Density Model for Harbor Porpoise (*Phocoena phocoena*) for the U.S. East Coast: Supplementary Report

Duke University Marine Geospatial Ecology Lab*

Model Version 3.4 - 2016-04-21

Citation

When referencing our methodology or results generally, please cite our open-access article:

Roberts JJ, Best BD, Mannocci L, Fujioka E, Halpin PN, Palka DL, Garrison LP, Mullin KD, Cole TVN, Khan CB, McLellan WM, Pabst DA, Lockhart GG (2016) Habitat-based cetacean density models for the U.S. Atlantic and Gulf of Mexico. Scientific Reports 6: 22615. doi: 10.1038/srep22615

To reference this specific model or Supplementary Report, please cite:

Roberts JJ, Best BD, Mannocci L, Fujioka E, Halpin PN, Palka DL, Garrison LP, Mullin KD, Cole TVN, Khan CB, McLellan WM, Pabst DA, Lockhart GG (2016) Density Model for Harbor Porpoise (*Phocoena phocoena*) for the U.S. East Coast Version 3.4, 2016-04-21, and Supplementary Report. Marine Geospatial Ecology Lab, Duke University, Durham, North Carolina.

Copyright and License

Revision History

Version	Date	Description of changes
1	2014-11-05	Initial version.
2	2014-12-03	Fixed bug that prevented 144 observations from the NE_narwss_1999_widgeon_hapo dataset from being used in the winter model. Refitted the winter model and updated the documentation.
3	2015-01-21	Refitted the detection function and density models to segments where Beaufort sea state was less than or equal to 2, as suggested by A. Read, to see if the abundance estimates better match NOAA's.
3.1	2015-03-06	Updated the documentation. No changes to the model.
3.2	2015-05-14	Updated calculation of CVs. Switched density rasters to logarithmic breaks. No changes to the model.
3.3	2015-09-26	Updated the documentation. No changes to the model.
3.4	2016-04-21	Switched calculation of monthly 5% and 95% confidence interval rasters to the method used to produce the year-round rasters. (We intended this to happen in version 3.2 but I did not implement it properly.) Updated the monthly CV rasters to have value 0 where we assumed the species was absent, consistent with the year-round CV raster. No changes to the other (non-zero) CV values, the mean abundance rasters, or the model itself.

*For questions, or to offer feedback about this model or report, please contact Jason Roberts (jason.roberts@duke.edu)

Survey Data

This analysis only considered effort segments and sightings where beaufort <= 2.

Survey	Period	Length (1000 km)	Hours	Sightings
NEFSC Aerial Surveys	1995-2008	32	192	461
NEFSC NARWSS Harbor Porpoise Survey	1999-1999	3	16	117
NEFSC North Atlantic Right Whale Sighting Survey	1999-2013	117	628	1014
NEFSC Shipboard Surveys	1995-2004	3	195	388
NJDEP Aerial Surveys	2008-2009	6	34	5
NJDEP Shipboard Surveys	2008-2009	6	366	33
SEFSC Atlantic Shipboard Surveys	1992-2005	6	420	0
SEFSC Mid Atlantic Tursiops Aerial Surveys	1995-2005	29	168	0
SEFSC Southeast Cetacean Aerial Surveys	1992-1995	6	28	0
UNCW Cape Hatteras Navy Surveys	2011-2013	4	31	0
UNCW Early Marine Mammal Surveys	2002-2002	8	44	0
UNCW Jacksonville Navy Surveys	2009-2013	35	232	0
UNCW Onslow Navy Surveys	2007-2011	19	117	0
UNCW Right Whale Surveys	2005-2008	61	316	0
Virginia Aquarium Aerial Surveys	2012-2014	3	18	0
Total		338	2805	2018

Table 2: Survey effort and sightings used in this model. Effort is tallied as the cumulative length of on-effort transects and hours the survey team was on effort. Sightings are the number of on-effort encounters of the modeled species for which a perpendicular sighting distance (PSD) was available. Off effort sightings and those without PSDs were omitted from the analysis.

Season	Months	Length (1000 km)	Hours	Sightings
Winter	Nov Dec Jan Feb Mar Apr May	183	1247	856
Summer	Jun Jul Aug Sep Oct	155	1557	1162

Table 3: Survey effort and on-effort sightings having perpendicular sighting distances, summarized by season.

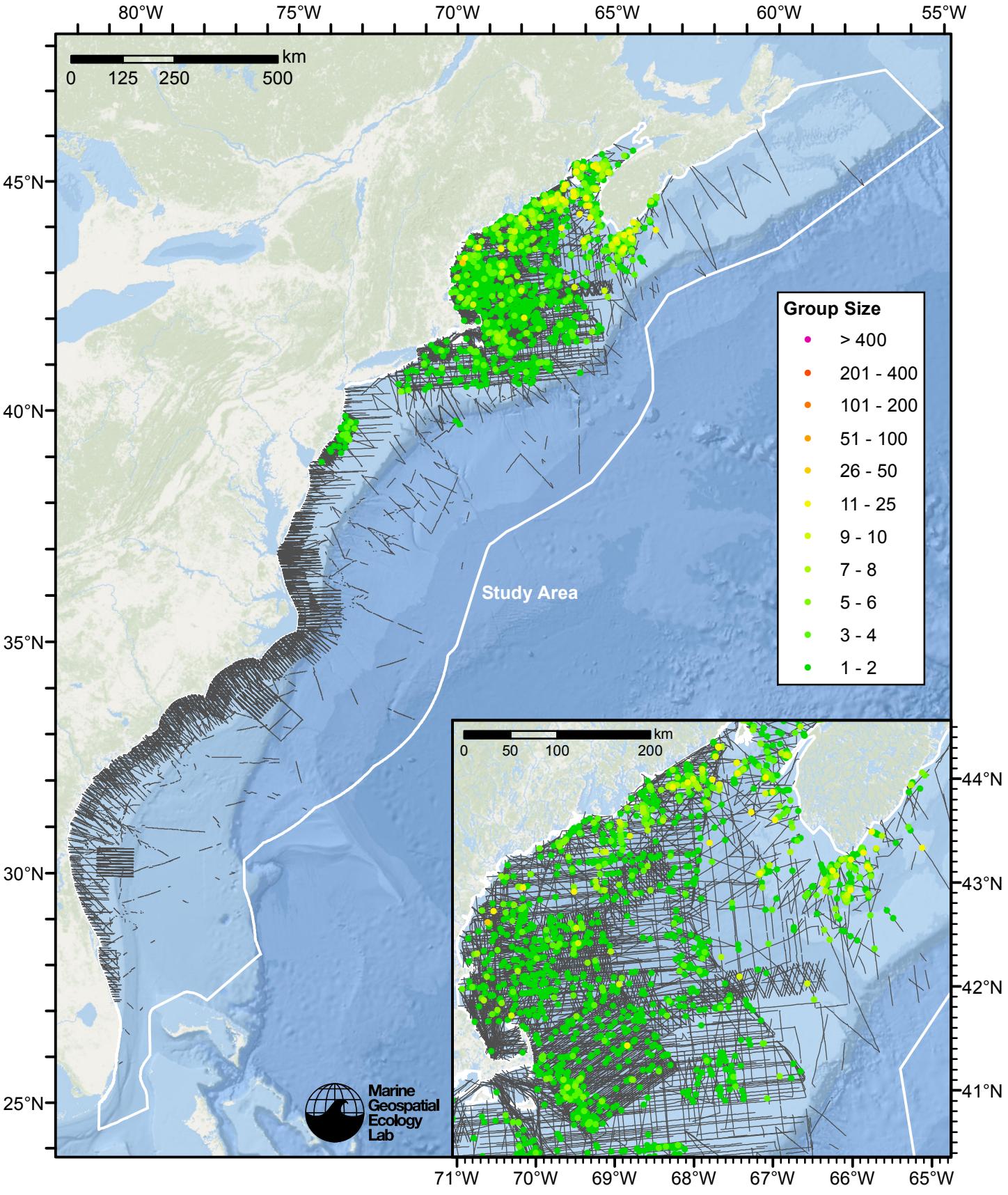

Figure 1: Harbor porpoise sightings and survey tracklines.

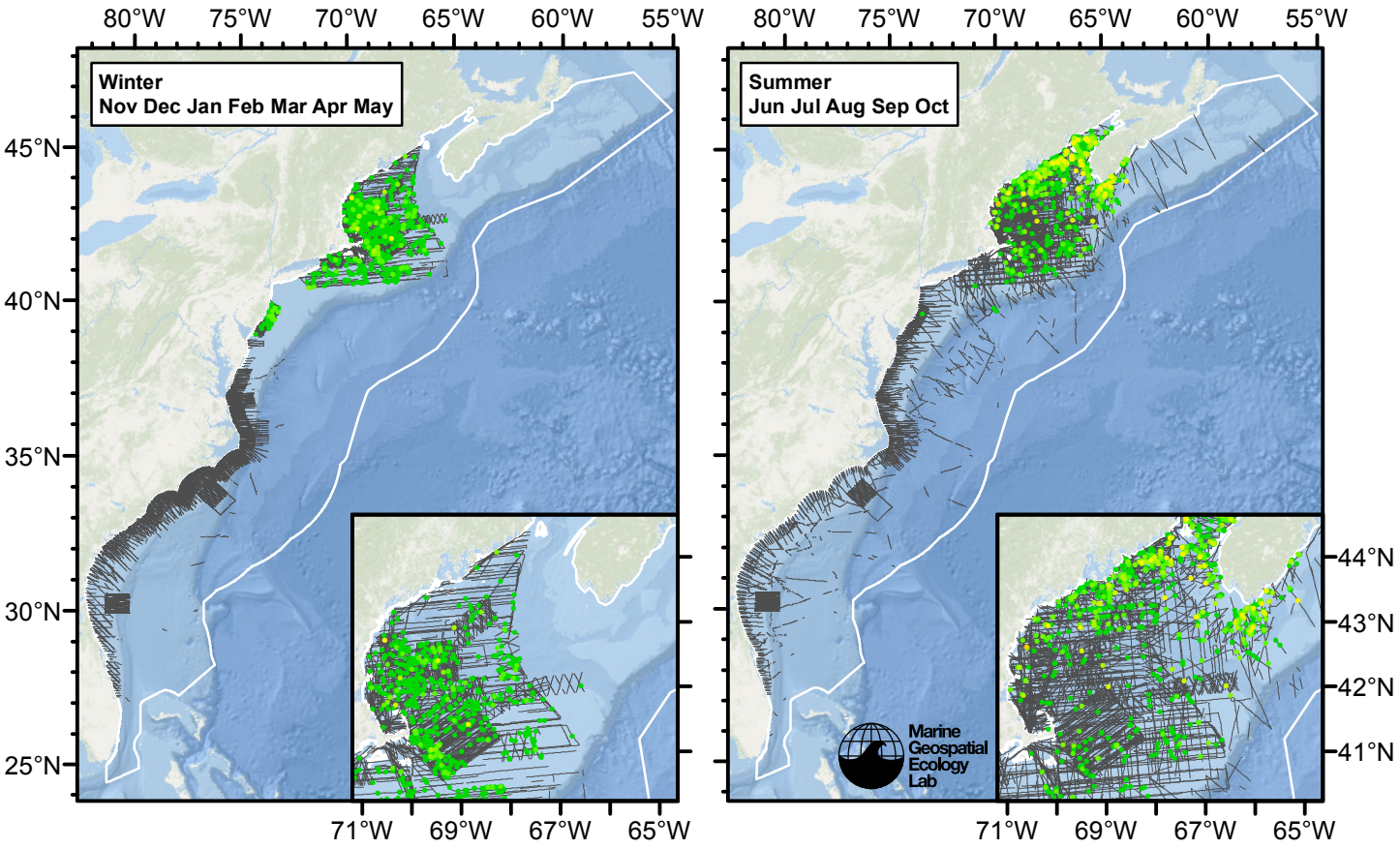

Figure 2: Harbor porpoise sightings and survey tracklines, by season. Sighting colors are the same as the previous figure.

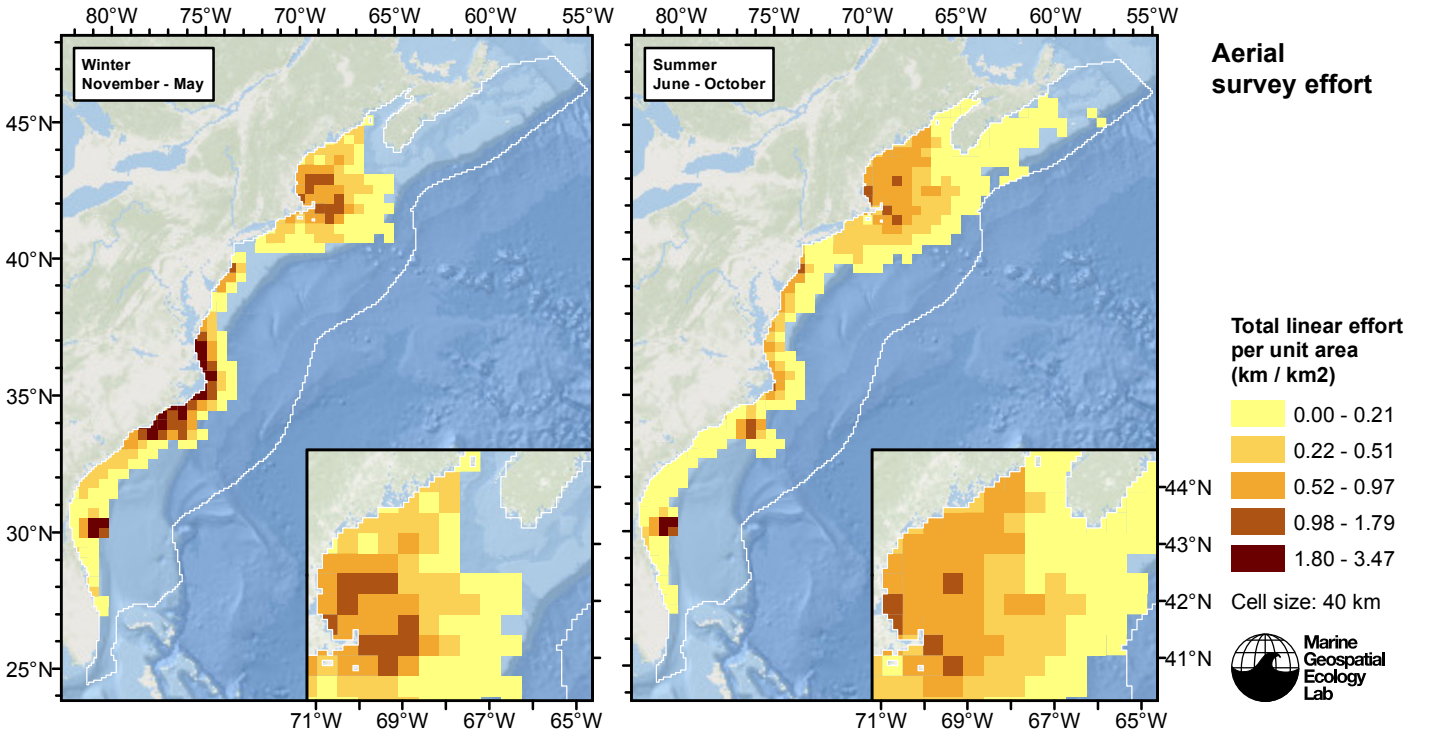

Figure 3: Aerial linear survey effort per unit area.

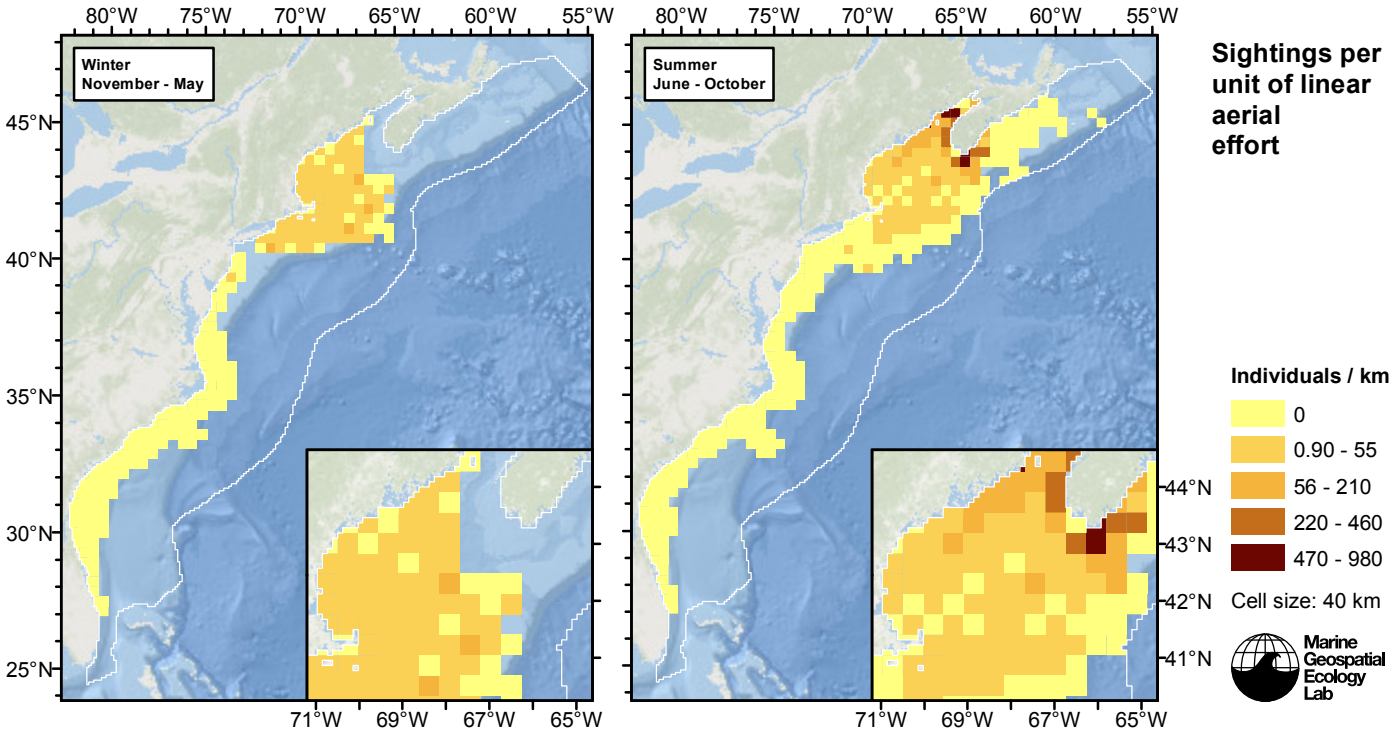

Figure 4: Harbor porpoise sightings per unit aerial linear survey effort.

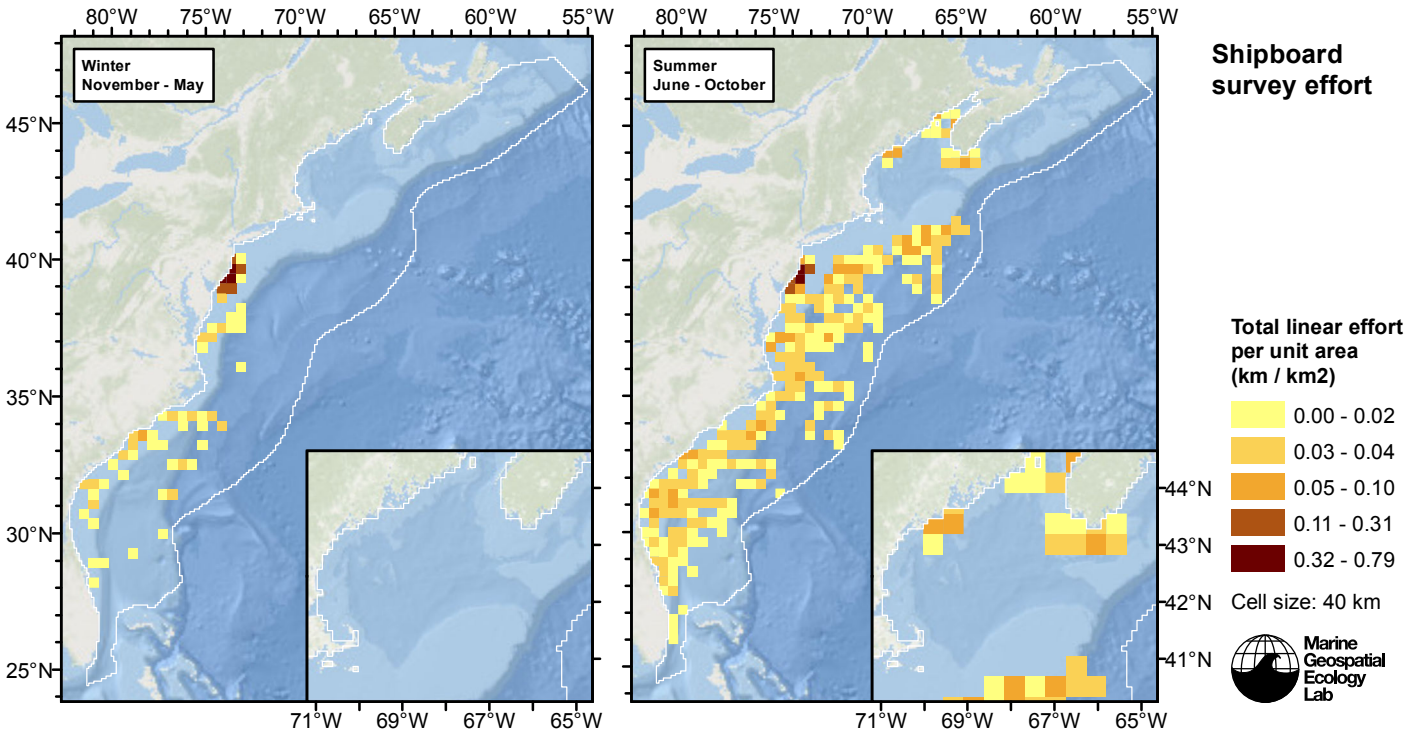

Figure 5: Shipboard linear survey effort per unit area.

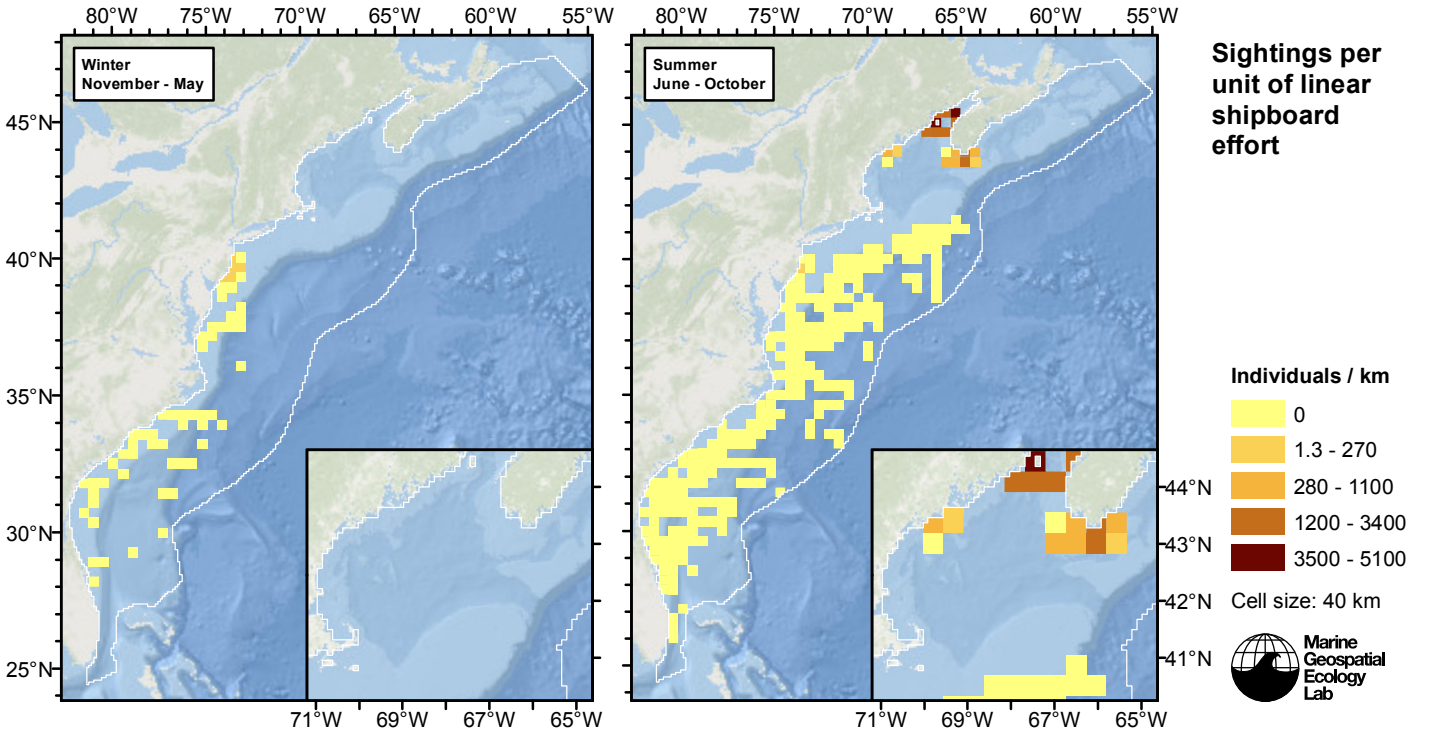

Figure 6: Harbor porpoise sightings per unit shipboard linear survey effort.

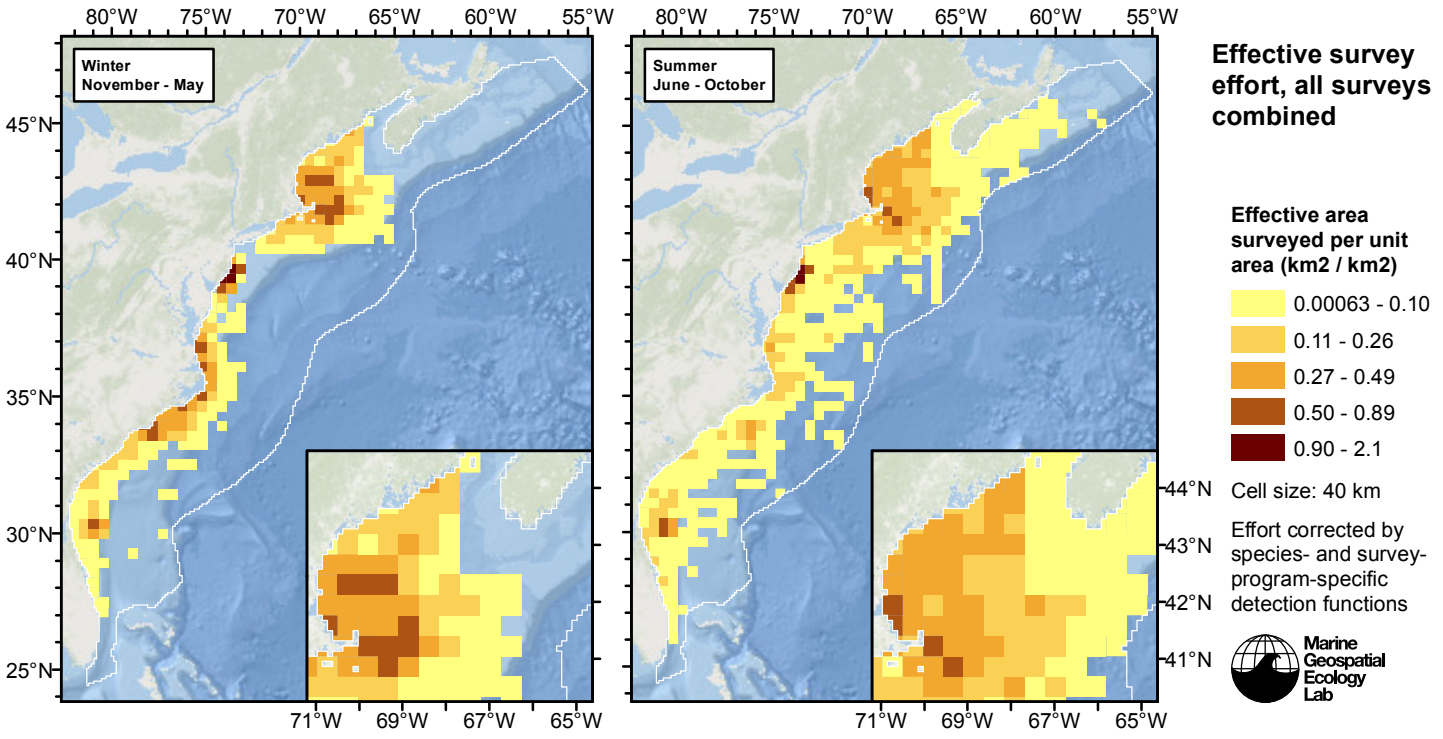

Figure 7: Effective survey effort per unit area, for all surveys combined. Here, effort is corrected by the species- and survey-program-specific detection functions used in fitting the density models.

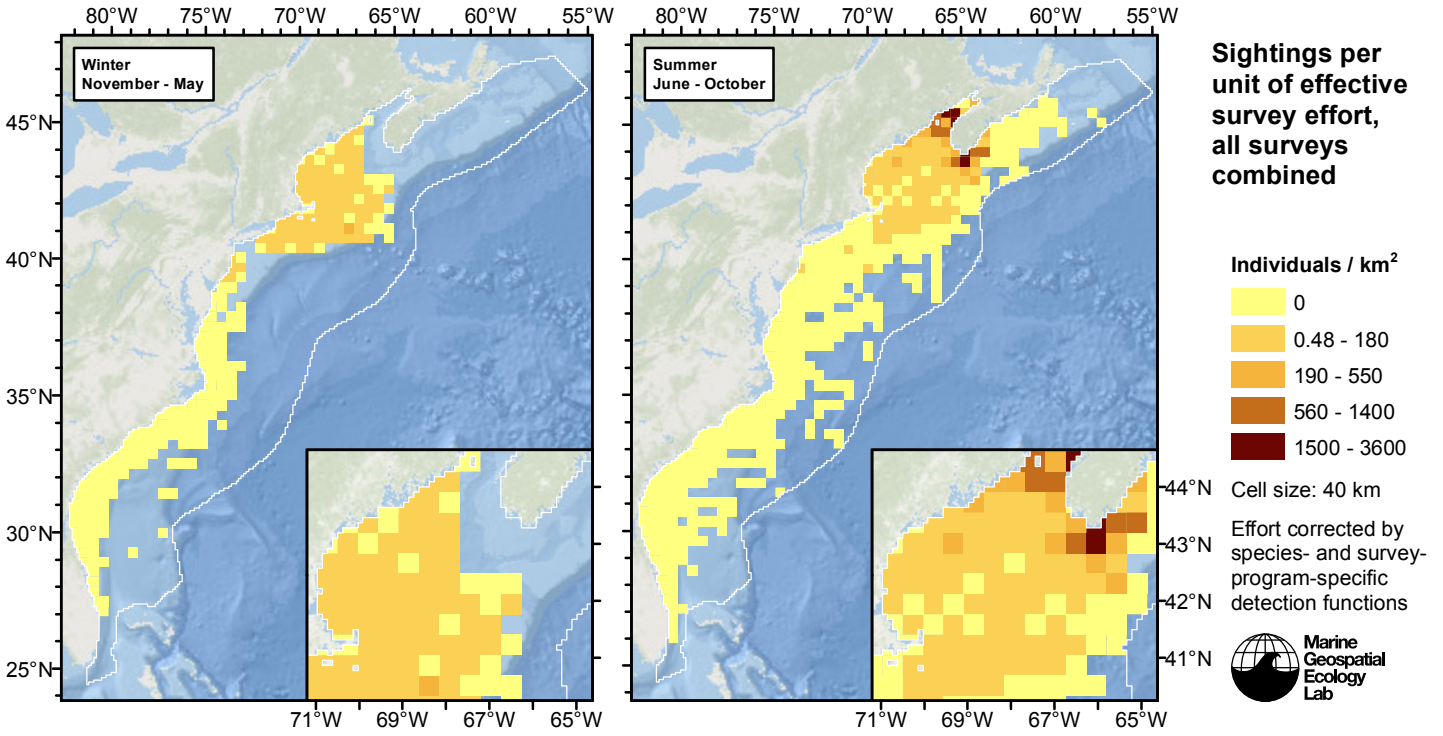

Figure 8: Harbor porpoise sightings per unit of effective survey effort, for all surveys combined. Here, effort is corrected by the species- and survey-program-specific detection functions used in fitting the density models.

Detection Functions

The detection hierarchy figures below show how sightings from multiple surveys were pooled to try to achieve Buckland et. al's (2001) recommendation that at least 60-80 sightings be used to fit a detection function. Leaf nodes, on the right, usually represent individual surveys, while the hierarchy to the left shows how they have been grouped according to how similar we believed the surveys were to each other in their detection performance.

At each node, the red or green number indicates the total number of sightings below that node in the hierarchy, and is colored green if 70 or more sightings were available, and red otherwise. If a grouping node has zero sightings–i.e. all of the surveys within it had zero sightings–it may be collapsed and shown as a leaf to save space.

Each histogram in the figure indicates a node where a detection function was fitted. The actual detection functions do not appear in this figure; they are presented in subsequent sections. The histogram shows the frequency of sightings by perpendicular sighting distance for all surveys contained by that node. Each survey (leaf node) recieves the detection function that is closest to it up the hierarchy. Thus, for common species, sufficient sightings may be available to fit detection functions deep in the hierarchy, with each function applying to only a few surveys, thereby allowing variability in detection performance between surveys to be addressed relatively finely. For rare species, so few sightings may be available that we have to pool many surveys together to try to meet Buckland's recommendation, and fit only a few coarse detection functions high in the hierarchy.

A blue Proxy Species tag indicates that so few sightings were available that, rather than ascend higher in the hierarchy to a point that we would pool grossly-incompatible surveys together, (e.g. shipboard surveys that used big-eye binoculars with those that used only naked eyes) we pooled sightings of similar species together instead. The list of species pooled is given in following sections.

Shipboard Surveys

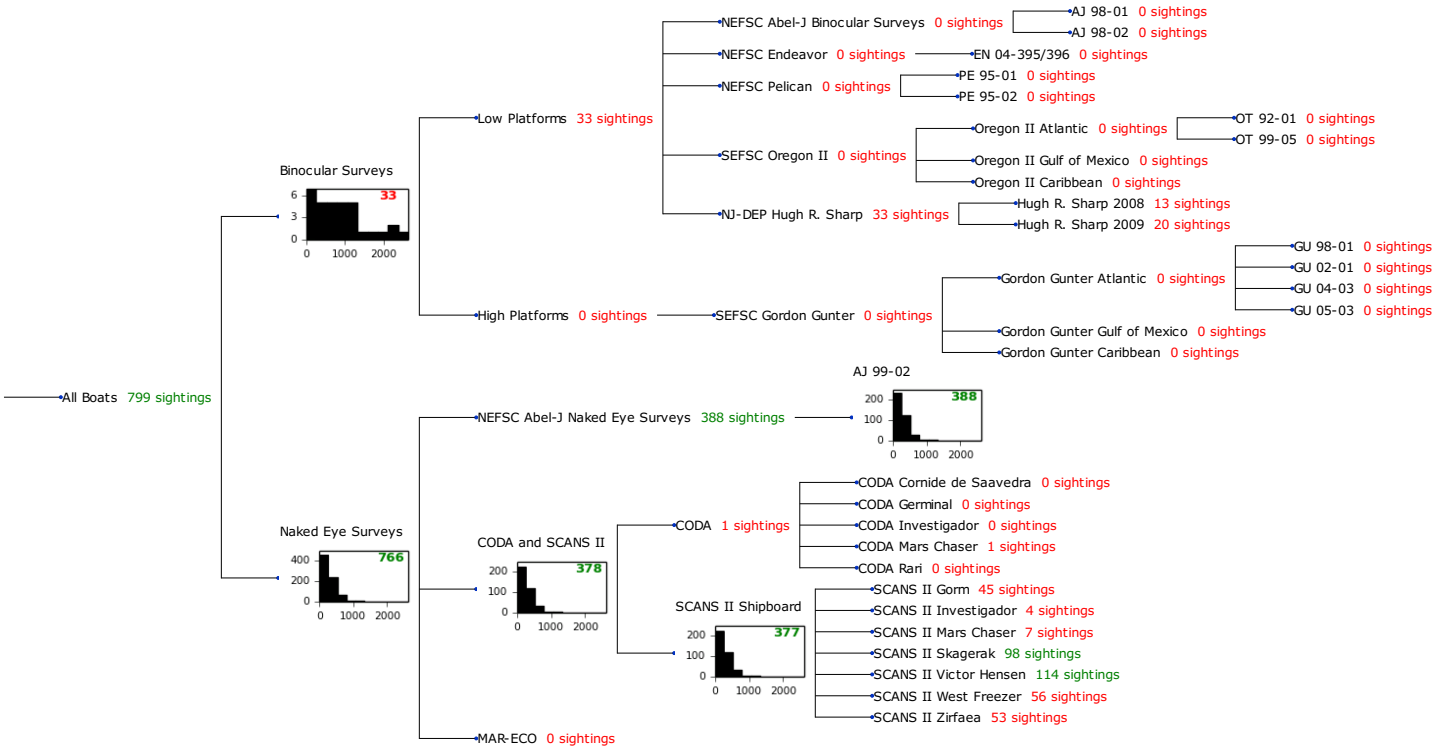

Figure 9: Detection hierarchy for shipboard surveys

Binocular Surveys

The sightings were right truncated at 2200m.

Key	Adjustment	Order	Covariates	Succeeded	Δ AIC	Mean ESHW (m)
hn				Yes	0.00	1177
hr				Yes	1.58	1418
hn	cos	2		Yes	1.84	1282
hn	cos	3		Yes	1.93	1100
hr	poly	2		Yes	3.56	1394
hr	poly	4		Yes	3.58	1418
hn	herm	4		No		

Table 4: Candidate detection functions for Binocular Surveys. The first one listed was selected for the density model.

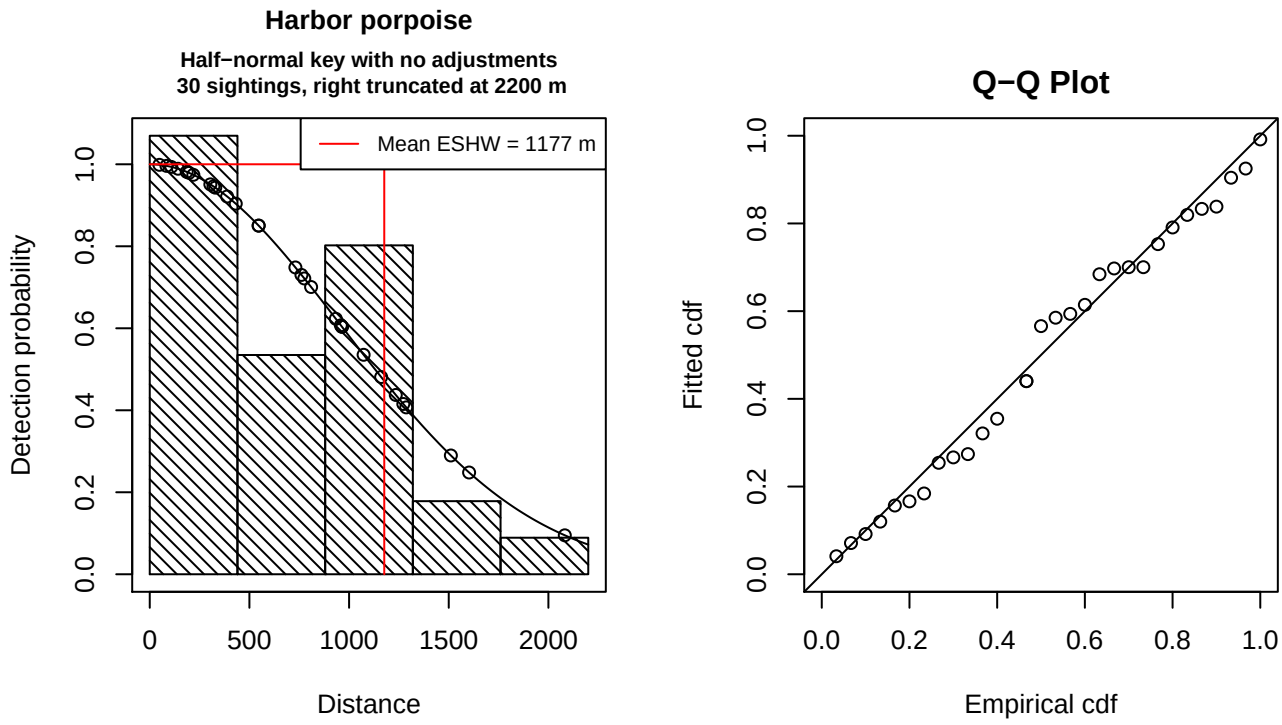

Figure 10: Detection function for Binocular Surveys that was selected for the density model

Statistical output for this detection function:

```
Summary for ds object
Number of observations :  30
Distance range         :  0  -  2200
AIC                    :  452.1663

Detection function:
 Half-normal key function

Detection function parameters
Scale Coefficients:
            estimate        se
(Intercept) 6.866704 0.1759982

                     Estimate          SE        CV
Average p            0.5348039  0.08140234 0.1522097
N in covered region 56.0953241 11.03158813 0.1966579
```

Naked Eye Surveys

The sightings were right truncated at 1000m.

Covariate	Description
beaufort	Beaufort sea state.
size	Estimated size (number of individuals) of the sighted group.

Table 5: Covariates tested in candidate "multi-covariate distance sampling" (MCDS) detection functions.

Key	Adjustment	Order	Covariates	Succeeded	Δ AIC	Mean ESHW (m)
hn				Yes	0.00	395
hn			beaufort	Yes	0.24	394
hn	cos	2		Yes	1.80	388
hn	cos	3		Yes	1.99	392
hr	poly	2		Yes	5.30	414
hr	poly	4		Yes	7.30	424
hr				Yes	14.81	447
hr			beaufort	Yes	16.47	448
hn	herm	4		No		
hn			size	No		
hr			size	No		
hn			beaufort, size	No		
hr			beaufort, size	No		

Table 6: Candidate detection functions for Naked Eye Surveys. The first one listed was selected for the density model.

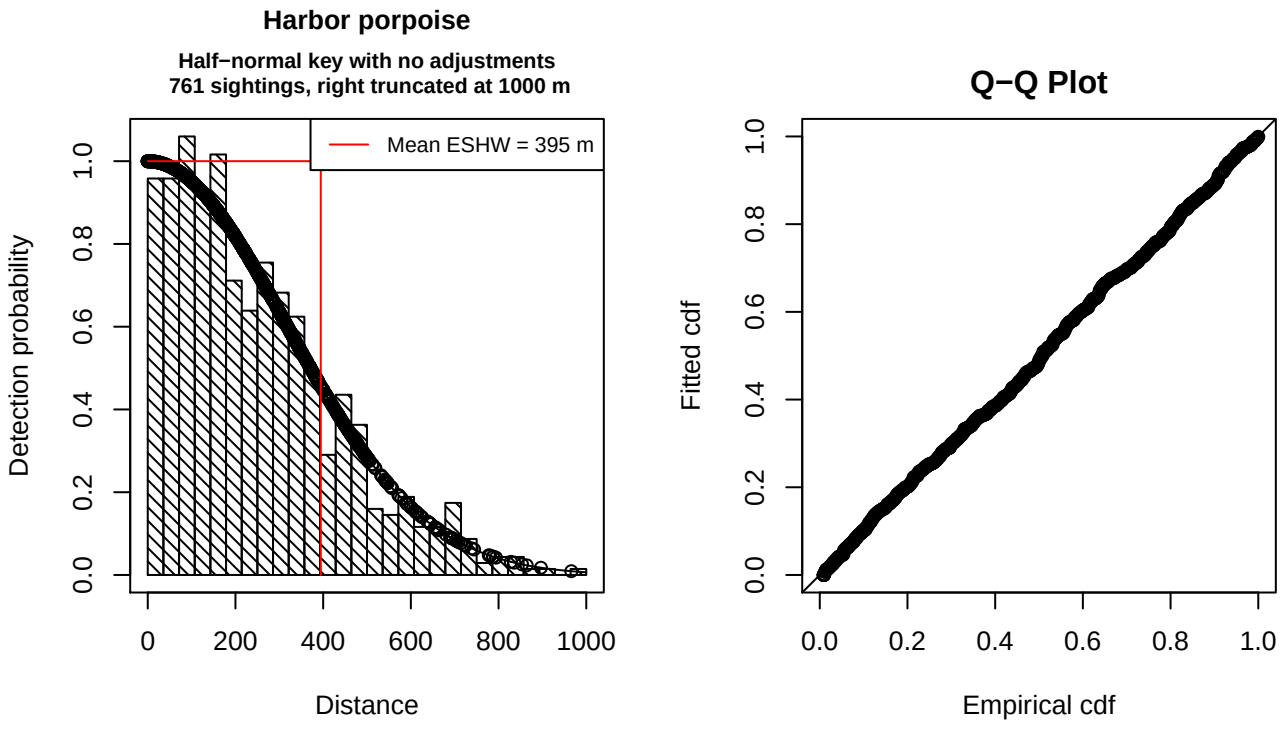

Figure 11: Detection function for Naked Eye Surveys that was selected for the density model

Statistical output for this detection function:

```
Summary for ds object
```

```
Number of observations :  761
Distance range         :  0  -  1000
AIC                    :  9848.572

Detection function:
 Half-normal key function

Detection function parameters
Scale Coefficients:
            estimate         se
(Intercept) 5.753511 0.02666397

                         Estimate          SE         CV
Average p              0.3945654  0.01034628 0.02622197
N in covered region 1928.7041978 74.27813234 0.03851194
```

Additional diagnostic plots:

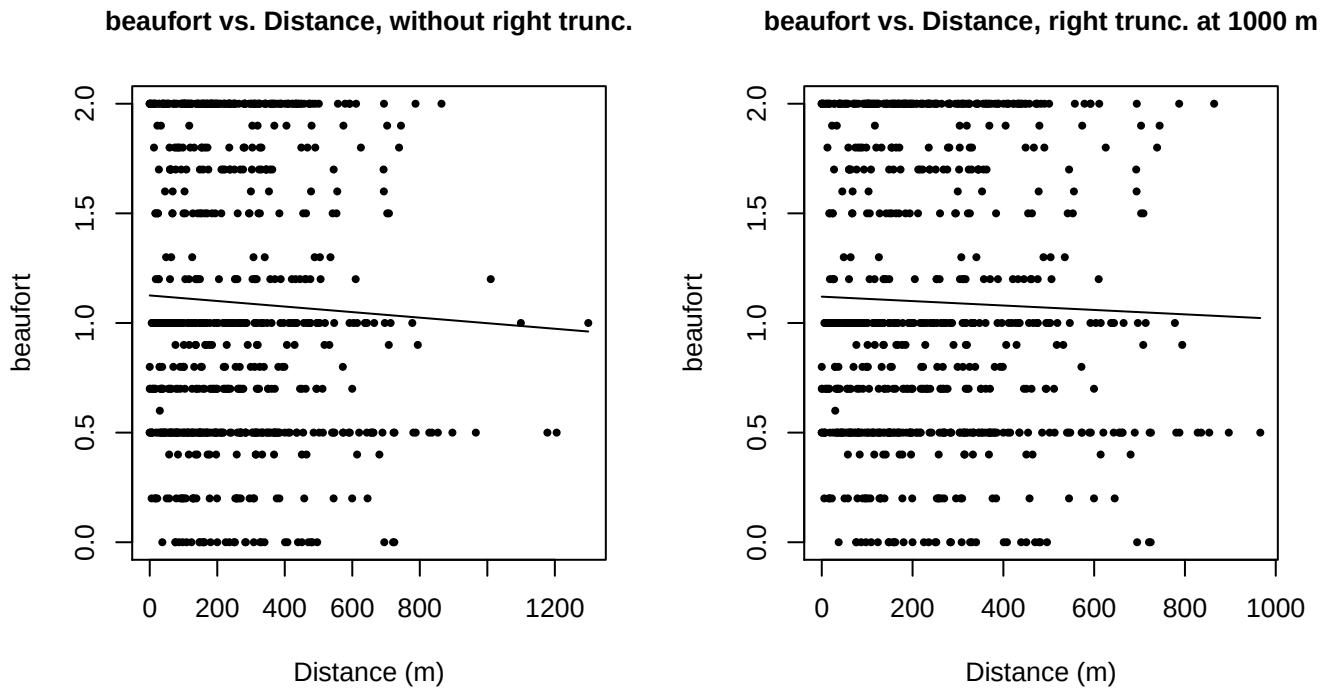

Figure 12: Scatterplots showing the relationship between Beaufort sea state and perpendicular sighting distance, for all sightings (left) and only those not right truncated (right). The line is a simple linear regression.

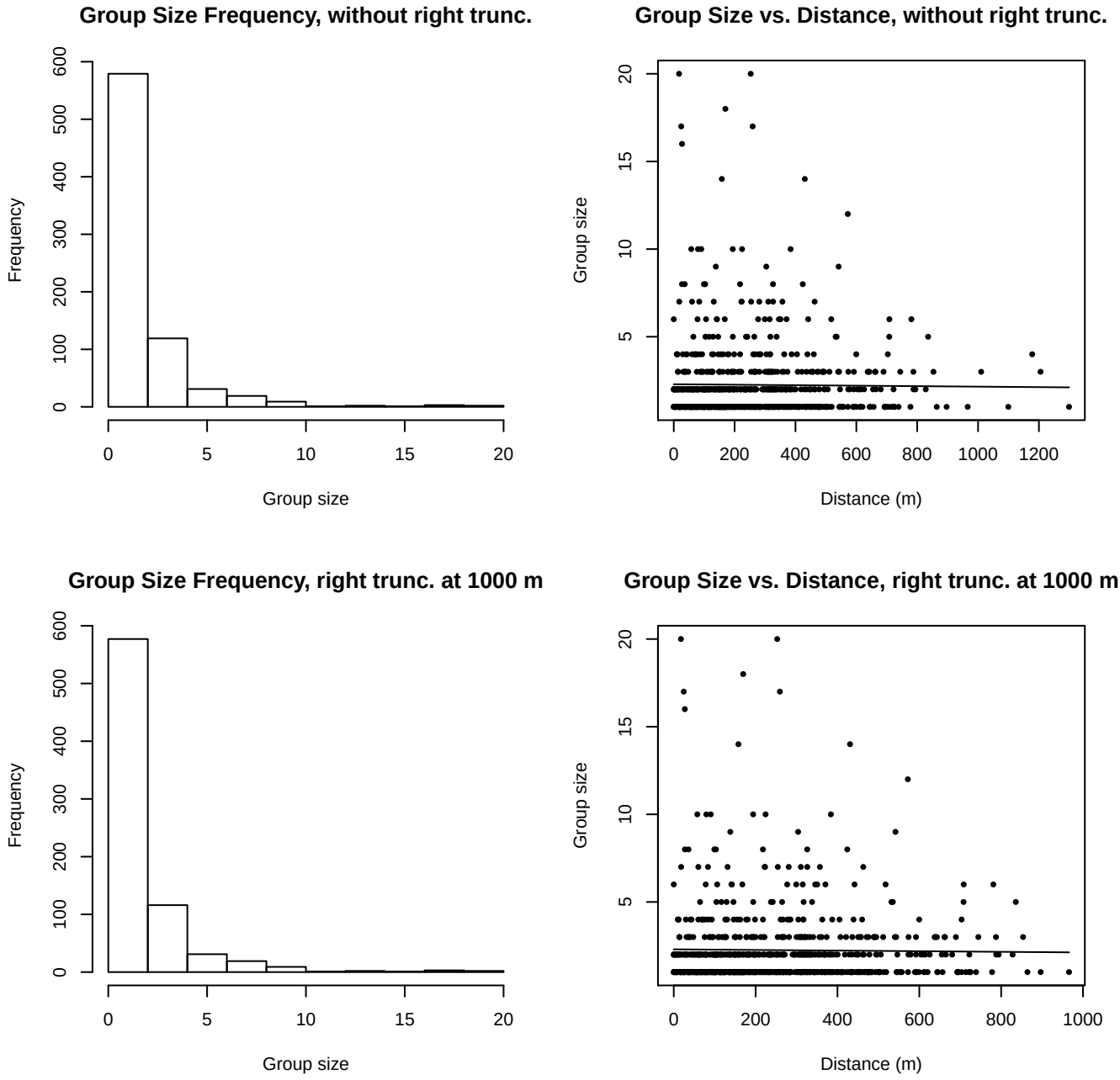

Figure 13: Histograms showing group size frequency and scatterplots showing the relationship between group size and perpendicular sighting distance, for all sightings (top row) and only those not right truncated (bottom row). In the scatterplot, the line is a simple linear regression.

NE_aj9902

The sightings were right truncated at 900m.

Covariate	Description
beaufort	Beaufort sea state.
quality	Survey-specific index of the quality of observation conditions, utilizing relevant factors other than Beaufort sea state (see methods).
size	Estimated size (number of individuals) of the sighted group.

Table 7: Covariates tested in candidate "multi-covariate distance sampling" (MCDS) detection functions.

Key	Adjustment	Order	Covariates	Succeeded	Δ AIC	Mean ESHW (m)
hn				Yes	0.00	388
hn			quality	Yes	1.27	387
hn	cos	3		Yes	1.82	399
hn	herm	4		Yes	2.00	387
hn	cos	2		Yes	2.00	388
hr	poly	2		Yes	4.14	414
hr	poly	4		Yes	4.70	425
hr				Yes	5.36	444
hn			beaufort	No		
hr			beaufort	No		
hr			quality	No		
hn			size	No		
hr			size	No		
hn			beaufort, quality	No		
hr			beaufort, quality	No		
hn			beaufort, size	No		
hr			beaufort, size	No		
hn			quality, size	No		
hr			quality, size	No		
hn			beaufort, quality, size	No		
hr			beaufort, quality, size	No		

Table 8: Candidate detection functions for NE_aj9902. The first one listed was selected for the density model.

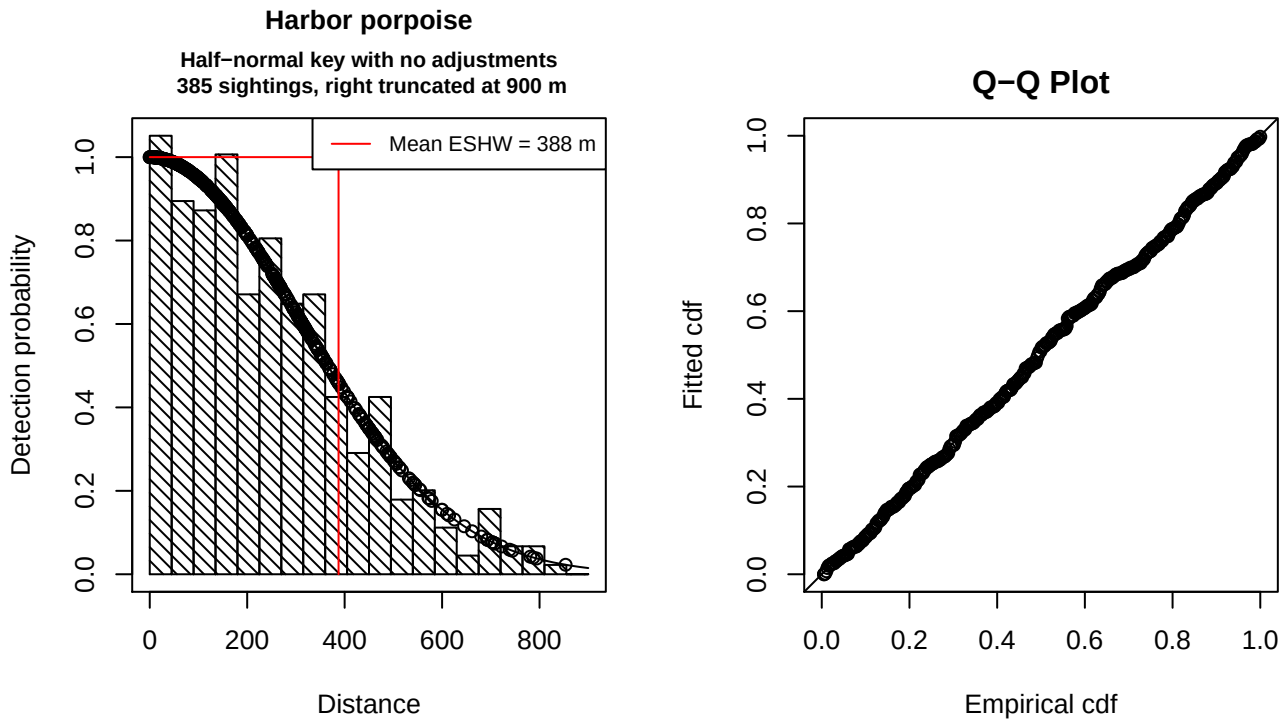

Figure 14: Detection function for NE_aj9902 that was selected for the density model

Statistical output for this detection function:

```
Summary for ds object
Number of observations :  385
Distance range         :  0  -  900
AIC                    :  4962.663

Detection function:
 Half-normal key function

Detection function parameters
Scale Coefficients:
            estimate         se
(Intercept) 5.737695 0.03931899

                      Estimate          SE         CV
Average p             0.4305691  0.01634285 0.03795639
N in covered region 894.1654479 48.31579378 0.05403451
```

Additional diagnostic plots:

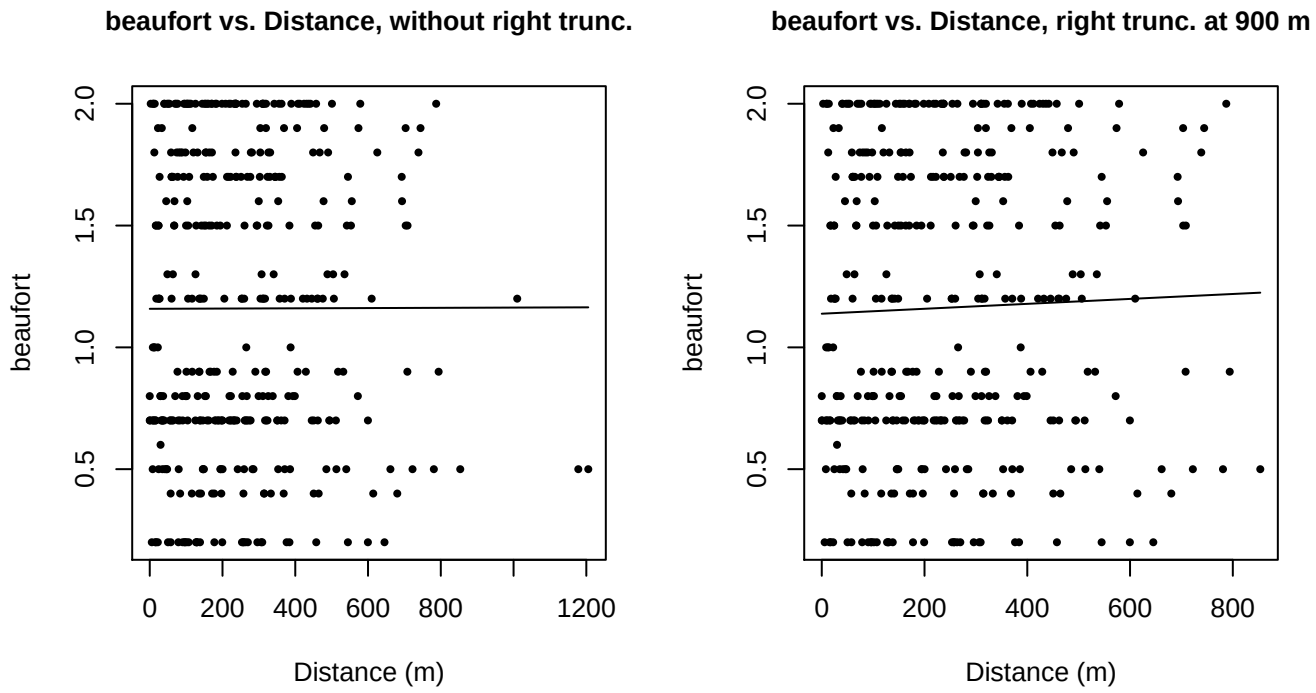

Figure 15: Scatterplots showing the relationship between Beaufort sea state and perpendicular sighting distance, for all sightings (left) and only those not right truncated (right). The line is a simple linear regression.

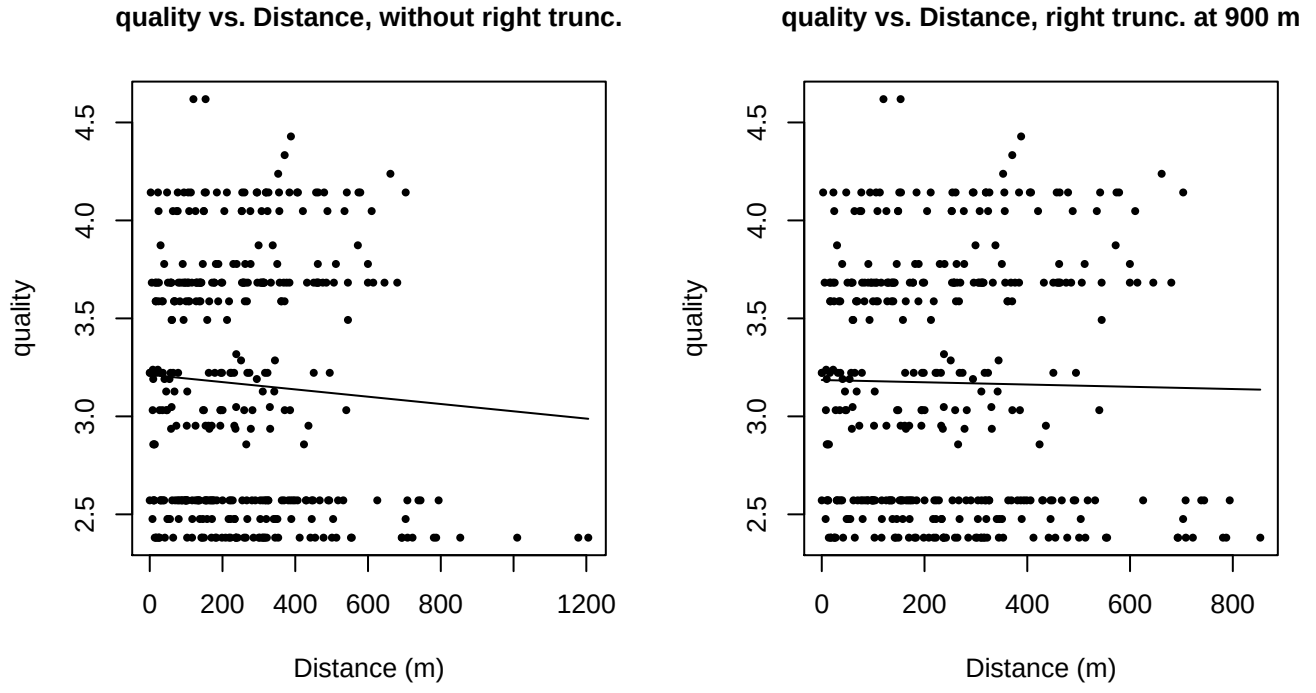

Figure 16: Scatterplots showing the relationship between the survey-specific index of the quality of observation conditions and perpendicular sighting distance, for all sightings (left) and only those not right truncated (right). Low values of the quality index correspond to better observation conditions. The line is a simple linear regression.

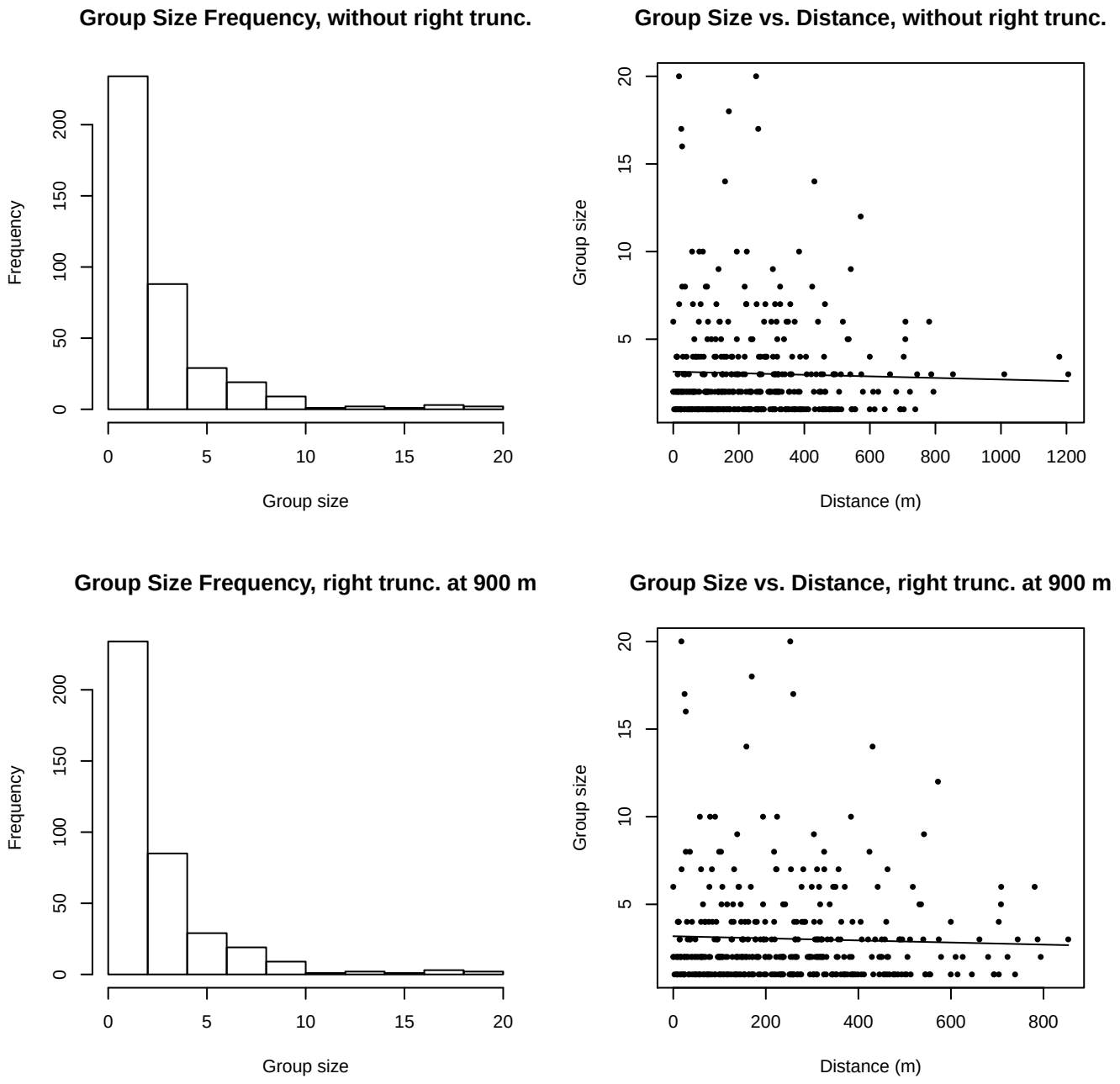

Figure 17: Histograms showing group size frequency and scatterplots showing the relationship between group size and perpendicular sighting distance, for all sightings (top row) and only those not right truncated (bottom row). In the scatterplot, the line is a simple linear regression.

CODA and SCANS II

The sightings were right truncated at 1000m.

Covariate	Description
beaufort	Beaufort sea state.
quality	Survey-specific index of the quality of observation conditions, utilizing relevant factors other than Beaufort sea state (see methods).
size	Estimated size (number of individuals) of the sighted group.

Table 9: Covariates tested in candidate "multi-covariate distance sampling" (MCDS) detection functions.

Key	Adjustment	Order	Covariates	Succeeded	Δ AIC	Mean ESHW (m)
hn			quality, size	Yes	0.00	402
hn			quality	Yes	0.78	403
hn			beaufort, size	Yes	7.32	404
hn			size	Yes	8.50	404
hn			beaufort	Yes	8.95	405
hr			quality, size	Yes	10.17	456
hn				Yes	10.28	405
hn	cos	2		Yes	11.54	388
hn	cos	3		Yes	12.11	394
hr			beaufort, quality, size	Yes	12.16	456
hr			quality	Yes	12.87	457
hr	poly	2		Yes	13.54	403
hr	poly	4		Yes	14.23	409
hr			size	Yes	14.83	434
hr			beaufort, size	Yes	14.98	444
hr				Yes	17.78	435
hr			beaufort	Yes	18.34	441
hn	herm	4		No		
hn			beaufort, quality	No		
hr			beaufort, quality	No		
hn			beaufort, quality, size	No		

Table 10: Candidate detection functions for CODA and SCANS II. The first one listed was selected for the density model.

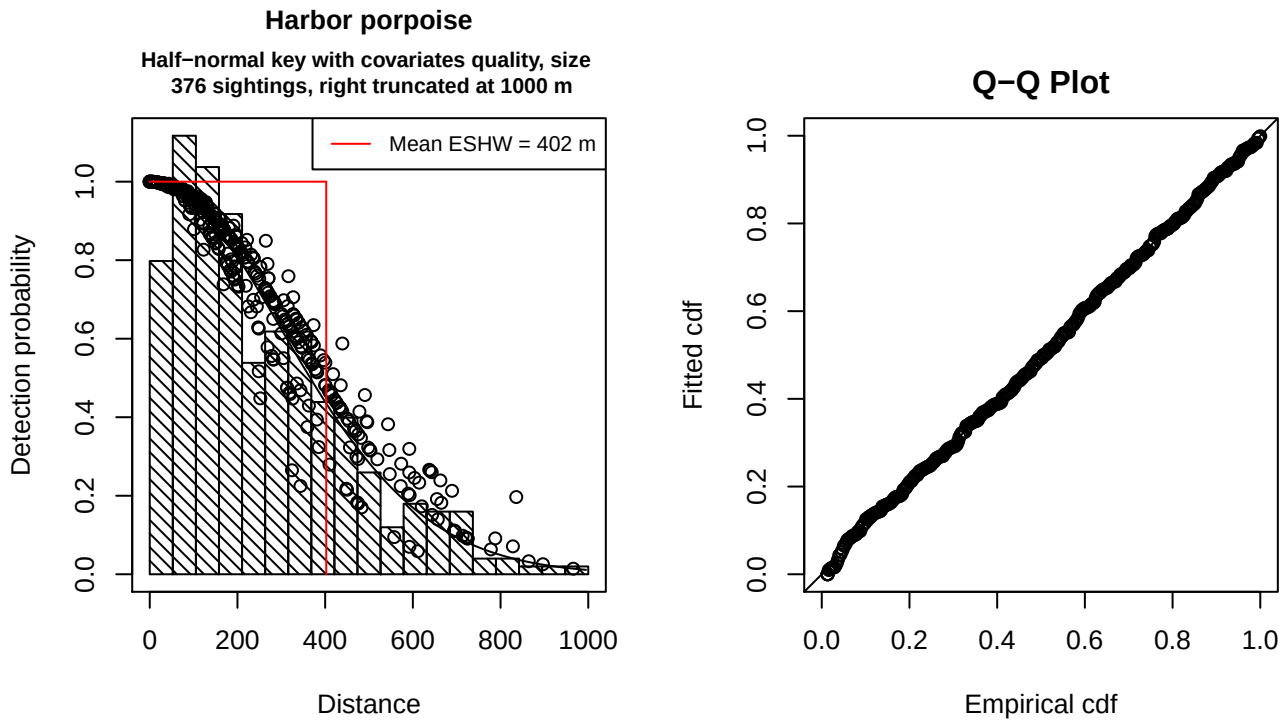

Figure 18: Detection function for CODA and SCANS II that was selected for the density model

Statistical output for this detection function:

```
Summary for ds object
Number of observations :  376
Distance range         :  0  -  1000
AIC                    :  4874.824

Detection function:
 Half-normal key function

Detection function parameters
Scale Coefficients:
               estimate         se
(Intercept)  5.71863595 0.09060314
quality     -0.15283736 0.05189857
size         0.08401323 0.05910341

                       Estimate         SE         CV
Average p             0.3947222  0.0162167 0.04108382
N in covered region 952.5686458 54.8716226 0.05760385
```

Additional diagnostic plots:

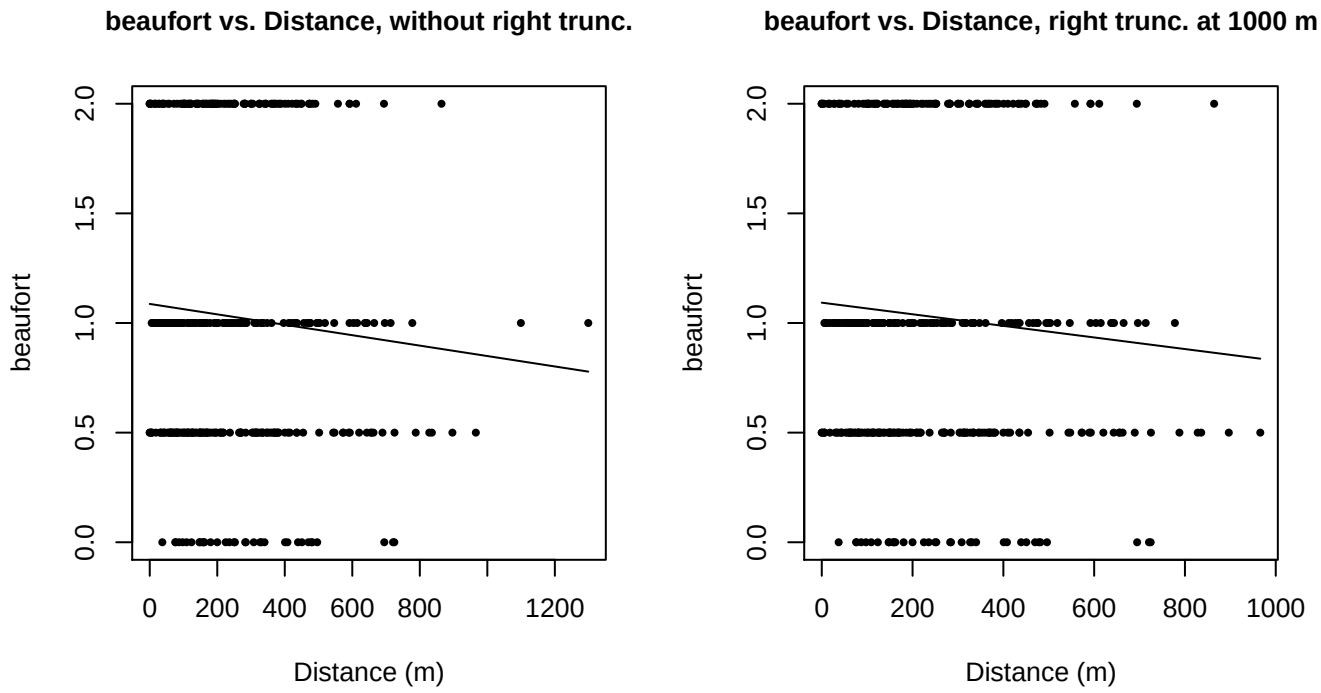

Figure 19: Scatterplots showing the relationship between Beaufort sea state and perpendicular sighting distance, for all sightings (left) and only those not right truncated (right). The line is a simple linear regression.

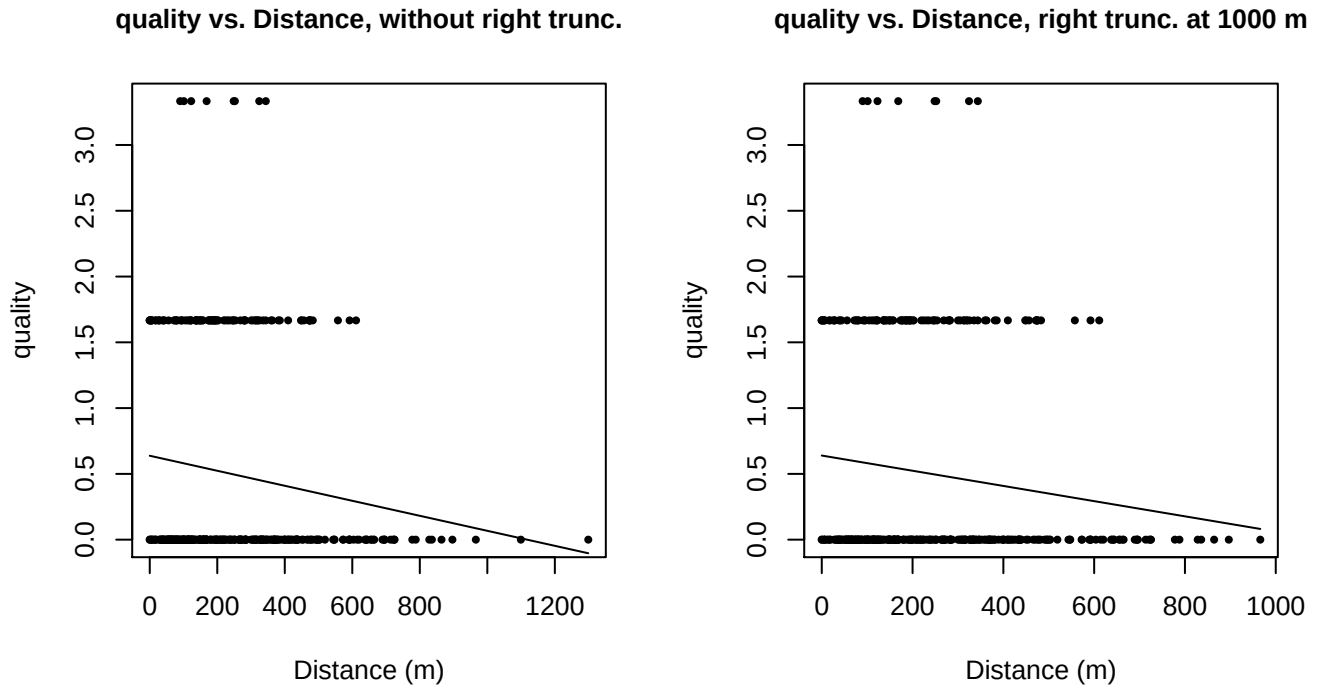

Figure 20: Scatterplots showing the relationship between the survey-specific index of the quality of observation conditions and perpendicular sighting distance, for all sightings (left) and only those not right truncated (right). Low values of the quality index correspond to better observation conditions. The line is a simple linear regression.

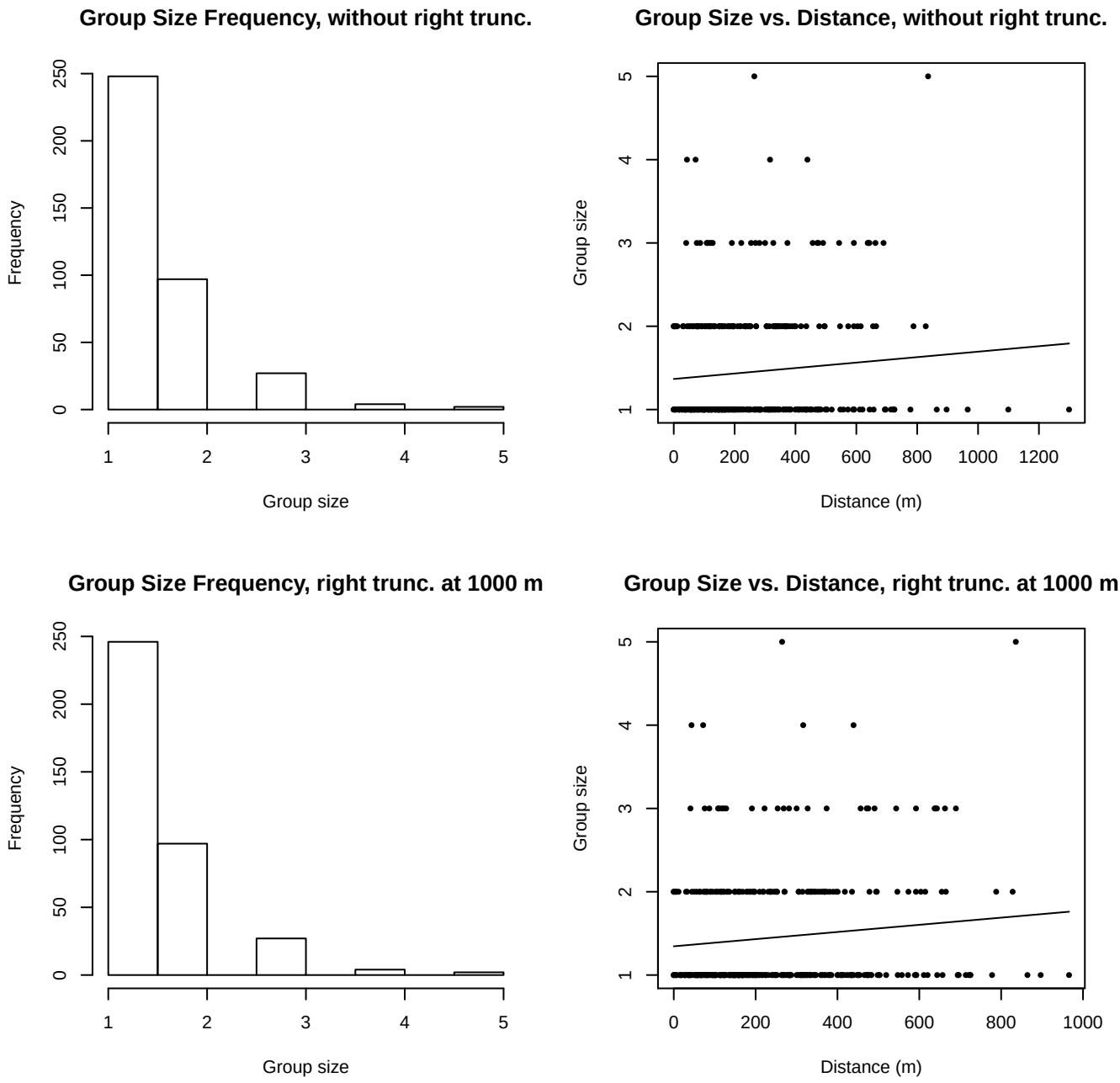

Figure 21: Histograms showing group size frequency and scatterplots showing the relationship between group size and perpendicular sighting distance, for all sightings (top row) and only those not right truncated (bottom row). In the scatterplot, the line is a simple linear regression.

SCANS II Shipboard

The sightings were right truncated at 1000m.

Covariate	Description
beaufort	Beaufort sea state.
quality	Survey-specific index of the quality of observation conditions, utilizing relevant factors other than Beaufort sea state (see methods).
size	Estimated size (number of individuals) of the sighted group.

vessel	Vessel from which the observation was made. This covariate allows the detection function to account for vessel-specific biases, such as the height of the survey platform.

Table 11: Covariates tested in candidate "multi-covariate distance sampling" (MCDS) detection functions.

Key	Adjustment	Order	Covariates	Succeeded	Δ AIC	Mean ESHW (m)
hn			quality, vessel	Yes	0.00	398
hn			vessel	Yes	0.26	400
hn			size, vessel	Yes	0.59	400
hn			quality, size, vessel	Yes	0.84	398
hn			beaufort, vessel	Yes	2.00	400
hn			beaufort, size, vessel	Yes	2.49	400
hr			quality, size, vessel	Yes	4.09	487
hr			quality, vessel	Yes	4.43	486
hr			size, vessel	Yes	4.87	488
hr			vessel	Yes	5.63	485
hn			quality, size	Yes	22.12	403
hn			quality	Yes	22.86	403
hn			beaufort, size	Yes	29.47	404
hn			size	Yes	30.65	405
hn			beaufort	Yes	31.08	405
hn				Yes	32.41	405
hr			quality, size	Yes	32.63	456
hn	cos	2		Yes	33.63	387
hn	cos	3		Yes	34.18	392
hn	herm	4		Yes	34.32	404
hr			beaufort, quality, size	Yes	34.62	456
hr			quality	Yes	35.26	457
hr	poly	2		Yes	35.63	401
hr	poly	4		Yes	36.34	407
hr			size	Yes	37.17	432
hr			beaufort, size	Yes	37.39	442
hr				Yes	40.14	434
hr			beaufort	Yes	40.74	440
hn			beaufort, quality	No		
hr			beaufort, quality	No		
hr			beaufort, vessel	No		
hn			beaufort, quality, size	No		
hn			beaufort, quality, vessel	No		

hr	beaufort, quality, vessel	No
hr	beaufort, size, vessel	No
hn	beaufort, quality, size, vessel	No
hr	beaufort, quality, size, vessel	No

Table 12: Candidate detection functions for SCANS II Shipboard. The first one listed was selected for the density model.

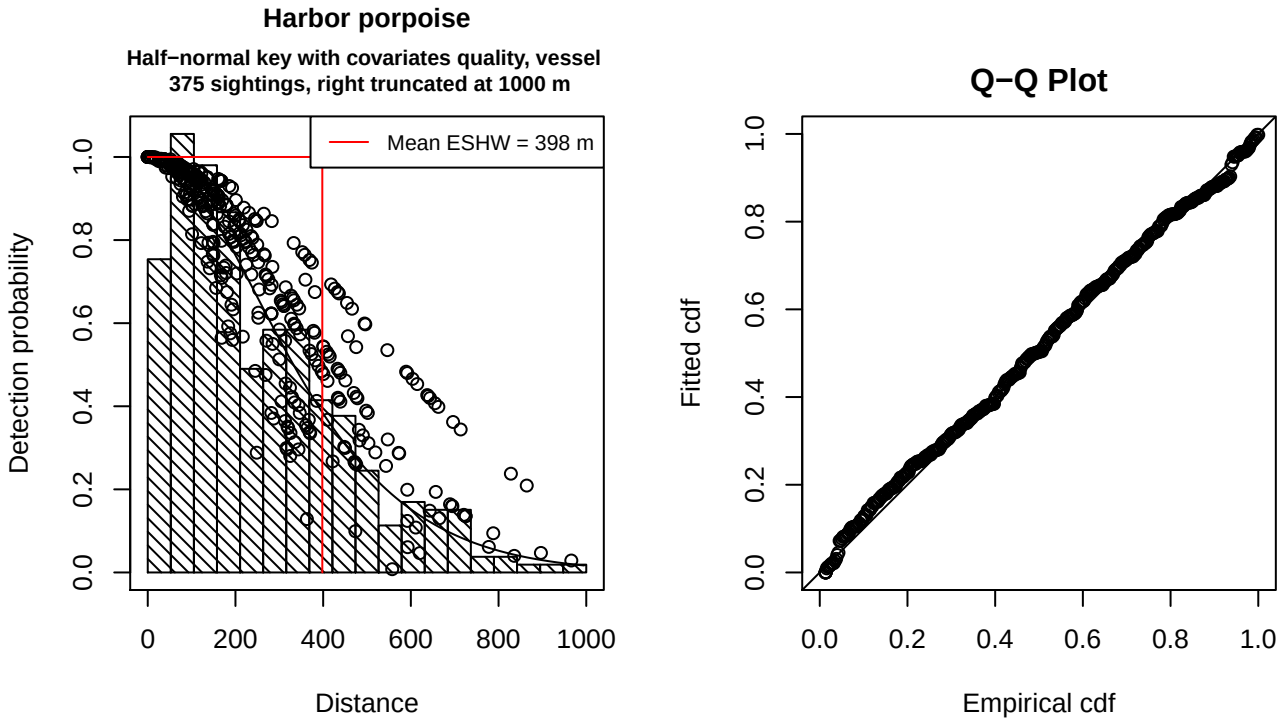

Figure 22: Detection function for SCANS II Shipboard that was selected for the density model

Statistical output for this detection function:

```
Summary for ds object
Number of observations :  375
Distance range         :  0  -  1000
AIC                    :  4840.026

Detection function:
 Half-normal key function

Detection function parameters
Scale Coefficients:
                     estimate         se
(Intercept)          5.31666827 0.13164505
quality             -0.07700794 0.06371585
vesselInvestigador   0.24537927 0.83024341
vesselMars Chaser    0.24236626 0.42214761
vesselSkagerak       0.57680438 0.14929156
vesselVictor Hensen  0.48066480 0.13523464
```

```
vesselWest Freezer   0.20677258 0.15104010
vesselZirfaea        0.87481431 0.21491944

                         Estimate          SE         CV
Average p                0.371992  0.01607041 0.04320095
N in covered region 1008.086297 60.57445406 0.06008856
```

Additional diagnostic plots:

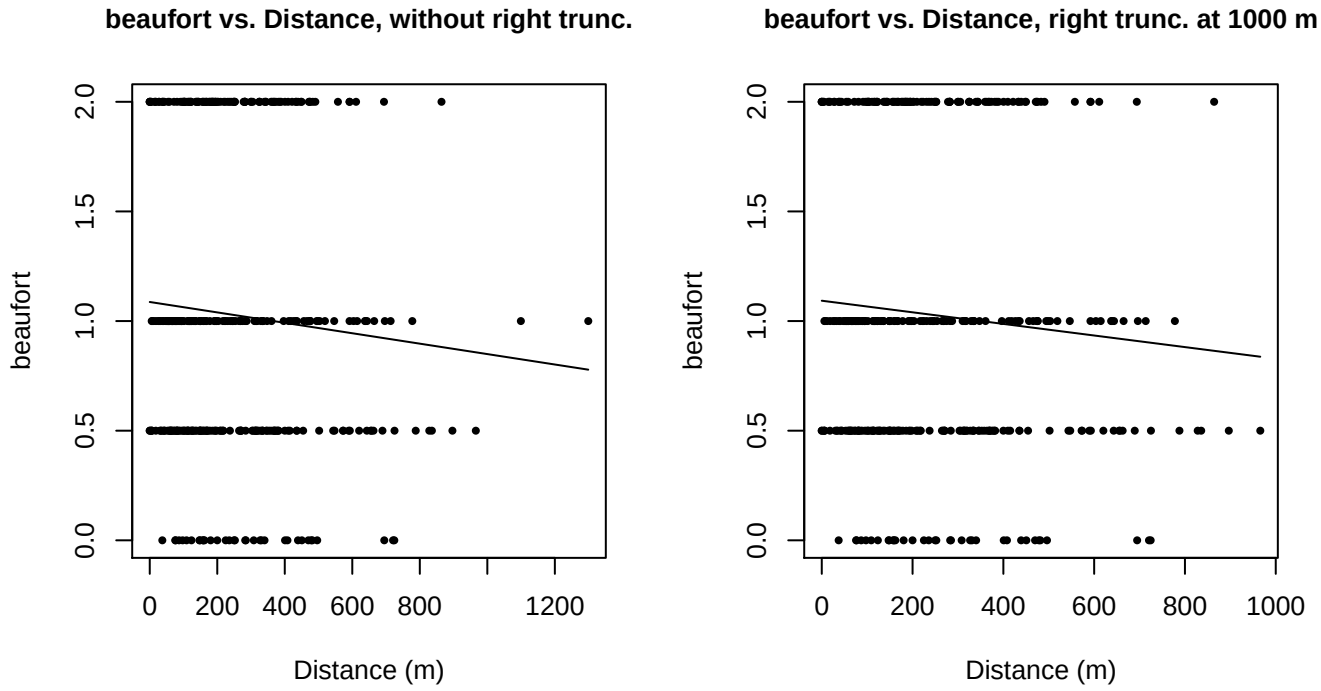

Figure 23: Scatterplots showing the relationship between Beaufort sea state and perpendicular sighting distance, for all sightings (left) and only those not right truncated (right). The line is a simple linear regression.

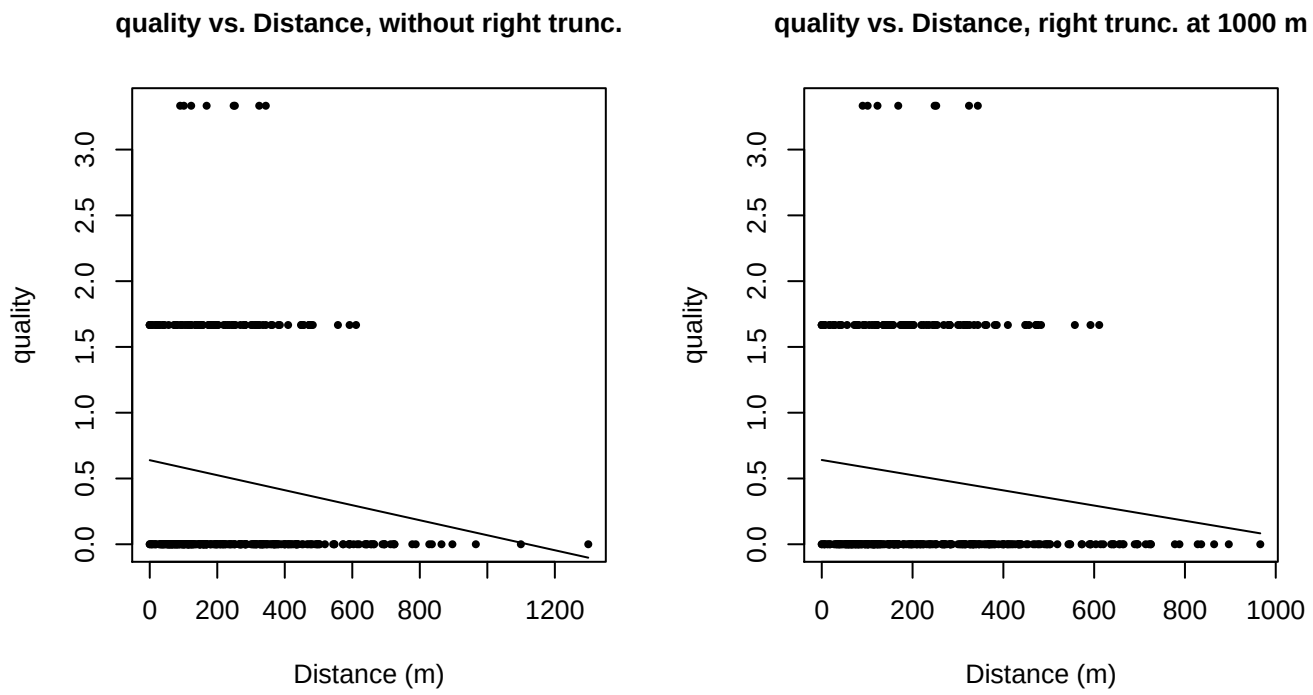

Figure 24: Scatterplots showing the relationship between the survey-specific index of the quality of observation conditions and perpendicular sighting distance, for all sightings (left) and only those not right truncated (right). Low values of the quality index correspond to better observation conditions. The line is a simple linear regression.

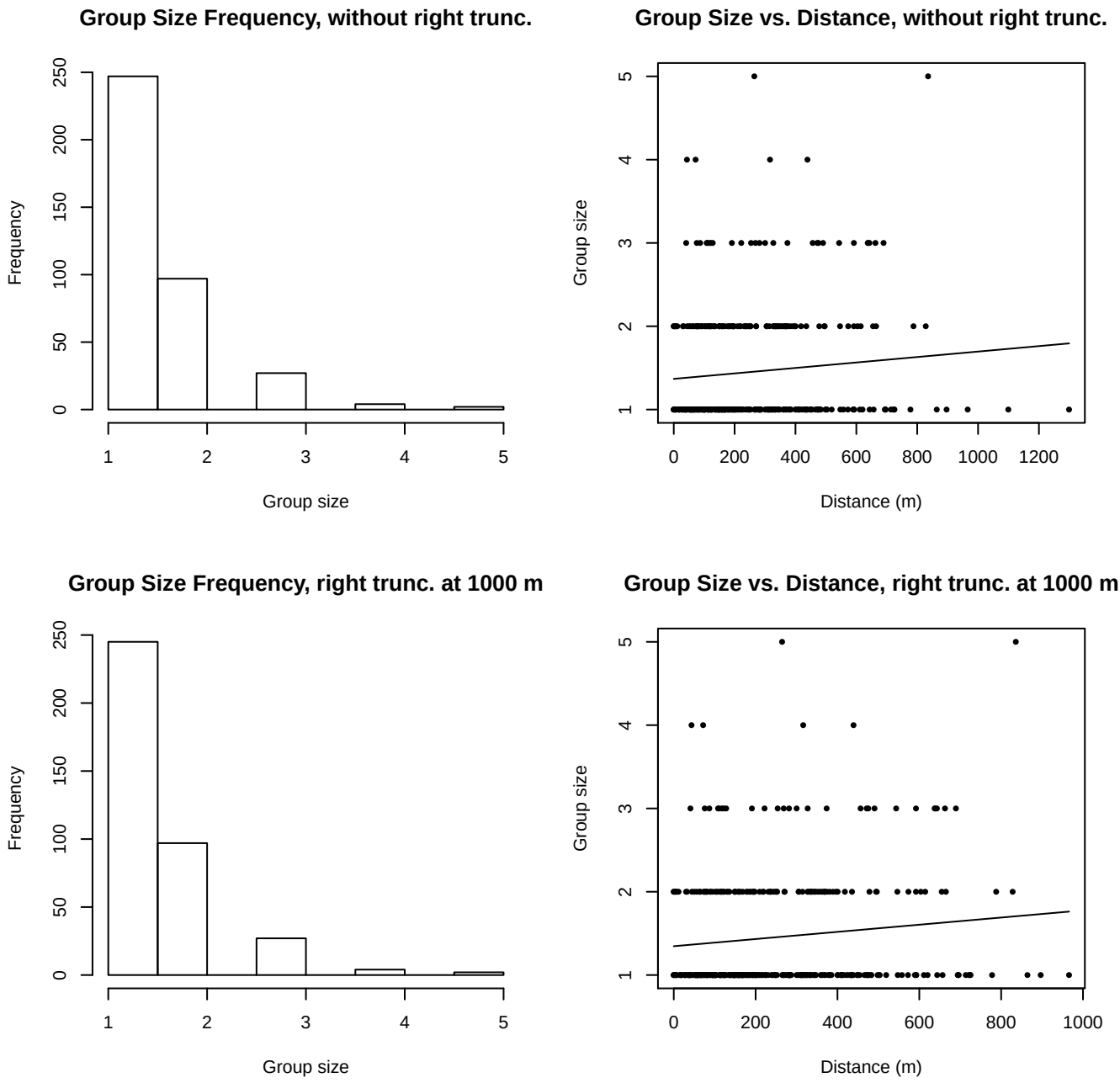

Figure 25: Histograms showing group size frequency and scatterplots showing the relationship between group size and perpendicular sighting distance, for all sightings (top row) and only those not right truncated (bottom row). In the scatterplot, the line is a simple linear regression.

Aerial Surveys

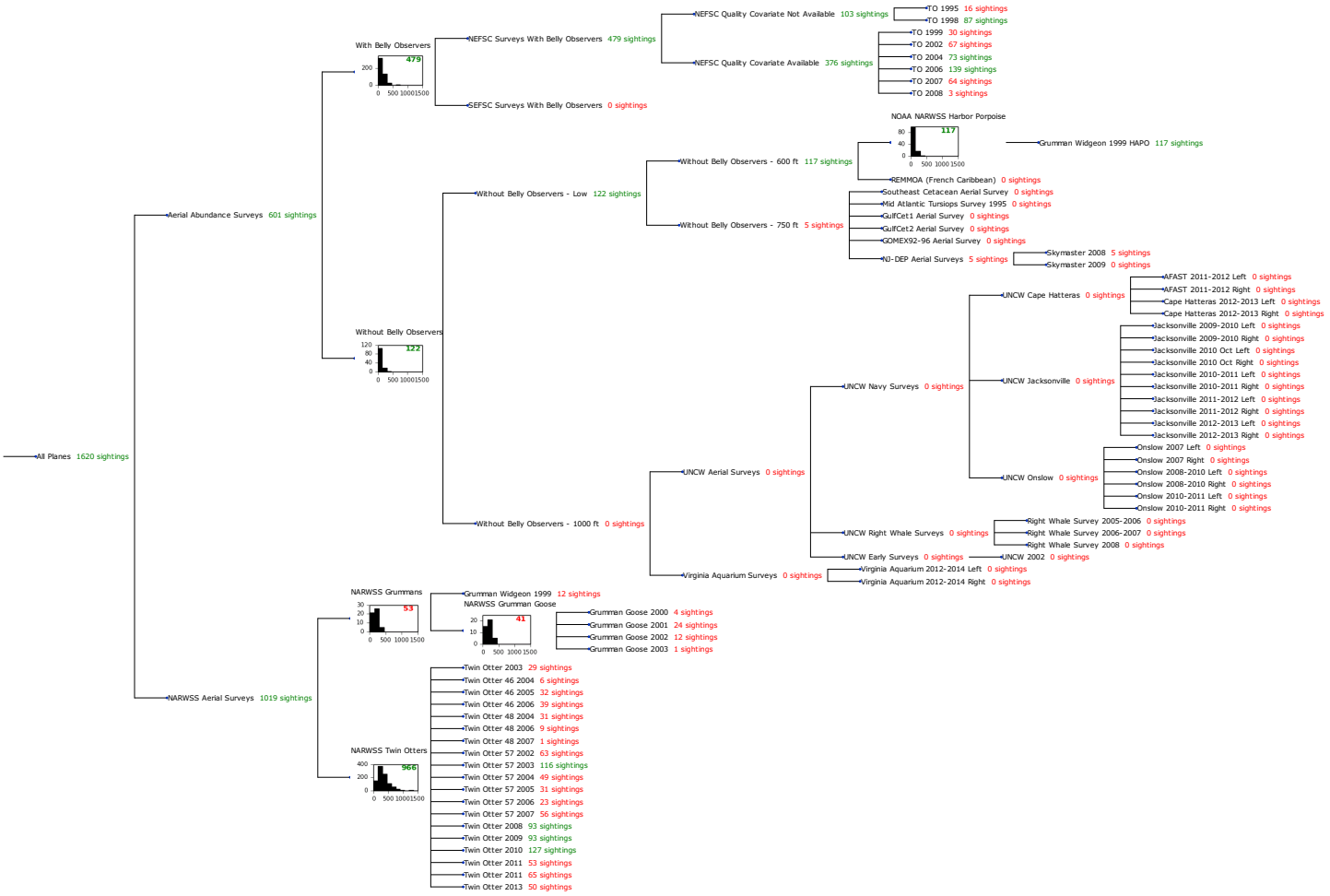

Figure 26: Detection hierarchy for aerial surveys

With Belly Observers

The sightings were right truncated at 500m.

Covariate	Description
beaufort	Beaufort sea state.
size	Estimated size (number of individuals) of the sighted group.

Table 13: Covariates tested in candidate "multi-covariate distance sampling" (MCDS) detection functions.

Key	Adjustment	Order	Covariates	Succeeded	Δ AIC	Mean ESHW (m)
hn			size	Yes	0.00	197
hn				Yes	3.33	197
hn	cos	2		Yes	3.67	186
hn	cos	3		Yes	4.93	190

hn	herm	4		Yes	5.23	196
hr			size	Yes	7.23	217
hr	poly	2		Yes	7.28	199
hr	poly	4		Yes	8.97	205
hr				Yes	14.16	219
hn			beaufort	No		
hr			beaufort	No		
hn			beaufort, size	No		
hr			beaufort, size	No		

Table 14: Candidate detection functions for With Belly Observers. The first one listed was selected for the density model.

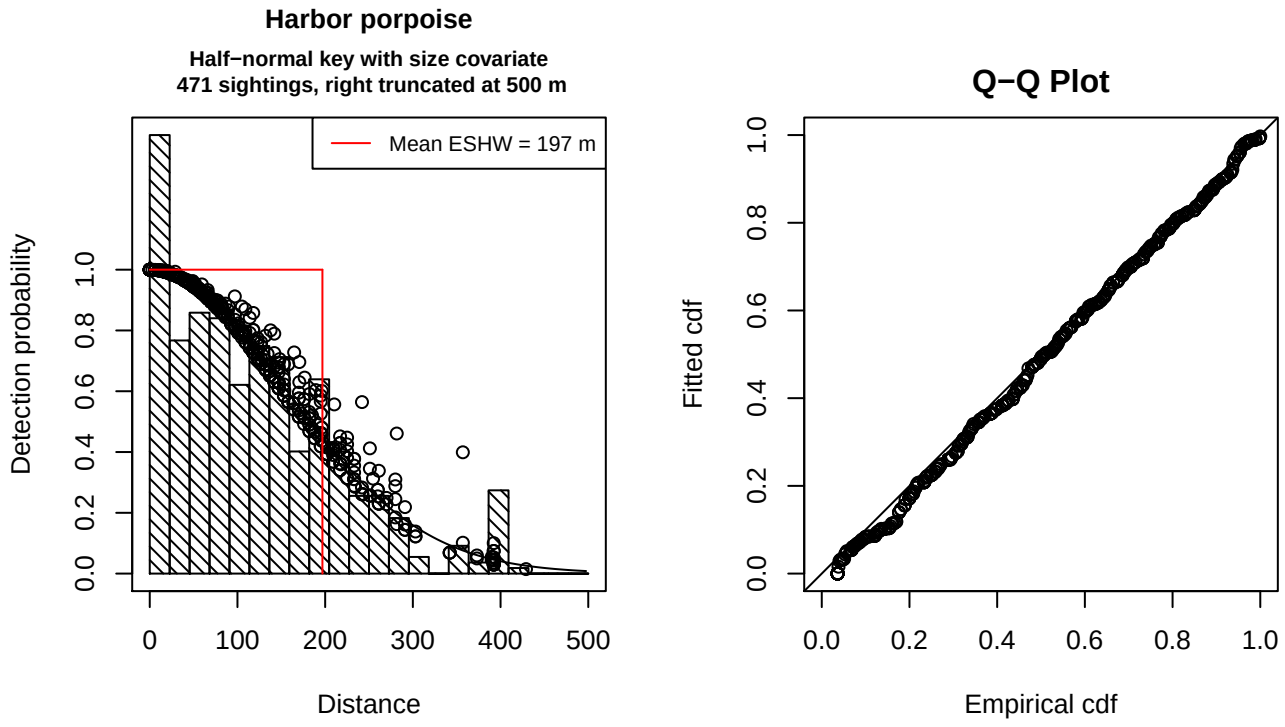

Figure 27: Detection function for With Belly Observers that was selected for the density model

Statistical output for this detection function:

```
Summary for ds object
Number of observations :  471
Distance range         :  0  -  500
AIC                    :  5438.119

Detection function:
 Half-normal key function

Detection function parameters
Scale Coefficients:
```

```
             estimate         se
(Intercept) 4.96562279 0.05129946
size        0.03040771 0.01600221

                         Estimate          SE         CV
Average p                0.3910381  0.01258862 0.03219282
N in covered region 1204.4860743 58.20425322 0.04832289
```

Additional diagnostic plots:

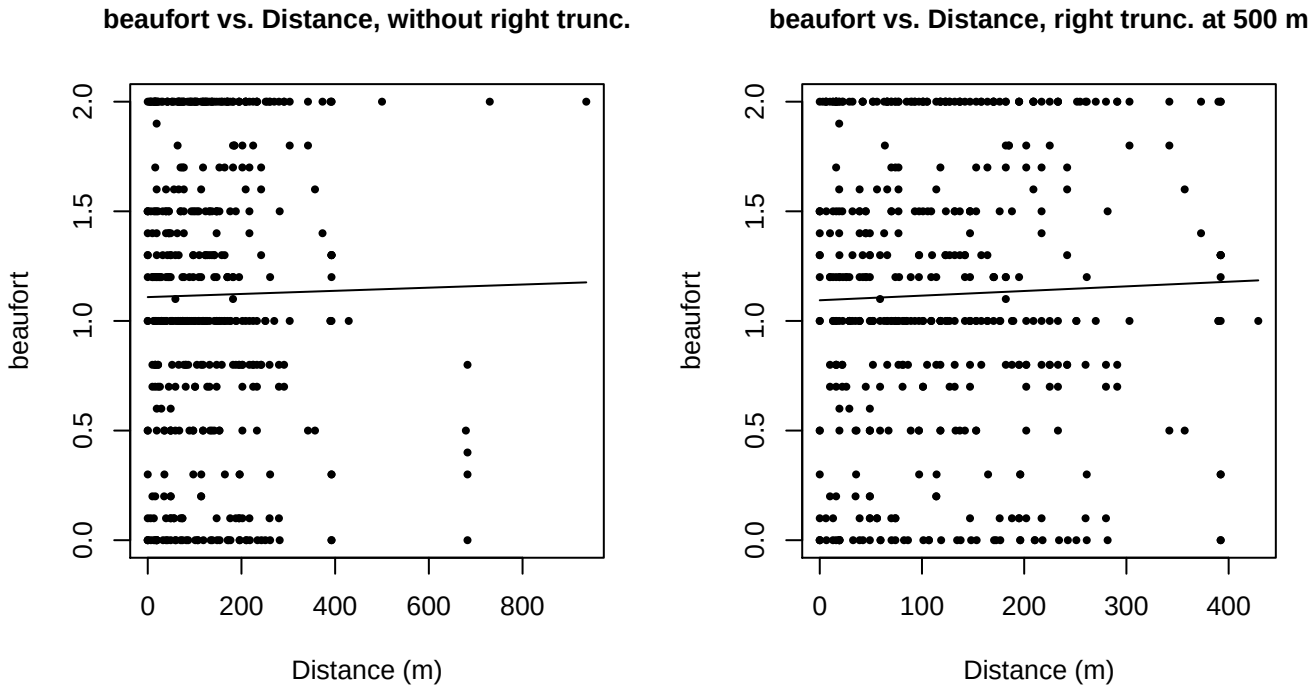

Figure 28: Scatterplots showing the relationship between Beaufort sea state and perpendicular sighting distance, for all sightings (left) and only those not right truncated (right). The line is a simple linear regression.

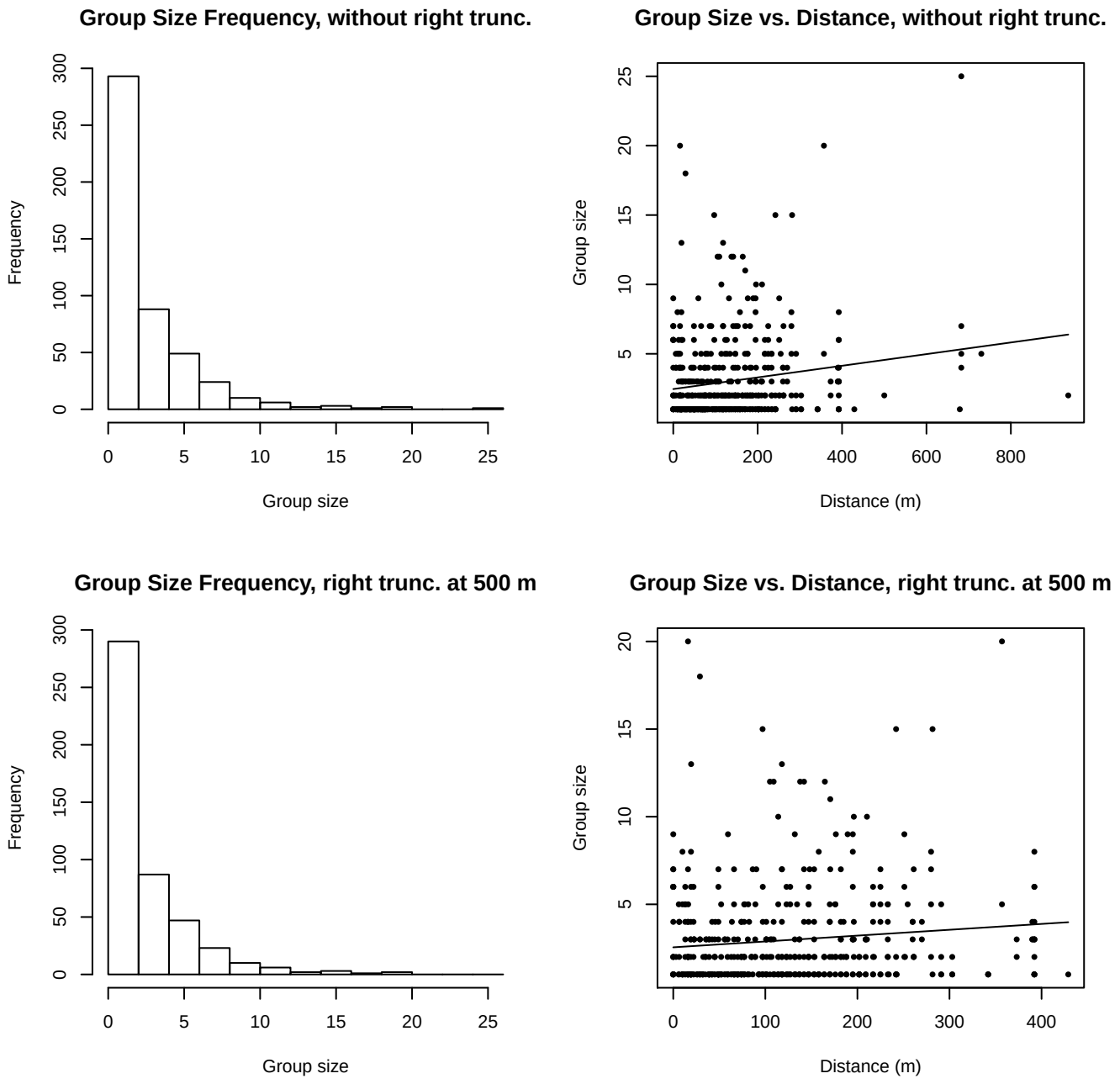

Figure 29: Histograms showing group size frequency and scatterplots showing the relationship between group size and perpendicular sighting distance, for all sightings (top row) and only those not right truncated (bottom row). In the scatterplot, the line is a simple linear regression.

Without Belly Observers

The sightings were right truncated at 400m. Due to a reduced frequency of sightings close to the trackline that plausibly resulted from the behavior of the observers and/or the configuration of the survey platform, the sightings were left truncted as well. Sightings closer than 32 m to the trackline were omitted from the analysis, and it was assumed that the the area closer to the trackline than this was not surveyed. This distance was estimated by inspecting histograms of perpendicular sighting distances.

Covariate	Description

beaufort	Beaufort sea state.
size	Estimated size (number of individuals) of the sighted group.

Table 15: Covariates tested in candidate "multi-covariate distance sampling" (MCDS) detection functions.

Key	Adjustment	Order	Covariates	Succeeded	Δ AIC	Mean ESHW (m)
hn				Yes	0.00	101
hn	cos	3		Yes	0.28	120
hn			beaufort	Yes	1.27	101
hn	cos	2		Yes	1.82	109
hn	herm	4		Yes	1.98	101
hn			beaufort, size	Yes	3.27	101
hn			size	No		

Table 16: Candidate detection functions for Without Belly Observers. The first one listed was selected for the density model.

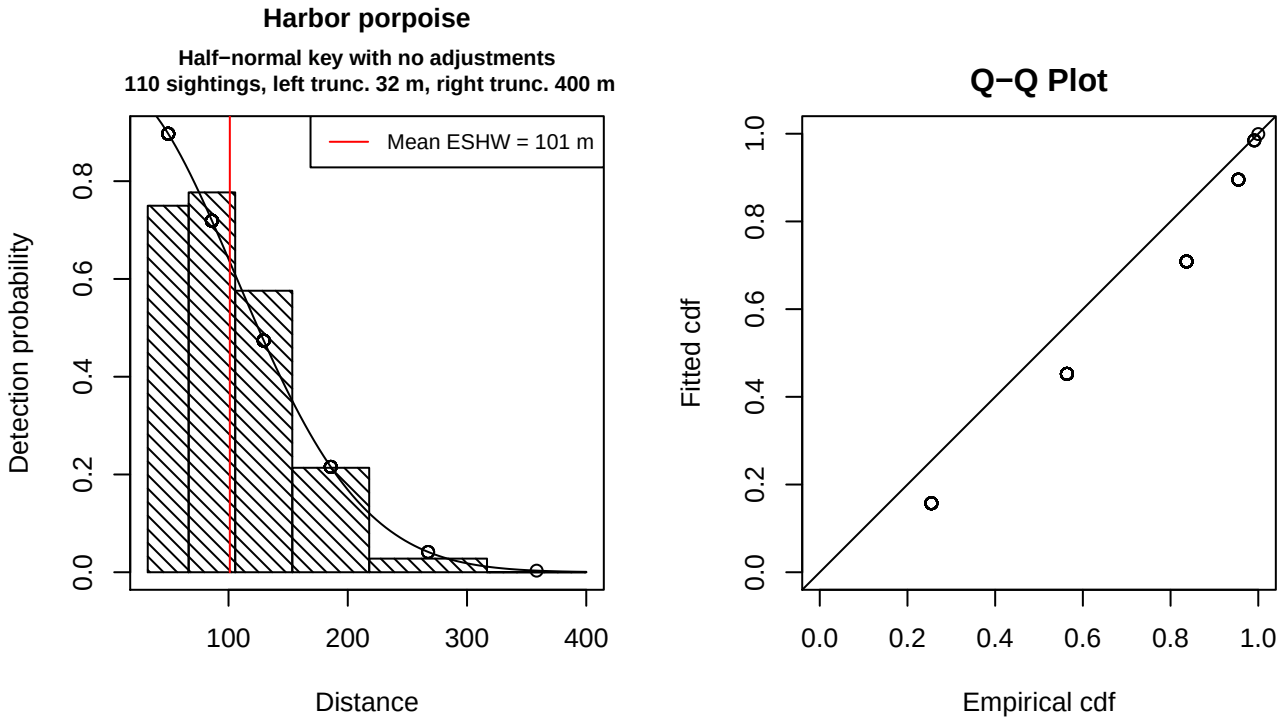

Figure 30: Detection function for Without Belly Observers that was selected for the density model

Statistical output for this detection function:

```
Summary for ds object
```

```
Number of observations :  110
Distance range         :  32.24668  -  400
AIC                    :  331.7133

Detection function:
 Half-normal key function

Detection function parameters
Scale Coefficients:
            estimate         se
(Intercept) 4.663474 0.06458825

                        Estimate          SE         CV
Average p             0.2526959  0.02124061 0.08405601
N in covered region 435.3059041 51.24622298 0.11772462
```

Additional diagnostic plots:

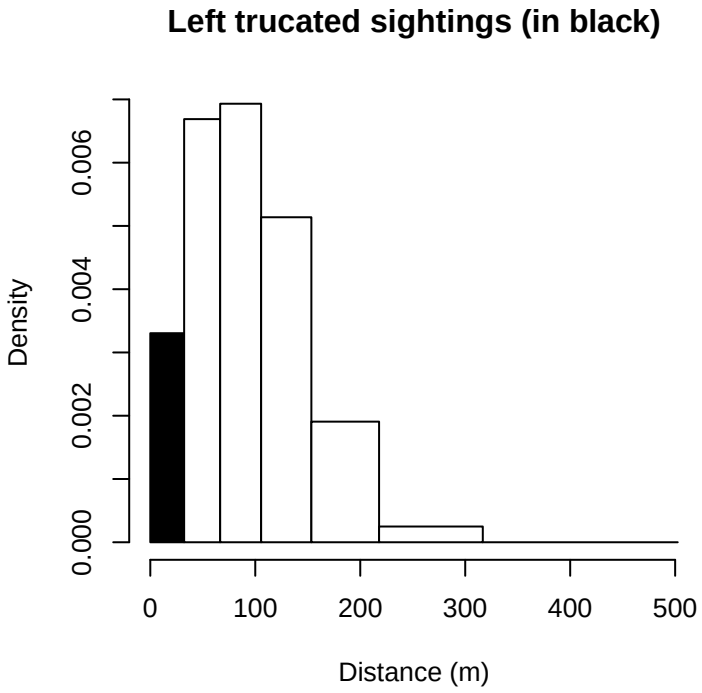

Figure 31: Density of sightings by perpendicular distance for Without Belly Observers. Black bars on the left show sightings that were left truncated.

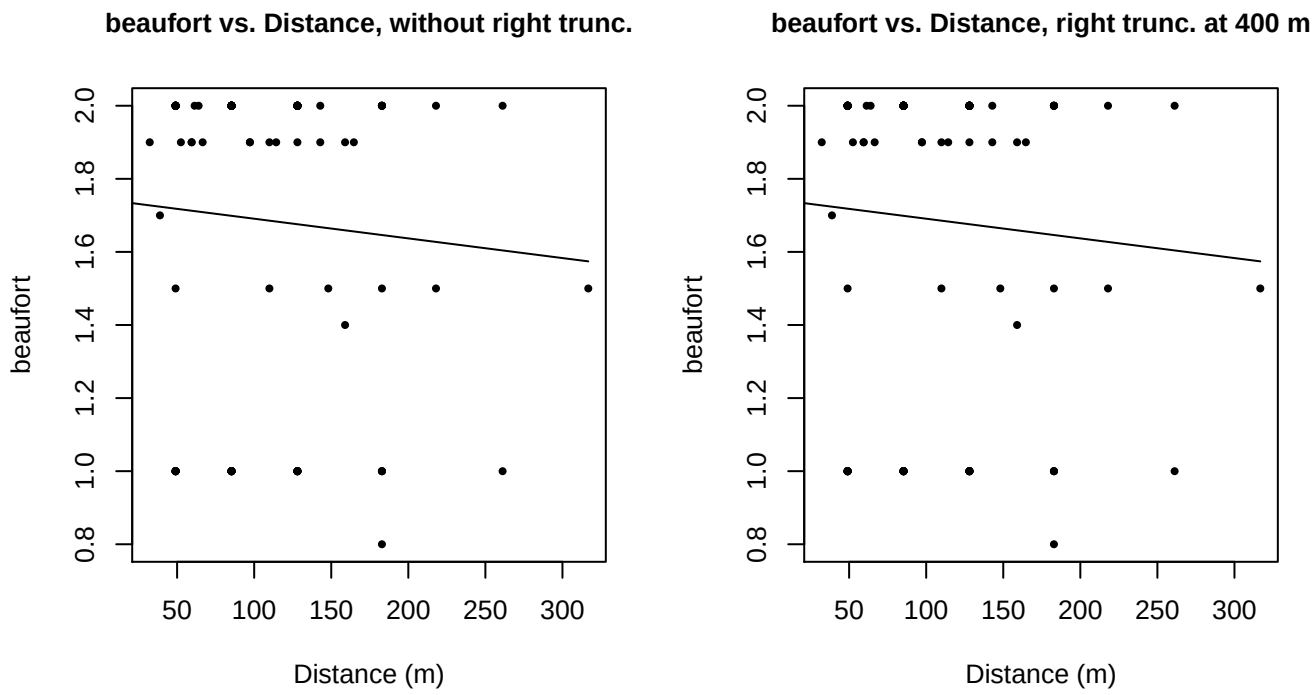

Figure 32: Scatterplots showing the relationship between Beaufort sea state and perpendicular sighting distance, for all sightings (left) and only those not right truncated (right). The line is a simple linear regression.

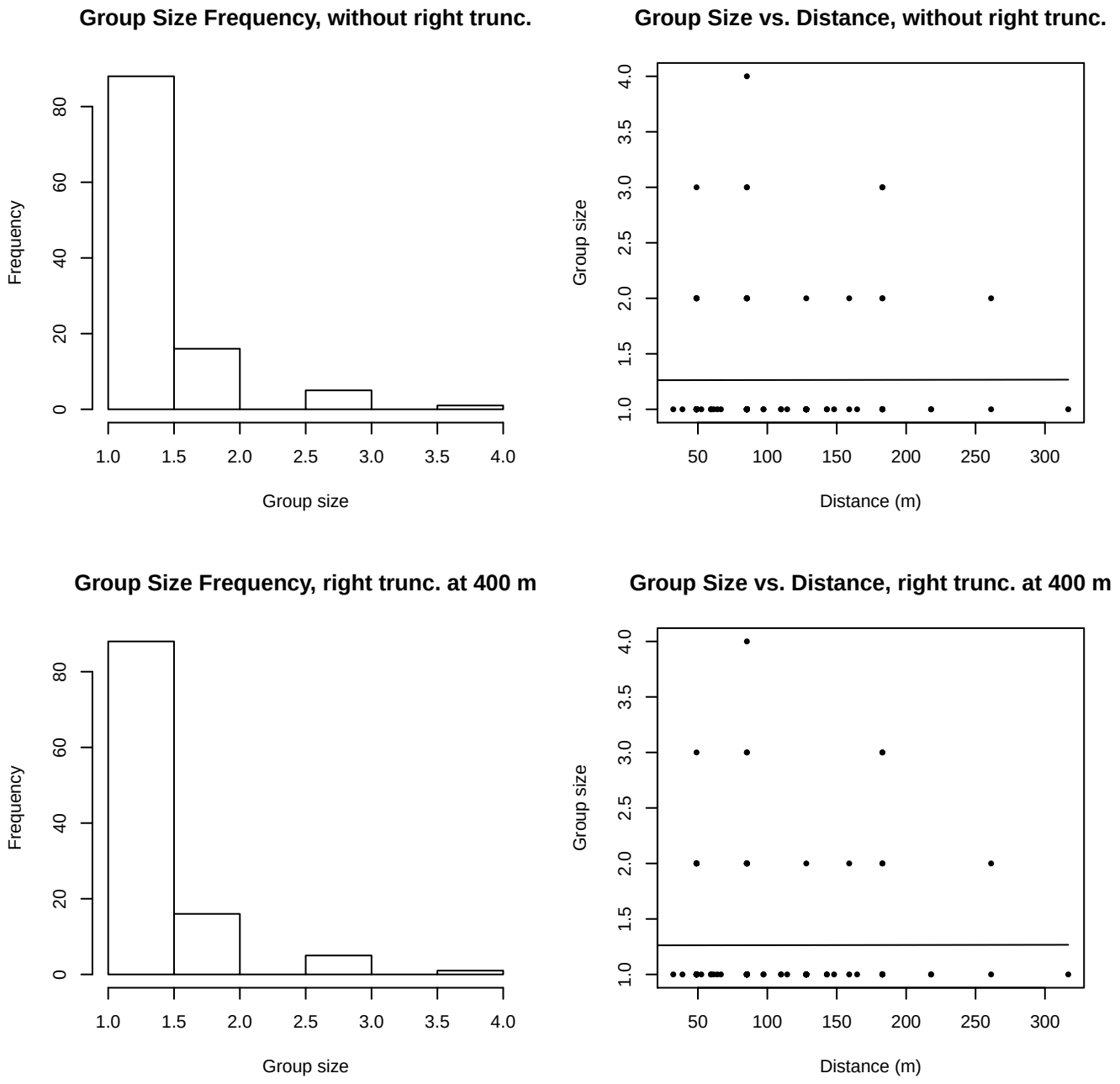

Figure 33: Histograms showing group size frequency and scatterplots showing the relationship between group size and perpendicular sighting distance, for all sightings (top row) and only those not right truncated (bottom row). In the scatterplot, the line is a simple linear regression.

NOAA NARWSS Harbor Porpoise

The sightings were right truncated at 400m. Due to a reduced frequency of sightings close to the trackline that plausibly resulted from the behavior of the observers and/or the configuration of the survey platform, the sightings were left truncted as well. Sightings closer than 32 m to the trackline were omitted from the analysis, and it was assumed that the the area closer to the trackline than this was not surveyed. This distance was estimated by inspecting histograms of perpendicular sighting distances. The vertical sighting angles were heaped at 10 degree increments up to 80 degrees and 1 degree increments thereafter, so the candidate detection functions were fitted using linear bins scaled accordingly.

Covariate	Description

beaufort	Beaufort sea state.
size	Estimated size (number of individuals) of the sighted group.

Table 17: Covariates tested in candidate "multi-covariate distance sampling" (MCDS) detection functions.

Key	Adjustment	Order	Covariates	Succeeded	Δ AIC	Mean ESHW (m)
hn	cos	3		Yes	0.00	121
hn				Yes	0.04	102
hn			beaufort	Yes	1.49	102
hn	cos	2		Yes	1.64	115
hn	herm	4		Yes	1.88	118
hn			size	No		
hn			beaufort, size	No		

Table 18: Candidate detection functions for NOAA NARWSS Harbor Porpoise. The first one listed was selected for the density model.

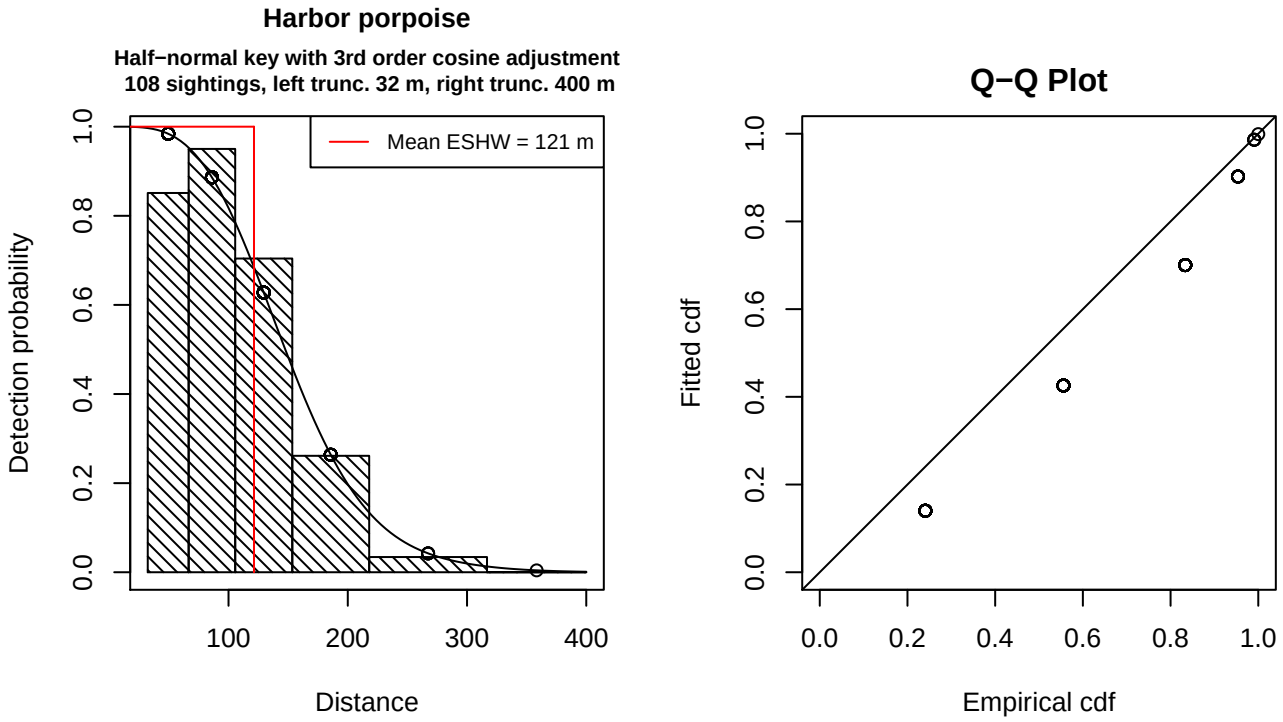

Figure 34: Detection function for NOAA NARWSS Harbor Porpoise that was selected for the density model

Statistical output for this detection function:

```
Summary for ds object
```

```
Number of observations :  108
Distance range         :  32.24668  -  400
AIC                    :  326.8852

Detection function:
 Half-normal key function with cosine adjustment term of order 3

Detection function parameters
Scale Coefficients:
            estimate        se
(Intercept) 4.666472 0.0653825

Adjustment term parameter(s):
               estimate        se
cos, order 3 -0.1376044 0.1899187


Monotonicity constraints were enforced.
                        Estimate           SE        CV
Average p              0.3033478   0.08308258 0.2738856
N in covered region 356.0269813 101.61672985 0.2854186

Monotonicity constraints were enforced.
```

Additional diagnostic plots:

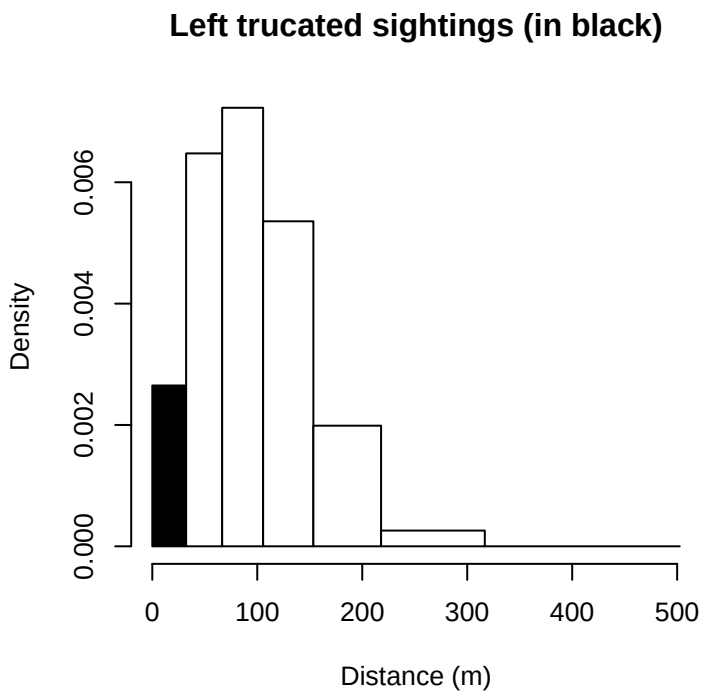

Figure 35: Density of sightings by perpendicular distance for NOAA NARWSS Harbor Porpoise. Black bars on the left show sightings that were left truncated.

Figure 36: Scatterplots showing the relationship between Beaufort sea state and perpendicular sighting distance, for all sightings (left) and only those not right truncated (right). The line is a simple linear regression.

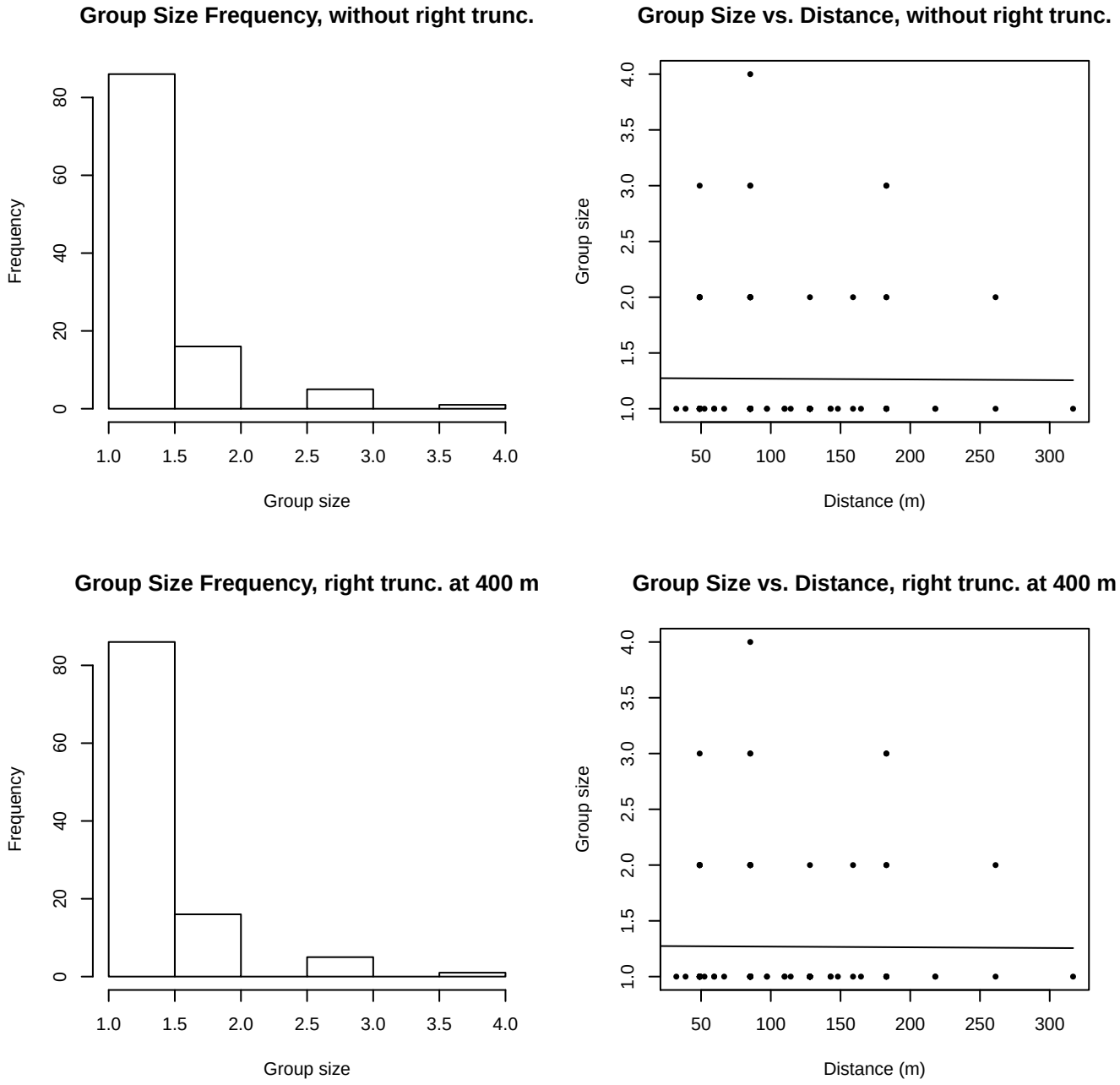

Figure 37: Histograms showing group size frequency and scatterplots showing the relationship between group size and perpendicular sighting distance, for all sightings (top row) and only those not right truncated (bottom row). In the scatterplot, the line is a simple linear regression.

NARWSS Grummans

The sightings were right truncated at 500m. Due to a reduced frequency of sightings close to the trackline that plausibly resulted from the behavior of the observers and/or the configuration of the survey platform, the sightings were left truncted as well. Sightings closer than 107 m to the trackline were omitted from the analysis, and it was assumed that the the area closer to the trackline than this was not surveyed. This distance was estimated by inspecting histograms of perpendicular sighting distances.

Covariate	Description

beaufort	Beaufort sea state.
quality	Survey-specific index of the quality of observation conditions, utilizing relevant factors other than Beaufort sea state (see methods).
size	Estimated size (number of individuals) of the sighted group.

Table 19: Covariates tested in candidate "multi-covariate distance sampling" (MCDS) detection functions.

Key	Adjustment	Order	Covariates	Succeeded	Δ AIC	Mean ESHW (m)
hn				Yes	0.00	108
hn			quality	Yes	1.34	108
hn			beaufort	Yes	1.55	108
hn	herm	4		Yes	1.91	122
hn			beaufort, quality	Yes	2.90	108
hn	cos	2		No		
hn	cos	3		No		
hn			size	No		
hn			beaufort, size	No		
hn			quality, size	No		
hn			beaufort, quality, size	No		

Table 20: Candidate detection functions for NARWSS Grummans. The first one listed was selected for the density model.

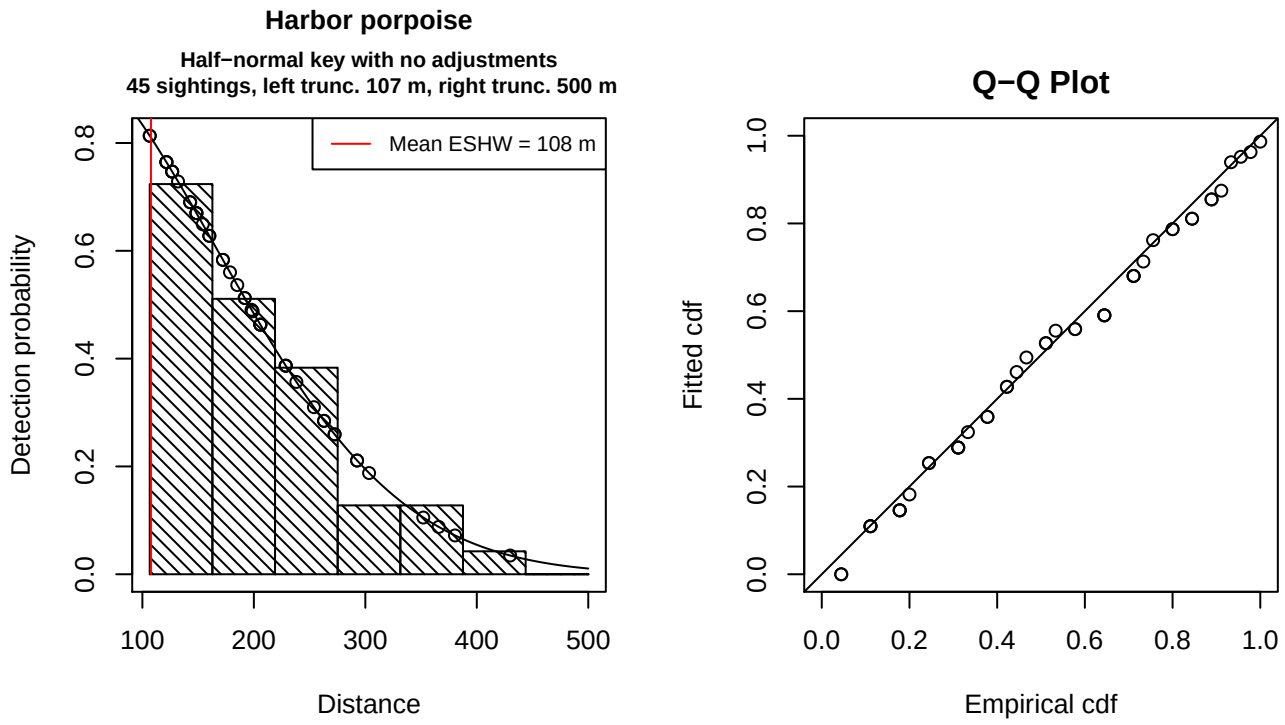

Figure 38: Detection function for NARWSS Grummans that was selected for the density model

Statistical output for this detection function:

```
Summary for ds object
Number of observations :  45
Distance range         :  106.5979  -  500
AIC                    :  502.1328

Detection function:
 Half-normal key function

Detection function parameters
Scale Coefficients:
            estimate        se
(Intercept) 5.111267 0.1075434

                     Estimate          SE        CV
Average p            0.215341  0.04066558 0.1888428
N in covered region 208.970932 48.15338558 0.2304310
```

Additional diagnostic plots:

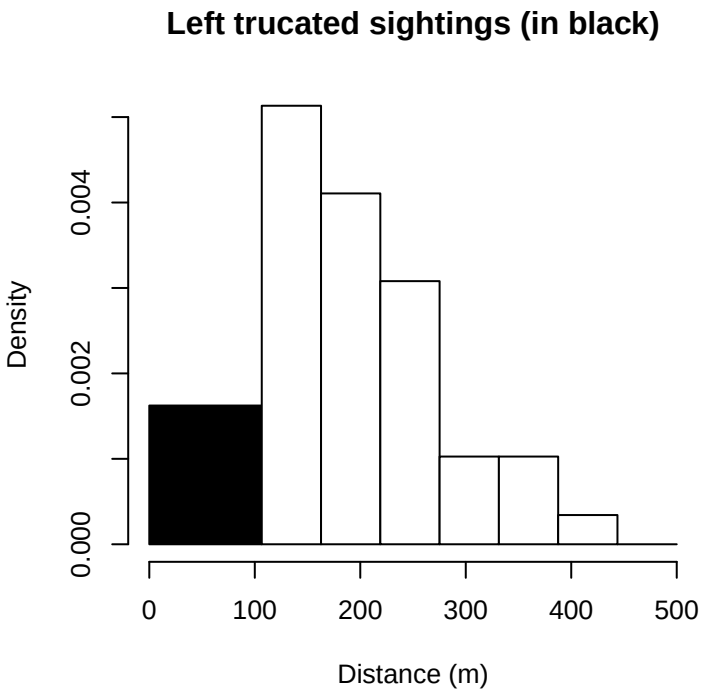

Figure 39: Density of sightings by perpendicular distance for NARWSS Grummans. Black bars on the left show sightings that were left truncated.

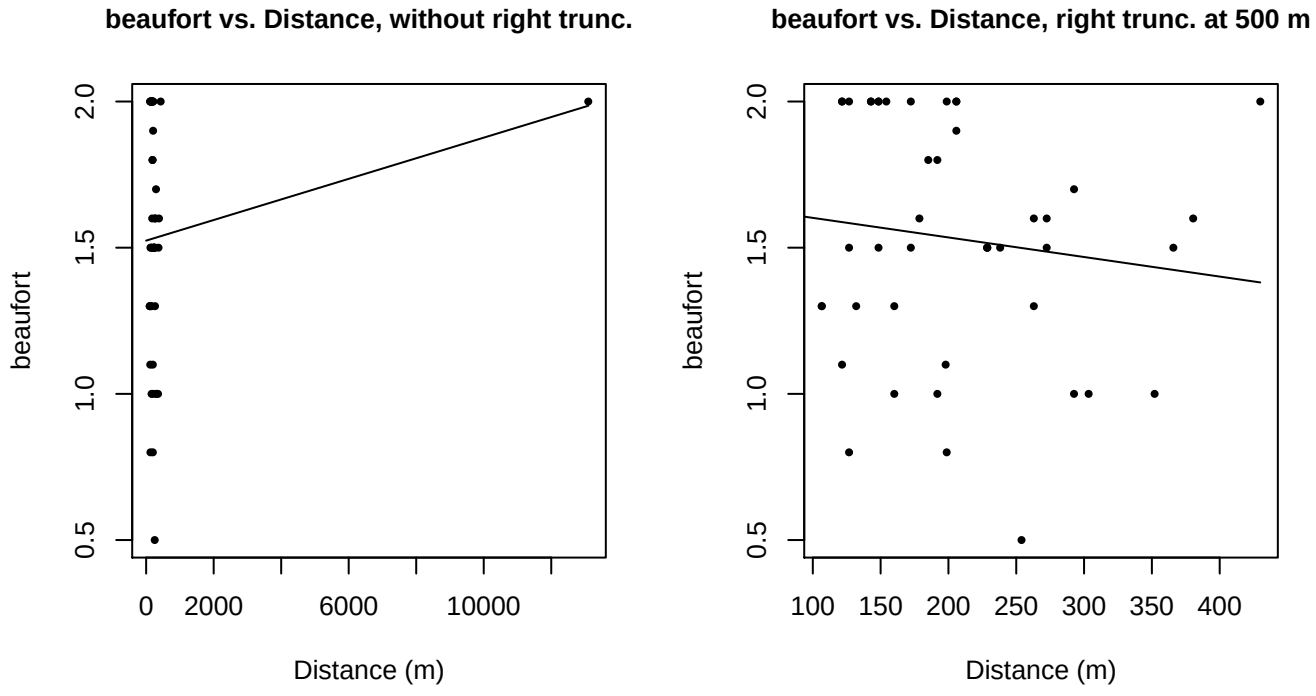

Figure 40: Scatterplots showing the relationship between Beaufort sea state and perpendicular sighting distance, for all sightings (left) and only those not right truncated (right). The line is a simple linear regression.

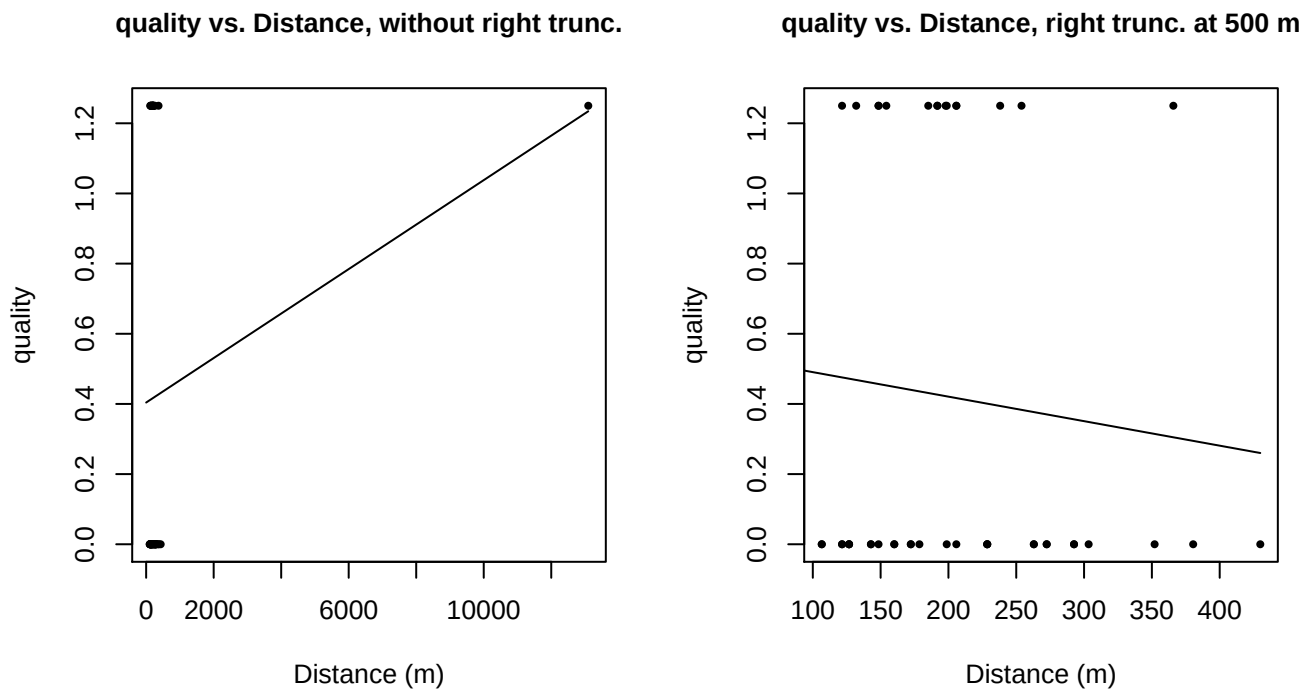

Figure 41: Scatterplots showing the relationship between the survey-specific index of the quality of observation conditions and perpendicular sighting distance, for all sightings (left) and only those not right truncated (right). Low values of the quality index correspond to better observation conditions. The line is a simple linear regression.

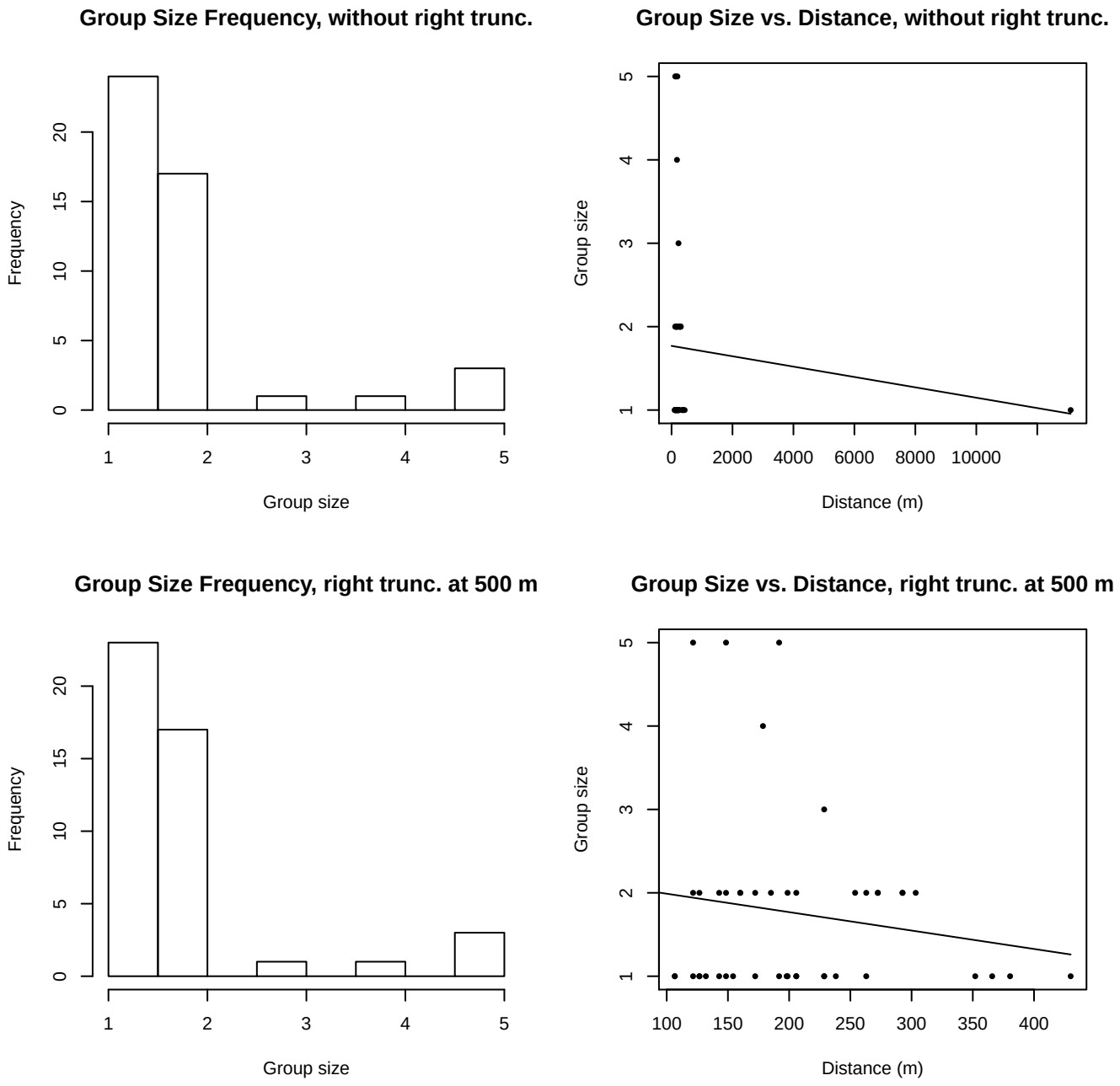

Figure 42: Histograms showing group size frequency and scatterplots showing the relationship between group size and perpendicular sighting distance, for all sightings (top row) and only those not right truncated (bottom row). In the scatterplot, the line is a simple linear regression.

NARWSS Grumman Goose

The sightings were right truncated at 500m. Due to a reduced frequency of sightings close to the trackline that plausibly resulted from the behavior of the observers and/or the configuration of the survey platform, the sightings were left truncted as well. Sightings closer than 107 m to the trackline were omitted from the analysis, and it was assumed that the the area closer to the trackline than this was not surveyed. This distance was estimated by inspecting histograms of perpendicular sighting distances.

Covariate	Description

beaufort	Beaufort sea state.
quality	Survey-specific index of the quality of observation conditions, utilizing relevant factors other than Beaufort sea state (see methods).
size	Estimated size (number of individuals) of the sighted group.

Table 21: Covariates tested in candidate "multi-covariate distance sampling" (MCDS) detection functions.

Key	Adjustment	Order	Covariates	Succeeded	Δ AIC	Mean ESHW (m)
hn				Yes	0.00	112
hn			quality	Yes	1.71	112
hn	herm	4		Yes	1.89	124
hn			beaufort	Yes	1.97	112
hn			beaufort, quality	Yes	3.68	113
hn	cos	2		No		
hn	cos	3		No		
hn			size	No		
hn			beaufort, size	No		
hn			quality, size	No		
hn			beaufort, quality, size	No		

Table 22: Candidate detection functions for NARWSS Grumman Goose. The first one listed was selected for the density model.

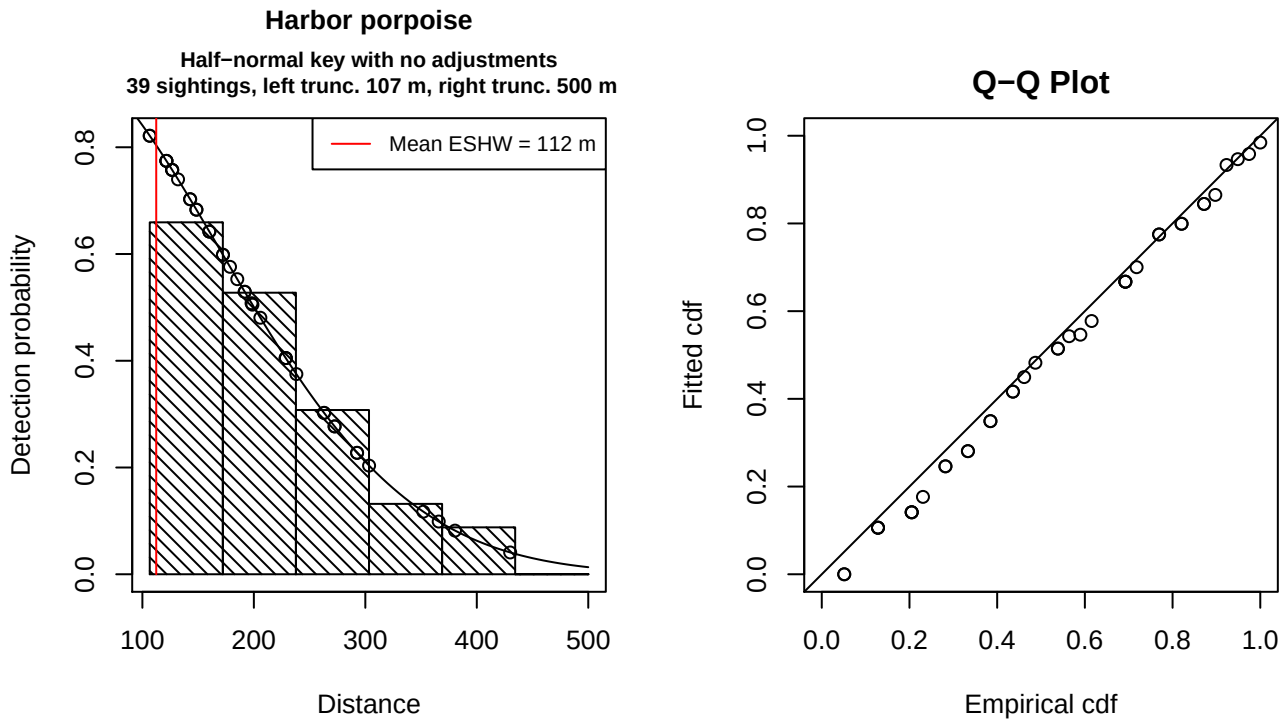

Figure 43: Detection function for NARWSS Grumman Goose that was selected for the density model

Statistical output for this detection function:

```
Summary for ds object
Number of observations :  39
Distance range         :  106.5979  -  500
AIC                    :  437.4127

Detection function:
 Half-normal key function

Detection function parameters
Scale Coefficients:
            estimate        se
(Intercept) 5.136039 0.1145746

                       Estimate         SE        CV
Average p             0.2248147  0.0443096 0.1970939
N in covered region 173.4762322 42.0380408 0.2423274
```

Additional diagnostic plots:

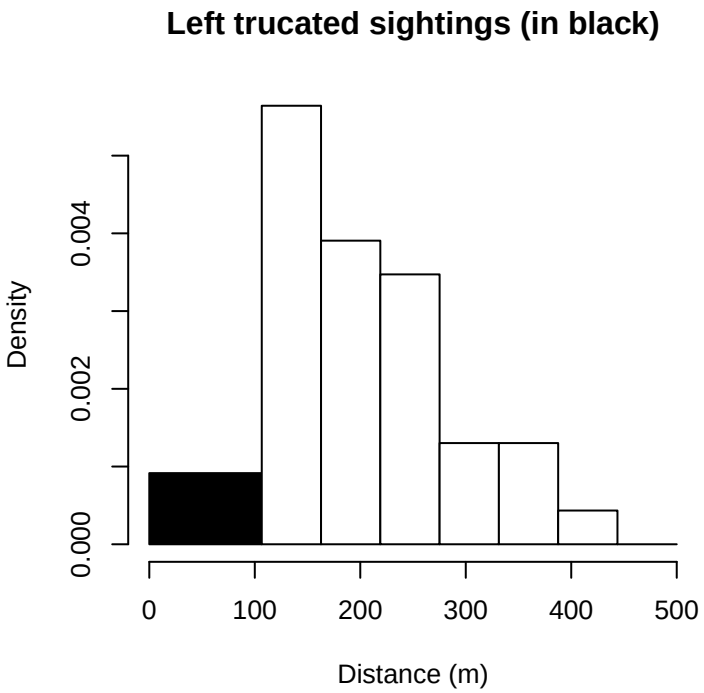

Figure 44: Density of sightings by perpendicular distance for NARWSS Grumman Goose. Black bars on the left show sightings that were left truncated.

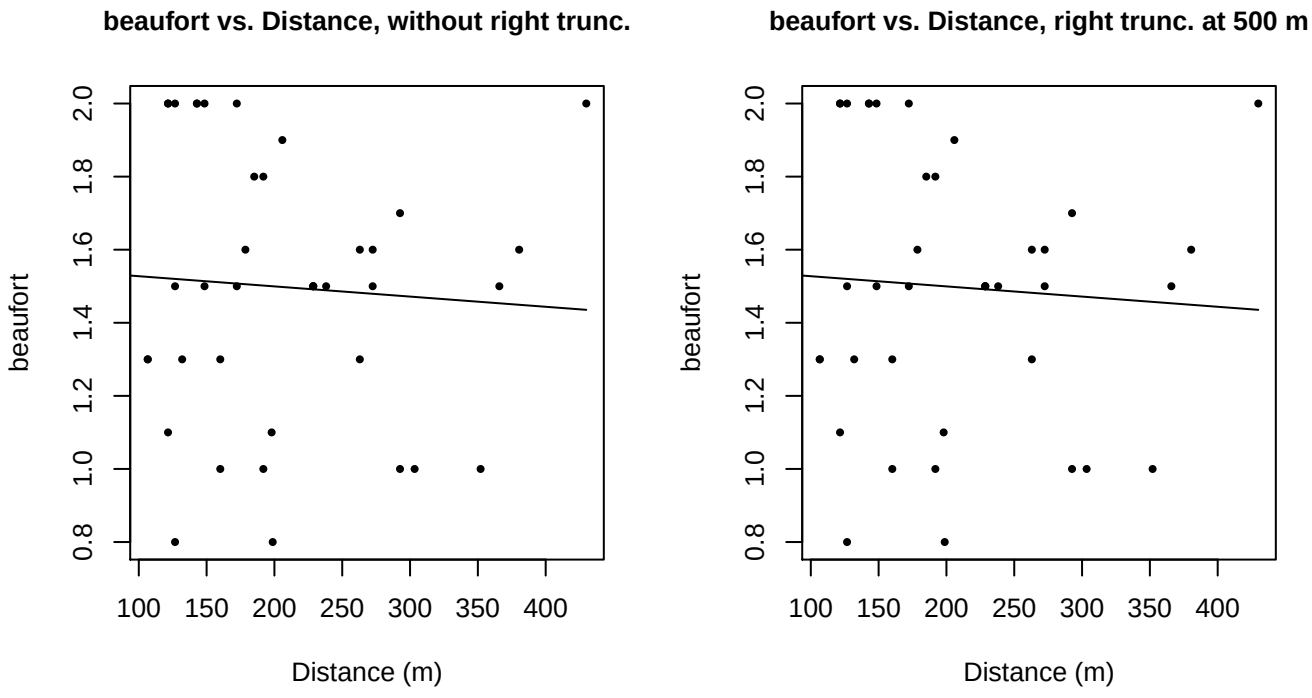

Figure 45: Scatterplots showing the relationship between Beaufort sea state and perpendicular sighting distance, for all sightings (left) and only those not right truncated (right). The line is a simple linear regression.

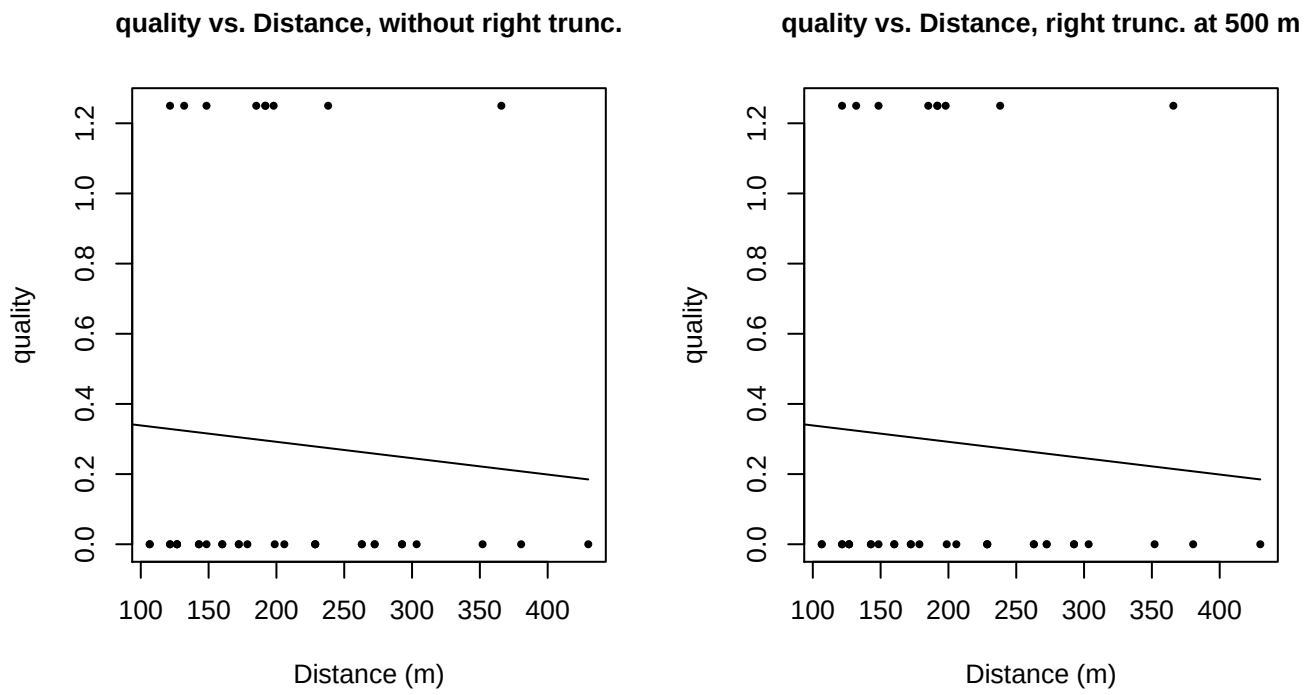

Figure 46: Scatterplots showing the relationship between the survey-specific index of the quality of observation conditions and perpendicular sighting distance, for all sightings (left) and only those not right truncated (right). Low values of the quality index correspond to better observation conditions. The line is a simple linear regression.

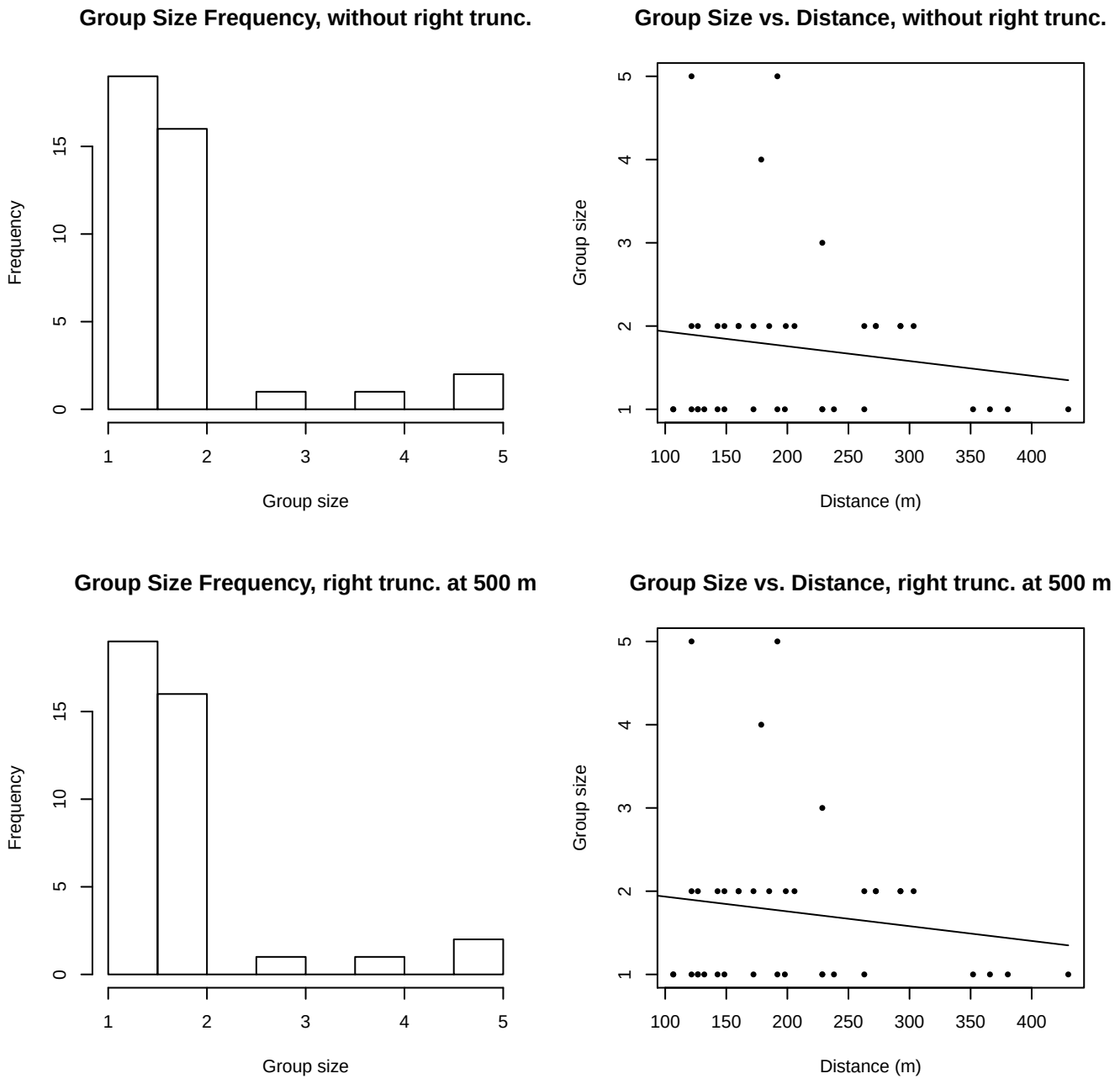

Figure 47: Histograms showing group size frequency and scatterplots showing the relationship between group size and perpendicular sighting distance, for all sightings (top row) and only those not right truncated (bottom row). In the scatterplot, the line is a simple linear regression.

NARWSS Twin Otters

The sightings were right truncated at 1366m. Due to a reduced frequency of sightings close to the trackline that plausibly resulted from the behavior of the observers and/or the configuration of the survey platform, the sightings were left truncted as well. Sightings closer than 160 m to the trackline were omitted from the analysis, and it was assumed that the the area closer to the trackline than this was not surveyed. This distance was estimated by inspecting histograms of perpendicular sighting distances. The vertical sighting angles were heaped at 10 degree increments up to 80 degrees and 1 degree increments thereafter, so the candidate detection functions were fitted using linear bins scaled accordingly.

Covariate	Description

beaufort	Beaufort sea state.
quality	Survey-specific index of the quality of observation conditions, utilizing relevant factors other than Beaufort sea state (see methods).
size	Estimated size (number of individuals) of the sighted group.

Table 23: Covariates tested in candidate "multi-covariate distance sampling" (MCDS) detection functions.

Key	Adjustment	Order	Covariates	Succeeded	Δ AIC	Mean ESHW (m)
hn			quality	Yes	0.00	268
hn			beaufort, quality	Yes	1.89	268
hn				Yes	4.35	268
hn	cos	2		Yes	5.50	254
hn	cos	3		Yes	5.93	250
hn			beaufort	Yes	6.04	268
hn	herm	4		Yes	6.29	268
hn			size	No		
hn			beaufort, size	No		
hn			quality, size	No		
hn			beaufort, quality, size	No		

Table 24: Candidate detection functions for NARWSS Twin Otters. The first one listed was selected for the density model.

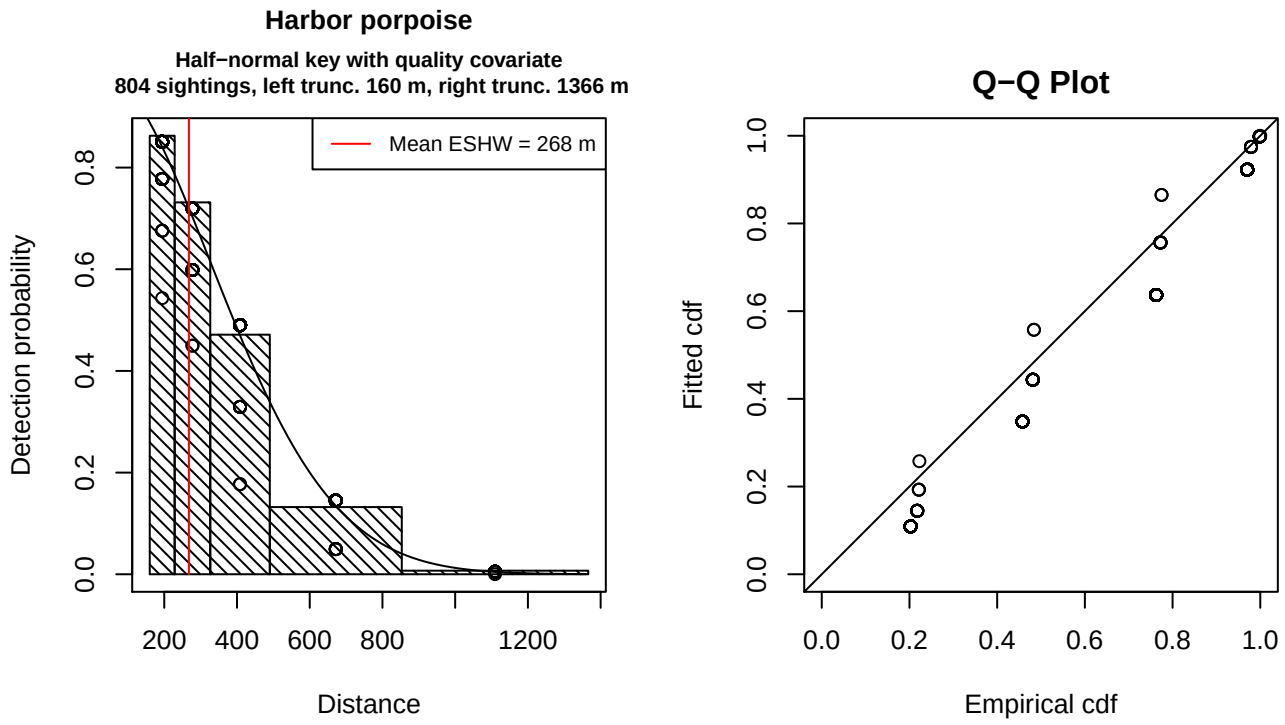

Figure 48: Detection function for NARWSS Twin Otters that was selected for the density model

Statistical output for this detection function:

```
Summary for ds object
Number of observations :  804
Distance range         :  160.0674  -  1366
AIC                    :  2330.374

Detection function:
 Half-normal key function

Detection function parameters
Scale Coefficients:
             estimate         se
(Intercept)  5.8345256 0.02533864
quality     -0.1772014 0.05577278

                        Estimate           SE         CV
Average p               0.1933093 7.267746e-03 0.03759647
N in covered region 4159.1385284 2.046116e+02 0.04919567
```

Additional diagnostic plots:

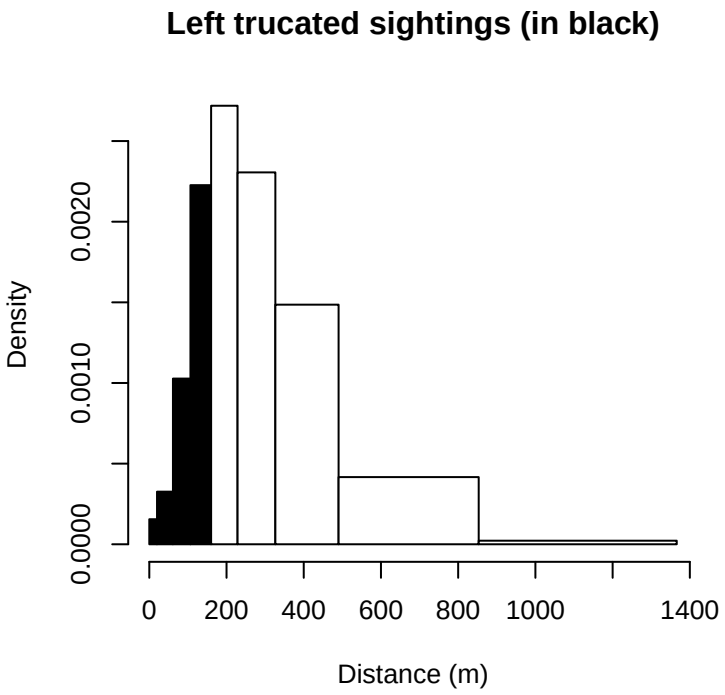

Figure 49: Density of sightings by perpendicular distance for NARWSS Twin Otters. Black bars on the left show sightings that were left truncated.

Figure 50: Scatterplots showing the relationship between Beaufort sea state and perpendicular sighting distance, for all sightings (left) and only those not right truncated (right). The line is a simple linear regression.

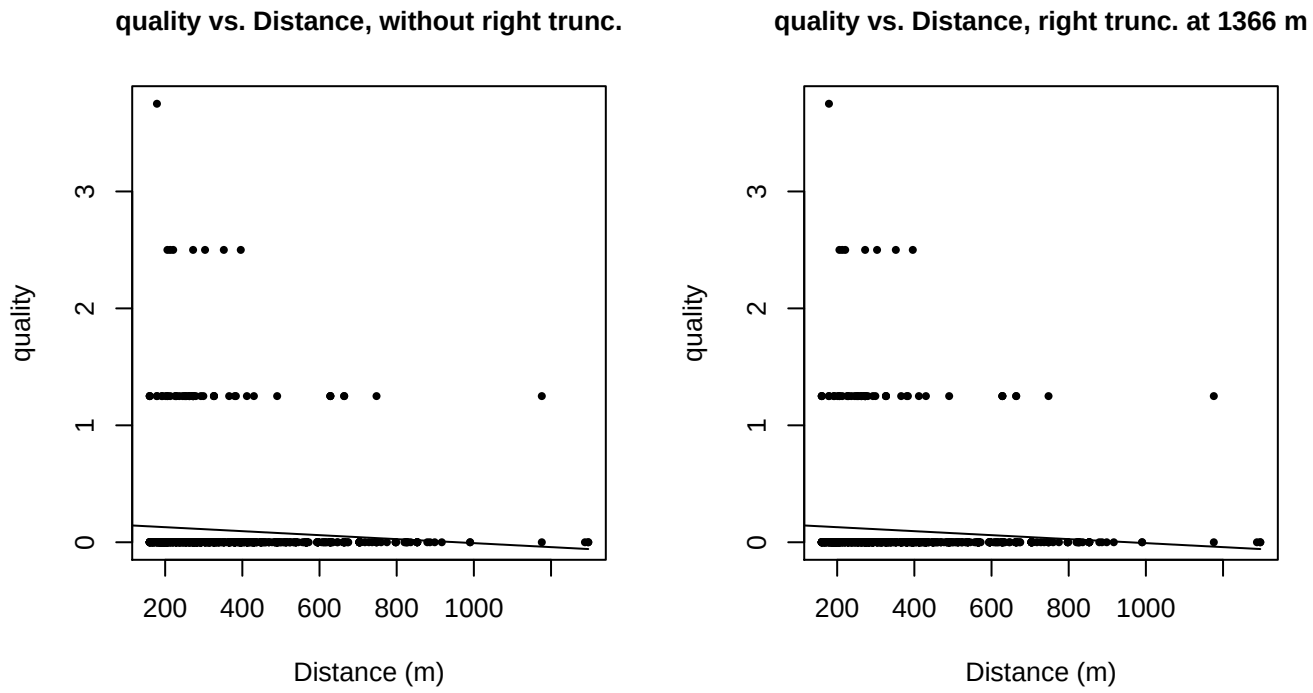

Figure 51: Scatterplots showing the relationship between the survey-specific index of the quality of observation conditions and perpendicular sighting distance, for all sightings (left) and only those not right truncated (right). Low values of the quality index correspond to better observation conditions. The line is a simple linear regression.

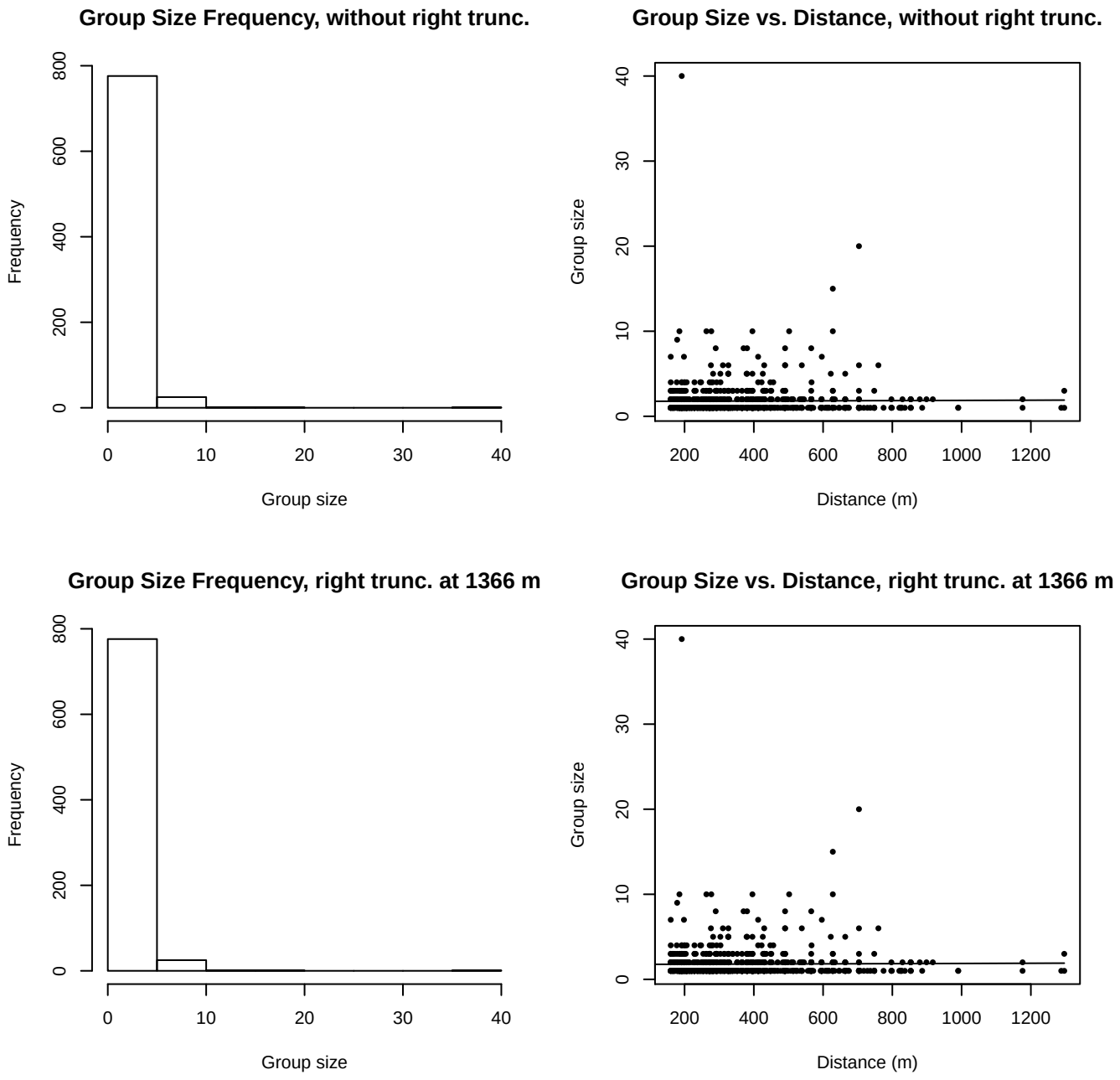

Figure 52: Histograms showing group size frequency and scatterplots showing the relationship between group size and perpendicular sighting distance, for all sightings (top row) and only those not right truncated (bottom row). In the scatterplot, the line is a simple linear regression.

g(0) Estimates

Platform	Surveys	Group Size	*g(0)*	Biases Addressed	Source
Shipboard	All	Any	0.35	Perception	Palka (2006)
Aerial	All	Any	0.36	Both	Palka (2006)

Table 25: Estimates of *g(0)* used in this density model.

Palka (2006) provided a survey-specific g(0) estimate for the 1999 Abel-J naked- eye survey, which reported over 90% of the shipboard sightings of harbor porpoises used in our models. This estimate used a dual-team methodology that accounted for perception bias but not availability bias. We used the estimate for the upper team, which was the primary team and the one for which we had sightings.

We could not find a harbor porpoise g(0) estimate in the literature for shipboard surveys that used bigeye binoculars, so we applied Palka's naked eye estimate to the shipboard surveys that used bigeye binoculars. There were only 36 sightings of harbor porpoises on these surveys, compared to over ten times as many on the naked eye survey, so any error introduced by this decision is likely to have a minor effect on our abundance models.

It has been suggested that harbor porpoises avoid ships (Palka 2000). We did not attempt to detect if this occurred; Palka (2006) did not report avoidance behavior in the 1999 Abel-J survey, nor again in a similar 2011 shipboard survey (Palka 2012) not used in our model here (NOAA did not provide it to us), but did report avoidance/attraction behavior in other species. If harbor porpoises did avoid the ship, it would result in an underestimation of abundance (Buckland et al. 2001).

For aerial surveys, we used Palka's (2006) estimate of g(0) for harbor porpoise, estimated from two years of aerial surveys using the Hiby (1999) circle-back method. This estimate accounted for both availability and perception bias.

Density Models

Harbor porpoises inhabit temperate and subarctic waters, often close to shore or at shallow depths. Analyses of genetic, chemical tracer, and life history data suggest there are four stocks in the North Atlantic: the Gulf of Maine/Bay of Fundy, Gulf of St. Lawrence, Newfoundland, and Greenland populations (Waring et al. 2014). Our study area encompasses much of the reported spatial extent of the the Gulf of Maine/Bay of Fundy stock. The northern part of the study area, along the Scotian Shelf, also partially overlaps with the southernmost extent of the Gulf of St. Lawrence stock. Although genetic data suggest there may be some mixing between these two stocks, they are fairly spatially distinct. Our objective was to model the Gulf of Maine/Bay of Fundy stock; the remainder of this document pertains to that stock, unless explicitly stated otherwise.

Palka et al. (1996) summarized the seasonal distribution of the Gulf of Maine/Bay of Fundy stock as follows. In July, the population migrates into the northern Gulf of Maine and lower Bay of Fundy region and remains there during summer. In September, it begins migrating out to unknown wintering grounds. During fall and spring, September to December and April to June, some harbor porpoises remain in the lower Gulf of Maine, at lower density than the northern summer aggregation. In winter, December through March, some of the population is presumed to be in the offshore mid-Atlantic, from North Carolina to Massachusetts (Palka et al. 1996).

In the surveys used in our study, the most southerly sighting made in the months of November through May was at the southern border of New Jersey. Strandings data support the posited mid-Atlantic winter distribution. In North Carolina, for the period 1997-2008, harbor porpoises tallied the second highest number of strandings of all marine mammals, second only to bottlenose dolphins (Byrd et al. 2014). All of these strandings occurred between January and May, with the peak in March (Hohn et al. 2013; Byrd et al. 2014). For the period 1995-2000, harbor porpoises were regularly caught in the mid-Atlantic coastal gillnet fishery, in numbers estimated from 21-446 per year (Rossman and Merrick 1999; Stenson 2014). Finally, two strandings of harbor porpoises were reported in Florida in 1984 and 1985; this is probably the southernmost extent of the population (Palka et al. 1996).

Based on the seasonal variation in distribution summarized by Palka et al. (1996), and on patterns in sightings we observed in the surveys we utilized, we developed a two-season model for harbor porpoise distribution, with winter spanning November through May and summer spanning June through October.

Harbor porpoises are a relatively difficult cetacean to sight on visual surveys, due to their small size, low group sizes (typically 2-4 animals) and cryptic behavior (Kraus et al. 1983). Rough seas exacerbate this problem (Palka 1996), potentially resulting in an underestimation of abundance. To mitigate against this, we restricted our analysis to survey segments in which the Beaufort sea state was 2 or less, as was done in a number of prior abundance studies of harbor porpoises (Barlow 1988; Hammond et al. 1995; Hammond et al. 2002; Hammond et al. 2013; Hansen and Heide-Jorgensen 2013).

Winter

In this season, the majority of harbor porpoise sightings occurred in the Gulf of Maine and off southern New England. Survey effort was relatively extensive on the continental shelf in this region; all surveys were from the NOAA NARWSS program. A second group of sightings occurred near coastal New Jersey, all reported by the NJ-DEP survey program, which extended only as far as 37 km from the shoreline. The majority of these sightings were reported in March.

No sightings were reported south of New Jersey, despite heavy survey coverage on the shelf in areas that harbor porpoises might be expected to inhabit. For example, no sightings were reported in coastal North Carolina, one of the heaviest surveyed regions in winter (Figure 53) and an area in which harbor porpoises are known to strand (Hohn et al. 2013; Byrd et al. 2014). No sightings were reported off the shelf in the mid-Atlantic region, although survey effort was very sparse except at three U.S. Navy operations areas that straddled the shelf break.

Given the lack of knowledge about the wintertime distribution of harbor porpoises and the suggestion that they may be in the offshore mid-Atlantic region (Palka et al. 1996), we constrained our model to a polygon, concave at a broad scale, that enclosed the survey tracklines. (This polygon was drawn prior to removing segments for which Beaufort sea state exceeded 2; many off-shelf segments were removed, resulting in very sparse off-shelf coverage.) The results should be viewed with caution, particularly on the shelf near New York and between central Virginia and 40 N, for which we had little survey effort during this season.

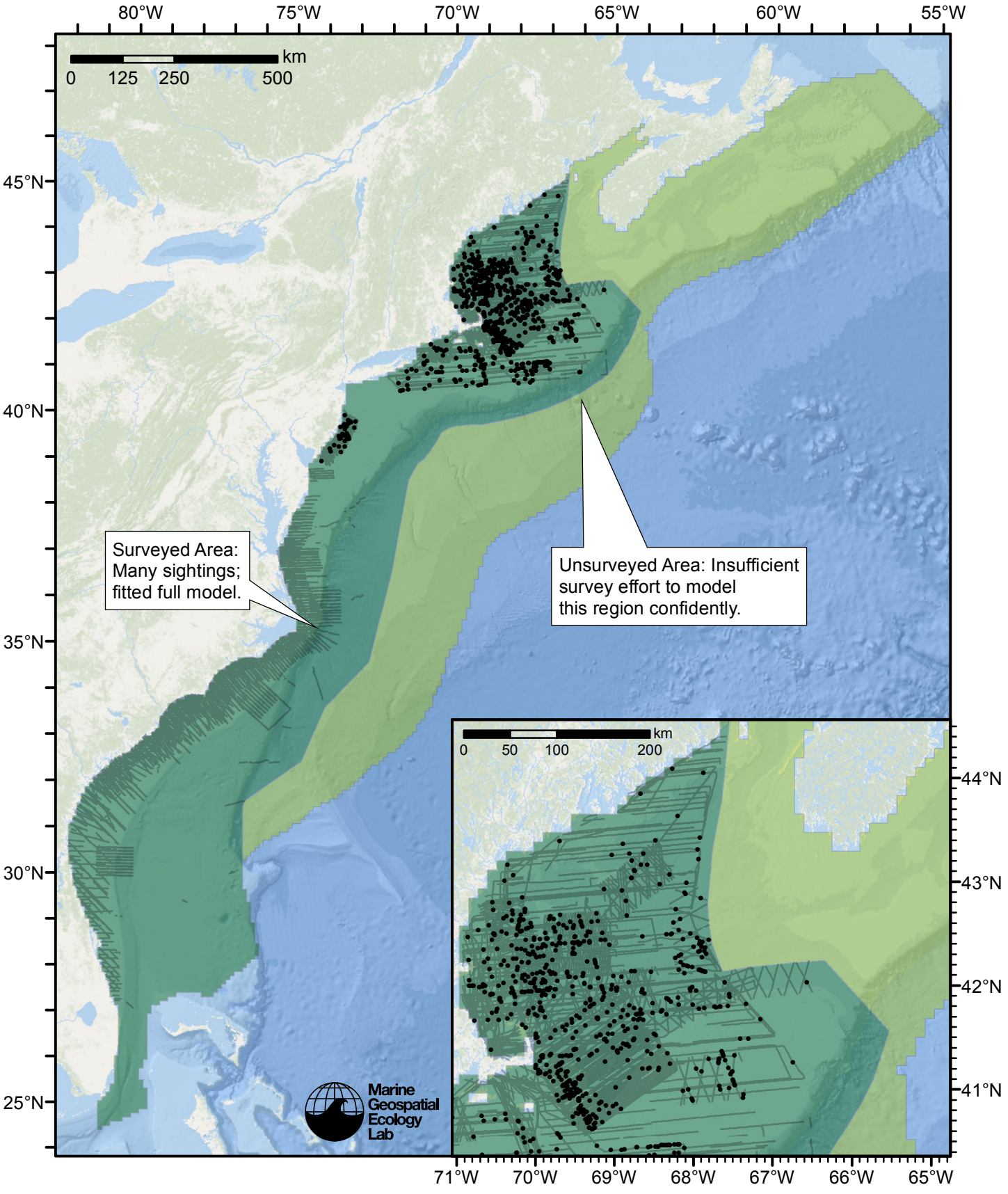

Figure 53: Harbor porpoise density model schematic for Winter season. All on-effort sightings are shown, including those that were truncated when detection functions were fitted.

Climatological Model

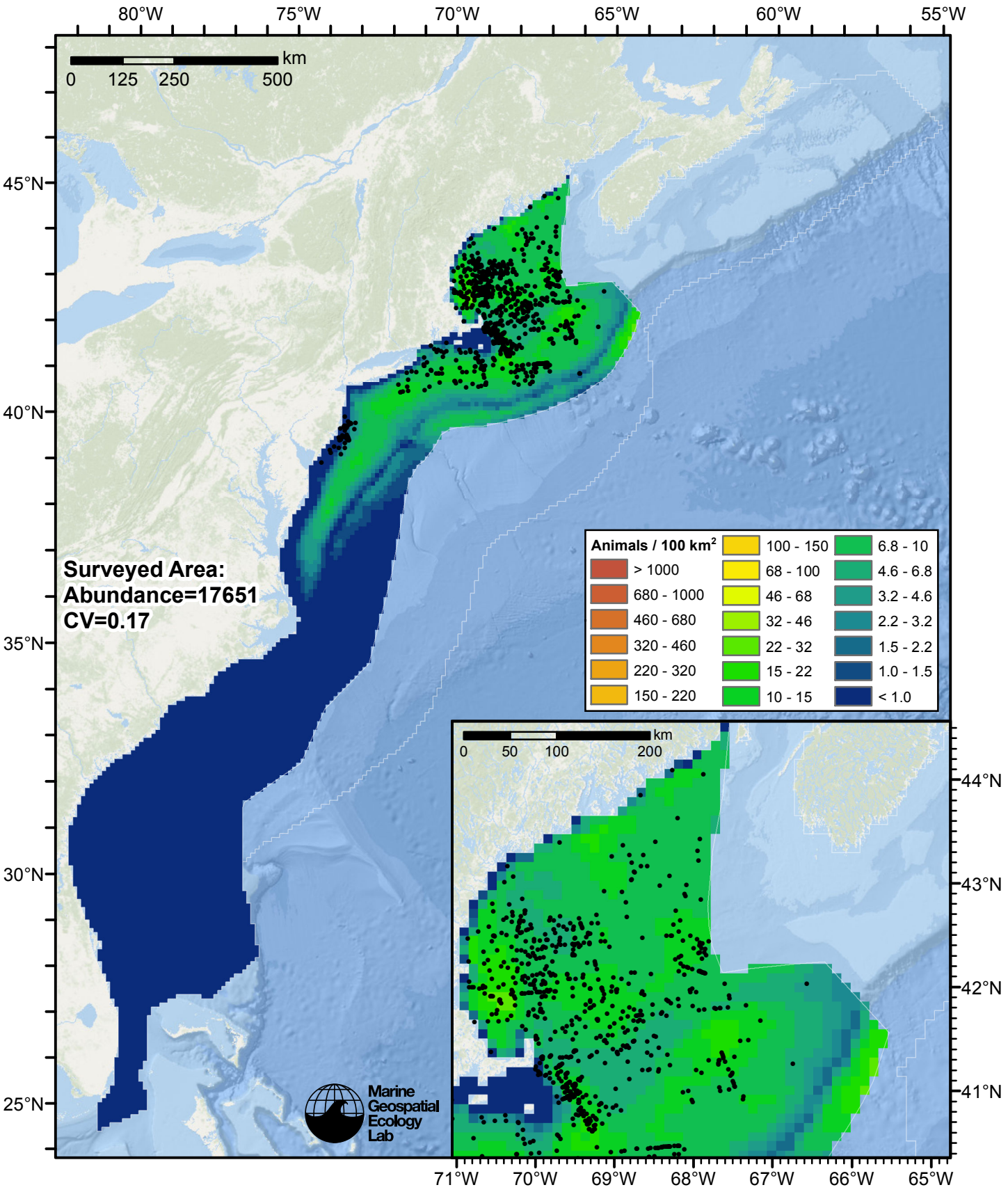

Figure 54: Harbor porpoise density predicted by the Winter season climatological model that explained the most deviance. Pixels are 10x10 km. The legend gives the estimated individuals per pixel; breaks are logarithmic. The same scale is used for all seasons. Abundance for each region was computed by summing the density cells occuring in that region.

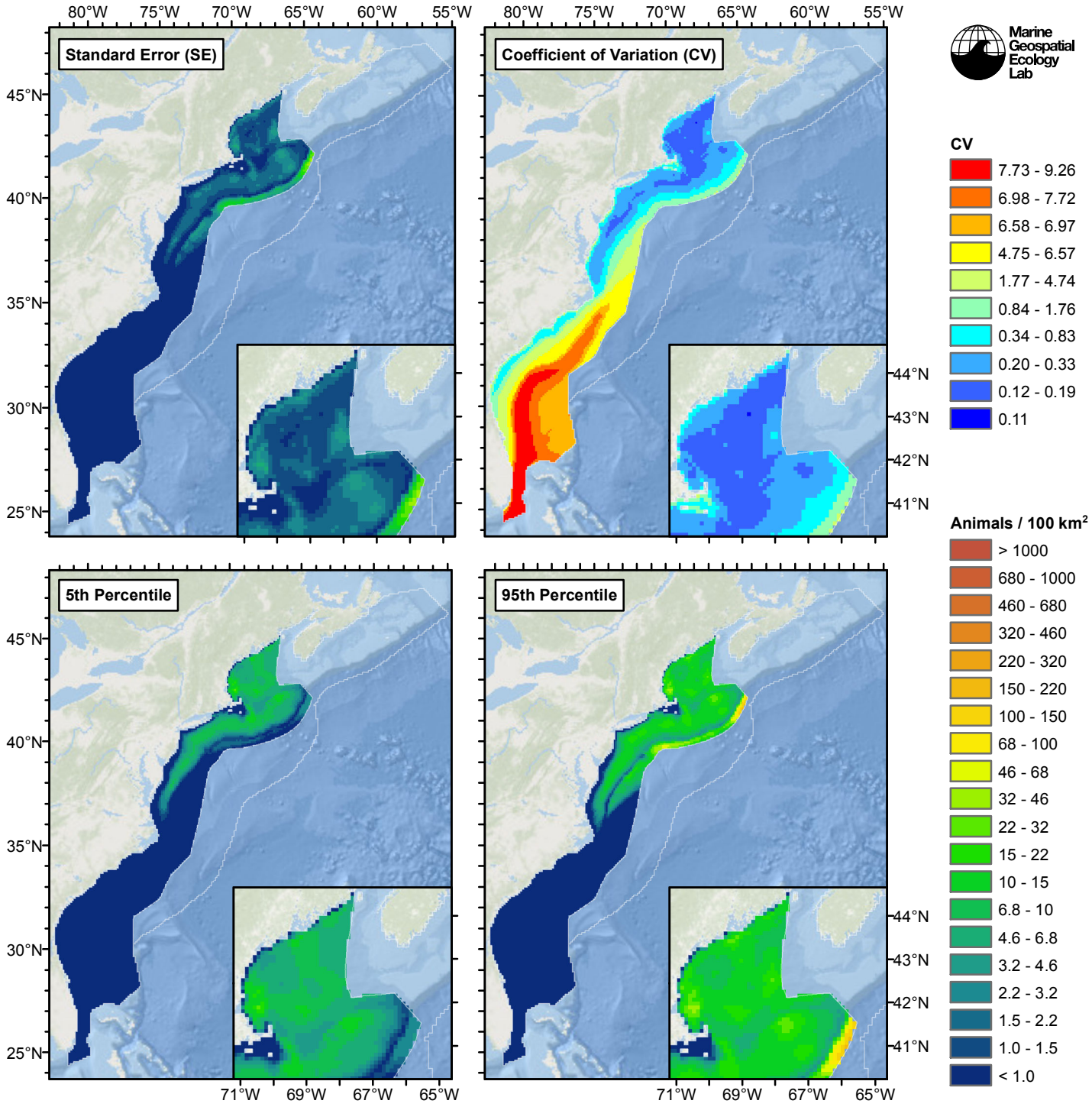

Figure 55: Estimated uncertainty for the Winter season climatological model that explained the most deviance. These estimates only incorporate the statistical uncertainty estimated for the spatial model (by the R mgcv package). They do not incorporate uncertainty in the detection functions, g(0) estimates, predictor variables, and so on.

Surveyed Area

Statistical output

```
Rscript.exe: This is mgcv 1.8-3. For overview type 'help("mgcv-package")'.


Family: Tweedie(p=1.29)
```

```
Link function: log

Formula:
abundance ~ offset(log(area_km2)) + s(log10(Depth), bs = "ts",
    k = 5) + s(sqrt(DistToShore/1000), bs = "ts", k = 5) + s(I(DistTo125m/1000),
    bs = "ts", k = 5) + s(I(DistTo300m/1000), bs = "ts", k = 5) +
    s(ClimSST, bs = "ts", k = 5) + s(I(ClimDistToFront1^(1/3)),
    bs = "ts", k = 5) + s(log10(pmax(ClimEKE, 1e-04)), bs = "ts",
    k = 5) + s(log10(pmax(ClimEpiMnkPP, 1e-06)), bs = "ts", k = 5)

Parametric coefficients:
            Estimate Std. Error t value Pr(>|t|)
(Intercept)  -10.738      2.157  -4.978 6.46e-07 ***
---
Signif. codes:  0 '***' 0.001 '**' 0.01 '*' 0.05 '.' 0.1 ' ' 1

Approximate significance of smooth terms:
                                     edf Ref.df      F  p-value
s(log10(Depth))                   3.6412      4  8.523 5.58e-08 ***
s(sqrt(DistToShore/1000))         3.0636      4  5.136 3.45e-05 ***
s(I(DistTo125m/1000))             3.3399      4  3.417 0.002154 **
s(I(DistTo300m/1000))             2.7899      4  7.109 3.79e-07 ***
s(ClimSST)                        2.5077      4 21.924  < 2e-16 ***
s(I(ClimDistToFront1^(1/3)))      1.0455      4  4.985 3.84e-06 ***
s(log10(pmax(ClimEKE, 1e-04)))    1.0973      4  6.340 1.48e-07 ***
s(log10(pmax(ClimEpiMnkPP, 1e-06))) 0.9617      4  2.559 0.000755 ***
---
Signif. codes:  0 '***' 0.001 '**' 0.01 '*' 0.05 '.' 0.1 ' ' 1

R-sq.(adj) =  0.0394   Deviance explained = 44.7%
-REML = 4018.4  Scale est. = 28.313    n = 21420

All predictors were significant. This is the final model.
Creating term plots.
Diagnostic output from gam.check():

Method: REML   Optimizer: outer newton
full convergence after 12 iterations.
Gradient range [-0.00166738,0.000105492]
(score 4018.433 & scale 28.31283).
Hessian positive definite, eigenvalue range [0.3481107,1685.341].
Model rank =  33 / 33

Basis dimension (k) checking results. Low p-value (k-index<1) may
indicate that k is too low, especially if edf is close to k'.

                                     k'   edf k-index p-value
s(log10(Depth))                   4.000 3.641   0.878    0.02
s(sqrt(DistToShore/1000))         4.000 3.064   0.884    0.03
s(I(DistTo125m/1000))             4.000 3.340   0.869    0.00
s(I(DistTo300m/1000))             4.000 2.790   0.815    0.00
s(ClimSST)                        4.000 2.508   0.762    0.00
s(I(ClimDistToFront1^(1/3)))      4.000 1.045   0.870    0.02
s(log10(pmax(ClimEKE, 1e-04)))    4.000 1.097   0.873    0.02
s(log10(pmax(ClimEpiMnkPP, 1e-06))) 4.000 0.962   0.886    0.07

Predictors retained during the model selection procedure: Depth, DistToShore, DistTo125m,
DistTo300m, ClimSST, ClimDistToFront1, ClimEKE, ClimEpiMnkPP
```

```
Predictors dropped during the model selection procedure: Slope
```

Model term plots

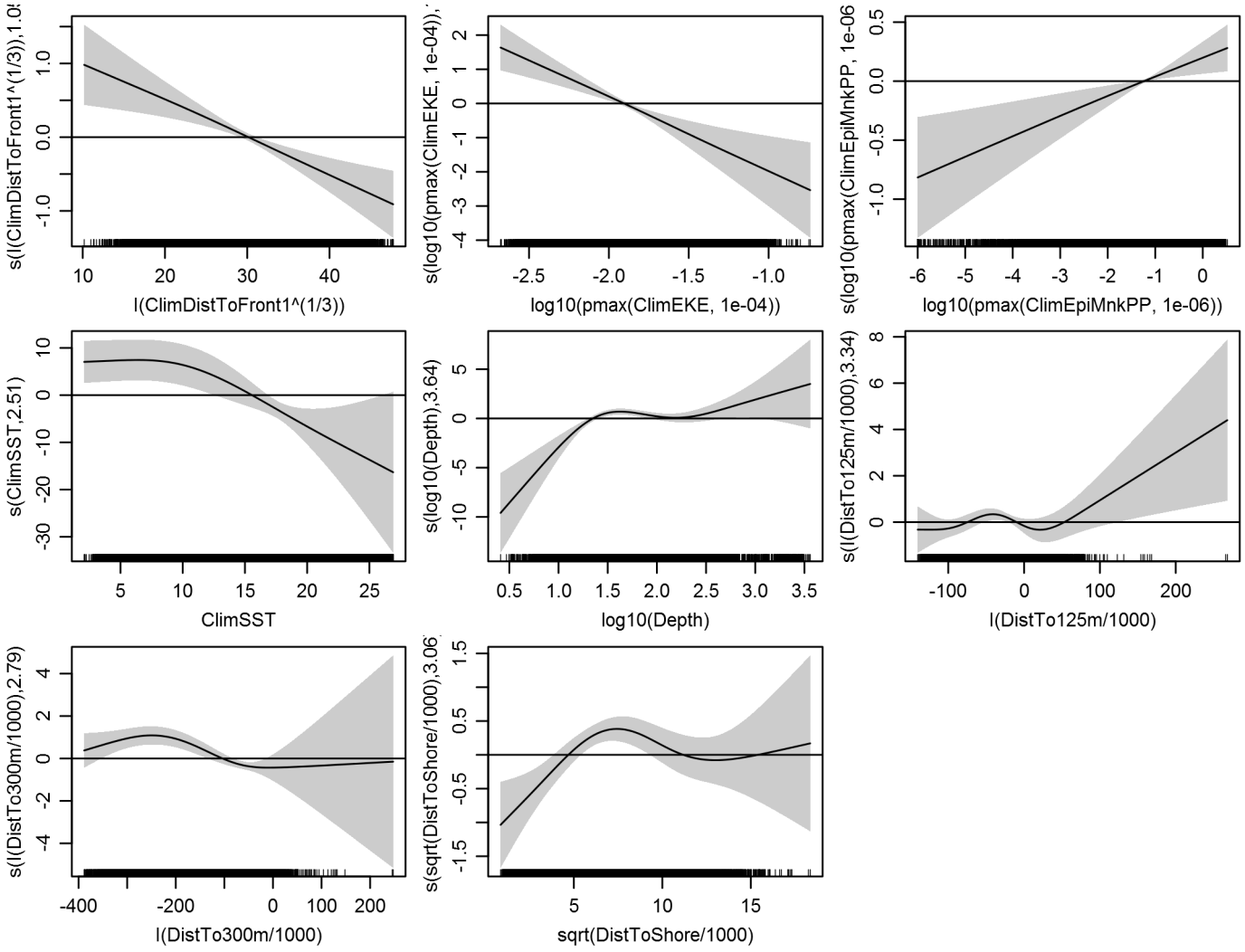

Diagnostic plots

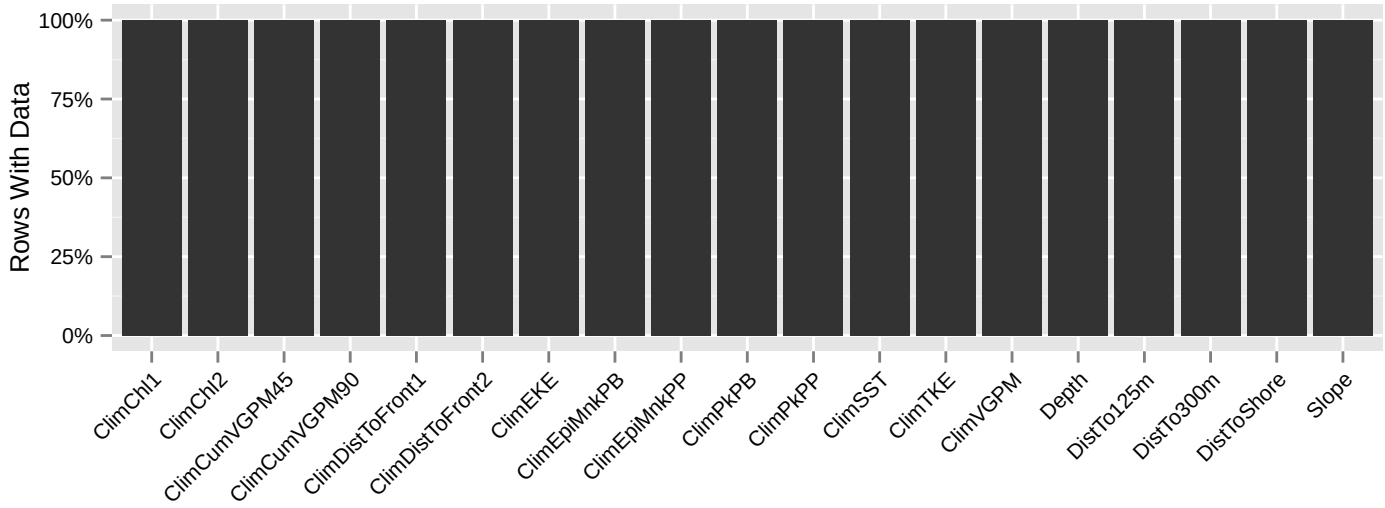

Figure 56: Segments with predictor values for the Harbor porpoise Climatological model, Winter season, Surveyed Area. This plot is used to assess how many segments would be lost by including a given predictor in a model.

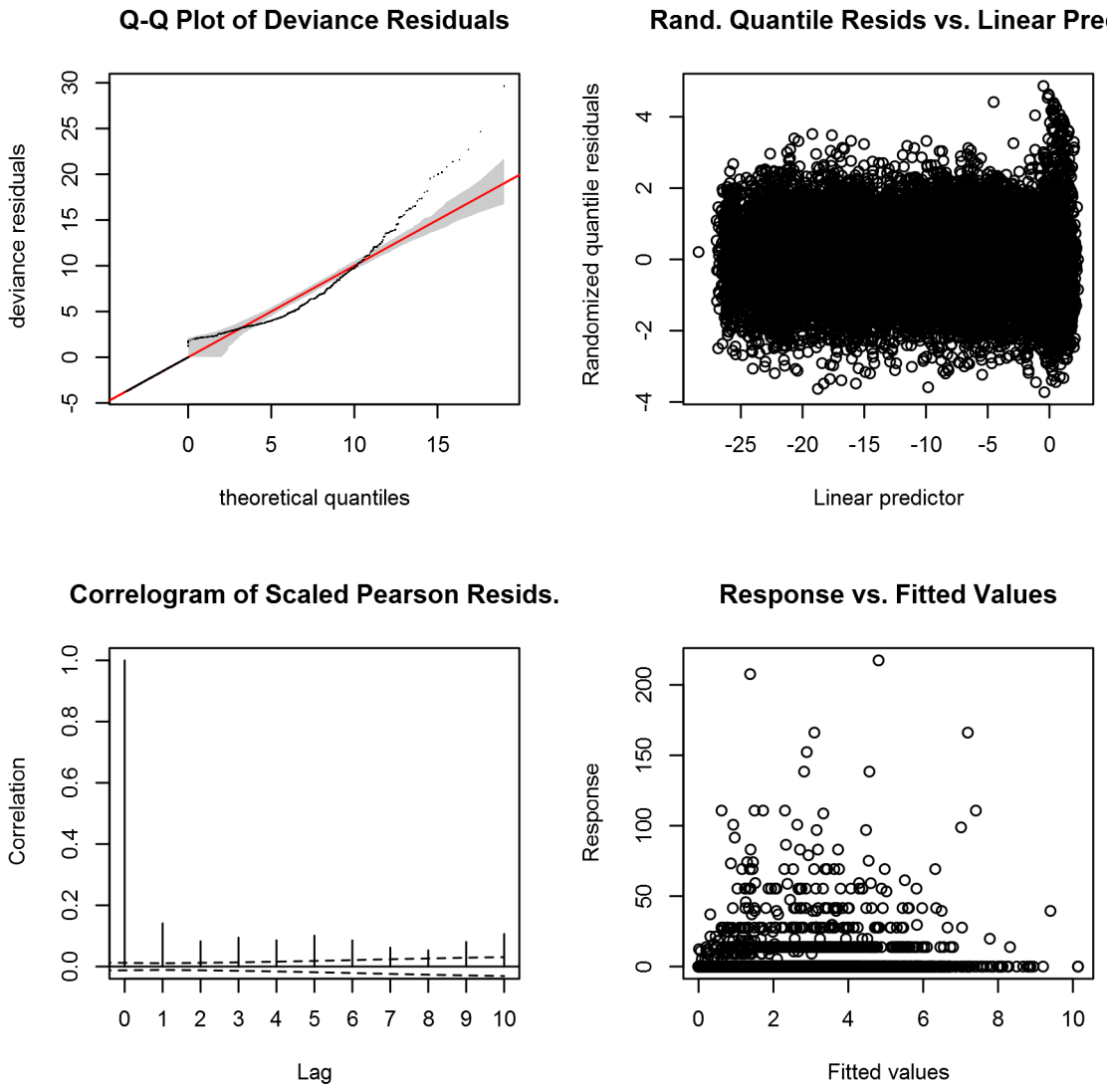

Figure 57: Statistical diagnostic plots for the Harbor porpoise Climatological model, Winter season, Surveyed Area.

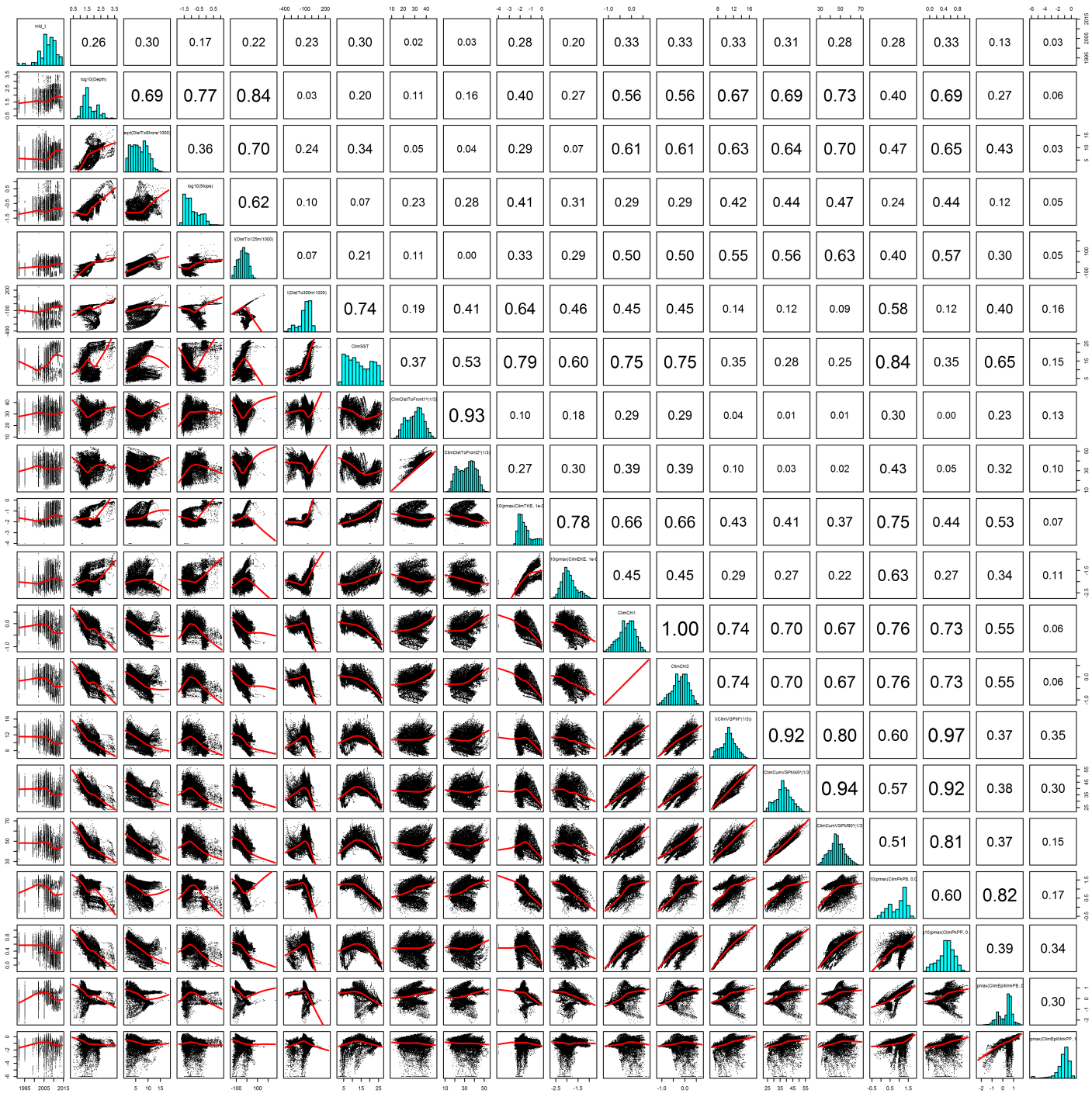

Figure 58: Scatterplot matrix for the Harbor porpoise Climatological model, Winter season, Surveyed Area. This plot is used to inspect the distribution of predictors (via histograms along the diagonal), simple correlation between predictors (via pairwise Pearson coefficients above the diagonal), and linearity of predictor correlations (via scatterplots below the diagonal). This plot is best viewed at high magnification.

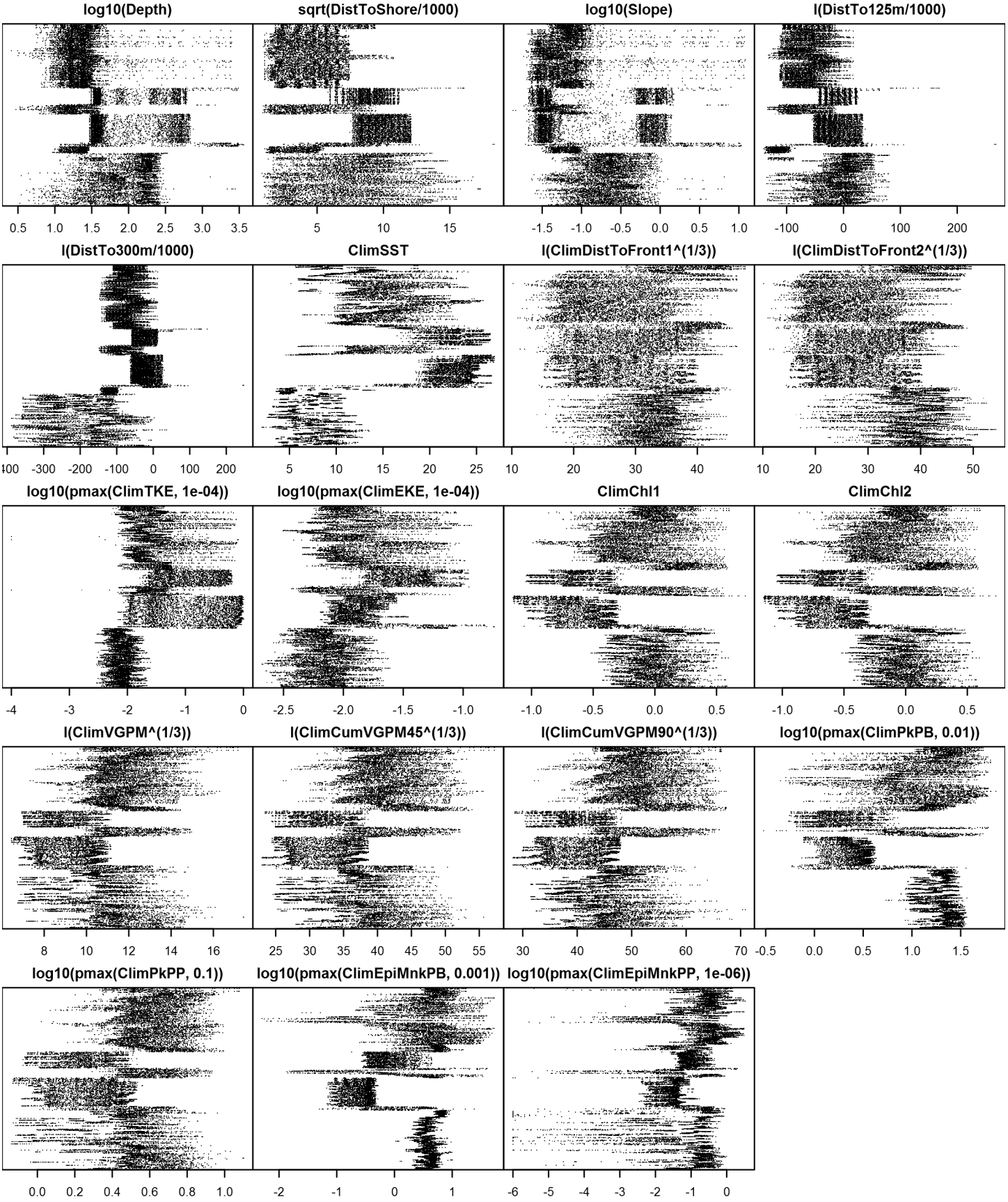

Figure 59: Dotplot for the Harbor porpoise Climatological model, Winter season, Surveyed Area. This plot is used to check for suspicious patterns and outliers in the data. Points are ordered vertically by transect ID, sequentially in time.

Unsurveyed Area

Density was not modeled for this region.

Contemporaneous Model

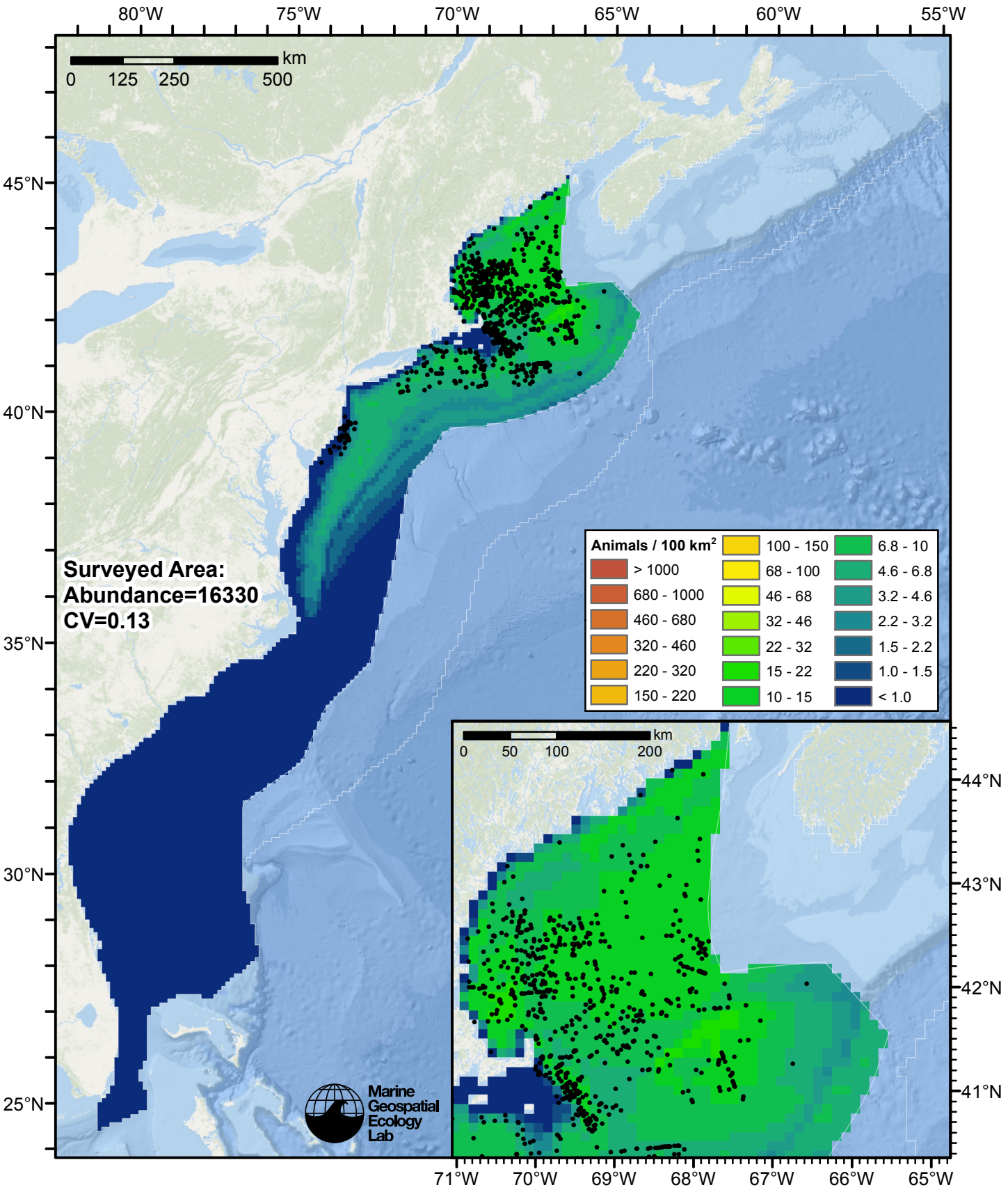

Figure 60: Harbor porpoise density predicted by the Winter season contemporaneous model that explained the most deviance. Pixels are 10x10 km. The legend gives the estimated individuals per pixel; breaks are logarithmic. The same scale is used for all seasons. Abundance for each region was computed by summing the density cells occuring in that region.

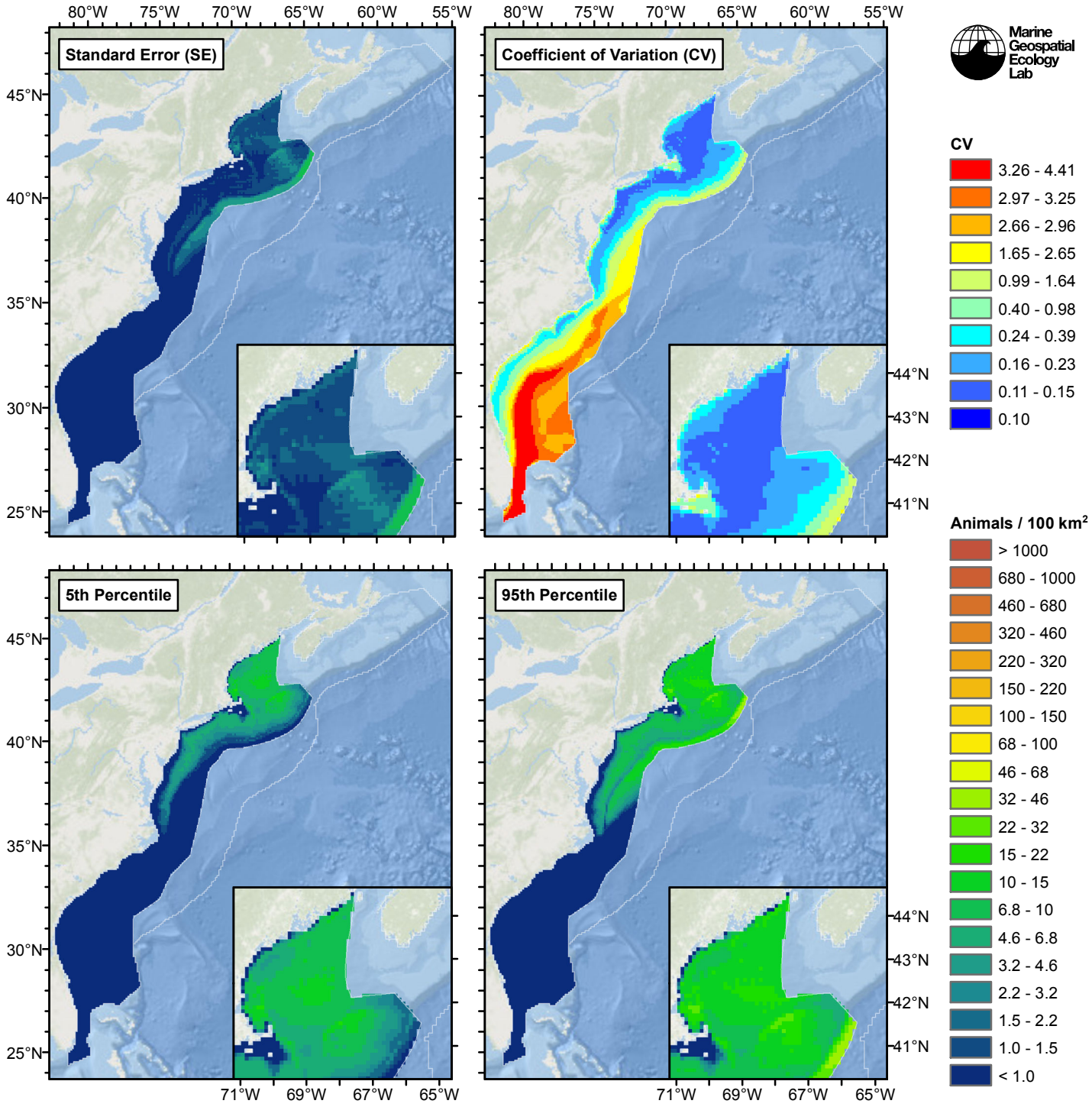

Figure 61: Estimated uncertainty for the Winter season contemporaneous model that explained the most deviance. These estimates only incorporate the statistical uncertainty estimated for the spatial model (by the R mgcv package). They do not incorporate uncertainty in the detection functions, g(0) estimates, predictor variables, and so on.

Surveyed Area

Statistical output

```
Rscript.exe: This is mgcv 1.8-3. For overview type 'help("mgcv-package")'.


Family: Tweedie(p=1.287)
```

```
Link function: log

Formula:
abundance ~ offset(log(area_km2)) + s(log10(Depth), bs = "ts",
    k = 5) + s(sqrt(DistToShore/1000), bs = "ts", k = 5) + s(I(DistTo300m/1000),
    bs = "ts", k = 5) + s(SST, bs = "ts", k = 5) + s(I(DistToFront2^(1/3)),
    bs = "ts", k = 5) + s(log10(pmax(EKE, 1e-04)), bs = "ts",
    k = 5) + s(log10(pmax(EpiMnkPP, 1e-06)), bs = "ts", k = 5)

Parametric coefficients:
            Estimate Std. Error t value Pr(>|t|)
(Intercept)  -7.8772     0.8821   -8.93   <2e-16 ***
---
Signif. codes:  0 '***' 0.001 '**' 0.01 '*' 0.05 '.' 0.1 ' ' 1

Approximate significance of smooth terms:
                                   edf Ref.df      F  p-value
s(log10(Depth))                 3.7948      4 18.963  < 2e-16 ***
s(sqrt(DistToShore/1000))       2.0526      4  3.626 0.000254 ***
s(I(DistTo300m/1000))           2.7542      4  9.457 2.17e-09 ***
s(SST)                          2.8435      4 16.503 2.14e-15 ***
s(I(DistToFront2^(1/3)))        0.9557      4  2.248 0.001506 **
s(log10(pmax(EKE, 1e-04)))      2.6427      4  3.398 0.001314 **
s(log10(pmax(EpiMnkPP, 1e-06))) 1.1333      4 10.545 2.56e-11 ***
---
Signif. codes:  0 '***' 0.001 '**' 0.01 '*' 0.05 '.' 0.1 ' ' 1

R-sq.(adj) =  0.037   Deviance explained = 41.9%
-REML = 4046.8  Scale est. = 28.807    n = 20611

All predictors were significant. This is the final model.
Creating term plots.
Diagnostic output from gam.check():

Method: REML   Optimizer: outer newton
full convergence after 11 iterations.
Gradient range [-7.671011e-05,5.110154e-05]
(score 4046.778 & scale 28.80746).
Hessian positive definite, eigenvalue range [0.2862555,1716.763].
Model rank =  29 / 29

Basis dimension (k) checking results. Low p-value (k-index<1) may
indicate that k is too low, especially if edf is close to k'.

                                  k'   edf k-index p-value
s(log10(Depth))                4.000 3.795   0.837    0.00
s(sqrt(DistToShore/1000))      4.000 2.053   0.881    0.12
s(I(DistTo300m/1000))          4.000 2.754   0.834    0.00
s(SST)                         4.000 2.844   0.784    0.00
s(I(DistToFront2^(1/3)))       4.000 0.956   0.842    0.00
s(log10(pmax(EKE, 1e-04)))     4.000 2.643   0.856    0.00
s(log10(pmax(EpiMnkPP, 1e-06))) 4.000 1.133   0.896    0.52

Predictors retained during the model selection procedure: Depth, DistToShore, DistTo300m, SST,
DistToFront2, EKE, EpiMnkPP

Predictors dropped during the model selection procedure: Slope, DistTo125m
```

Model term plots

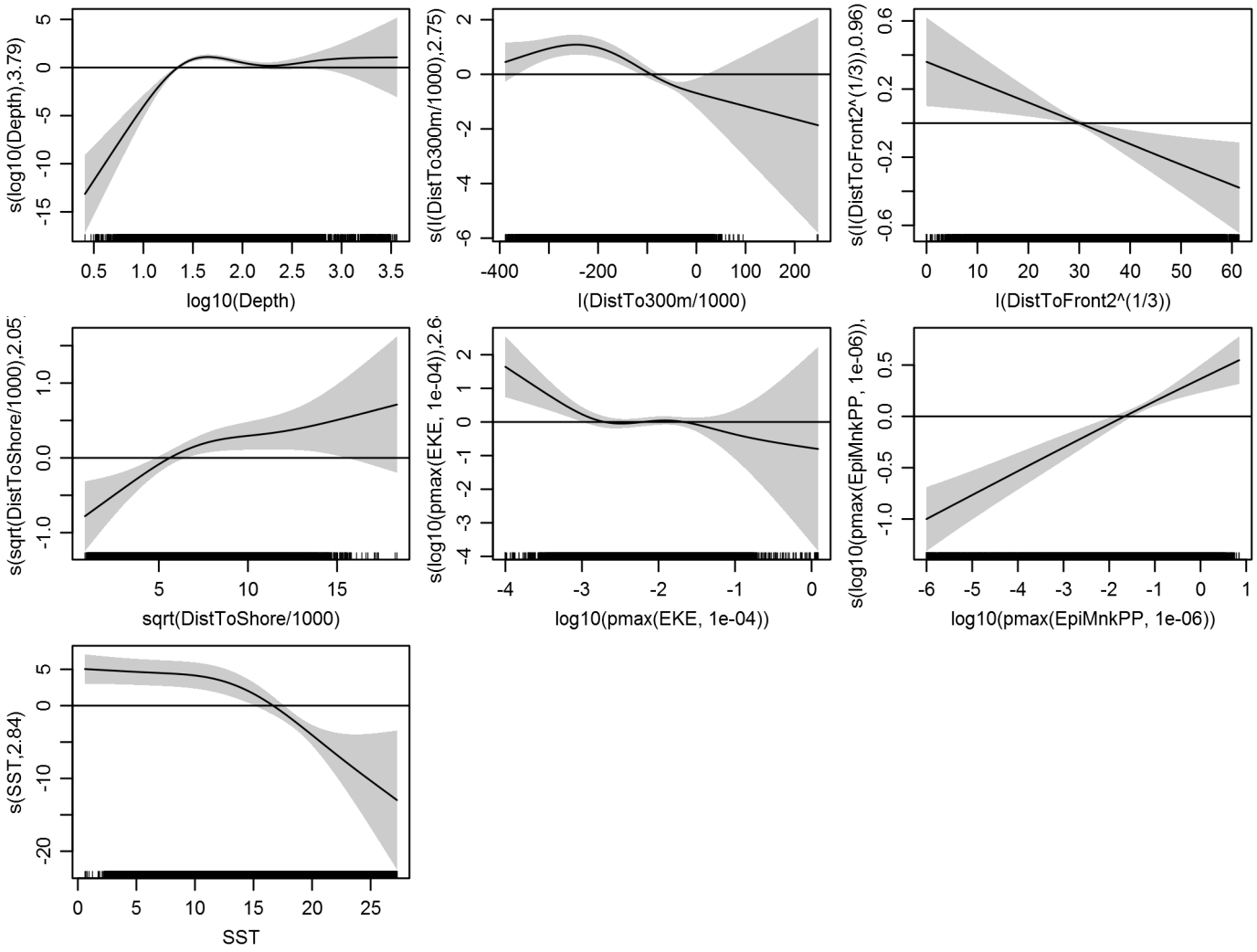

Diagnostic plots

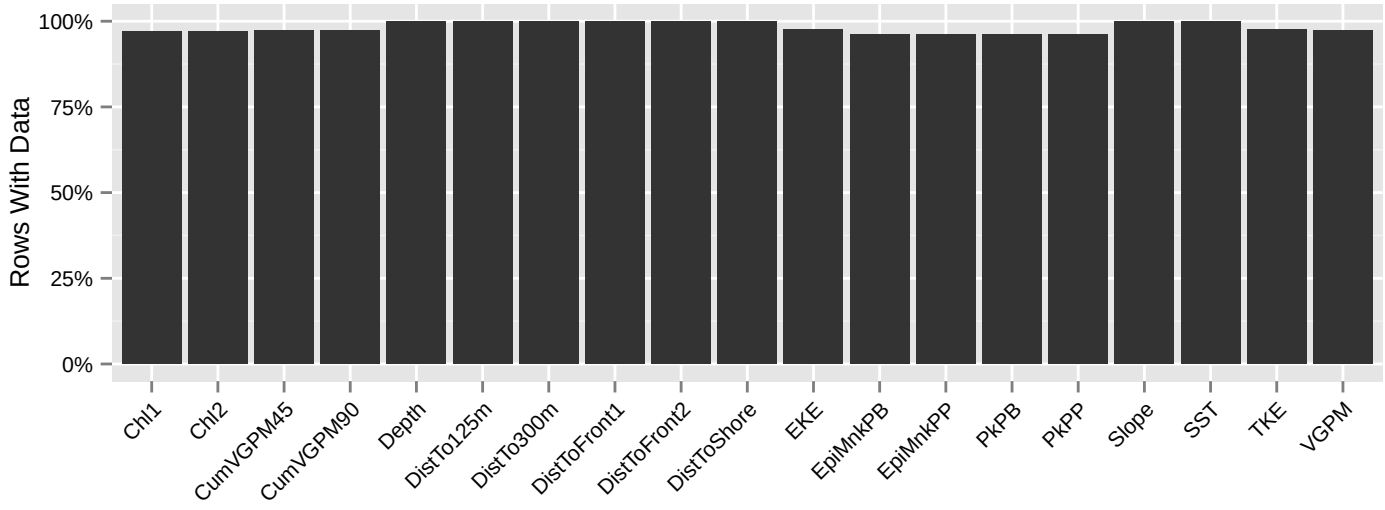

Figure 62: Segments with predictor values for the Harbor porpoise Contemporaneous model, Winter season, Surveyed Area. This plot is used to assess how many segments would be lost by including a given predictor in a model.

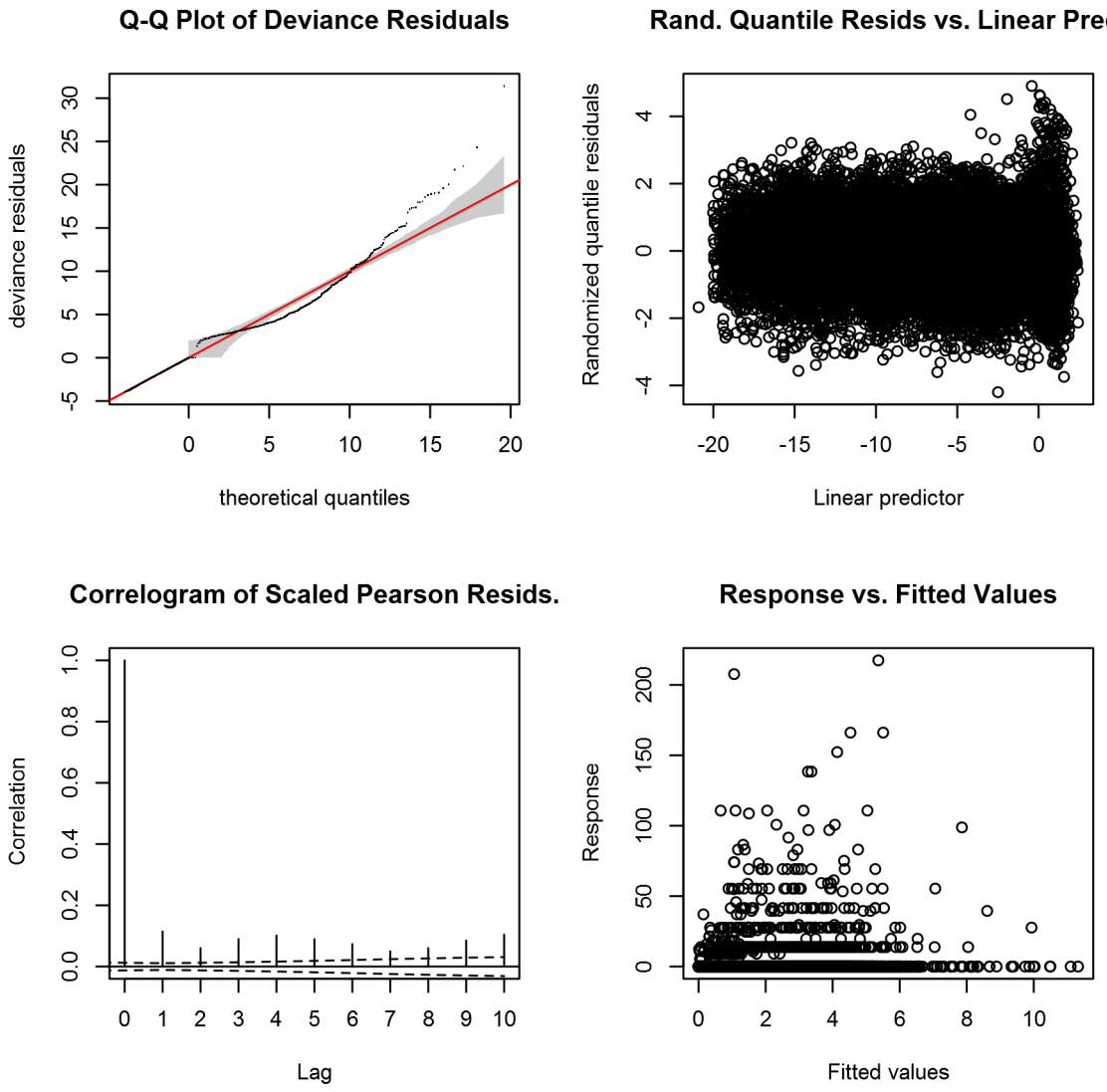

Figure 63: Statistical diagnostic plots for the Harbor porpoise Contemporaneous model, Winter season, Surveyed Area.

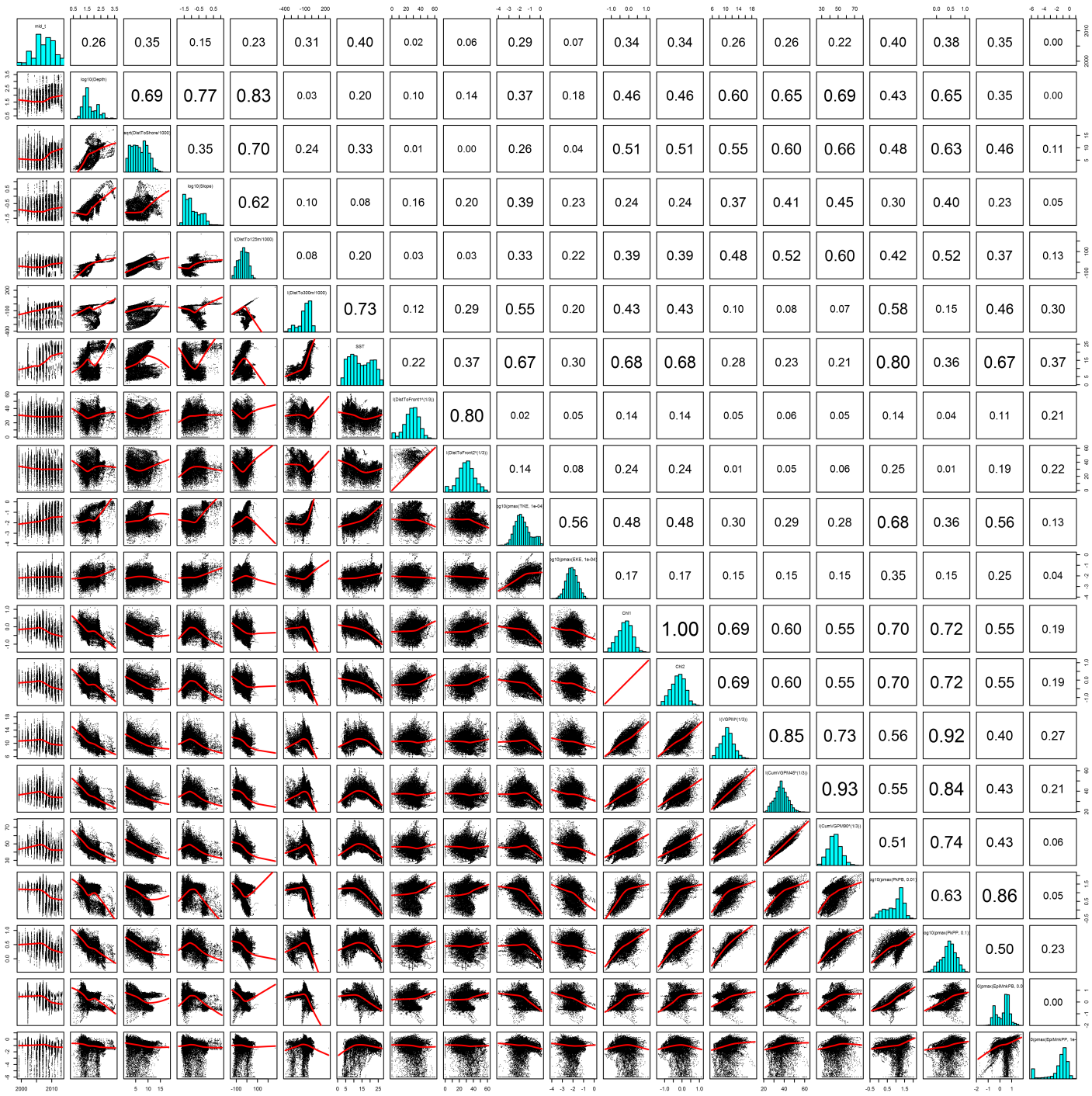

Figure 64: Scatterplot matrix for the Harbor porpoise Contemporaneous model, Winter season, Surveyed Area. This plot is used to inspect the distribution of predictors (via histograms along the diagonal), simple correlation between predictors (via pairwise Pearson coefficients above the diagonal), and linearity of predictor correlations (via scatterplots below the diagonal). This plot is best viewed at high magnification.

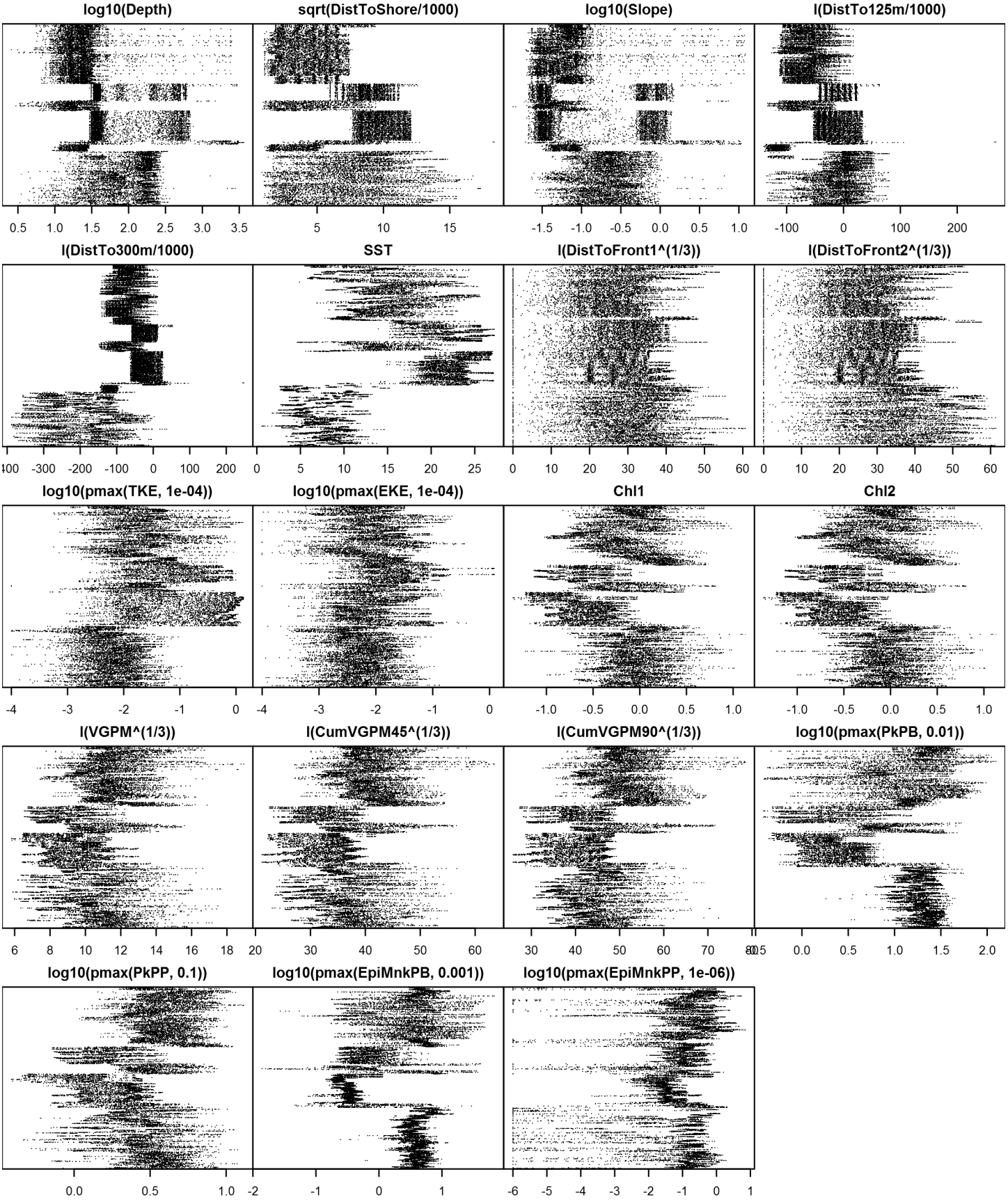

Figure 65: Dotplot for the Harbor porpoise Contemporaneous model, Winter season, Surveyed Area. This plot is used to check for suspicious patterns and outliers in the data. Points are ordered vertically by transect ID, sequentially in time.

Unsurveyed Area

Density was not modeled for this region.

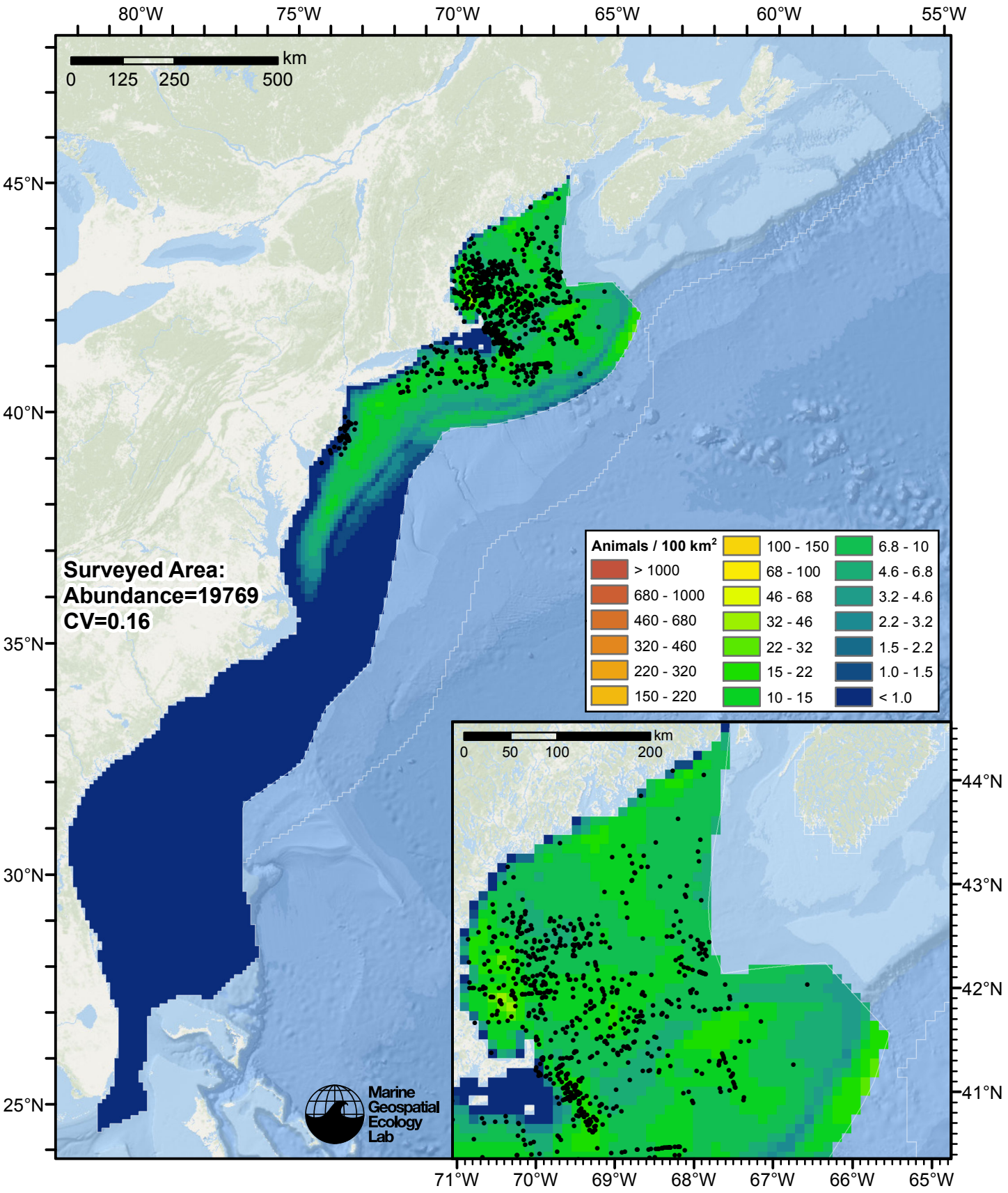

Figure 66: Harbor porpoise density predicted by the Winter season climatological same segments model that explained the most deviance. Pixels are 10x10 km. The legend gives the estimated individuals per pixel; breaks are logarithmic. The same scale is used for all seasons. Abundance for each region was computed by summing the density cells occuring in that region.

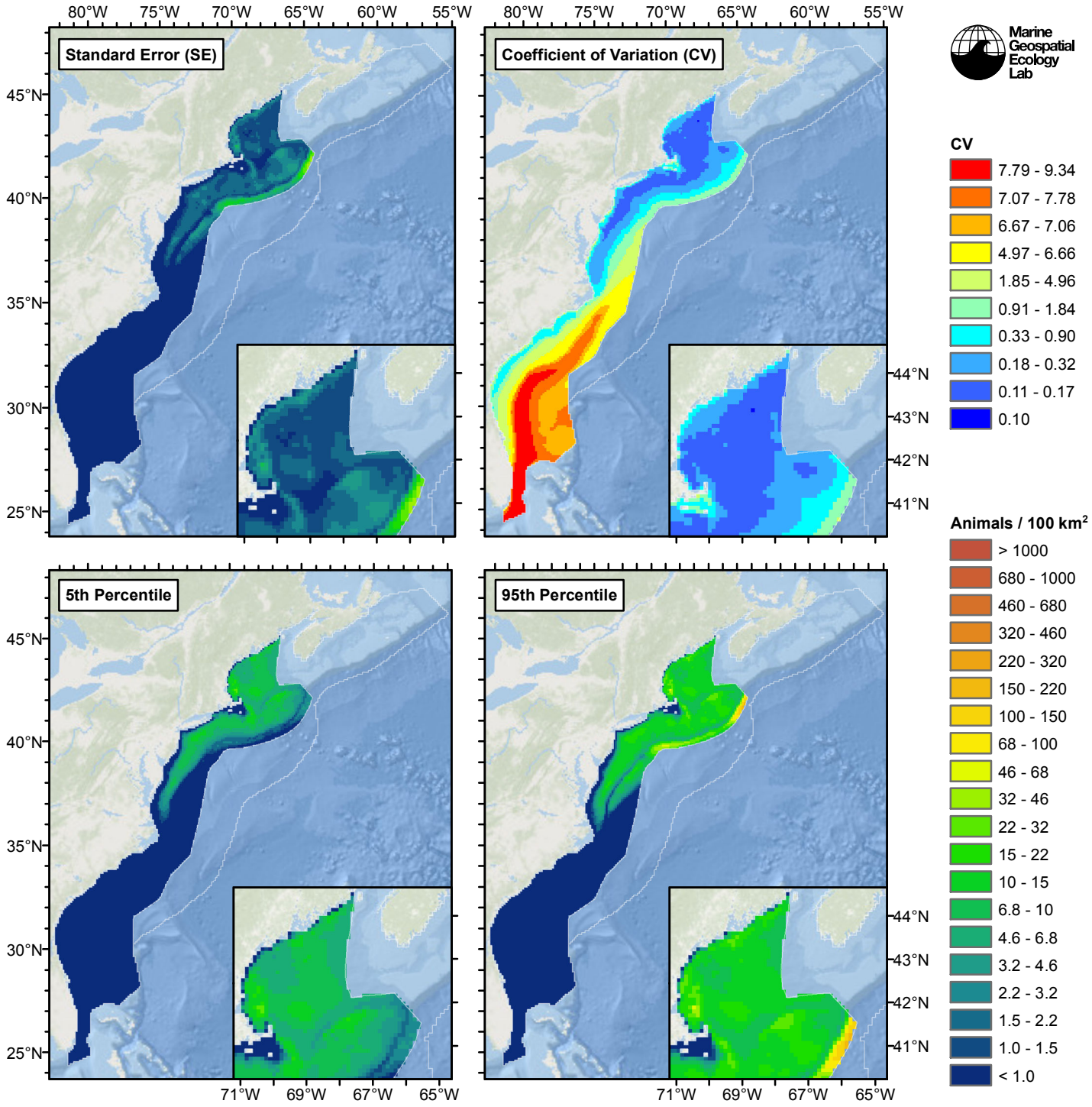

Figure 67: Estimated uncertainty for the Winter season climatological same segments model that explained the most deviance. These estimates only incorporate the statistical uncertainty estimated for the spatial model (by the R mgcv package). They do not incorporate uncertainty in the detection functions, g(0) estimates, predictor variables, and so on.

Surveyed Area

Statistical output

```
Rscript.exe: This is mgcv 1.8-3. For overview type 'help("mgcv-package")'.


Family: Tweedie(p=1.293)
```

```
Link function: log

Formula:
abundance ~ offset(log(area_km2)) + s(log10(Depth), bs = "ts",
    k = 5) + s(sqrt(DistToShore/1000), bs = "ts", k = 5) + s(I(DistTo125m/1000),
    bs = "ts", k = 5) + s(I(DistTo300m/1000), bs = "ts", k = 5) +
    s(ClimSST, bs = "ts", k = 5) + s(I(ClimDistToFront1^(1/3)),
    bs = "ts", k = 5) + s(log10(pmax(ClimEKE, 1e-04)), bs = "ts",
    k = 5)

Parametric coefficients:
            Estimate Std. Error t value Pr(>|t|)
(Intercept)   -10.48       2.19  -4.787 1.71e-06 ***
---
Signif. codes:  0 '***' 0.001 '**' 0.01 '*' 0.05 '.' 0.1 ' ' 1

Approximate significance of smooth terms:
                                edf Ref.df      F  p-value
s(log10(Depth))               3.7039      4 14.564 3.55e-13 ***
s(sqrt(DistToShore/1000))     3.0721      4  4.876 6.61e-05 ***
s(I(DistTo125m/1000))         0.8734      4  1.506  0.00658 **
s(I(DistTo300m/1000))         2.7515      4  5.700 1.00e-05 ***
s(ClimSST)                    2.5244      4 20.594  < 2e-16 ***
s(I(ClimDistToFront1^(1/3)))  1.0361      4  4.385 1.47e-05 ***
s(log10(pmax(ClimEKE, 1e-04))) 1.0772     4  6.663 6.80e-08 ***
---
Signif. codes:  0 '***' 0.001 '**' 0.01 '*' 0.05 '.' 0.1 ' ' 1

R-sq.(adj) =  0.036   Deviance explained = 43.7%
-REML = 4020.3  Scale est. = 28.532    n = 20920

All predictors were significant. This is the final model.
Creating term plots.
Diagnostic output from gam.check():

Method: REML   Optimizer: outer newton
full convergence after 16 iterations.
Gradient range [-0.000510429,0.0002547975]
(score 4020.297 & scale 28.53214).
Hessian positive definite, eigenvalue range [0.3573469,1676.063].
Model rank =  29 / 29

Basis dimension (k) checking results. Low p-value (k-index<1) may
indicate that k is too low, especially if edf is close to k'.

                                k'   edf k-index p-value
s(log10(Depth))               4.000 3.704   0.863    0.00
s(sqrt(DistToShore/1000))     4.000 3.072   0.901    0.22
s(I(DistTo125m/1000))         4.000 0.873   0.888    0.02
s(I(DistTo300m/1000))         4.000 2.752   0.819    0.00
s(ClimSST)                    4.000 2.524   0.798    0.00
s(I(ClimDistToFront1^(1/3)))  4.000 1.036   0.876    0.00
s(log10(pmax(ClimEKE, 1e-04))) 4.000 1.077   0.866    0.01

Predictors retained during the model selection procedure: Depth, DistToShore, DistTo125m,
DistTo300m, ClimSST, ClimDistToFront1, ClimEKE

Predictors dropped during the model selection procedure: Slope
```

Model term plots

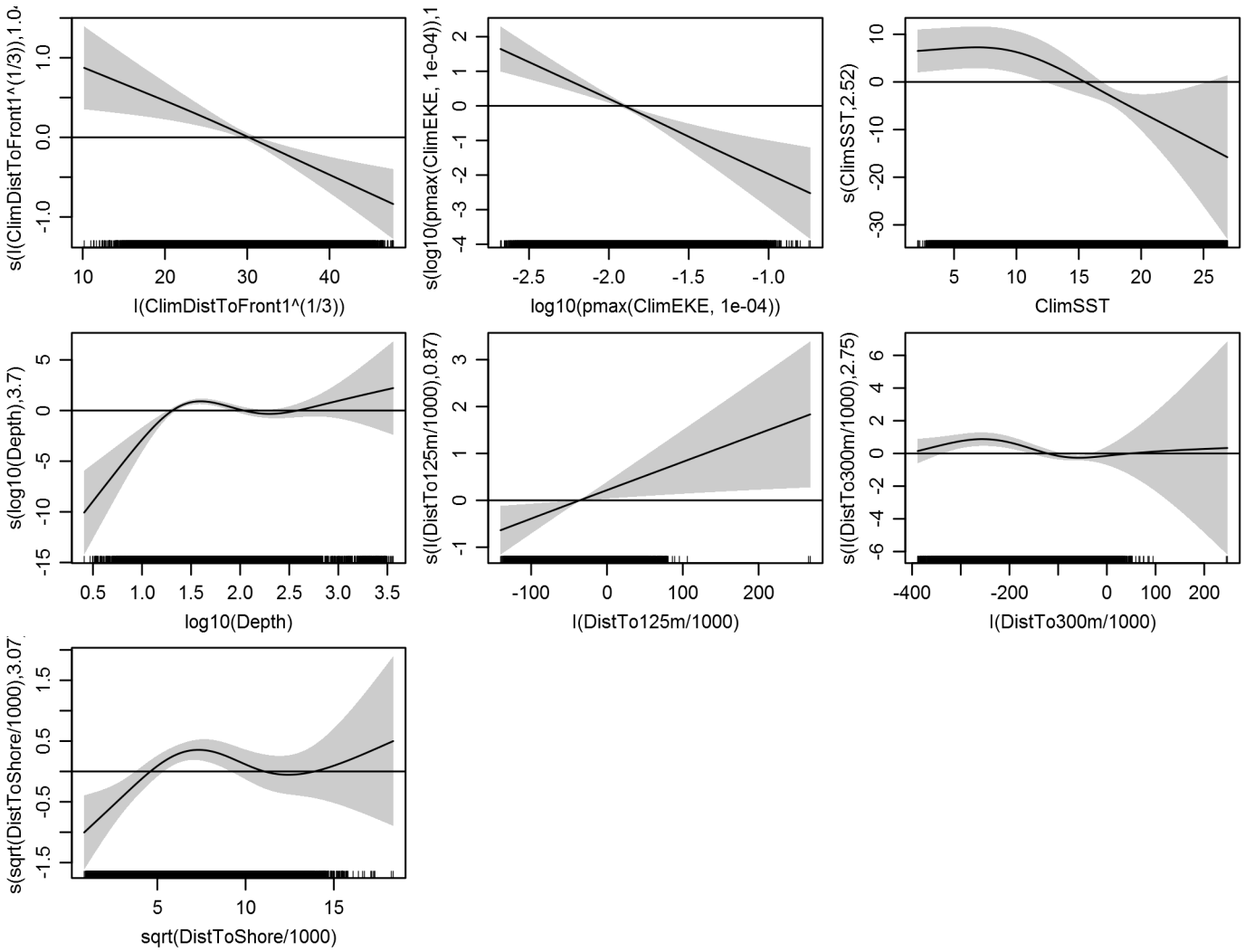

Diagnostic plots

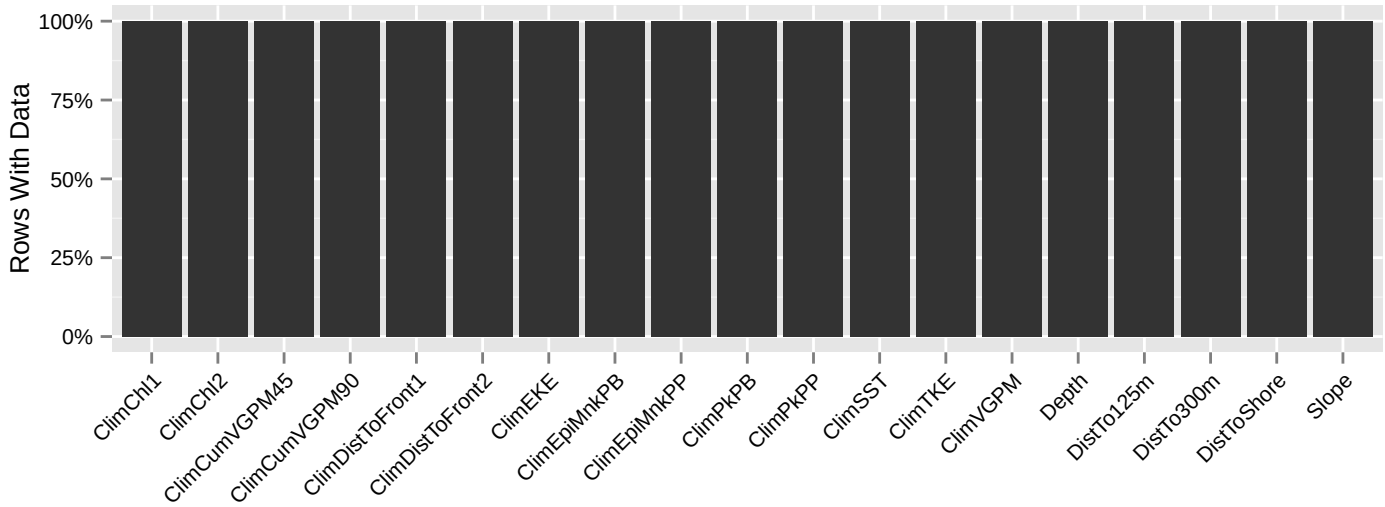

Figure 68: Segments with predictor values for the Harbor porpoise Climatological model, Winter season, Surveyed Area. This plot is used to assess how many segments would be lost by including a given predictor in a model.

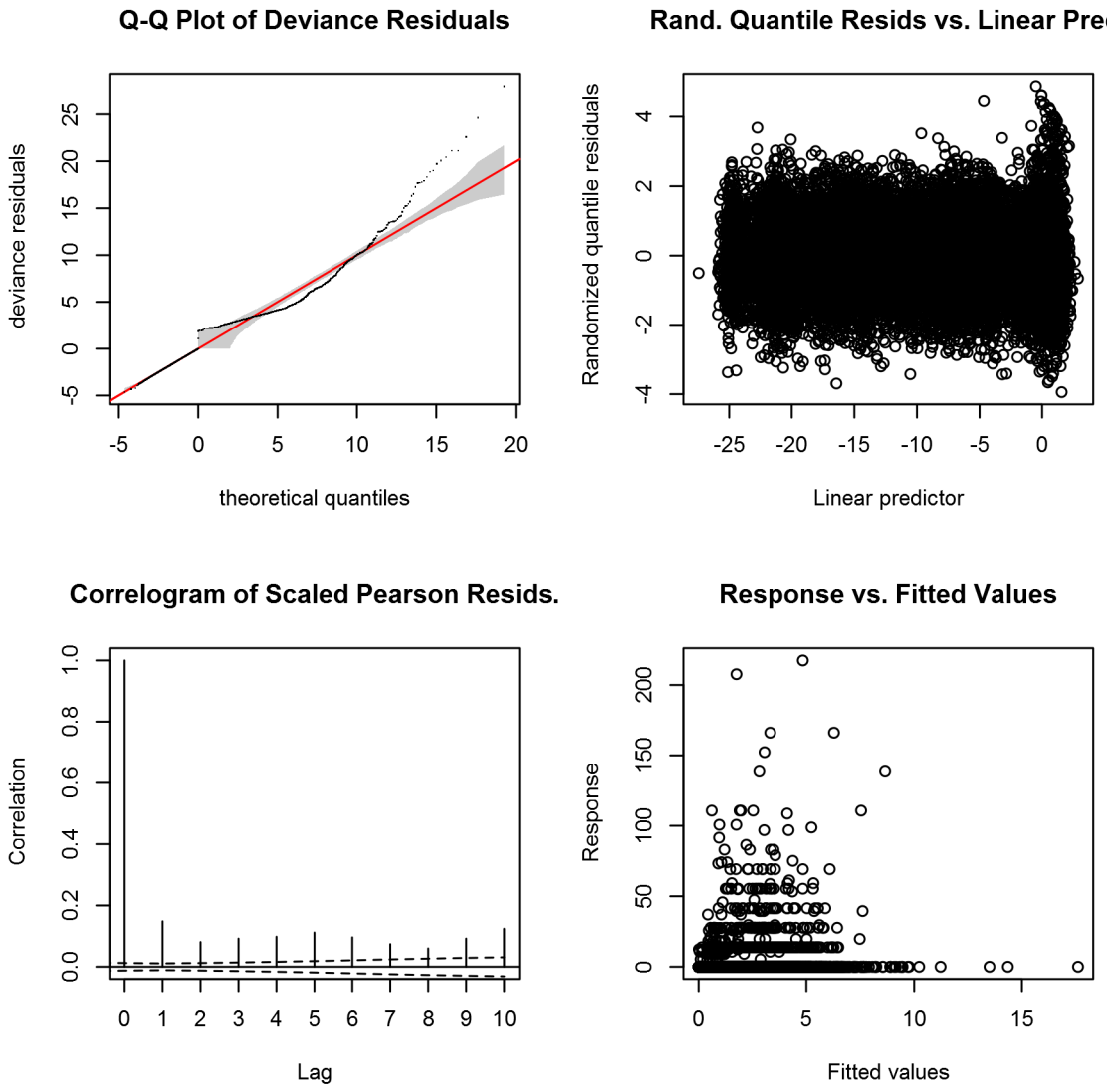

Figure 69: Statistical diagnostic plots for the Harbor porpoise Climatological model, Winter season, Surveyed Area.

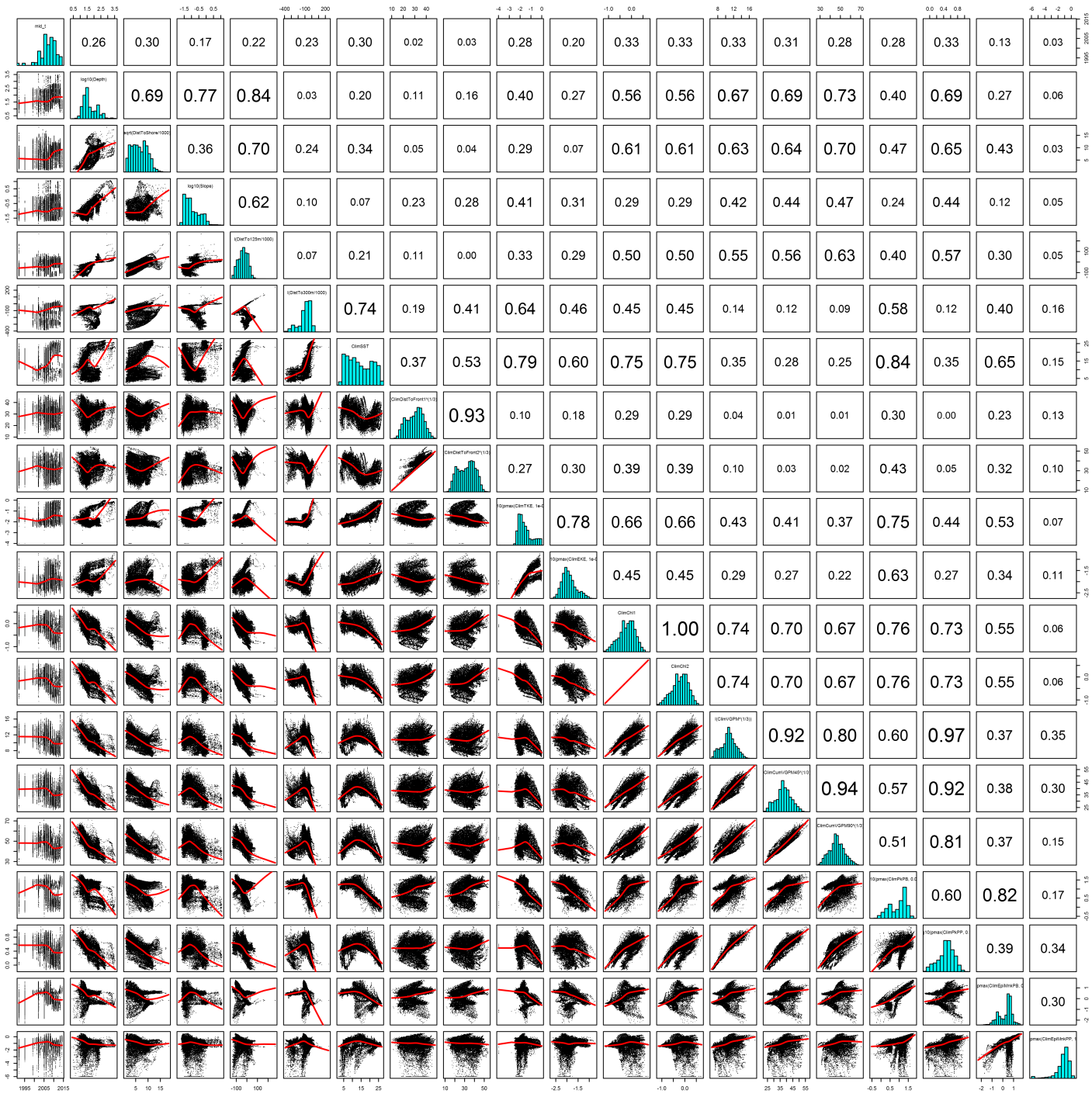

Figure 70: Scatterplot matrix for the Harbor porpoise Climatological model, Winter season, Surveyed Area. This plot is used to inspect the distribution of predictors (via histograms along the diagonal), simple correlation between predictors (via pairwise Pearson coefficients above the diagonal), and linearity of predictor correlations (via scatterplots below the diagonal). This plot is best viewed at high magnification.

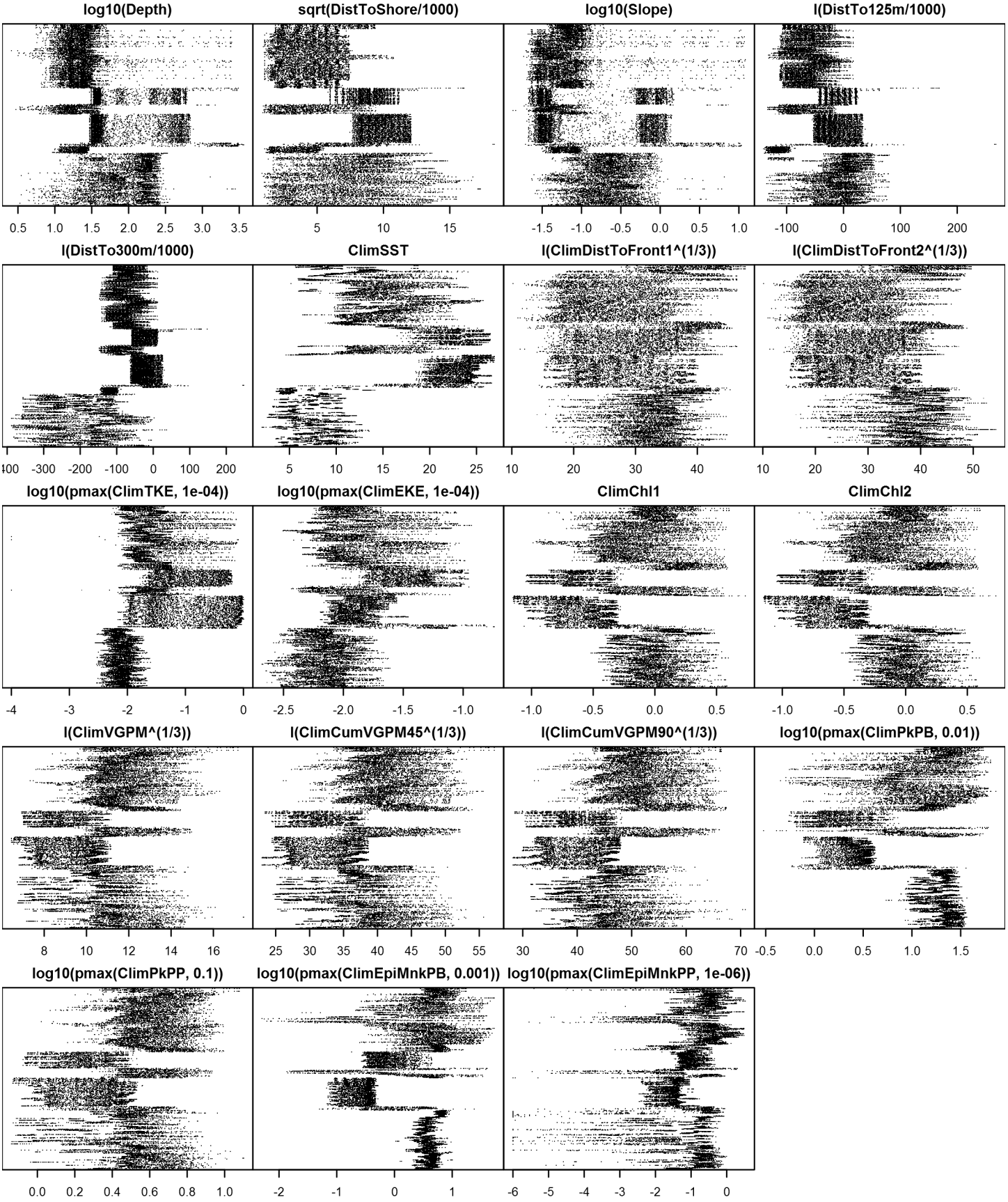

Figure 71: Dotplot for the Harbor porpoise Climatological model, Winter season, Surveyed Area. This plot is used to check for suspicious patterns and outliers in the data. Points are ordered vertically by transect ID, sequentially in time.

Unsurveyed Area

Density was not modeled for this region.

Summer

In this season, the entire study area was surveyed, with the most effort occurring on the continental shelf, particularly in the southern Gulf of Maine and off New England. In the south, we split the study area at the north wall of the Gulf Stream and assumed that harbor porpoises were absent in the southern area, where no sightings were reported for the duration of the study. In the north, we split the study area again about half way between the southern tip of Nova Scotia and the northernmost extent of the study area. Survey effort was sparse on the Scotian Shelf, and our objective was not to model the Gulf of St. Lawrence stock, which we presumed was progressively more likely occur than the Gulf of Maine/Bay of Fundy stock as we progressed north up the Scotian Shelf.

When we included this Northern Scotian Shelf region in our model, it predicted very high abundance near Cape Breton Island and Sable Island. We found no support for this in the literature and opted not to offer a prediction for this region, rather than offer the high prediction. We note that our model could likely be improved in the Scotian Shelf region by incorporating the Canadian TNASS survey from July 2007 (Lawson and Gosselin, 2009). We made several attempts to contact J. Lawson regarding this survey, in the hope of incorporating it into our model, but received no response. We remain hopeful that a collaboration can be established in the future, and the Canadian TNASS data may be incorporated into a new version of our model.

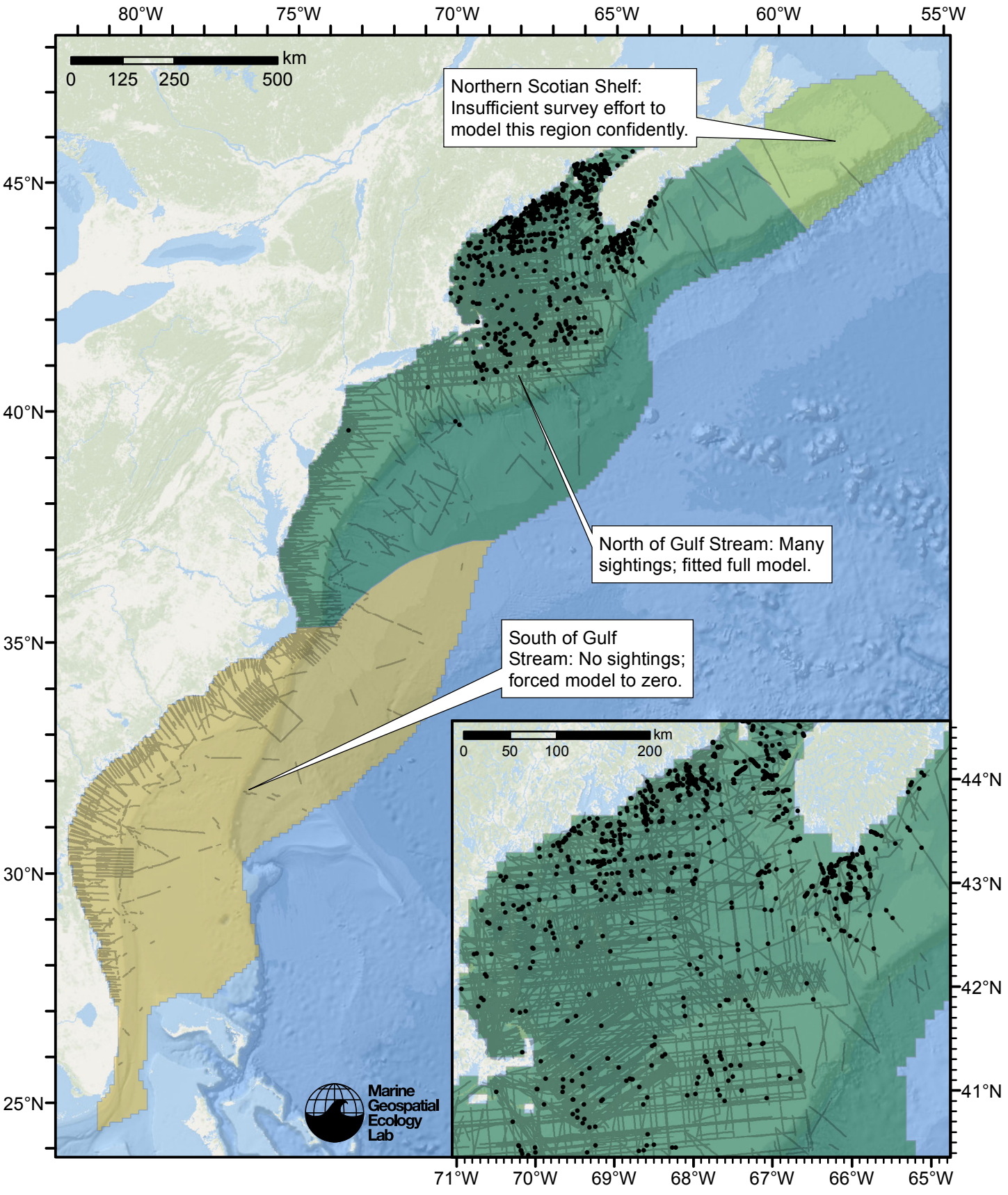

Figure 72: Harbor porpoise density model schematic for Summer season. All on-effort sightings are shown, including those that were truncated when detection functions were fitted.

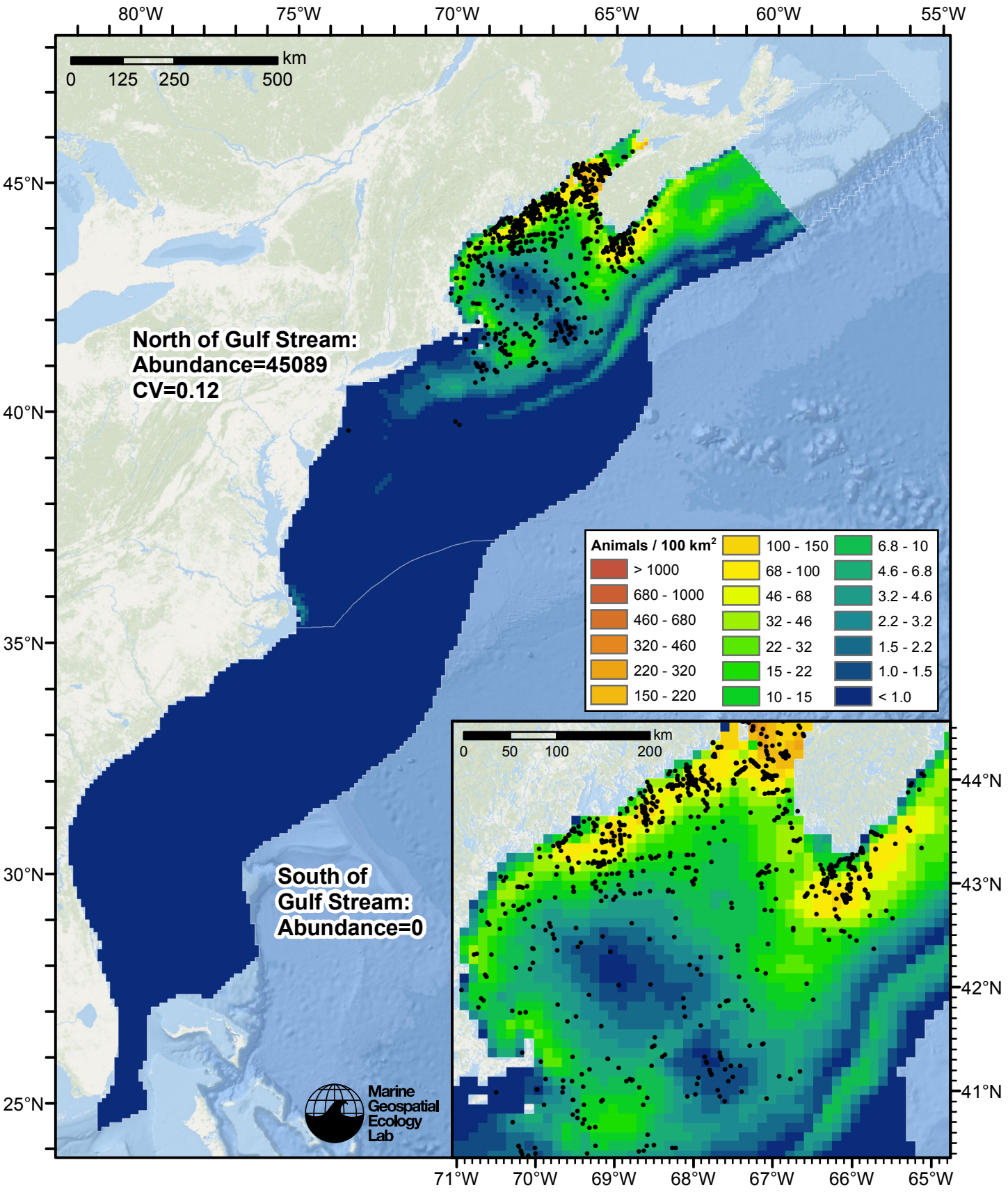

Figure 73: Harbor porpoise density predicted by the Summer season climatological model that explained the most deviance. Pixels are 10x10 km. The legend gives the estimated individuals per pixel; breaks are logarithmic. The same scale is used for all seasons. Abundance for each region was computed by summing the density cells occuring in that region.

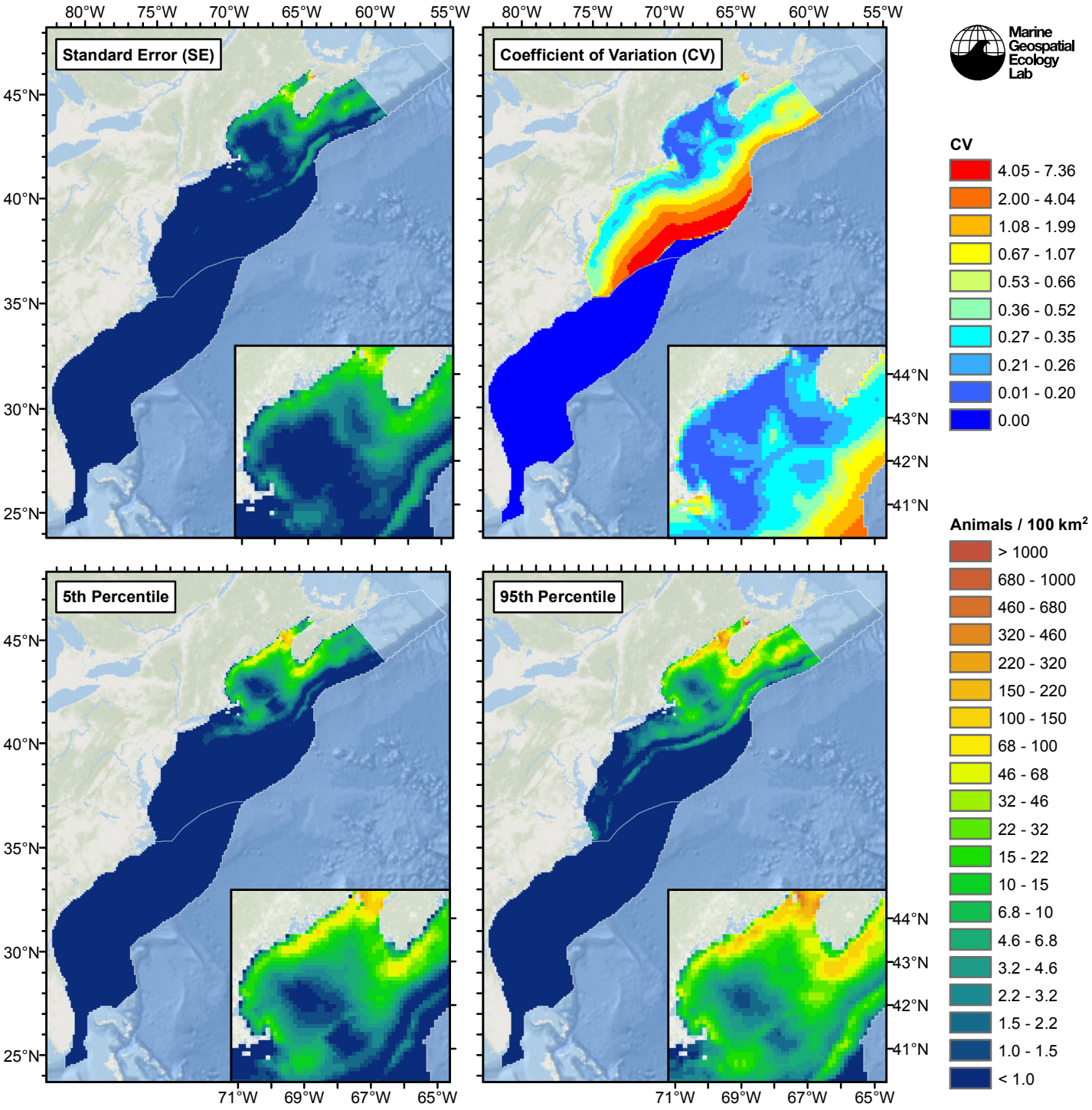

Figure 74: Estimated uncertainty for the Summer season climatological model that explained the most deviance. These estimates only incorporate the statistical uncertainty estimated for the spatial model (by the R mgcv package). They do not incorporate uncertainty in the detection functions, g(0) estimates, predictor variables, and so on.

North of Gulf Stream

Statistical output

```
Rscript.exe: This is mgcv 1.8-3. For overview type 'help("mgcv-package")'.


Family: Tweedie(p=1.374)
```

```
Link function: log

Formula:
abundance ~ offset(log(area_km2)) + s(log10(Depth), bs = "ts",
    k = 5) + s(sqrt(DistToShore/1000), bs = "ts", k = 5) + s(I(DistTo125m/1000),
    bs = "ts", k = 5) + s(I(DistTo300m/1000), bs = "ts", k = 5) +
    s(ClimSST, bs = "ts", k = 5) + s(log10(pmax(ClimEKE, 1e-04)),
    bs = "ts", k = 5) + s(log10(pmax(ClimPkPP, 0.1)), bs = "ts",
    k = 5)

Parametric coefficients:
            Estimate Std. Error t value Pr(>|t|)
(Intercept)  -4.1203     0.1498  -27.51   <2e-16 ***
---
Signif. codes:  0 '***' 0.001 '**' 0.01 '*' 0.05 '.' 0.1 ' ' 1

Approximate significance of smooth terms:
                                edf Ref.df      F  p-value
s(log10(Depth))               3.459      4 16.463 3.26e-16 ***
s(sqrt(DistToShore/1000))     2.745      4 29.834  < 2e-16 ***
s(I(DistTo125m/1000))         1.871      4  9.874 3.08e-11 ***
s(I(DistTo300m/1000))         3.839      4 22.612  < 2e-16 ***
s(ClimSST)                    3.234      4 38.029  < 2e-16 ***
s(log10(pmax(ClimEKE, 1e-04))) 3.032      4  7.886 1.06e-07 ***
s(log10(pmax(ClimPkPP, 0.1)))  1.220      4 10.717 9.51e-12 ***
---
Signif. codes:  0 '***' 0.001 '**' 0.01 '*' 0.05 '.' 0.1 ' ' 1

R-sq.(adj) =  0.0903   Deviance explained = 37.8%
-REML = 3845.3  Scale est. = 42.798    n = 11393

All predictors were significant. This is the final model.
Creating term plots.
Diagnostic output from gam.check():

Method: REML   Optimizer: outer newton
full convergence after 14 iterations.
Gradient range [-0.0004580228,0.0001176233]
(score 3845.35 & scale 42.7983).
Hessian positive definite, eigenvalue range [0.3404671,1169.564].
Model rank =  29 / 29

Basis dimension (k) checking results. Low p-value (k-index<1) may
indicate that k is too low, especially if edf is close to k'.

                                k'   edf k-index p-value
s(log10(Depth))               4.000 3.459   0.722    0.00
s(sqrt(DistToShore/1000))     4.000 2.745   0.749    0.28
s(I(DistTo125m/1000))         4.000 1.871   0.733    0.00
s(I(DistTo300m/1000))         4.000 3.839   0.731    0.02
s(ClimSST)                    4.000 3.234   0.655    0.00
s(log10(pmax(ClimEKE, 1e-04))) 4.000 3.032   0.738    0.06
s(log10(pmax(ClimPkPP, 0.1)))  4.000 1.220   0.750    0.45

Predictors retained during the model selection procedure: Depth, DistToShore, DistTo125m,
DistTo300m, ClimSST, ClimEKE, ClimPkPP

Predictors dropped during the model selection procedure: Slope, ClimDistToFront1
```

Model term plots

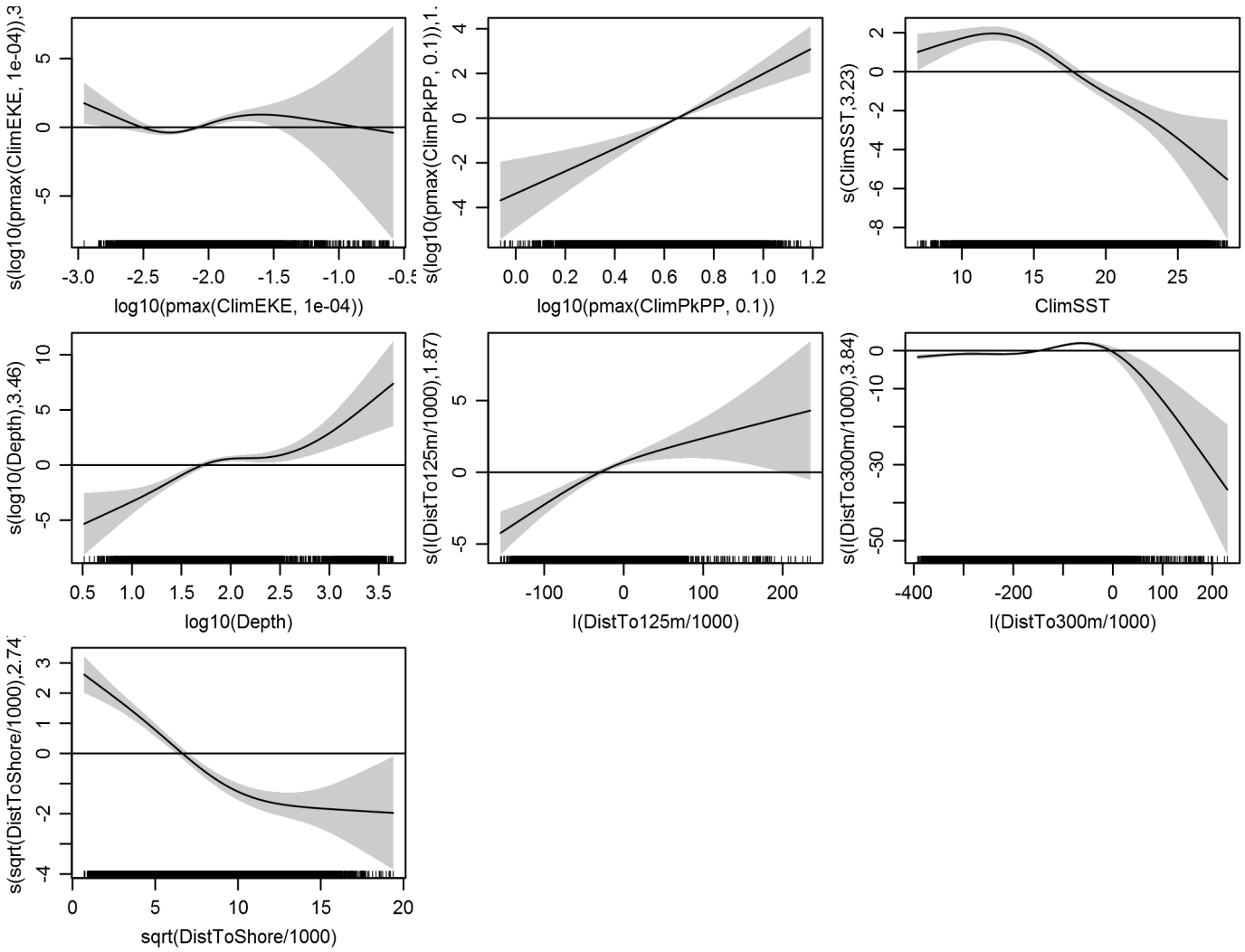

Diagnostic plots

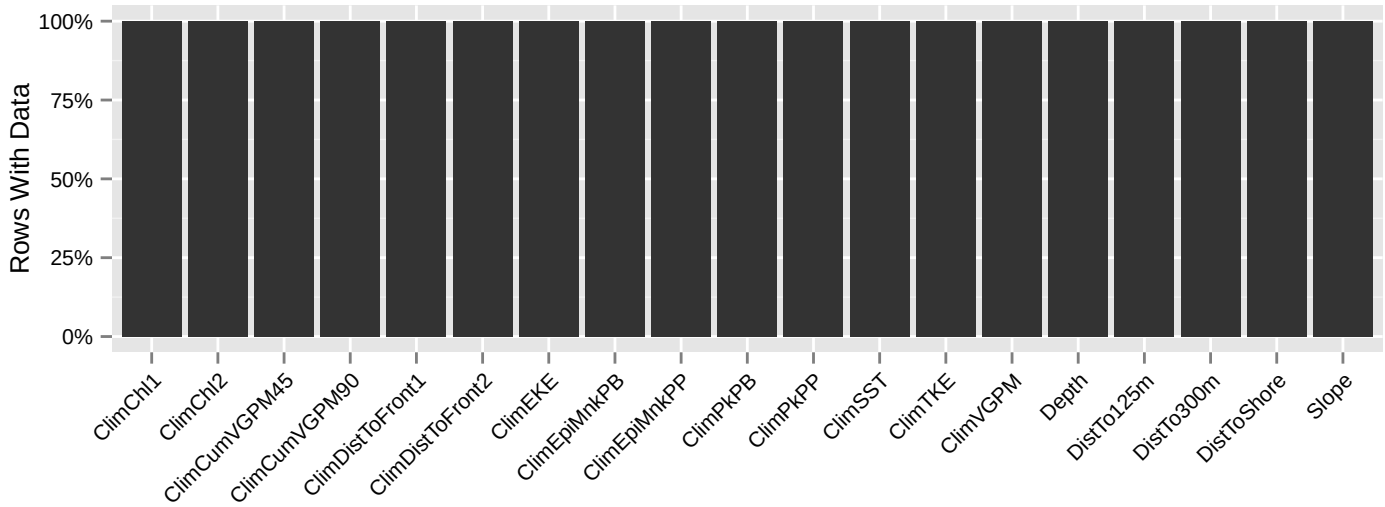

Figure 75: Segments with predictor values for the Harbor porpoise Climatological model, Summer season, North of Gulf Stream. This plot is used to assess how many segments would be lost by including a given predictor in a model.

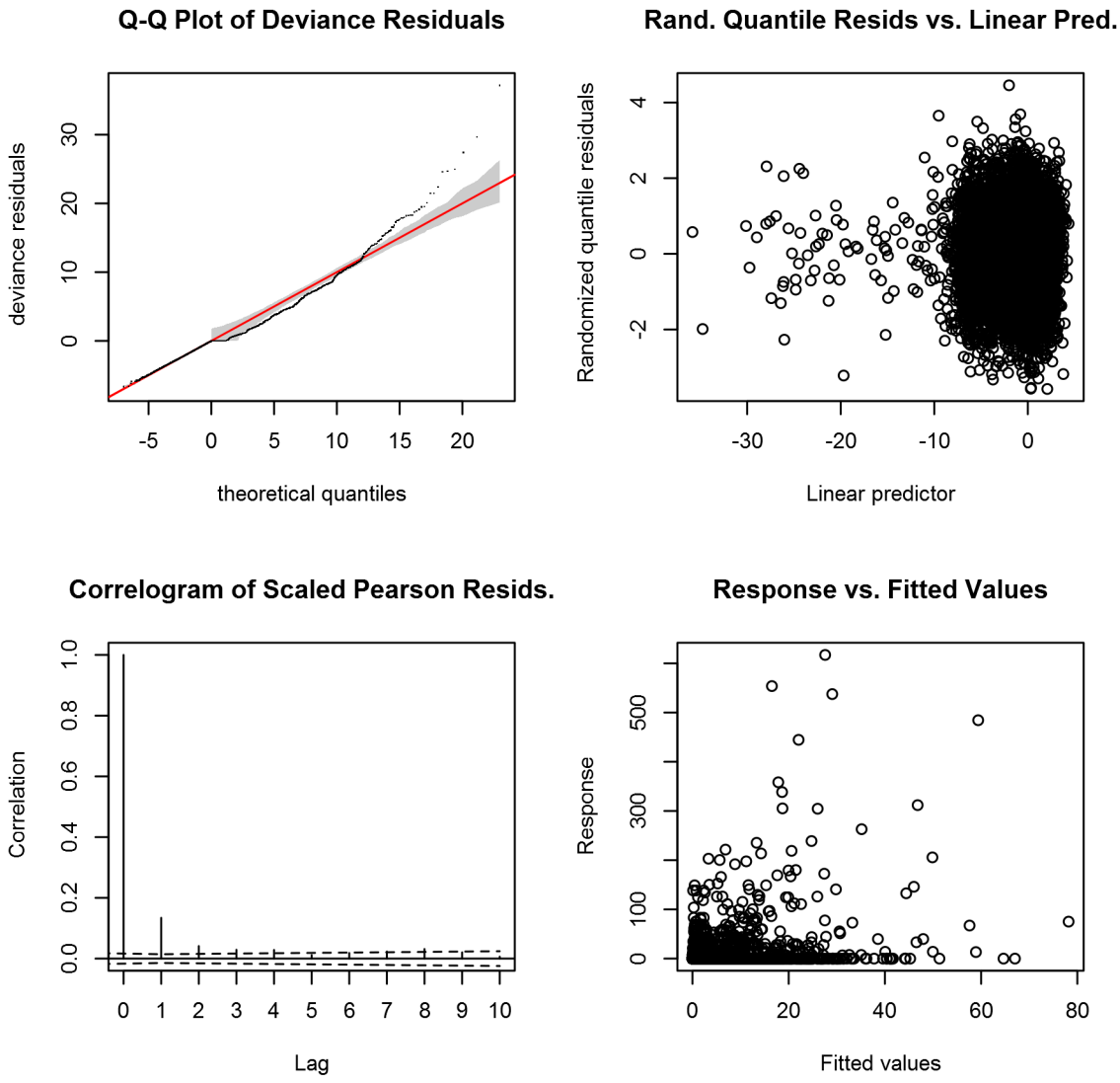

Figure 76: Statistical diagnostic plots for the Harbor porpoise Climatological model, Summer season, North of Gulf Stream.

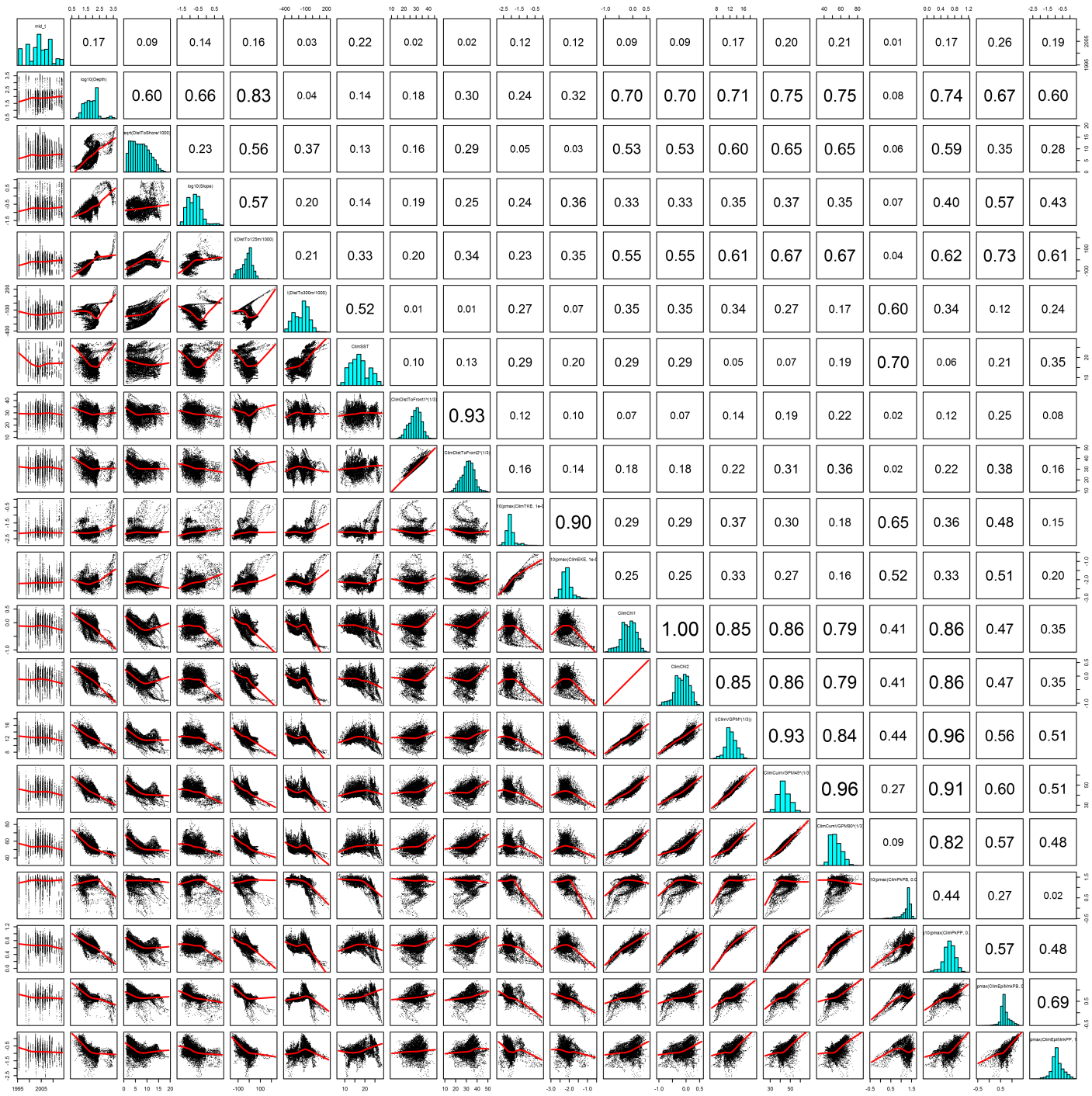

Figure 77: Scatterplot matrix for the Harbor porpoise Climatological model, Summer season, North of Gulf Stream. This plot is used to inspect the distribution of predictors (via histograms along the diagonal), simple correlation between predictors (via pairwise Pearson coefficients above the diagonal), and linearity of predictor correlations (via scatterplots below the diagonal). This plot is best viewed at high magnification.

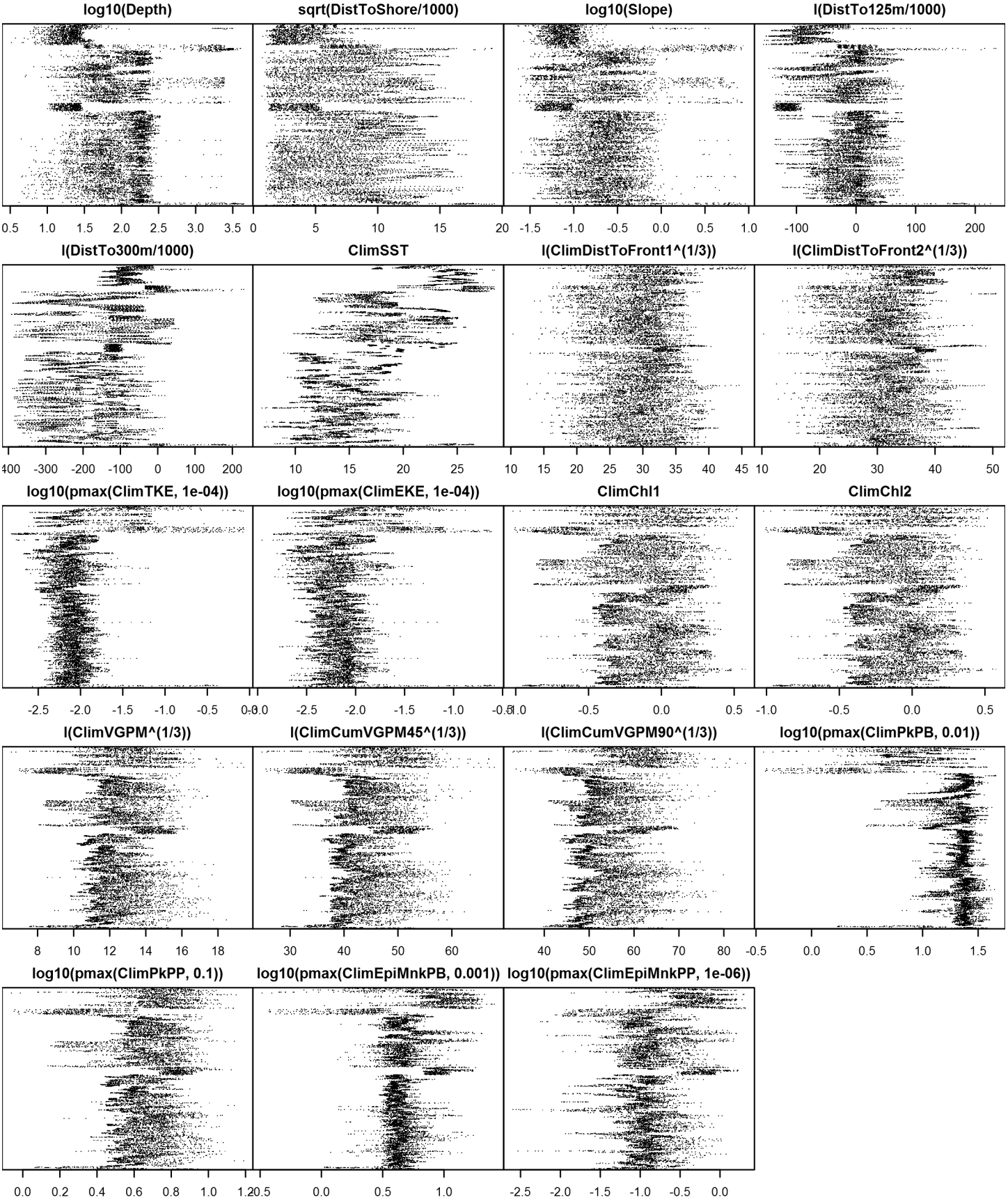

Figure 78: Dotplot for the Harbor porpoise Climatological model, Summer season, North of Gulf Stream. This plot is used to check for suspicious patterns and outliers in the data. Points are ordered vertically by transect ID, sequentially in time.

Northern Scotian Shelf

Density was not modeled for this region.

South of Gulf Stream

Density assumed to be 0 in this region.

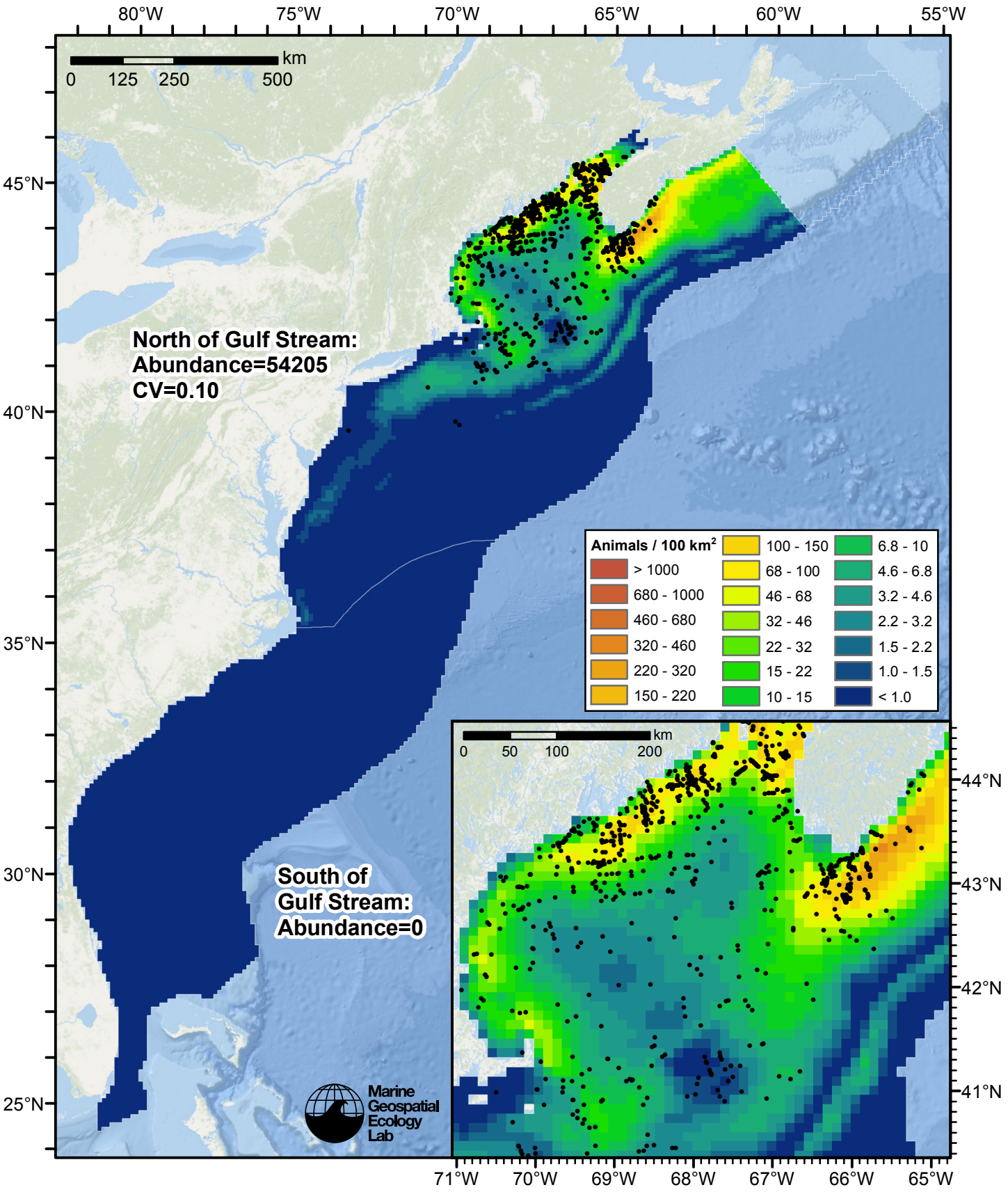

Figure 79: Harbor porpoise density predicted by the Summer season contemporaneous model that explained the most deviance. Pixels are 10x10 km. The legend gives the estimated individuals per pixel; breaks are logarithmic. The same scale is used for all seasons. Abundance for each region was computed by summing the density cells occuring in that region.

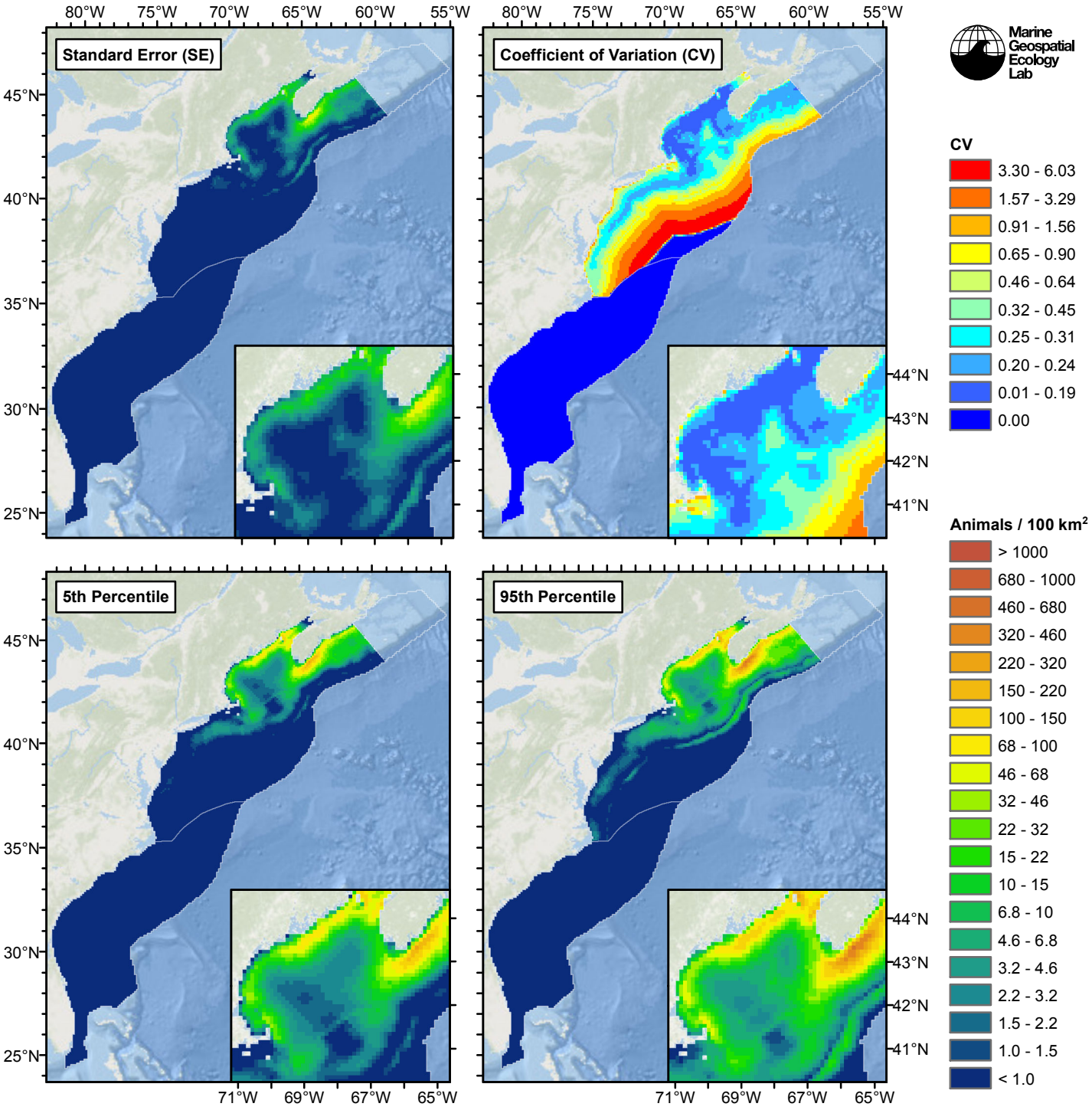

Figure 80: Estimated uncertainty for the Summer season contemporaneous model that explained the most deviance. These estimates only incorporate the statistical uncertainty estimated for the spatial model (by the R mgcv package). They do not incorporate uncertainty in the detection functions, g(0) estimates, predictor variables, and so on.

North of Gulf Stream

Statistical output

```
Rscript.exe: This is mgcv 1.8-3. For overview type 'help("mgcv-package")'.


Family: Tweedie(p=1.386)
```

```
Link function: log

Formula:
abundance ~ offset(log(area_km2)) + s(log10(Depth), bs = "ts",
    k = 5) + s(sqrt(DistToShore/1000), bs = "ts", k = 5) + s(I(DistTo125m/1000),
    bs = "ts", k = 5) + s(I(DistTo300m/1000), bs = "ts", k = 5) +
    s(SST, bs = "ts", k = 5) + s(I(DistToFront1^(1/3)), bs = "ts",
    k = 5) + s(log10(pmax(TKE, 1e-04)), bs = "ts", k = 5)

Parametric coefficients:
            Estimate Std. Error t value Pr(>|t|)
(Intercept)   -3.903      0.131  -29.79   <2e-16 ***
---
Signif. codes:  0 '***' 0.001 '**' 0.01 '*' 0.05 '.' 0.1 ' ' 1

Approximate significance of smooth terms:
                              edf Ref.df      F  p-value
s(log10(Depth))            3.6538      4 14.436 1.67e-13 ***
s(sqrt(DistToShore/1000))  3.5111      4 40.472  < 2e-16 ***
s(I(DistTo125m/1000))      2.1831      4 10.627 2.21e-11 ***
s(I(DistTo300m/1000))      3.8868      4 17.121 8.20e-15 ***
s(SST)                     3.2585      4 26.806  < 2e-16 ***
s(I(DistToFront1^(1/3)))   0.8806      4  1.272   0.0139 *
s(log10(pmax(TKE, 1e-04))) 2.3434      4  5.527 6.16e-06 ***
---
Signif. codes:  0 '***' 0.001 '**' 0.01 '*' 0.05 '.' 0.1 ' ' 1

R-sq.(adj) =  0.0695   Deviance explained = 34.5%
-REML =   3890  Scale est. = 44.87     n = 11393

All predictors were significant. This is the final model.
Creating term plots.
Diagnostic output from gam.check():

Method: REML   Optimizer: outer newton
full convergence after 11 iterations.
Gradient range [-1.530788e-06,2.043466e-07]
(score 3890.046 & scale 44.86982).
Hessian positive definite, eigenvalue range [0.3382015,1152.942].
Model rank =  29 / 29

Basis dimension (k) checking results. Low p-value (k-index<1) may
indicate that k is too low, especially if edf is close to k'.

                              k'   edf k-index p-value
s(log10(Depth))            4.000 3.654   0.705    0.02
s(sqrt(DistToShore/1000))  4.000 3.511   0.724    0.26
s(I(DistTo125m/1000))      4.000 2.183   0.707    0.00
s(I(DistTo300m/1000))      4.000 3.887   0.716    0.11
s(SST)                     4.000 3.259   0.695    0.00
s(I(DistToFront1^(1/3)))   4.000 0.881   0.738    0.80
s(log10(pmax(TKE, 1e-04))) 4.000 2.343   0.730    0.46

Predictors retained during the model selection procedure: Depth, DistToShore, DistTo125m,
DistTo300m, SST, DistToFront1, TKE

Predictors dropped during the model selection procedure: Slope
```

Model term plots

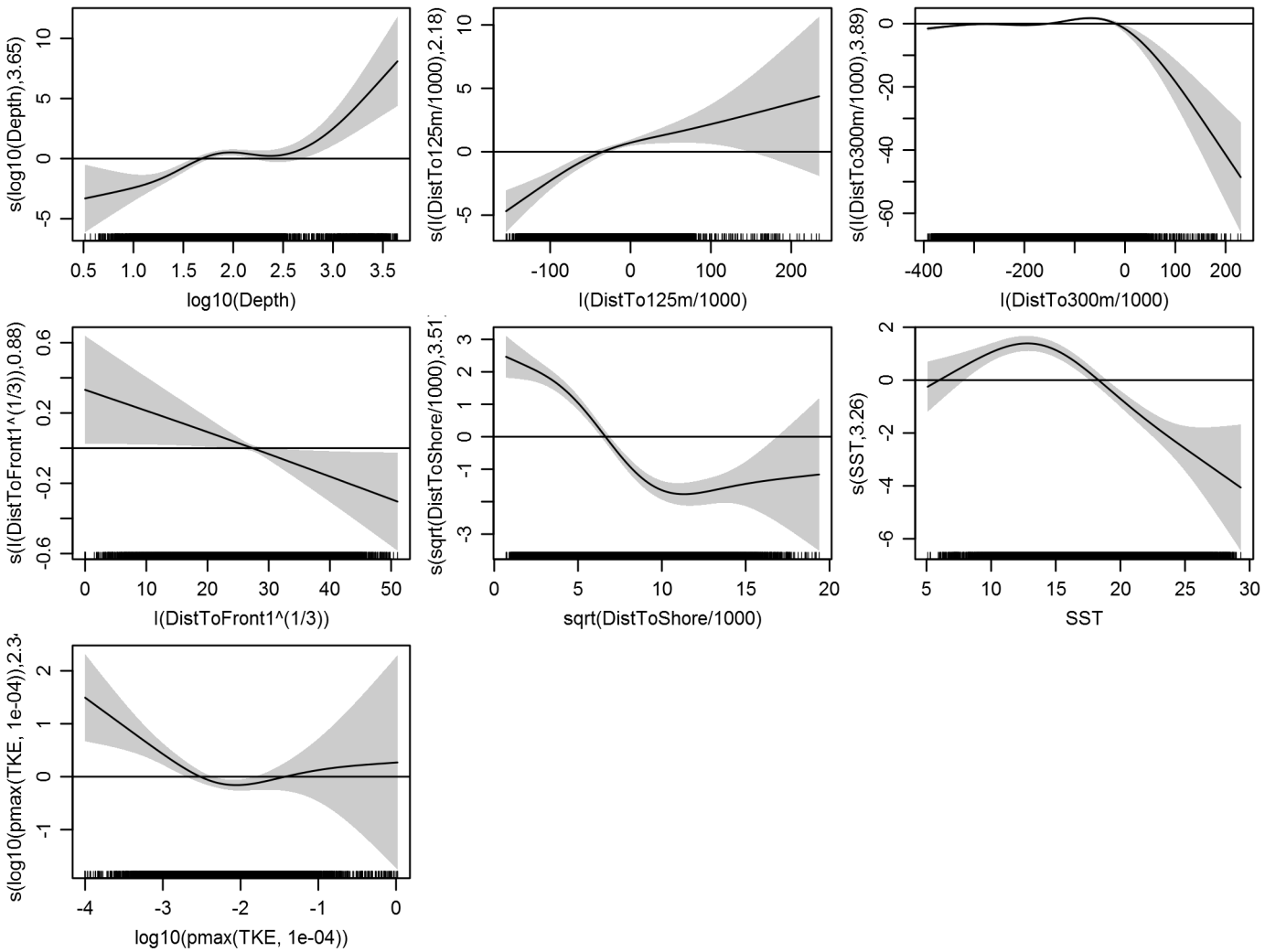

Diagnostic plots

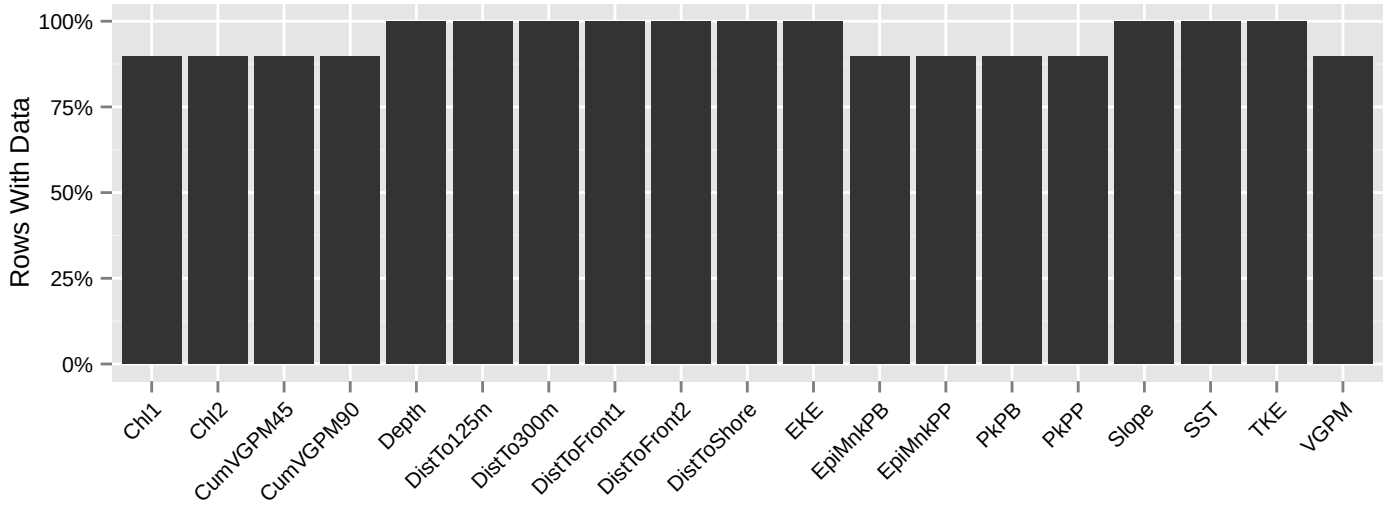

Figure 81: Segments with predictor values for the Harbor porpoise Contemporaneous model, Summer season, North of Gulf Stream. This plot is used to assess how many segments would be lost by including a given predictor in a model.

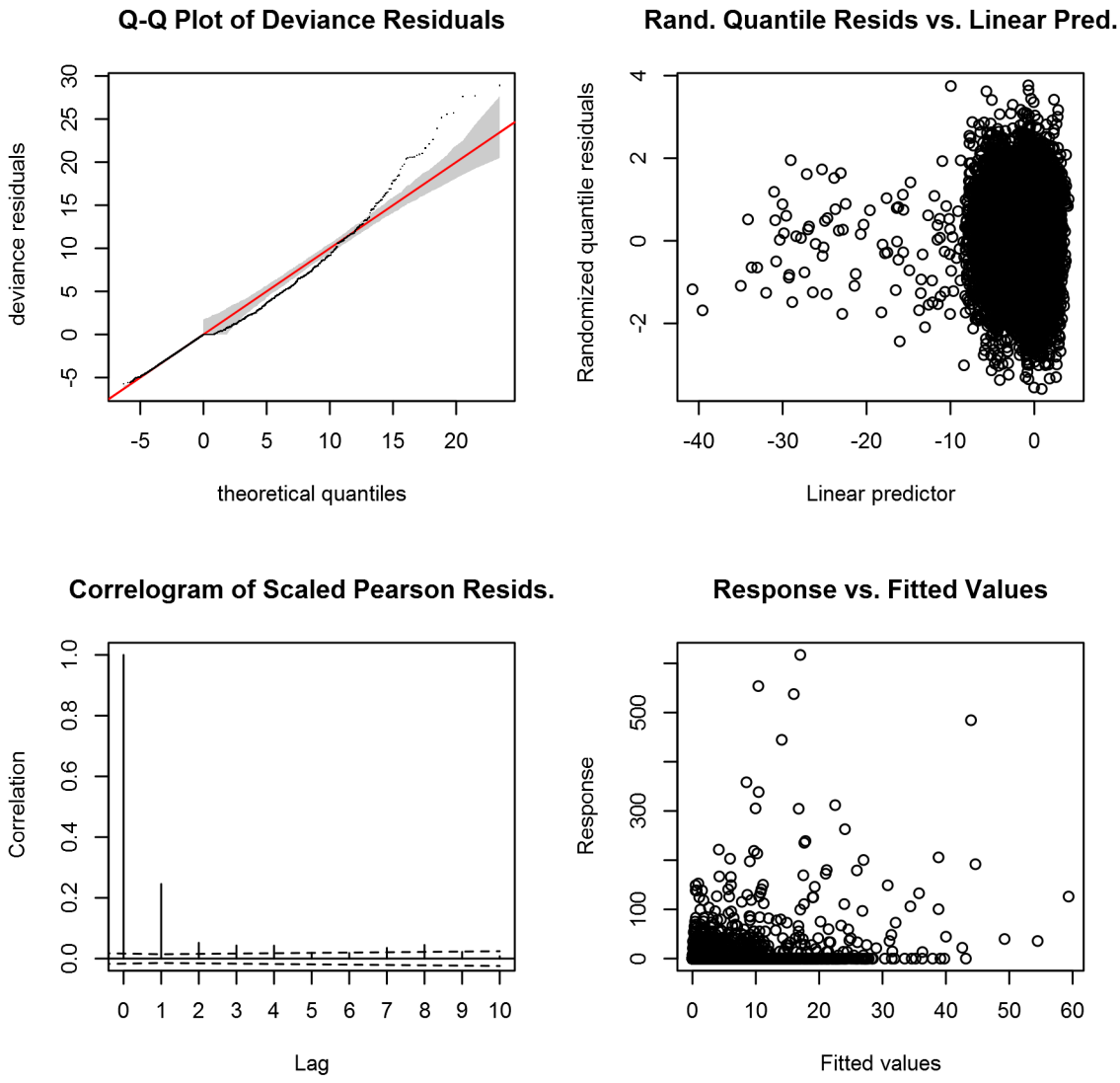

Figure 82: Statistical diagnostic plots for the Harbor porpoise Contemporaneous model, Summer season, North of Gulf Stream.

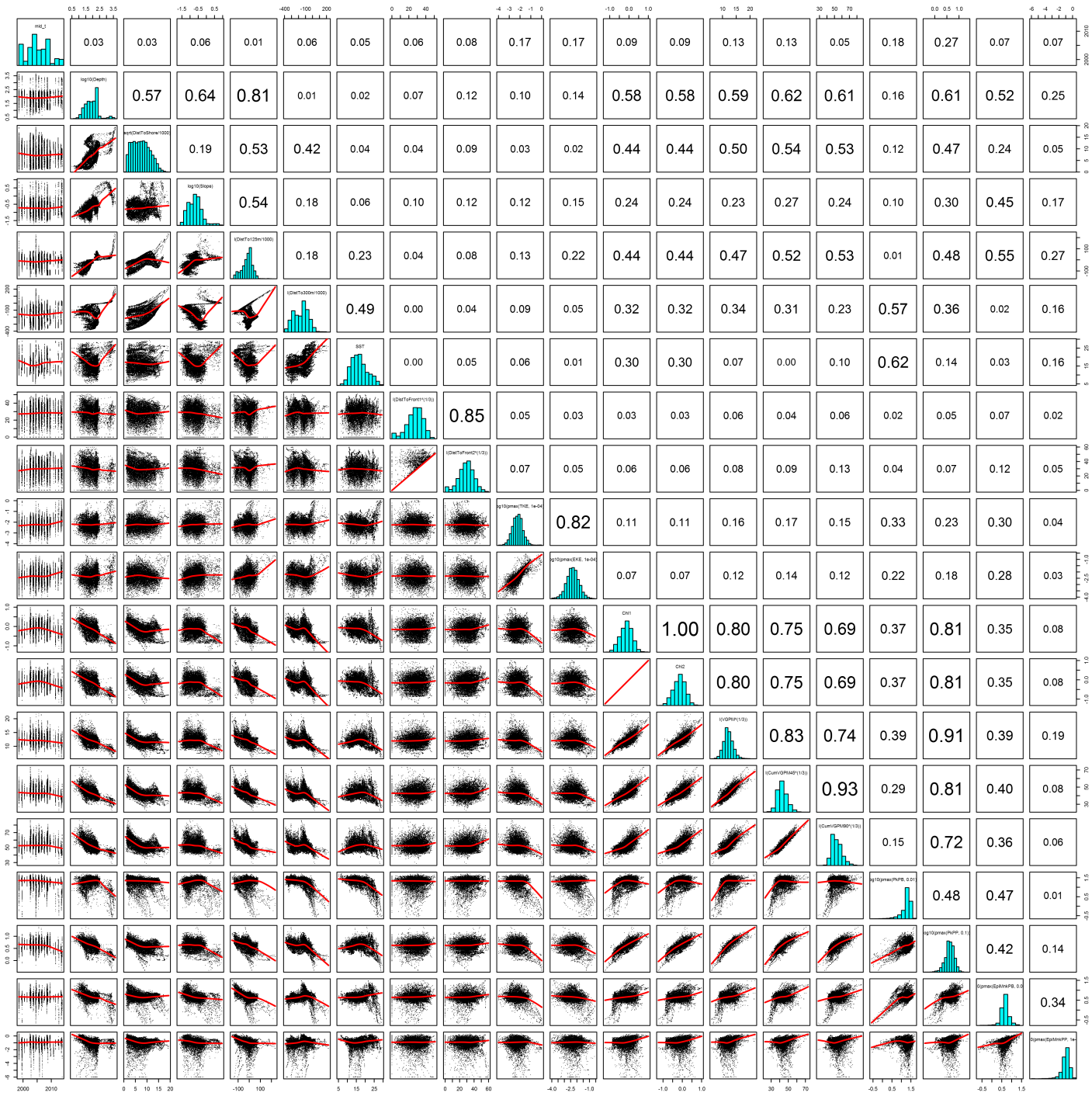

Figure 83: Scatterplot matrix for the Harbor porpoise Contemporaneous model, Summer season, North of Gulf Stream. This plot is used to inspect the distribution of predictors (via histograms along the diagonal), simple correlation between predictors (via pairwise Pearson coefficients above the diagonal), and linearity of predictor correlations (via scatterplots below the diagonal). This plot is best viewed at high magnification.

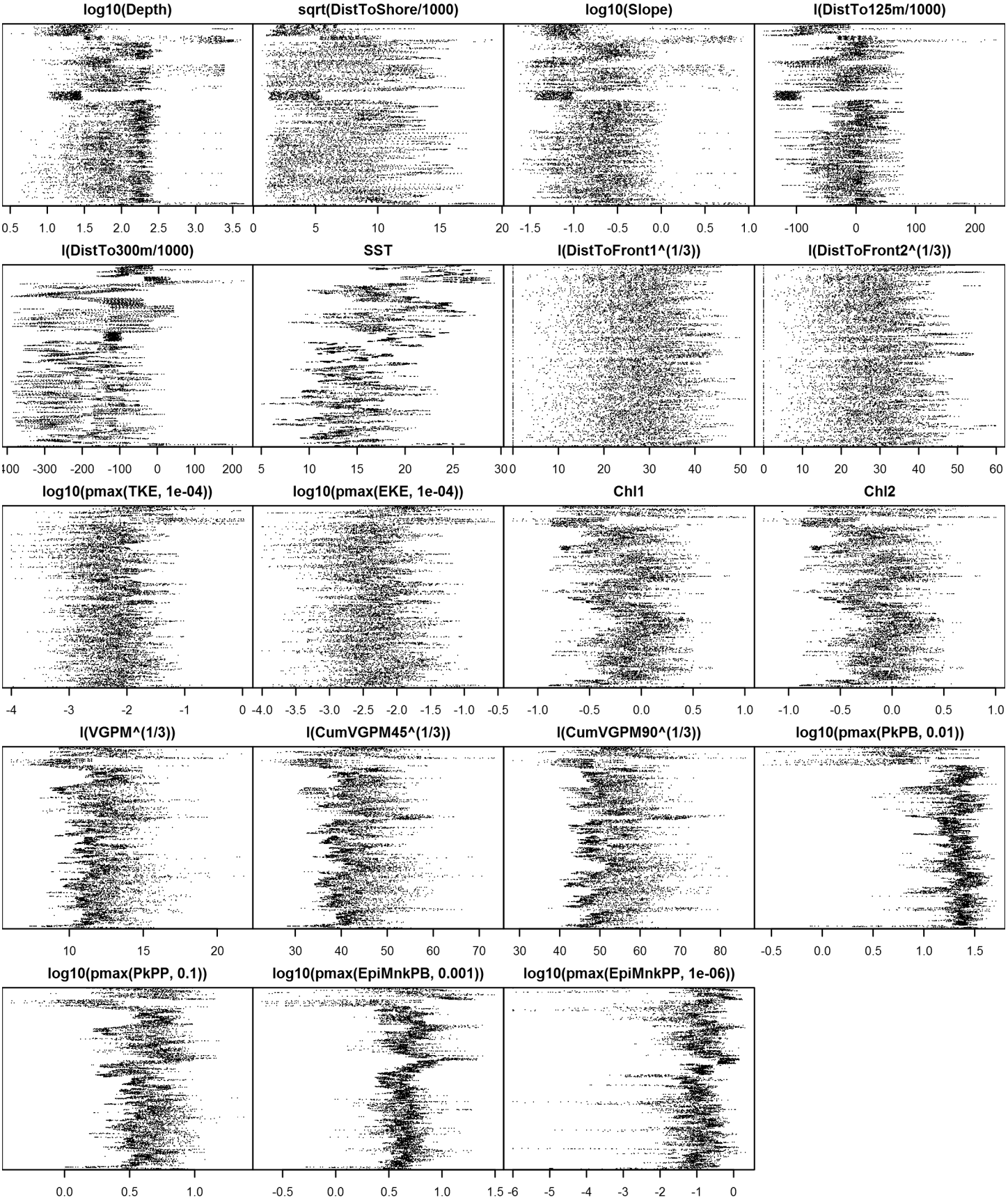

Figure 84: Dotplot for the Harbor porpoise Contemporaneous model, Summer season, North of Gulf Stream. This plot is used to check for suspicious patterns and outliers in the data. Points are ordered vertically by transect ID, sequentially in time.

Northern Scotian Shelf

Density was not modeled for this region.

South of Gulf Stream

Density assumed to be 0 in this region.

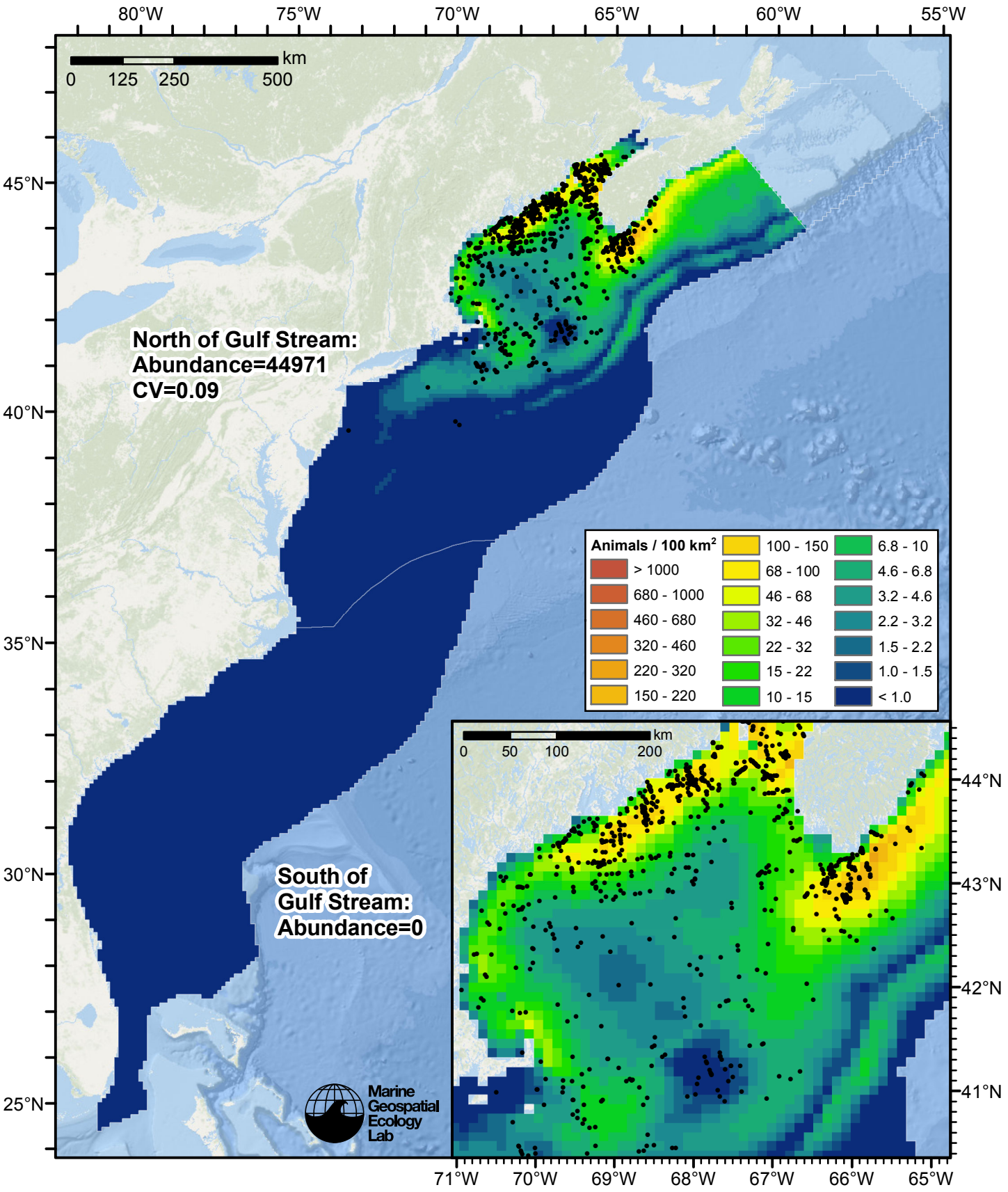

Figure 85: Harbor porpoise density predicted by the Summer season climatological same segments model that explained the most deviance. Pixels are 10x10 km. The legend gives the estimated individuals per pixel; breaks are logarithmic. The same scale is used for all seasons. Abundance for each region was computed by summing the density cells occuring in that region.

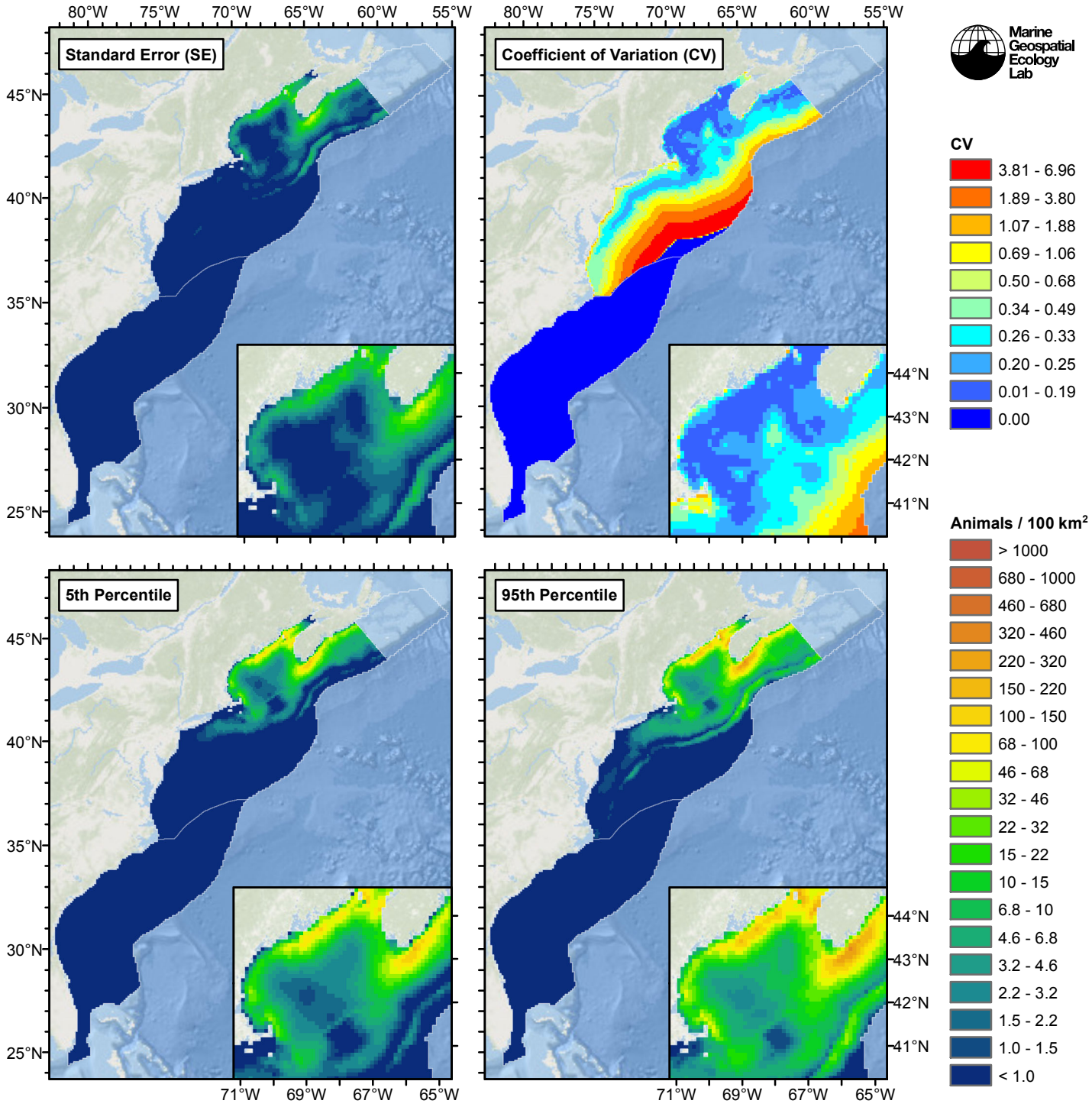

Figure 86: Estimated uncertainty for the Summer season climatological same segments model that explained the most deviance. These estimates only incorporate the statistical uncertainty estimated for the spatial model (by the R mgcv package). They do not incorporate uncertainty in the detection functions, g(0) estimates, predictor variables, and so on.

North of Gulf Stream

Statistical output

```
Rscript.exe: This is mgcv 1.8-3. For overview type 'help("mgcv-package")'.


Family: Tweedie(p=1.388)
```

```
Link function: log

Formula:
abundance ~ offset(log(area_km2)) + s(log10(Depth), bs = "ts",
    k = 5) + s(sqrt(DistToShore/1000), bs = "ts", k = 5) + s(I(DistTo125m/1000),
    bs = "ts", k = 5) + s(I(DistTo300m/1000), bs = "ts", k = 5) +
    s(ClimSST, bs = "ts", k = 5) + s(I(ClimDistToFront1^(1/3)),
    bs = "ts", k = 5)

Parametric coefficients:
            Estimate Std. Error t value Pr(>|t|)
(Intercept)  -4.0925     0.1516     -27   <2e-16 ***
---
Signif. codes:  0 '***' 0.001 '**' 0.01 '*' 0.05 '.' 0.1 ' ' 1

Approximate significance of smooth terms:
                                edf Ref.df      F  p-value
s(log10(Depth))              3.6147      4 13.860 4.38e-13 ***
s(sqrt(DistToShore/1000))    3.3871      4 39.296  < 2e-16 ***
s(I(DistTo125m/1000))        1.9571      4  7.534 1.51e-08 ***
s(I(DistTo300m/1000))        3.8466      4 13.987 3.60e-12 ***
s(ClimSST)                   3.4059      4 35.843  < 2e-16 ***
s(I(ClimDistToFront1^(1/3))) 0.9292      4  2.010  0.00228 **
---
Signif. codes:  0 '***' 0.001 '**' 0.01 '*' 0.05 '.' 0.1 ' ' 1

R-sq.(adj) =  0.0612   Deviance explained = 35.4%
-REML = 3871.4  Scale est. = 44.417    n = 11393

All predictors were significant. This is the final model.
Creating term plots.
Diagnostic output from gam.check():

Method: REML   Optimizer: outer newton
full convergence after 12 iterations.
Gradient range [-0.001167911,0.0001763663]
(score 3871.364 & scale 44.41728).
Hessian positive definite, eigenvalue range [0.1799804,1141.421].
Model rank =  25 / 25

Basis dimension (k) checking results. Low p-value (k-index<1) may
indicate that k is too low, especially if edf is close to k'.

                               k'   edf k-index p-value
s(log10(Depth))             4.000 3.615   0.737    0.12
s(sqrt(DistToShore/1000))   4.000 3.387   0.757    0.77
s(I(DistTo125m/1000))       4.000 1.957   0.733    0.06
s(I(DistTo300m/1000))       4.000 3.847   0.730    0.04
s(ClimSST)                  4.000 3.406   0.726    0.02
s(I(ClimDistToFront1^(1/3))) 4.000 0.929   0.756    0.64

Predictors retained during the model selection procedure: Depth, DistToShore, DistTo125m,
DistTo300m, ClimSST, ClimDistToFront1

Predictors dropped during the model selection procedure: Slope
```

Model term plots

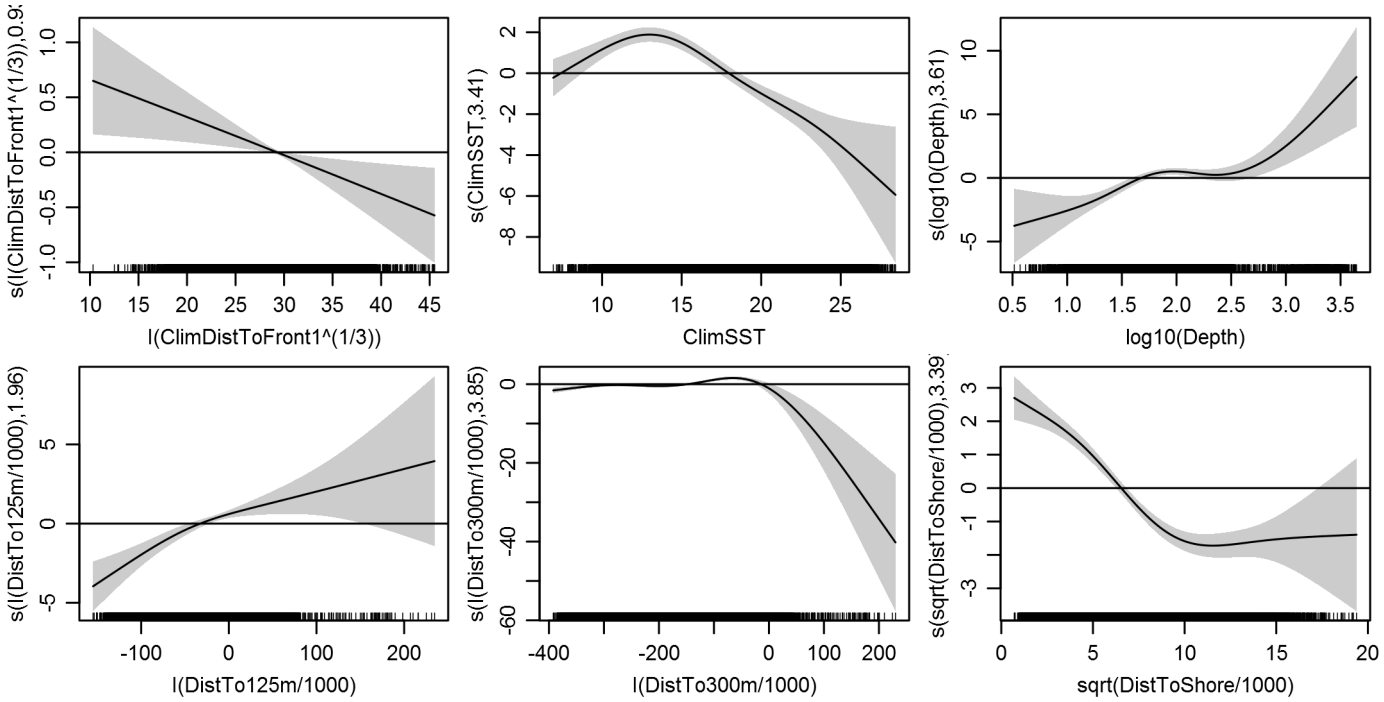

Diagnostic plots

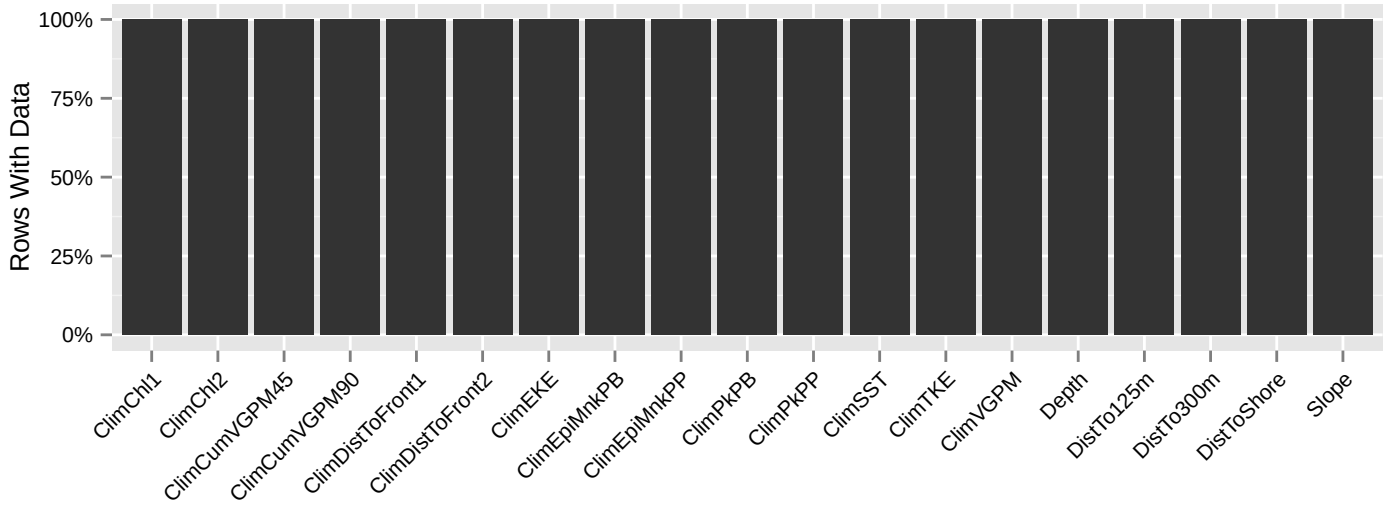

Figure 87: Segments with predictor values for the Harbor porpoise Climatological model, Summer season, North of Gulf Stream. This plot is used to assess how many segments would be lost by including a given predictor in a model.

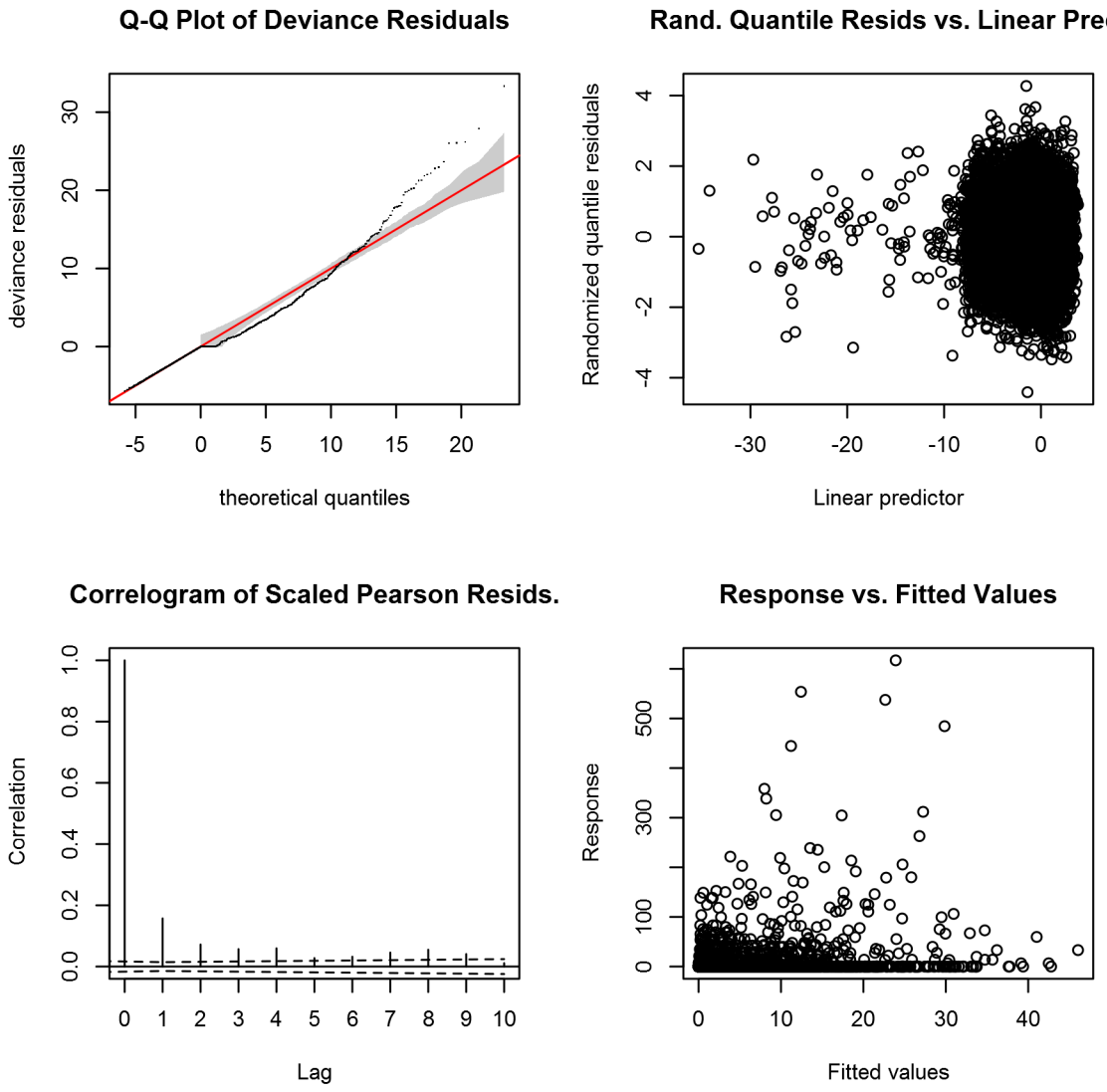

Figure 88: Statistical diagnostic plots for the Harbor porpoise Climatological model, Summer season, North of Gulf Stream.

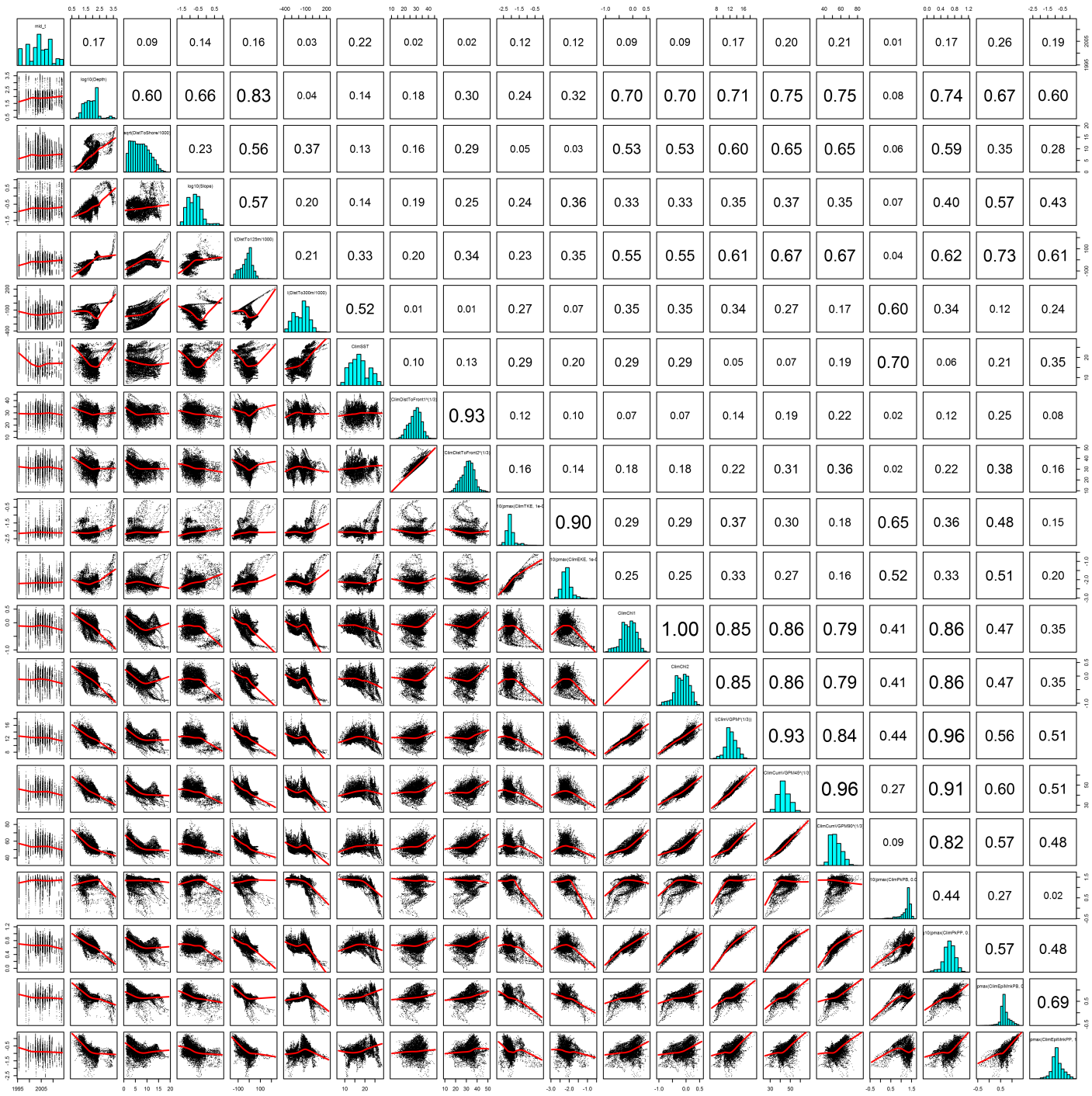

Figure 89: Scatterplot matrix for the Harbor porpoise Climatological model, Summer season, North of Gulf Stream. This plot is used to inspect the distribution of predictors (via histograms along the diagonal), simple correlation between predictors (via pairwise Pearson coefficients above the diagonal), and linearity of predictor correlations (via scatterplots below the diagonal). This plot is best viewed at high magnification.

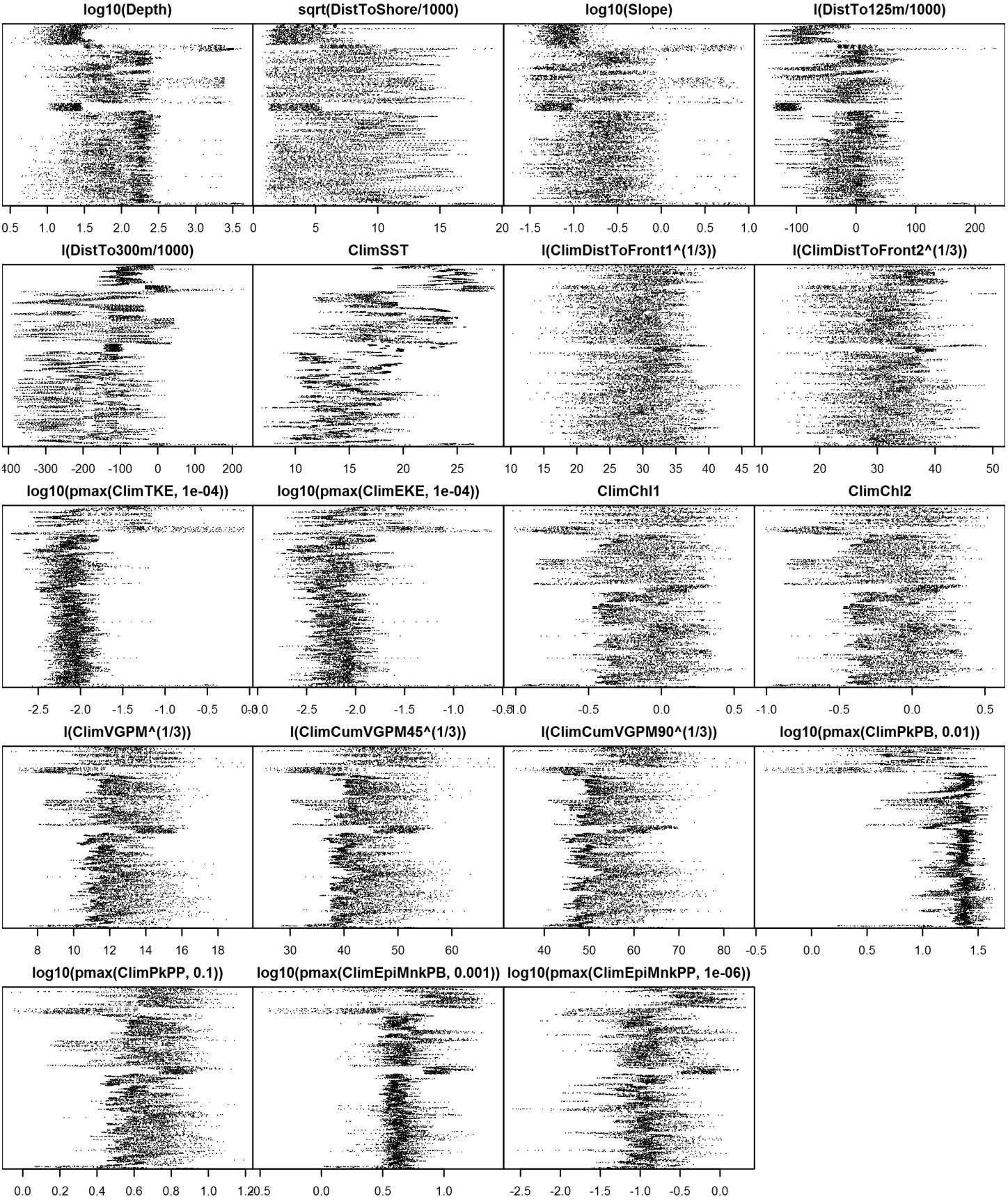

Figure 90: Dotplot for the Harbor porpoise Climatological model, Summer season, North of Gulf Stream. This plot is used to check for suspicious patterns and outliers in the data. Points are ordered vertically by transect ID, sequentially in time.

Northern Scotian Shelf

Density was not modeled for this region.

South of Gulf Stream

Density assumed to be 0 in this region.

Model Comparison

Spatial Model Performance

The table below summarizes the performance of the candidate spatial models that were tested. For each season, the first model contained only physiographic predictors. Subsequent models added additional suites of predictors of based on when they became available via remote sensing.

For each model, three versions were fitted; the % Dev Expl columns give the % deviance explained by each one. The "climatological" models were fitted to 8-day climatologies of the environmental predictors. Because the environmental predictors were always available, no segments were lost, allowing these models to consider the maximal amount of survey data. The "contemporaneous" models were fitted to day-of-sighting images of the environmental predictors; these were smoothed to reduce data loss due to clouds, but some segments still failed to retrieve environmental values and were lost. Finally, the "climatological same segments" models fitted climatological predictors to the segments retained by the contemporaneous model, so that the explantory power of the two types of predictors could be directly compared. For each of the three models, predictors were selected independently via shrinkage smoothers; thus the three models did not necessarily utilize the same predictors.

Predictors derived from ocean currents first became available in January 1993 after the launch of the TOPEX/Poseidon satellite; productivity predictors first became available in September 1997 after the launch of the SeaWiFS sensor. Contemporaneous and climatological same segments models considering these predictors usually suffered data loss. Date Range shows the years spanned by the retained segments. The Segments column gives the number of segments retained; % Lost gives the percentage lost.

Season	Predictors	Climatol % Dev Expl	Contemp % Dev Expl	Climatol Same Segs % Dev Expl	Segments	% Lost	Date Range
Winter							
	Phys	37.9			21420		1992-2014
	Phys+SST	43.1	41.6	43.1	21420	0.0	1992-2014
	Phys+SST+Curr	44.5	41.1	43.7	20920	2.3	1995-2013
	Phys+SST+Curr+Prod	44.7	41.9	43.7	20611	3.8	1999-2013
Summer							
	Phys	29.9			11393		1995-2013
	Phys+SST	35.4	33.6	35.4	11393	0.0	1995-2013
	Phys+SST+Curr	35.0	34.5	35.0	11393	0.0	1995-2013
	Phys+SST+Curr+Prod	37.8	33.8	35.4	10226	10.2	1998-2013

Table 26: Deviance explained by the candidate density models.

Abundance Estimates

The table below shows the estimated mean abundance (number of animals) within the study area, for the models that explained the most deviance for each model type. Mean abundance was calculated by first predicting density maps for a series of time steps, then computing the abundance for each map, and then averaging the abundances. For the climatological models, we used 8-day climatologies, resulting in 46 abundance maps. For the contemporaneous models, we used daily images, resulting in 365 predicted abundance maps per year that the prediction spanned. The Dates column gives the dates to which the estimates apply. For our models, these are the years for which both survey data and remote sensing data were available.

The Assumed g(0)=1 column specifies whether the abundance estimate assumed that detection was certain along the survey trackline. Studies that assumed this did not correct for availability or perception bias, and therefore underestimated abundance. The In our models column specifies whether the survey data from the study was also used in our models. If not, the study provides a completely independent estimate of abundance.

Season	Dates	Model or study	Estimated abundance	CV	Assumed g(0)=1	In our models
Winter						
	1992-2014	Climatological model*	17651	0.17	No	
	1999-2013	Contemporaneous model	16330	0.13	No	
	1992-2014	Climatological same segments model	19769	0.16	No	
Summer						
	1995-2013	Climatological model*	45089	0.12	No	
	1995-2013	Contemporaneous model	54205	0.10	No	
	1995-2013	Climatological same segments model	44971	0.09	No	
	Jun-Aug 2011	Central Virginia to lower Bay of Fundy (Waring et al. 2014)	79883	0.32	No	No
	Jun-Aug 2011	Central Florida to central Virginia (Waring et al. 2014)	0	0.00	No	No
	Jul-Aug 2007	Scotian Shelf to Northern Labrador (Lawson and Gosselin 2011)	12732	0.61	No	No
	August 2006	Southern Georges Bank to Bay of Fundy and Gulf of St. Lawrence (Waring et al. 2014)	89054	0.47	No	Yes
	Jun-Aug 2004	Southern Georges Bank to lower Bay of Fundy (Waring et al. 2014)	51520	0.65	No	Yes

Table 27: Estimated mean abundance within the study area. We selected the model marked with * as our best estimate of the abundance and distribution of this taxon. For comparison, independent abundance estimates from NOAA technical reports and/or the scientific literature are shown. Please see the Discussion section below for our evaluation of our models compared to the other estimates. Our coefficients of variation (CVs) underestimate the true uncertainty in our estimates, as they only incorporated the uncertainty of the GAM stage of our models. Other sources of uncertainty include the detection functions and g(0) estimates. It was not possible to incorporate these into our CVs without undertaking a computationally-prohibitive bootstrap; we hope to attempt that in a future version of our models.

Density Maps

Climatological Model

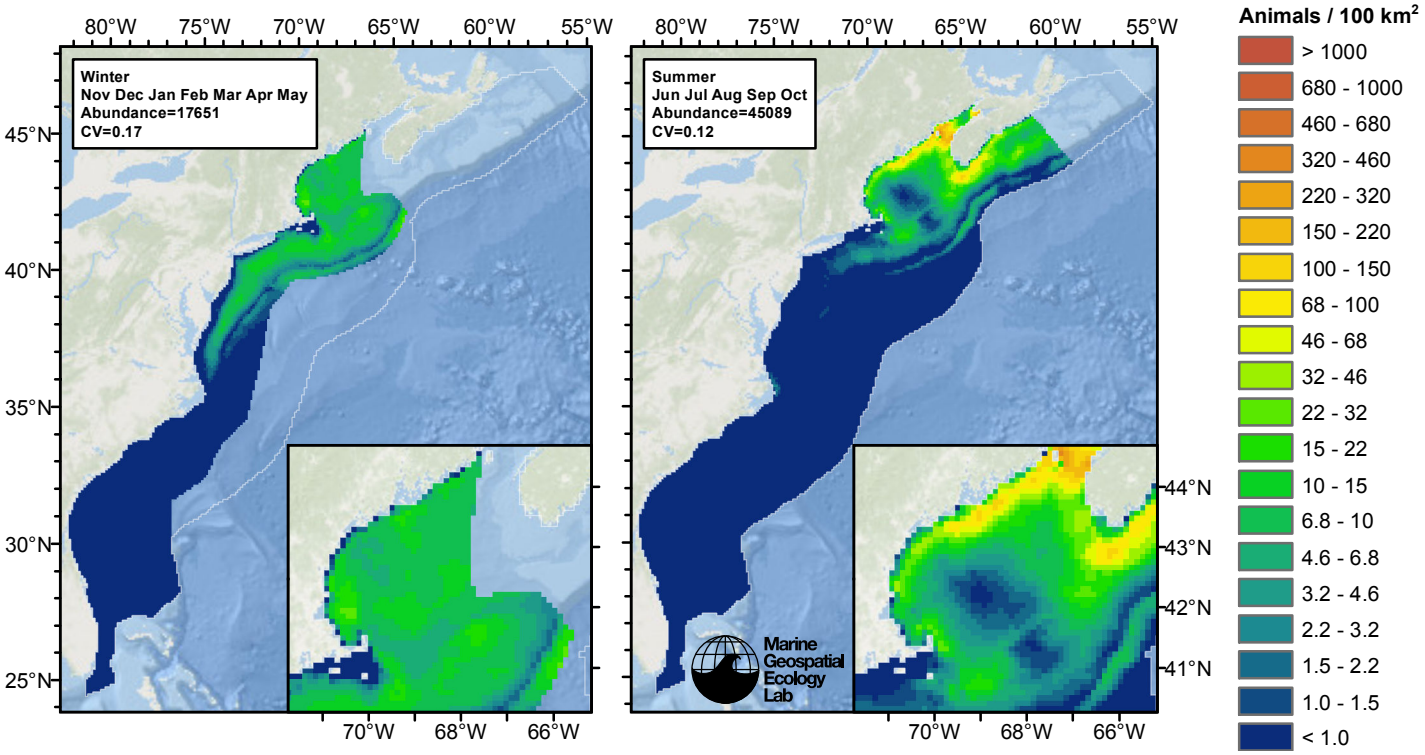

Figure 91: Harbor porpoise density and abundance predicted by the climatological model that explained the most deviance. Regions inside the study area (white line) where the background map is visible are areas we did not model (see text).

Contemporaneous Model

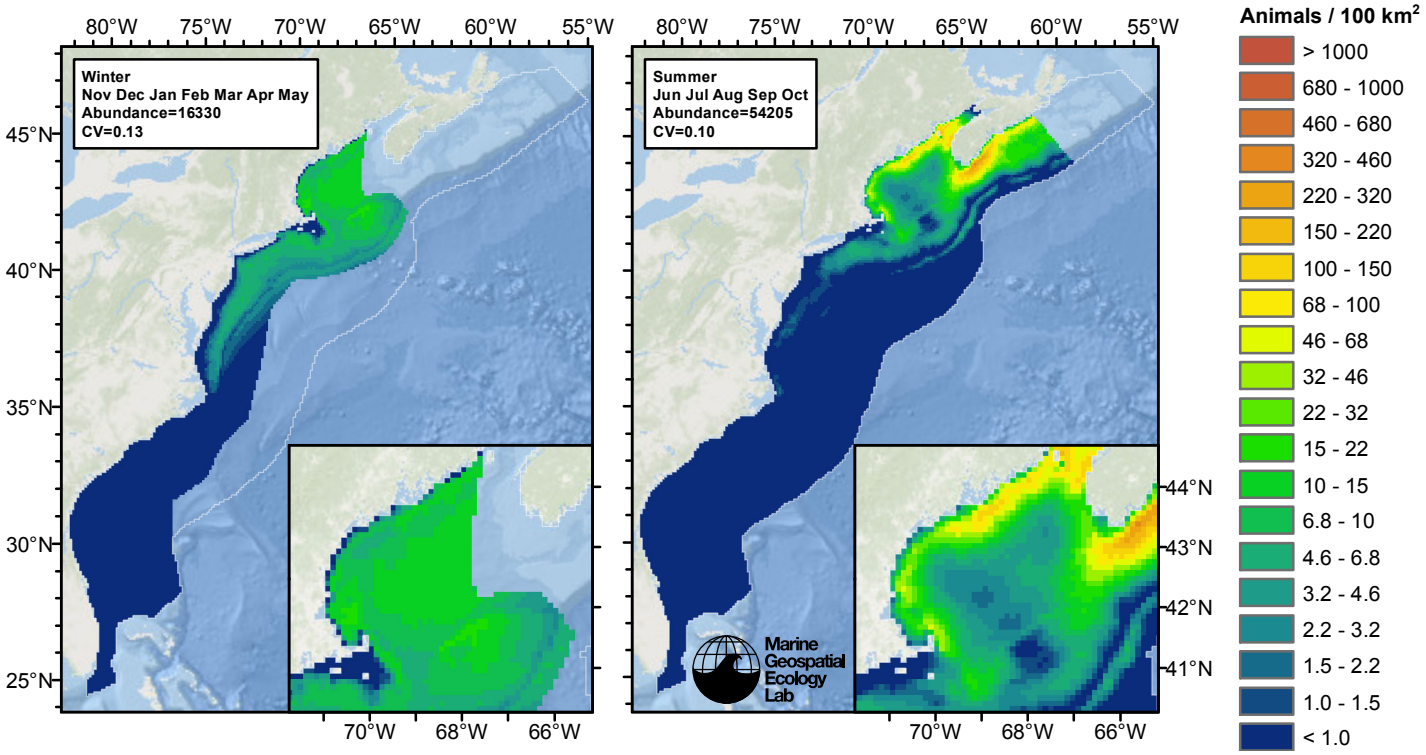

Figure 92: Harbor porpoise density and abundance predicted by the contemporaneous model that explained the most deviance. Regions inside the study area (white line) where the background map is visible are areas we did not model (see text).

Climatological Same Segments Model

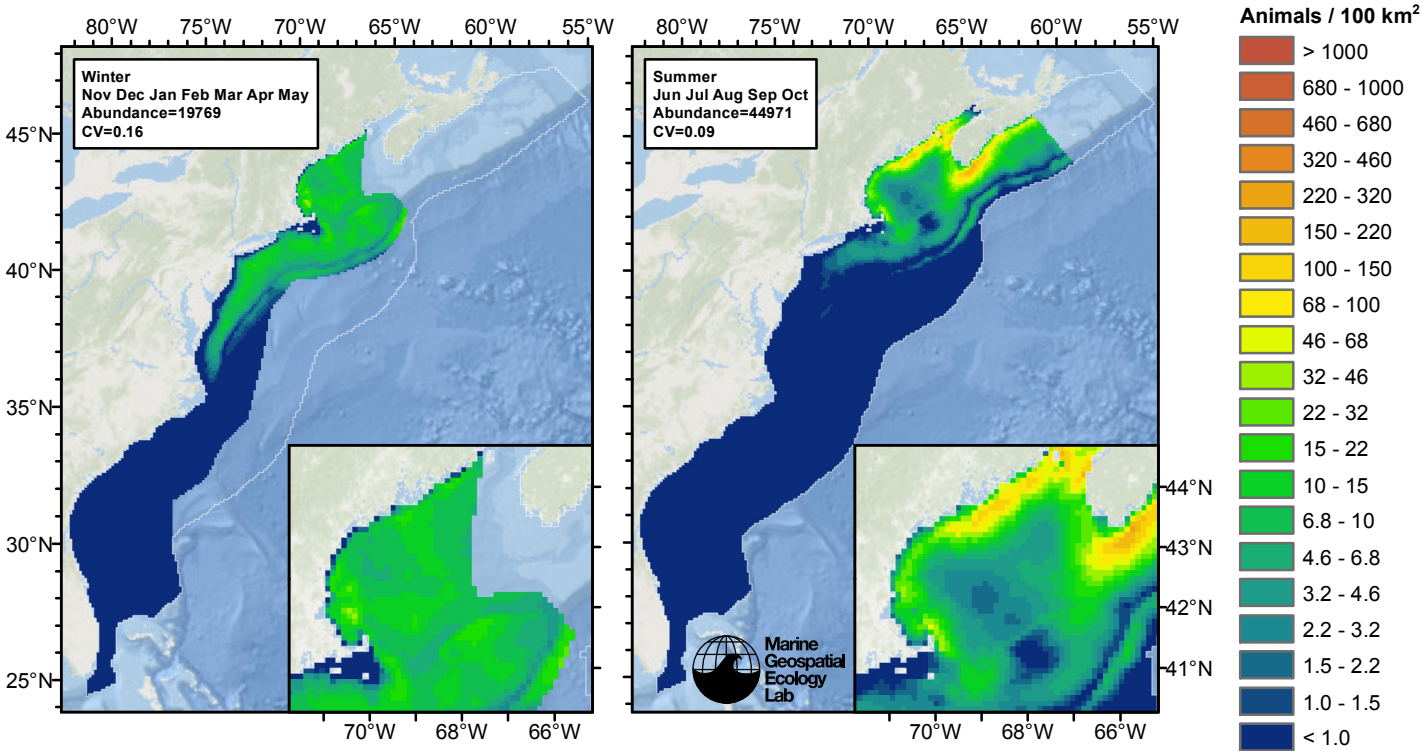

Figure 93: Harbor porpoise density and abundance predicted by the climatological same segments model that explained the most deviance. Regions inside the study area (white line) where the background map is visible are areas we did not model (see text).

Temporal Variability

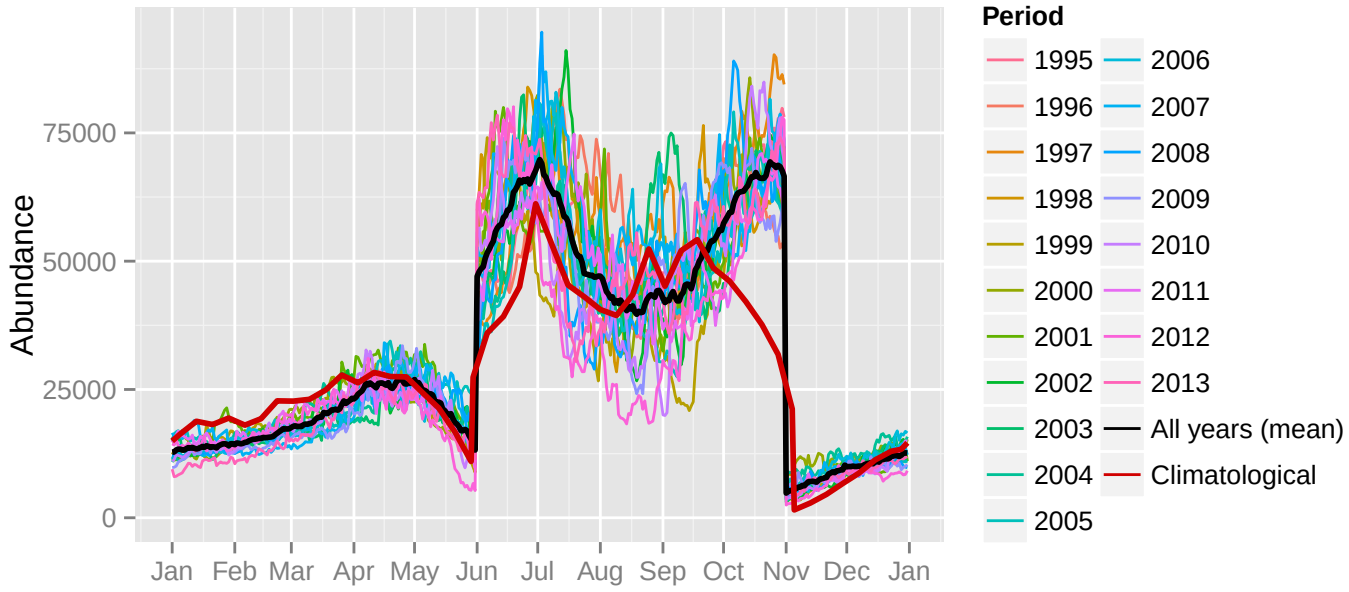

Figure 94: Comparison of Harbor porpoise abundance predicted at a daily time step for different time periods. Individual years were predicted using contemporaneous models. "All years (mean)" averages the individual years, giving the mean annual abundance of the contemporaneous model. "Climatological" was predicted using the climatological model. The results for the climatological same segments model are not shown.

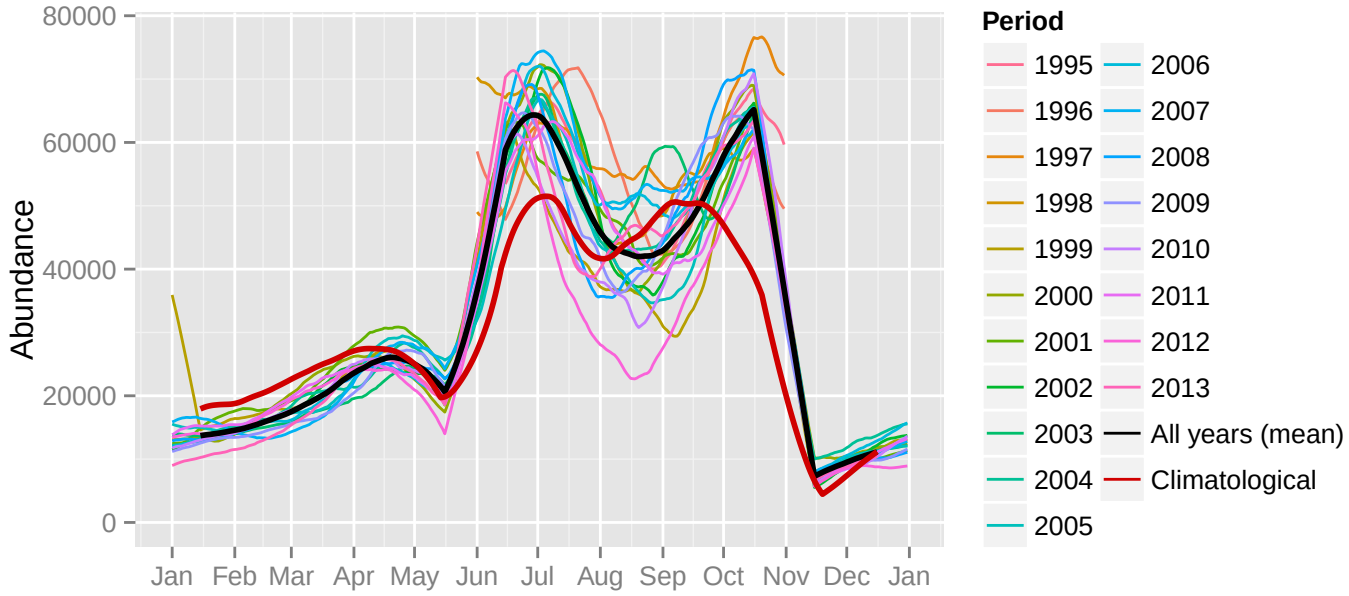

Figure 95: The same data as the preceding figure, but with a 30-day moving average applied.

Climatological Model

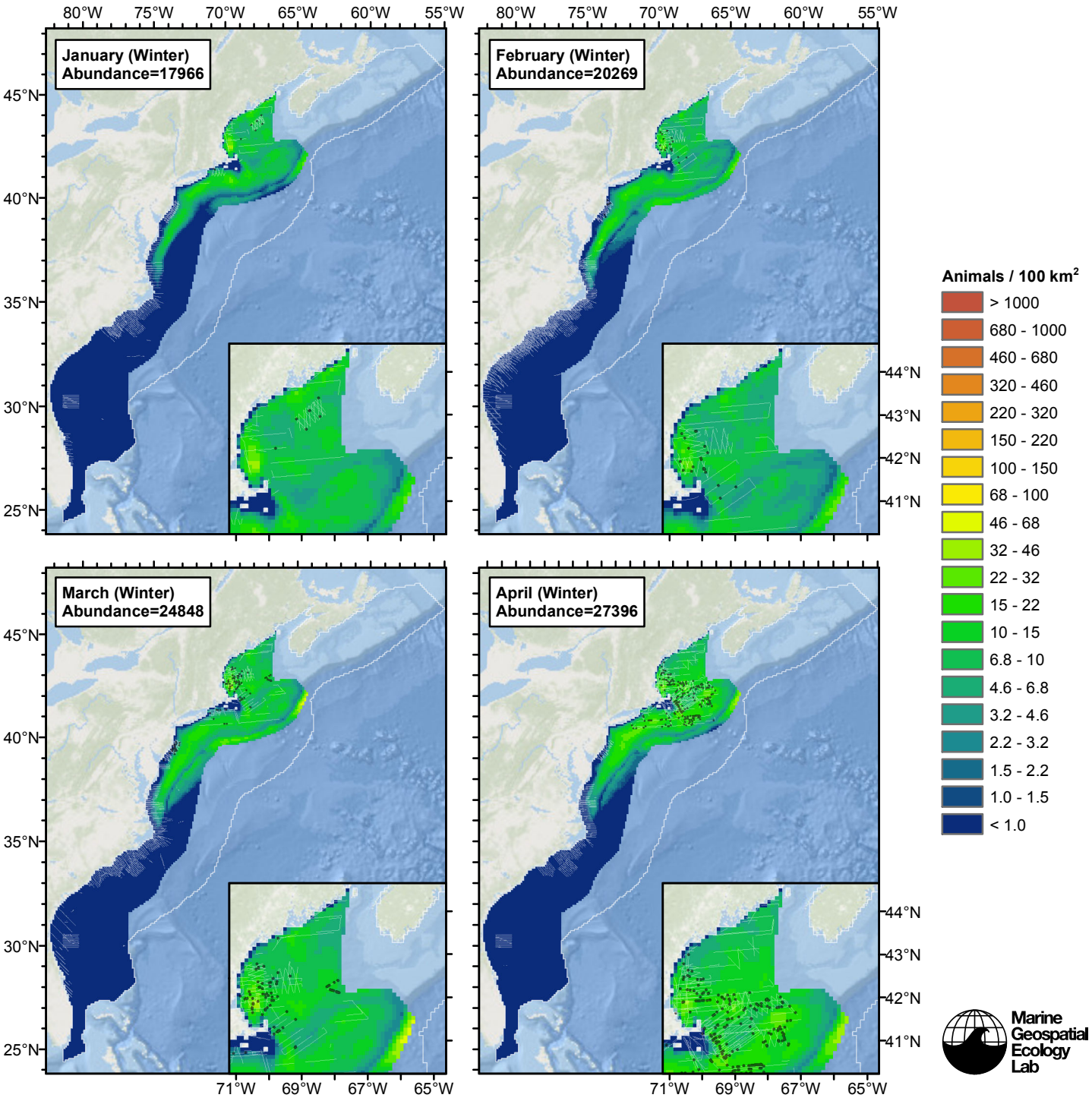

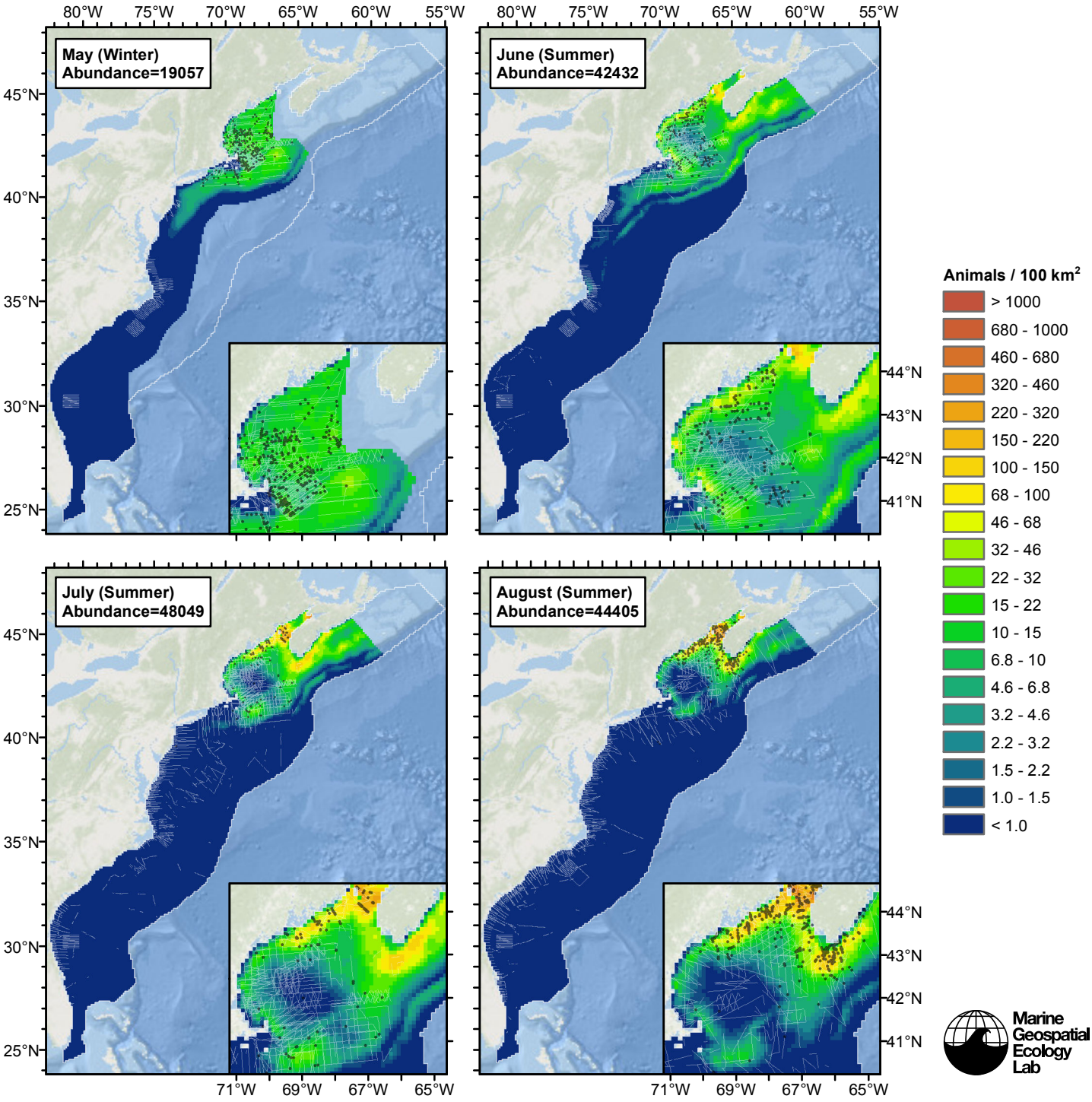
May (Winter)
Abundance=19057
June (Summer)
Abundance=42432
July (Summer)
Abundance=48049
August (Summer)
Abundance=44405
80°W
75°W
70°W
65°W
60°W
55°W
45°N
40°N
35°N
30°N
25°N
44°N
43°N
42°N
41°N
71°W
69°W
67°W
65°W
Animals / 100 km²
> 1000
680 - 1000
460 - 680
320 - 460
220 - 320
150 - 220
100 - 150
68 - 100
46 - 68
32 - 46
22 - 32
15 - 22
10 - 15
6.8 - 10
4.6 - 6.8
3.2 - 4.6
2.2 - 3.2
1.5 - 2.2
1.0 - 1.5
< 1.0
Marine
Geospatial
Ecology
Lab

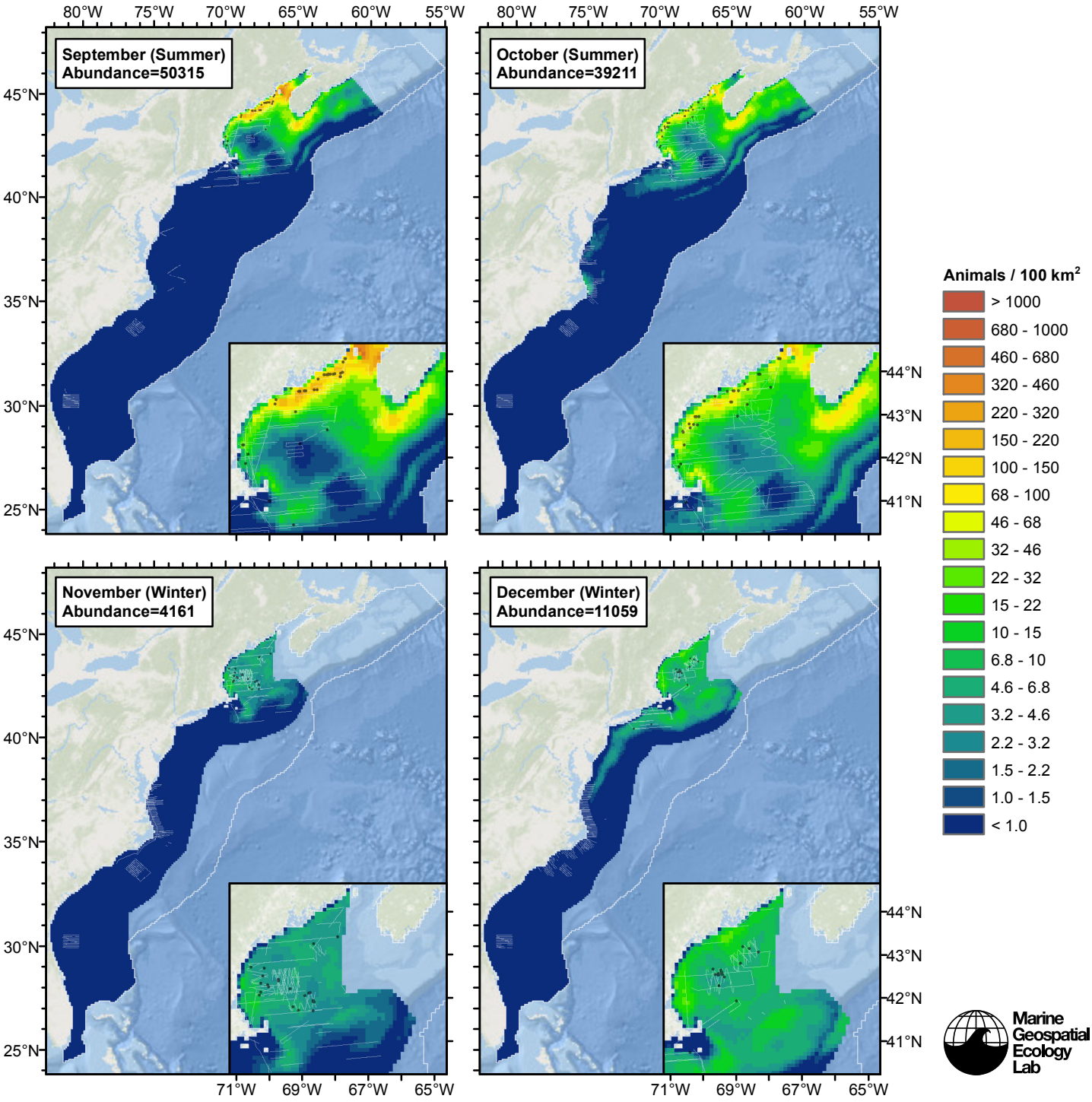
September (Summer)
Abundance=50315
October (Summer)
Abundance=39211
November (Winter)
Abundance=4161
December (Winter)
Abundance=11059
80°W
75°W
70°W
65°W
60°W
55°W
45°N
40°N
35°N
30°N
25°N
44°N
43°N
42°N
41°N
71°W
69°W
67°W
65°W
Animals / 100 km²
> 1000
680 - 1000
460 - 680
320 - 460
220 - 320
150 - 220
100 - 150
68 - 100
46 - 68
32 - 46
22 - 32
15 - 22
10 - 15
6.8 - 10
4.6 - 6.8
3.2 - 4.6
2.2 - 3.2
1.5 - 2.2
1.0 - 1.5
< 1.0
Marine
Geospatial
Ecology
Lab

Contemporaneous Model

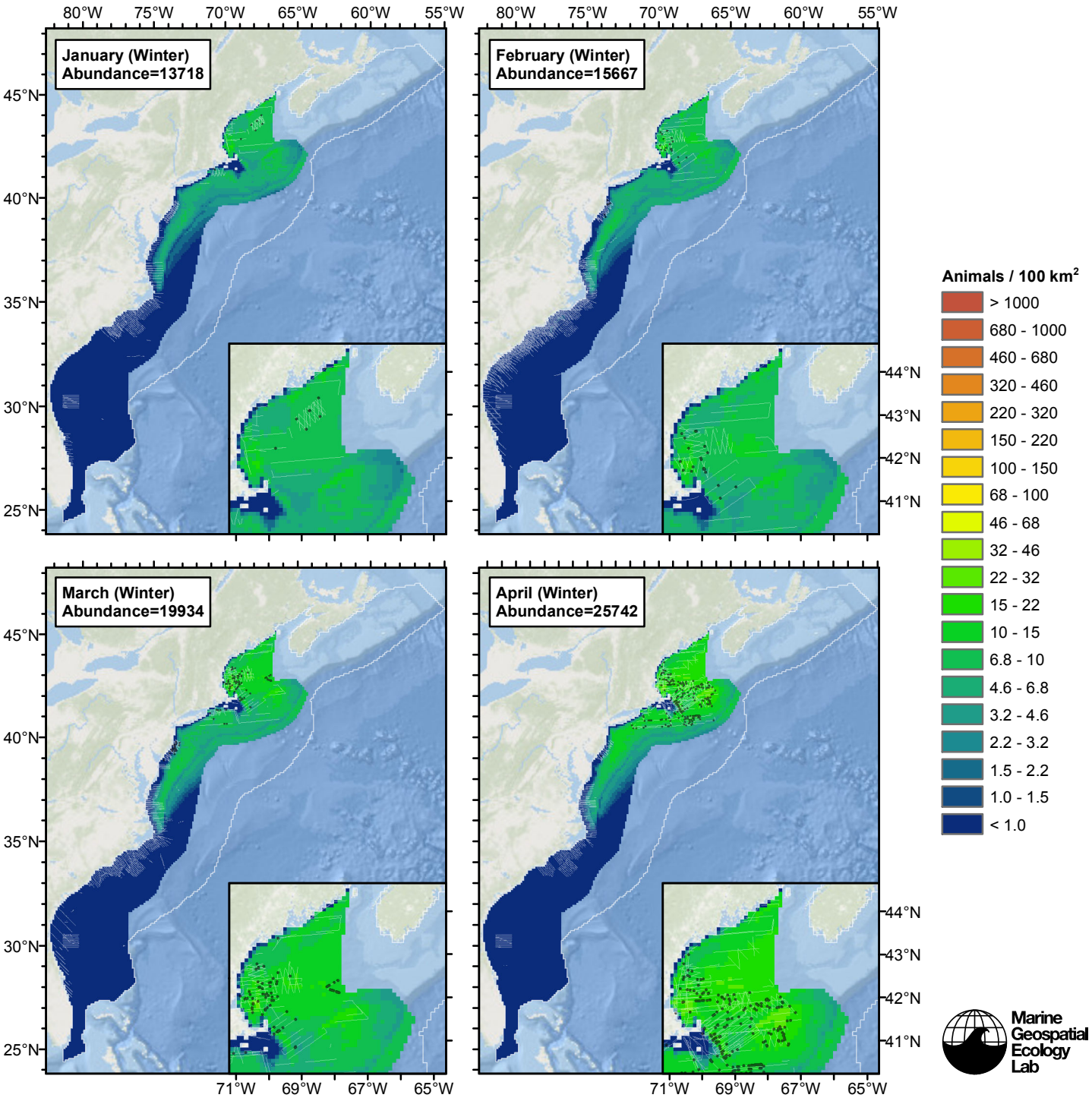

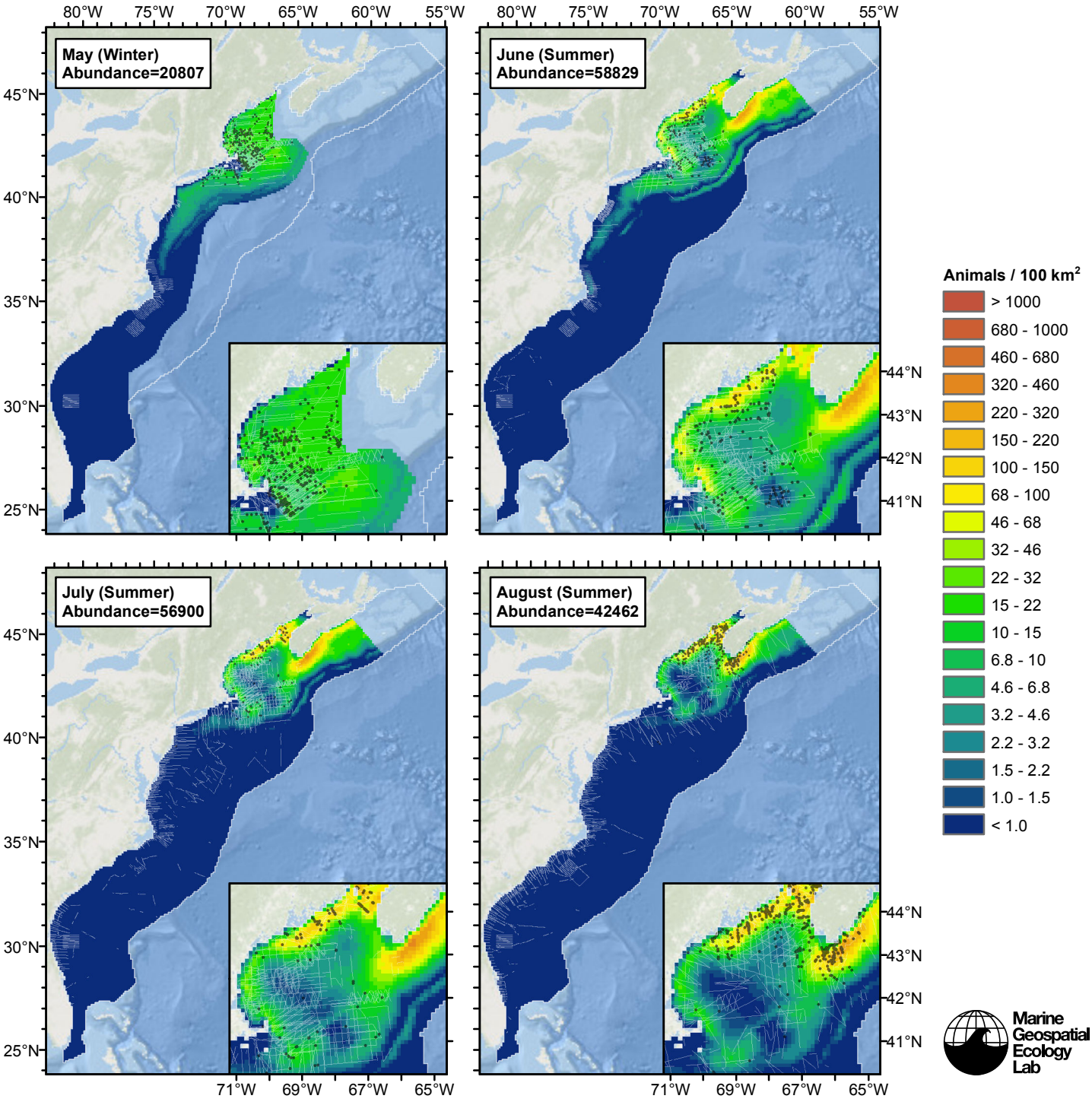
May (Winter)
Abundance=20807
June (Summer)
Abundance=58829
July (Summer)
Abundance=56900
August (Summer)
Abundance=42462
80°W
75°W
70°W
65°W
60°W
55°W
45°N
40°N
35°N
30°N
25°N
44°N
43°N
42°N
41°N
71°W
69°W
67°W
65°W
Animals / 100 km²
> 1000
680 - 1000
460 - 680
320 - 460
220 - 320
150 - 220
100 - 150
68 - 100
46 - 68
32 - 46
22 - 32
15 - 22
10 - 15
6.8 - 10
4.6 - 6.8
3.2 - 4.6
2.2 - 3.2
1.5 - 2.2
1.0 - 1.5
< 1.0
Marine
Geospatial
Ecology
Lab

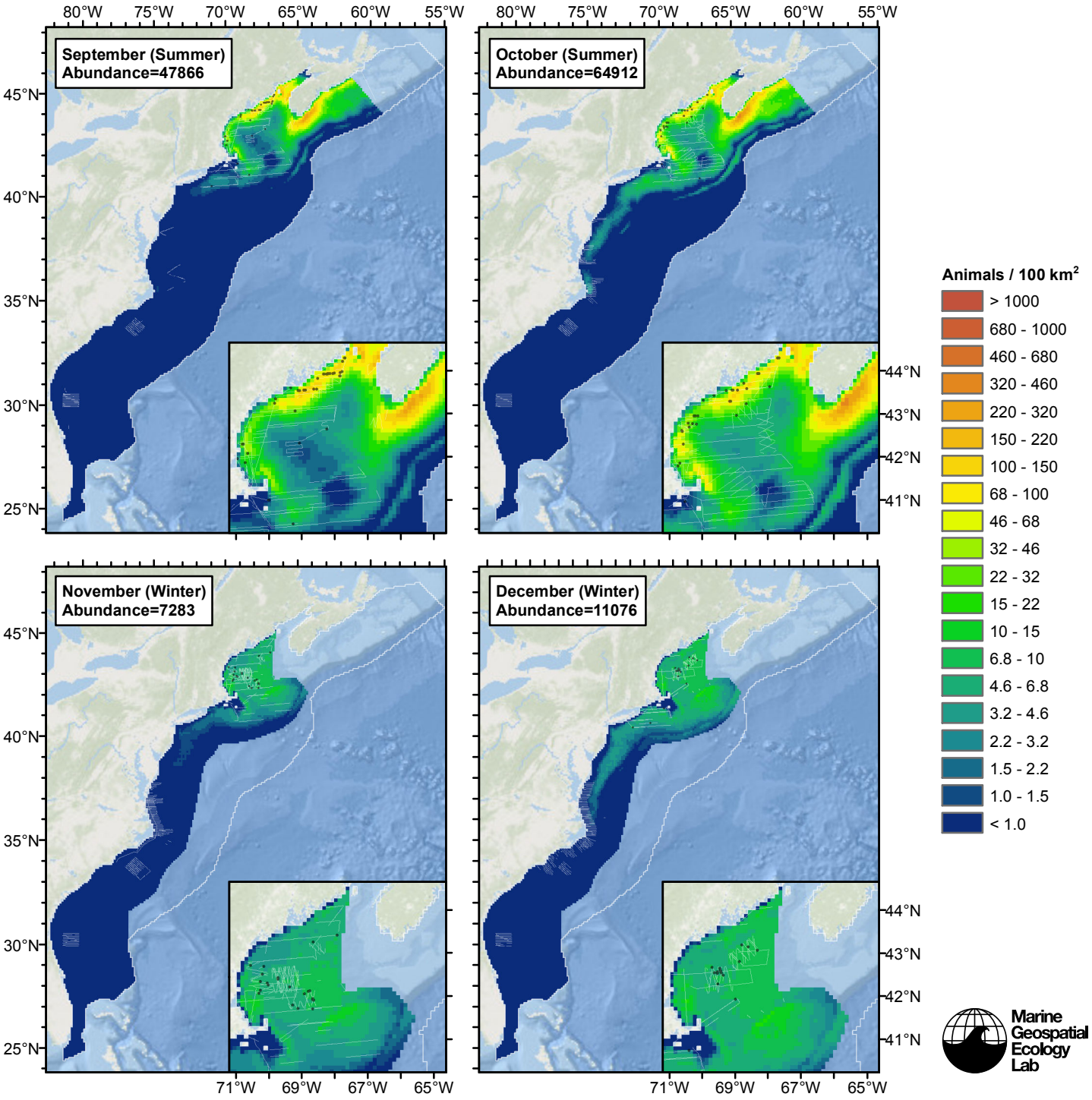
September (Summer)
Abundance=47866
October (Summer)
Abundance=64912
November (Winter)
Abundance=7283
December (Winter)
Abundance=11076
80°W
75°W
70°W
65°W
60°W
55°W
45°N
40°N
35°N
30°N
25°N
44°N
43°N
42°N
41°N
71°W
69°W
67°W
65°W
Animals / 100 km²
> 1000
680 - 1000
460 - 680
320 - 460
220 - 320
150 - 220
100 - 150
68 - 100
46 - 68
32 - 46
22 - 32
15 - 22
10 - 15
6.8 - 10
4.6 - 6.8
3.2 - 4.6
2.2 - 3.2
1.5 - 2.2
1.0 - 1.5
< 1.0
Marine
Geospatial
Ecology
Lab

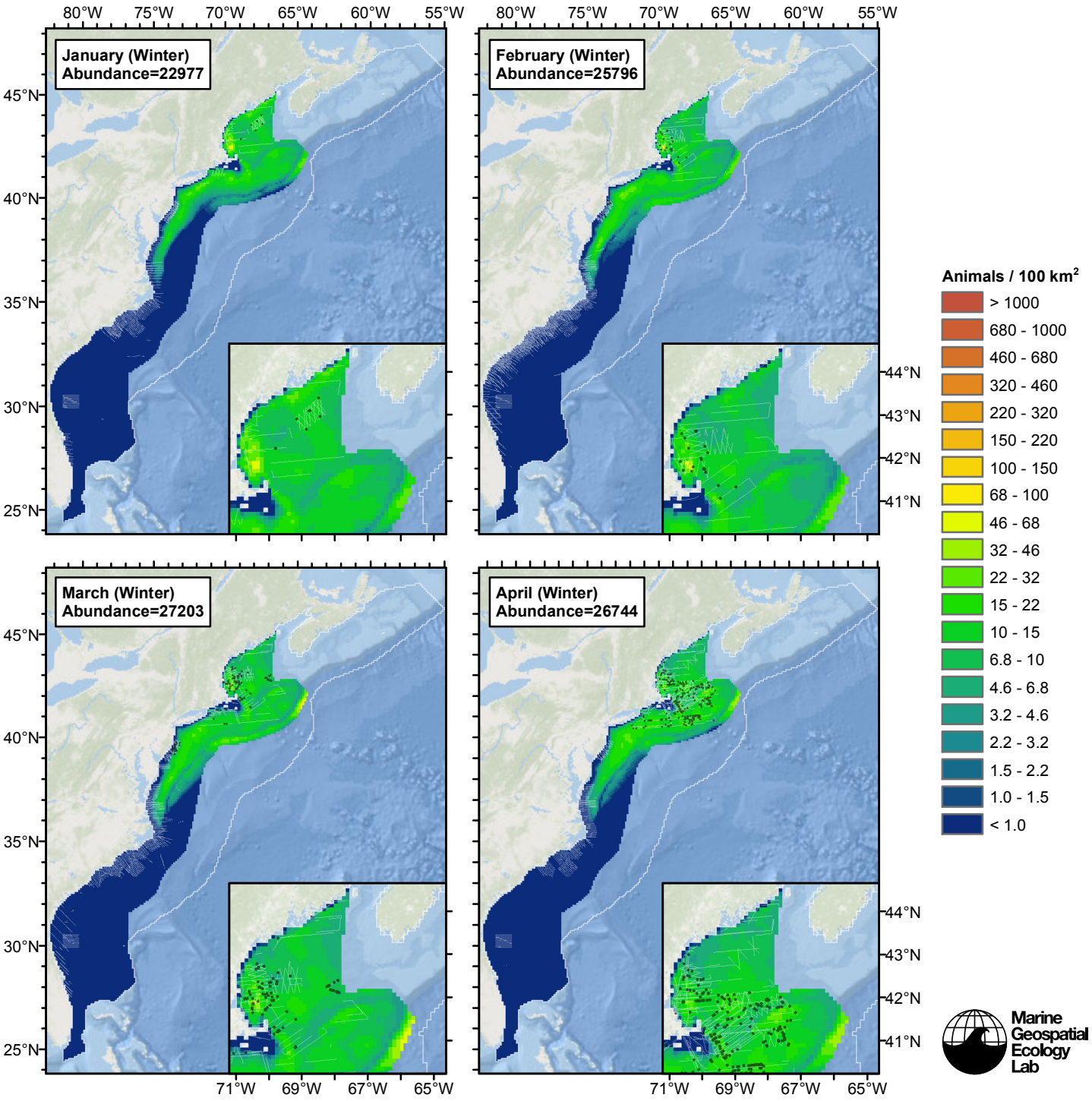
January (Winter)
Abundance=22977
February (Winter)
Abundance=25796
March (Winter)
Abundance=27203
April (Winter)
Abundance=26744
80°W
75°W
70°W
65°W
60°W
55°W
45°N
40°N
35°N
30°N
25°N
44°N
43°N
42°N
41°N
71°W
69°W
67°W
65°W
Animals / 100 km²
> 1000
680 - 1000
460 - 680
320 - 460
220 - 320
150 - 220
100 - 150
68 - 100
46 - 68
32 - 46
22 - 32
15 - 22
10 - 15
6.8 - 10
4.6 - 6.8
3.2 - 4.6
2.2 - 3.2
1.5 - 2.2
1.0 - 1.5
< 1.0
Marine
Geospatial
Ecology
Lab

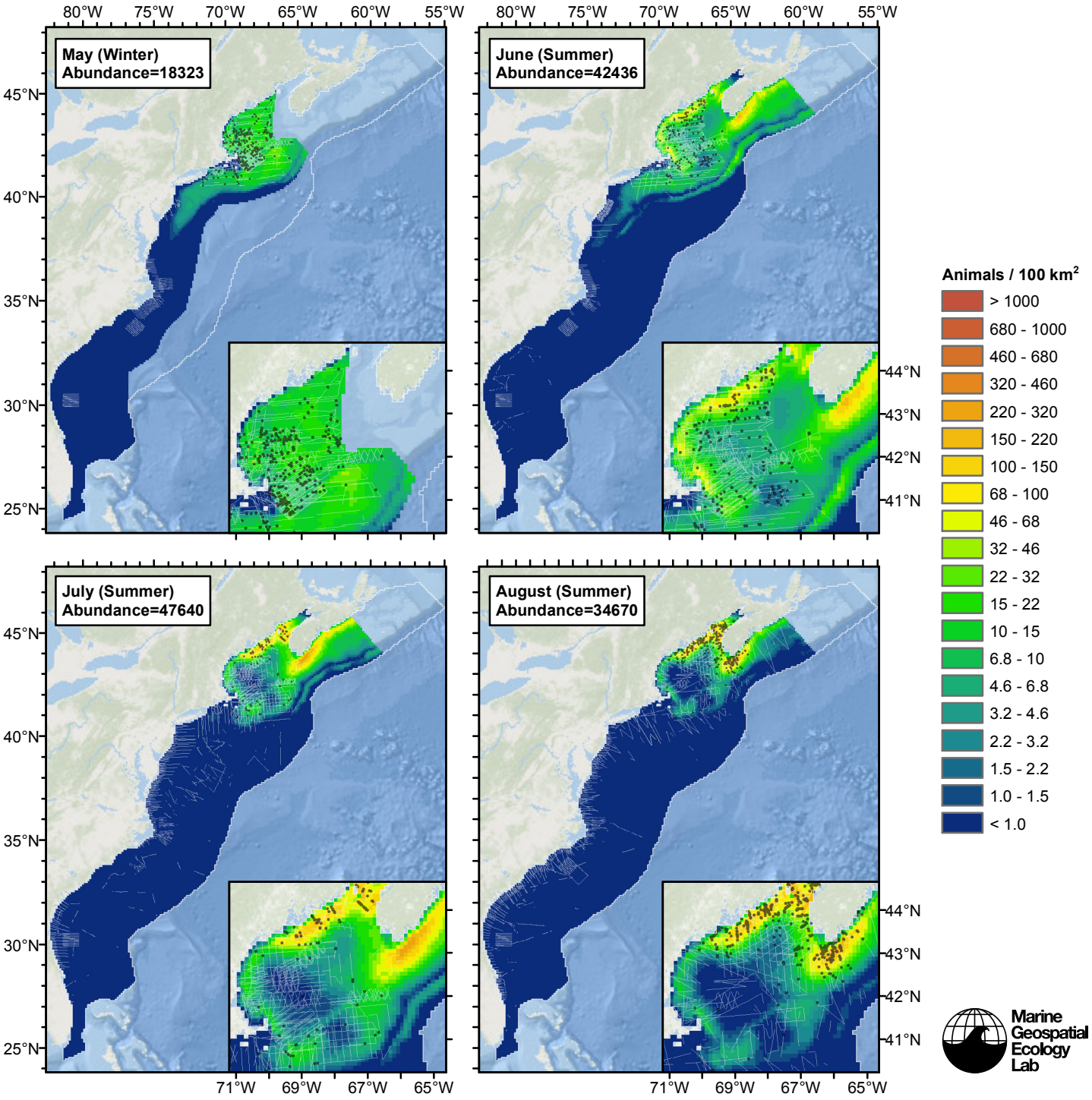
May (Winter)
Abundance=18323
June (Summer)
Abundance=42436
July (Summer)
Abundance=47640
August (Summer)
Abundance=34670
80°W
75°W
70°W
65°W
60°W
55°W
45°N
40°N
35°N
30°N
25°N
44°N
43°N
42°N
41°N
71°W
69°W
67°W
65°W
Animals / 100 km²
> 1000
680 - 1000
460 - 680
320 - 460
220 - 320
150 - 220
100 - 150
68 - 100
46 - 68
32 - 46
22 - 32
15 - 22
10 - 15
6.8 - 10
4.6 - 6.8
3.2 - 4.6
2.2 - 3.2
1.5 - 2.2
1.0 - 1.5
< 1.0
Marine
Geospatial
Ecology
Lab

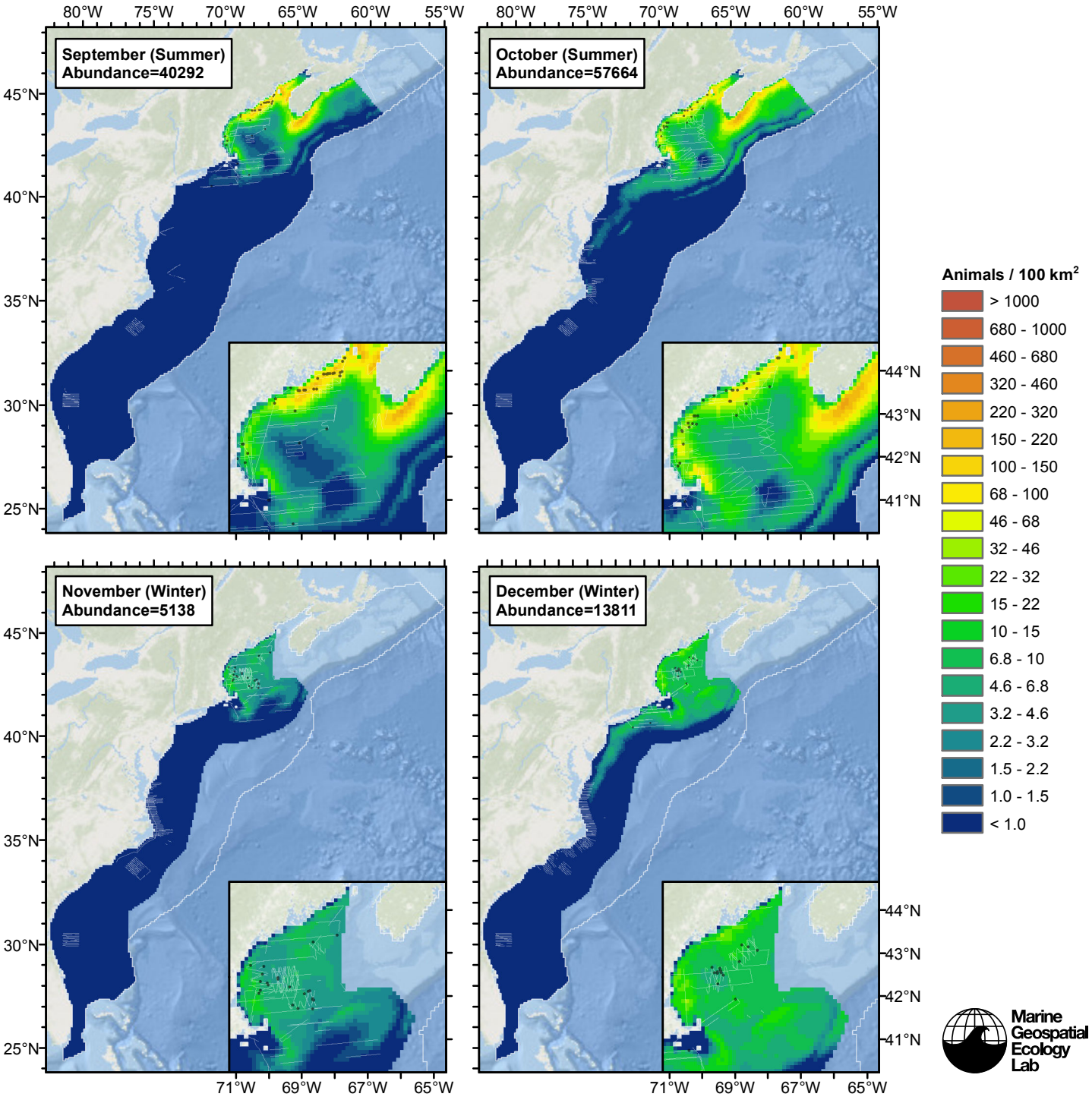

Discussion

Winter

In this season, the models that used climatological predictor variables outperformed the models that used contemporaneous predictors, explaining slightly more deviance. The spatial distributions of predicted abundance were similar across all models. The total abundance predicted by the climatological model that considered all segments was about 10% less than the climatological model that considered only the contemporaneous model's segments. The contemporaneous model's prediction was about 20% less than the climatological model that considered the same segments. Given the overall similarity between the models, we selected the climatological model that considered all segments as our best estimate of wintertime harbor porpoise

distribution and abundance, on the basis of its higher explained deviance and consideration of more survey data.

While we believe our model offers the best presently-available, spatiotemporally-explicit estimate of the wintertime distribution of Gulf of Maine/Bay of Fundy harbor porpoises, we note two important deficiencies. First, the total abundance predicted by our winter model is three to five times lower than the abundance predicted by our summer models or by NOAA's models. Either our winter model is greatly underestimating abundance or harbor porpoises inhabit some unmodeled area during this season (e.g. U.S. off-shelf waters, or Canadian waters on or off the shelf).

Second, despite numerous wintertime strandings in North Carolina (Hohn et al. 2013; Byrd et al. 2014), our model predicts very low density near to and south of North Carolina. Most of the strandings occurred north of Cape Hatteras (Byrd et al. 2014). Between New England and Cape Hatteras, currents on the shelf generally flow south, following the shelf, until they are entrained in the Gulf Stream at Cape Hatteras (Lentz 2008). This raises the possibility that the strandings in northern North Carolina were of animals that died at sea further north, were carried south by ocean currents, and washed up in northern North Carolina. But 13% of the strandings of harbor porpoises in the period 1997-2008 occurred between Cape Hatteras and Cape Lookout (Byrd et al. 2014). It seems unlikely that dead porpoises would drift around Cape Hatteras to the south without becoming entrained in the Gulf Stream. This raises the possibility that harbor porpoises could inhabit coastal North Carolina in winter, or even areas farther south.

We advise caution until these problems can be addressed. Kraus et al. (1983) argued that shipboard surveys are superior to aerial surveys for estimating harbor porpoise distribution and abundance. Keeping that in mind, we note that the NJ-DEP inshore shipboard surveys reported 36 sightings, the most sightings of harbor porpoises for any survey south of New England, while the NJ-DEP aerial surveys in the same region reported only 6 sightings. It is possible that harbor porpoises are just too difficult to observe effectively from aircraft in winter in this region. We recommend additional shipboard surveying of the mid-Atlantic states and North Carolina in winter, using naked eyes if possible. If such surveys are carried out, they should use dual observer teams or some other approach that allows perception bias to be estimated.

Summer

As with the winter season, the models that used climatological predictor variables outperformed the models that used contemporaneous predictors, explaining slightly more deviance. The spatial distributions of predicted abundance were similar across all models. The climatological models predicted higher abundance in the northern Bay of Fundy, while the contemporaneous model predicted higher abundance along the Scotian Shelf, close to shore. The total abundance predicted by the climatological models was about 20% less than the contemporaneous model. The contemporaneous model exhibited higher variability, with August abundance roughly 30% lower than June or October.

Given the overall similarity between the models, we selected the climatological model that considered all segments as our best estimate of summertime harbor porpoise distribution and abundance, on the basis of its higher explained deviance, consideration of more survey data, and a more plausible pattern of monthly abundance predictions.

Our model's mean prediction was about 10% lower than NOAA's estimate from 2004, but 40-50% lower than NOAA's 2006 and 2011 estimates. We suspect an important reason for this difference lies in our use of the NARWSS surveys. The NARWSS surveys were not ideally suited for observing harbor porpoises. Although they occurred mainly on the same Twin Otter aircraft as the NOAA marine mammal abundance surveys that NOAA's estimates are based on, they did not utilize a belly observer, they flew at 750 ft rather than 600 ft, and, most importantly, their observers scanned most frequently at 1-1.5 miles out from the trackline (T. Cole, pers. comm.) rather than "guarding the trackline" as is recommended for abundance estimation. While this protocol was appropriate for the NARWSS program's primary mission of finding and photographing right whales, it resulted in relatively few harbor porpoise sightings close to the trackline (see NARWSS Twin Otters detection functions above).

We addressed this by left truncating the sightings and fitting a half-normal detection function that extrapolated back to zero (Buckland et al. 2001). Vertical angles were often rounded in these data, and we had to heap them at 10 degree intervals. As a result, we had to discard 4 of 9 bins and fit the detection function to only the 5 most distant bins.

The resulting detection function seemed reasonable, but the mean effective strip half width (268 m) was wider than what we obtained (197 m) for our detection function for the NOAA marine mammal abundance surveys (called "With Belly Observers" above), even after accounting for the portion of the strip lost due to left-truncation. This may be an overestimate of the NARWSS surveys' effectiveness; if so, it would result in an underestimation of abundance. And because this detection function was applied to over twice as many sightings as the detection function for the marine mammal abundance surveys (1014 sightings vs. 461), it exercised a strong influence on our model.

This raises the question: should we have removed the NARWSS surveys from our model? We considered the question carefully and determined that we should not. The NARWSS surveys provided irreplaceable temporal coverage of the Gulf of Maine,

which allowed the models to capture seasonal dynamics in distribution that could not be captured by the NOAA marine mammal abundance surveys, which occurred mainly in July and August. For example, the NARWSS surveys reported numerous harbor porpoise sightings in May in the southern Gulf of Maine; our May prediction reflects this (see Temporal Variability section above). Palka (2006), based on the 1999, 2002, and 2004 marine mammal abundance surveys, estimated zero harbor porpoises in this area (the Gulf of Maine South (GOMS) stratum of Palka's analysis).

In conclusion, we find the spatiotemporal dynamics of our model plausible and in agreement with what has been reported in the literature, but the absolute abundance prediction may be low. We suggest that our monthly predictions be used for federal regulatory purposes and marine spatial planning applications, so that the seasonality of the species be accounted for, but we advise caution in all months and areas due to the possibility that we underestimated abundance.

References

Byrd BL, Harms CA, Hohn AA, McLellan WA, Lovewell GN, et al. (2014) Strandings as indicators of marine mammal biodiversity and human interactions off the coast of North Carolina. Fishery Bulletin 112: 1-23.

Hammond PS, Benke H, Breggren P, Collet A, Heide-Jorgensen MP, et al. (1995) The distribution and abundance of harbour porpoises and other small cetaceans in the North Sea and adjacent waters. ICES CM Document 1995/N:10. Available online: http://brage.bibsys.no/xmlui/handle/11250/105477

Hammond PS, Berggren P, Benke H, Borchers DL, Collet A, et al. (2002) Abundance of harbour porpoise and other cetaceans in the North Sea and adjacent waters. Journal of Applied Ecology. 39: 361-376.

Hammond PS, Macleod K, Berggren P, Borchers DL, Burt L, et al. (2013) Cetacean abundance and distribution in European Atlantic shelf waters to inform conservation and management. Biological Conservation 164: 107-122.

Hansen RG, Heide-Jorgensen MP. (2013) Spatial trends in abundance of long-finned pilot whales, white-beaked dolphins and harbour porpoises in West Greenland. Mar Biol. 160: 2929-2941.

Hiby L (1999) The objective identification of duplicate sightings in aerial survey for porpoise. In: Marine Mammal Survey and Assessment Methods (Garner GW, Amstrup SC, Laake JL, Manly BFJ, McDonald LL, Robertson DG, eds.). Balkema, Rotterdam, pp. 179-189.

Hohn AA, Rotstein DS, Byrd BL (2013) Unusual Mortality Events of Harbor Porpoise Strandings in North Carolina, 1997-2009. Journal of Marine Biology: 1-13.

Kraus SD, Gilbert JR, Prescott JH. (1983) A comparison of aerial, shipboard, and land-based survey methodology for the harbor porpoise, Phocoena phocoena. Fishery Bulletin 81: 910-913.

Lawson JW, Gosselin J-F (2011) Fully-corrected cetacean abundance estimates from the Canadian TNASS survey. Working Paper 10. National Marine Mammal Peer Review Meeting. Ottawa, Can. 28 p.

Lentz SJ (2008) Observations and a Model of the Mean Circulation over the Middle Atlantic Bight Continental Shelf. Journal of Physical Oceanography 38: 1203-1221.

Palka DL (1996) Effects of Beaufort sea state on the sightability of harbor porpoises in the Gulf of Maine. Rep Int Whal Comm. 46: 575-582.

Palka DL (2000) Abundance of the Gulf of Maine/Bay of Fundy harbor porpoise based on shipboard and aerial surveys during 1999. US Dept Commer, Northeast Fish Sci Cent Ref Doc. 00-07.

Palka DL (2006) Summer Abundance Estimates of Cetaceans in US North Atlantic Navy Operating Areas. US Dept Commer, Northeast Fish Sci Cent Ref Doc. 06-03: 41 p.

Palka DL (2012) Cetacean abundance estimates in US northwestern Atlantic Ocean waters from summer 2011 line transect survey. US Dept Commer, Northeast Fish Sci Cent Ref Doc. 12-29. 37 p.

Palka DL, Read AJ, Westgate AJ, Johnston DW (1996) Summary of current knowledge of harbour porpoises in US and Canadian Atlantic waters. Rep Int Whal Comm. 46: 559-565.

Rossman MC, Merrick RL (1999) Harbor porpoise bycatch in the Northeast multispecies sink gillnet fishery and the Mid-Atlantic coastal gillnet fishery in 1998 and during January-May 1999. Northeast Fish Sci Cent Ref Doc: 99-17. 36 p.

Stenson GB (2014) Harbour porpoise (Phocoena phocoena) in the North Atlantic: Abundance, removals, and sustainability of removals. NAMMCO Scientific Publications 5: 271-302.

Waring GT, Josephson E, Maze-Foley K, Rosel PE, eds. (2014) U.S. Atlantic and Gulf of Mexico Marine Mammal Stock Assessments – 2013. NOAA Tech Memo NMFS NE 228; 464 p.